The mean-field theory of nuclear structure and dynamics

J. W. Negele

Center for Theoretical Physics, Laboratory for Nuclear Science and Department of Physics, Massachusetts Institute of Technology, Cambridge, Massachusetts 02139

The physical and theoretical foundations are presented for the mean-field theory of nuclear structure and dynamics. Salient features of the many-body theory of stationary states are reviewed to motivate the time-dependent mean-field approximation. The time-dependent Hartree-Fock approximation and its limitations are discussed and general theoretical formulations are presented which yield time-dependent mean-field equations in lowest approximation and provide suitable frameworks for overcoming various conceptual and practical limitations of the mean-field theory. Particular emphasis is placed on recent developments utilizing functional integral techniques to obtain a quantum mean-field theory applicable to quantized eigenstates, spontaneous fission, the nuclear partition function, and scattering problems. Applications to a number of simple, idealized systems are presented to verify the approximations for solvable problems and to elucidate the essential features of mean-field dynamics. Finally, calculations utilizing moderately realistic geometries and interactions are reviewed which address heavy-ion collisions, fusion, strongly damped collisions, and fission.

CONTENTS

I. INTRODUCTION

A fundamental challenge pervading theoretical physics is the problem of understanding the properties of systems possessing large or infinite numbers of degrees of freedom in terms of the underlying interactions between constituents. The particular case addressed in this review, the structure and dynamics of self-bound composite systems governed by nonrelativistic quantum mechanics and interacting via a static two-body potential, retains much of the challenge of the general many-body problem, while incorporating sufficient simplifications to render it tractable.

Whereas the essential elements of the theory are of general applicability to a variety of many-particle systems, there are compelling reasons for investigating the mean-field theory within the context of nuclear physics. In the first place, the role of the mean field in nuclear ground states is already well understood and provides a natural foundation for exploration of dynamics. Furthermore, the phenomena and modes of excitation observable in nuclei are exceedingly rich and varied. Even in nuclear ground states, one observes strong interplay between single-particle structure and shape degrees of freedom. The phenomenology of excited states is even richer, with the full spectrum of single-particle and collective degrees of freedom arising in appropriate reactions. The accessibility of nuclei to diverse probes allows the methodical exploration of the charge, current, and magnetization densities with electromagnetic probes and the systematic excitation of states of most desired quantum numbers with mesonic and hadronic probes. Finally, the possibility of studying reactions with projectiles ranging from a single nucleon to the heaviest nuclei at energies ranging up to hundreds of MeV per nucleon offers incomparable opportunities to investigate dynamics under diverse conditions. For all these reasons, then, nuclear physics provides a natural testing ground in which to try out our first tentative ideas in formulating a general dynamical theory.

Given the complexity of the full time-dependent many-body problem, it is desirable to formulate a general hierarchy of successive approximations such that the lowest order contains the physics of the mean field. Certainly one great appeal of such a systematic approach is the freedom in each order from any adjustable parameters or adjustable assumptions. Given the nuclear Hamiltonian and appropriate initial conditions, the theory itself determines the relevant collective or single-particle degrees of freedom. If some significant feature of the force is changed, the system responds appropriately. By simply changing the initial conditions, one should be able to obtain a single unified description of such diverse phenomena as transitions to excited states induced by external fields, large amplitude collective oscillations, fission, fusion, compound nucleus formation, dissipation, strongly damped collisions, fragmentation, and high-density self-sustaining spin-isospin instabilities.

Such a microscopic description is in marked contrast to the plethora of models which, guided by the phenomenology, have deliberately built into them just those features one ultimately wishes to observe in a particular application. Only certain degrees of freedom are included, and no change in the interaction or initial conditions can bring in other, suppressed degrees of freedom. When one changes from the description of one phenomenon to another, a new model with different degrees of freedom and assumptions is invoked, thereby losing all contact with a general unified description. Not only is there no systematic program of successive corrections to a hydrodynamic model, various friction models, or the assumption of random nuclear matrix elements, but often, due to the multiplicity of adjustable parameters and assumptions, it is not even possible to perform a definitive test of the underlying theory. Indeed, it is most worthwhile to fully savor the essential shortcomings of such models so as to be adequately tolerant of numerical difficulties associated with solving the self-consistent time-dependent mean-field equations arising from the microscopic theory.

A. The mean field

Since the mean field plays a central role in the present formulation, it is useful at the outset to review the physical rationale for a mean-field description of low-energy dynamics. One of the best justifications is Hartree's original intuitive argument for the static problem that an individual particle should respond to the average field generated by interactions with surrounding particles. In dynamics, this average field is the obvious candidate to communicate collective information. In contrast to other formulations which single out several assumed collective coordinates, the mean field may be viewed as a collective field containing an infinite number of degrees of freedom. A subset of these degrees of freedom, of course, includes all the familiar surface deformations and shape degrees of freedom, but the essential feature is that the theory contains from the outset all the relevant collective degrees of freedom, with different collective variables coming into play as the specific situation demands.

The fact that a one-body mean field governs the structure and low-energy dynamics of nuclei in spite of the exceedingly strong two-body interactions described by the nucleon-nucleon potential arises primarily from the Pauli exclusion principle. The question of whether one-body behavior or two-body collisions dominate depends essentially on whether the nucleon mean-free path is much longer or shorter than the nuclear size. The simple estimate $\lambda \sim (\sigma\rho)^{-1}$ yielding a mean-free path of several

Fermis is qualitatively altered by Pauli blocking and the density of states in the nuclear medium. For a single nucleon of energy ε outside of a Fermi gas of Fermi energy ε_F (Galitskii, 1958) the result is

$$\lambda=\frac{4}{3\langle\sigma\rho\rangle}\left[\frac{\varepsilon_F}{\varepsilon-\varepsilon_F}\right]^2, \tag{1.1}$$

yielding greatly enhanced mean-free paths for energies sufficiently close to ε_F.

An estimate far more relevant to nuclear collisions is a calculation of the decay time for the edges of the Fermi spheres representing two interpenetrating Fermi gases. Given one gas, representing a projectile, with an energy per particle E_p relative to the other gas, corresponding to a target, the decay time is approximately (Bertsch, 1978b)

$$\tau\approx\frac{1000\ \text{MeV fm c}^{-1}}{E_p}. \tag{1.2}$$

This simple formula is in qualitative agreement with explicit numerical calculations (Bertsch, 1977a). At incident energies greater than roughly 8 MeV per nucleon, nuclei essentially pass through each other, so a characteristic decay length is the distance two nuclei would interpenetrate at the incident velocity during the decay time τ

$$\lambda\sim\left[\frac{2E_p}{m}\right]^{1/2}\tau=\frac{46.1}{\sqrt{E_p}}\ \text{fm MeV}^{1/2}. \tag{1.3}$$

At an incident energy of 10 MeV per nucleon, $\lambda=15$ fm, so the relevant decay length is comparable to the diameter of the largest existing nuclei. At lower energies, Pauli blocking is even more effective in increasing the mean-free path. In addition, the nonlocality of the mean field decreases the density of states near the Fermi surface, thereby significantly increasing the mean-free path in nuclear matter beyond that due to the Pauli principle alone (Fantoni, Friman, and Pandharipande, 1981; Negele and Yazaki, 1981). Hence it is reasonable to expect the mean field to provide a valid description for dynamics up to energies of the order of 10 MeV per particle. The precise value of 10 MeV is, of course, subject to the obvious uncertainties in all mean-free path arguments, but there must surely exist a distinct low-energy regime in which nuclear dimensions are smaller than the characteristic dimension at which two-body collisions begin to dominate mean-field dynamics.

Whereas the concept of a mean field has the clear physical foundations discussed above and is crucial to our present understanding of nuclear ground states and the shell model, one must ultimately face the fact that it is purely an artificial theoretical construct. It cannot be uniquely defined and it does not correspond to any observable operator which even in principle could be measured. Thus, it is inevitable that reference to the mean field will necessarily be imprecise, and that different formalisms addressing alternative features of the physics will yield somewhat different definitions of the mean field. The one limit in which essentially all formulations of mean-field theories merge is in the limit of an arbitrarily weak interaction, in which case the mean field simply becomes the Hartree-Fock potential produced by the integral of the antisymmetrized two-body potential with the instantaneous one-body density matrix. This Hartree-Fock limit has given rise to a certain imprecision in terminology, in which time-dependent theories involving mean fields defined in terms of effective interactions instead of the bare two-body potential are often loosely referred to as the time-dependent Hartree-Fock (TDHF) approximation.

B. Phenomenology

Although I shall attempt to formulate a theory which is microscopic at the level of nuclear structure, until present qualitative ideas concerning meson exchange and interactions between bags of quarks are replaced by a tractable quantitative theory of strong interactions, the theory will necessarily remain phenomenological at the level of the nucleon-nucleon interaction. The approach in this present work is simply to postulate the existence of a static nucleon-nucleon potential and to let its spatial, spin, and isospin dependence be determined phenomenologically from two-body scattering data and properties of the deuteron. Whereas essential fundamental limitations are imposed by the suppression of underlying meson and quark degrees of freedom and lack of experimental constraints on the off-shell behavior of the phenomenological potential, the potential approximation yields a well-defined many-body problem which may be addressed by microscopic theory.

The validity of this approach has already been explored for nuclear matter and the ground states of finite nuclei. Whereas the qualitative features are correctly reproduced by a potential such as the Reid potential (Reid, 1968), the equilibrium density of nuclear matter and corresponding interior densities of finite nuclei are quantitatively in error.

To establish detailed quantitative contact with real nuclei, then, a second level of phenomenology must necessarily be introduced. In the framework of effective operators, it is possible to include the physics of suppressed degrees of freedom by defining effective operators in a restricted model space which reproduce the same expectation values as the true operators acting within the full space. In this language, then, meson exchanges between one nucleon and two others which overlap in time or involve virtual isobar excitation give rise to three-body effective interactions. Similar processes in which a photon couples to a virtual nucleon-antinucleon pair or isobar which is created or annihilated by interaction with another nucleon in the medium give rise to two- and higher-body contributions to the effective electromagnetic current operator. The fact that perturbative estimates based on the longest-range meson contributions yield many-body effective interactions and current operators of the required order of magnitude, renders such many-body

effective operators the most physical explanation of the discrepancies arising in the theory including only two-body potentials. The second level of phenomenology is thus introduced by postulating a three-body effective interaction which is phenomenologically defined to reproduce the known density and binding energy of bulk nuclear matter.

Since we are lacking a fundamental theory of nuclear interactions, the ultimate test of this phenomenological potential theory is its consistency. As will be reviewed in Sec. II, one obtains a consistent theory of ground states of nuclei throughout the Periodic Table, so it is physically plausible that the same potentials should adequately describe low-energy nuclear dynamics. As unpleasant as any recourse to phenomenology may seem, it is important to bear in mind that the theoretical developments presented in this review concerning many-body dynamics with static potentials stand on their own merits, independent of specific limitations of our present knowledge of nuclear interactions. Furthermore, it is possible that future progress in deriving effective many-body interactions in the nucleon-nucleon space will produce fundamental interactions sufficiently close to the phenomenological ones used at present that the framework envisioned in this review will prove essentially correct. Alternatively, some enlargement of the space may ultimately turn out to be forced upon us. A particularly innocuous enlargement would be to include Δ isobars coupled to nucleons with static transition potentials, in which case the present theory would carry over immediately with only the technical complications of carrying an additional spinlike label distinguishing nucleon and Δ states. Only if one is forced to the explicit inclusion of mesons, antiparticles, or quark and gluon degrees of freedom will the essential simplicity of the present approach be seriously compromised.

C. Outline

This review is organized according to the following outline. For the reasons discussed in this introduction, Sec. II reviews the status of microscopic many-body theory for stationary states. Subject to the two levels of phenomenology explained above, it is shown that mean-field theory yields a quantitative description of binding energies and matter distributions throughout the Periodic Table. The systematics of density distributions and shapes of intrinsic states are particularly relevant, since such shape degrees of freedom play a crucial role in low-energy dynamics. Several explicit comparisons of theoretical predictions with electron scattering data are included to emphasize the level of quantitative precision presently obtained.

As an introduction to dynamics, the simplest version of the time-dependent mean-field theory, the TDHF initial-value problem, is presented in Sec. III. Instead of deriving it as the first step in a systematic hierarchy, I have utilized the concise form provided by the time-dependent variational principle. Salient properties of the TDHF equations are presented, and special limiting cases are reviewed. Finally, the need for more systematic general approaches is motivated by discussion of two fundamental limitations of the TDHF initial-value problem: the omission of multiparticle correlations and the conceptual ambiguities associated with description of a quantum many-body problem in terms of an equation of motion and initial condition for a one-body density matrix. One solution to the first problem is presented in Sec. IV, in which alternative truncations of hierarchies of coupled equations for many-particle correlation functions are discussed and it is argued that the time-dependent coupled-cluster expansion is a particularly economical and practical approach.

The problem of systematically approximating exact expressions for quantum observables in such a way as to obtain a first approximation to the time-dependent mean-field form is addressed in Sec. V. Using alternative functional integral representations for the evolution operator, application of the stationary-phase approximation yields self-consistent time-dependent mean-field equations which, in principle, may be systematically corrected by expanding the corrections to the stationary-phase result. Applications are presented to the calculation of quantized states of large-amplitude collective motion, tunneling decay in spontaneous fission, and response to an external potential.

Applications of the general theory of Secs. II–V to a variety of model and realistic problems are presented in the last two sections. Section VI addresses simple, idealized systems. Exact and mean-field approximations are compared for two solvable models: particles in one spatial dimension interacting via an attractive delta-function two-body potential and the two-level Lipkin model (Meshkov, Glick, and Lipkin, 1965). As a prelude to realistic three-dimensional geometry, numerical solutions for a one-dimensional saturating model and semi-infinite slabs of matter with nontrivial spatial dependence in only one dimension are presented for a variety of dynamical processes. Applications to nuclear physics are presented in Sec. VII. Following a survey of approximations required to implement practical numerical calculations, three aspects of heavy-ion collisions are reviewed: the systematics of fusion cross sections, qualitative features of strongly damped collisions, and the onset of spin-isospin instabilities. In addition to these scattering problems, preliminary efforts to understand the dynamics of induced and spontaneous fission are discussed.

II. MICROSCOPIC THEORY OF STATIONARY STATES

As a prelude to dynamics, it is useful to address a number of questions concerning the present status of many-body theory for stationary states. Just how reliably can one calculate observables with a two-body potential possessing the properties of the Reid potential: strong long-range attraction, an extremely repulsive short-range core, pronounced spin-isospin and angular momentum depen-

dence, and a strong tensor force? How much of the full theory may be embedded in a suitable definition of the mean field? What are the systematic shortcomings of a theory based on a static nucleon-nucleon potential, and to what extent can they be resolved by introducing a phenomenological effective interaction with few parameters? Finally, to what extent does the resulting mean-field theory correctly describe the observable properties of finite nuclei, and what is its predictive power?

A. Many-body theory

To address these and other related questions, it is appropriate to review several relevant topics of quantum many-body theory.

1. Expectation values of few-body operators

At the outset, it is essential to accept the fact that, whereas many-body theory may under certain circumstances yield excellent approximations to expectation values of few-body operators, it is inevitably inadequate to describe the full N-body wave function. Consider the familiar example of a fully interacting N-particle ground state in which each particle has a small probability ε of being excited out of its normally occupied single-particle state. Whereas a determinant of the occupied single-particle states will reproduce expectation values of few-body operators to order $\varepsilon^{1/2}$, the probability of all N particles' simultaneously being in the occupied states is $(1-\varepsilon)^N \sim e^{-\varepsilon N}$, rendering the overlap between the determinant and the exact wave function exponentially small. An alternative physical argument may be made in coordinate space. Whereas the mean value of a finite-range two-body operator is obviously sensitive to two-body correlations, it is unaffected by multiparticle correlations specifying what additional particles are simultaneously doing far away elsewhere in the system. The error in describing the behavior of other particles far away from a correctly correlated pair simply contributes an arbitrary normalization factor which cancels out of the numerator and denominator of $\langle \mathcal{O} \rangle = \langle \psi | \mathcal{O} | \psi \rangle / \langle \psi | \psi \rangle$. In contrast, full knowledge of N-particle correlations and hence at least N orders of perturbation theory are required to describe adequately the full wave function. For large systems we must therefore give up all pretense of calculating wave functions and deal exclusively with mean values of few-body operators.

The distinction between mean values and overlaps of N-body wave functions is particularly crucial in addressing time-dependent problems. Sloppiness in making the corresponding distinction for stationary states is seldom disastrous, because virtually all experimental measurements deal with expectation values of one- or two-body operators. Thus binding energies, removal energies, and charge density distributions do not really probe the full wave function, but rather just the expectation value of the Hamiltonian and one-body density operator. Similarly, despite loose talk concerning testing wave functions, in practice only transition densities induced by one-body operators can be compared with experiment. Time-dependent applications, however, are far more demanding, since experimentalists insist on confronting theorists with S-matrix elements, which are overlaps of N-body wave functions evolved through some interaction time with other appropriate N-particle wave functions describing final asymptotic states. Only in very special cases is an S-matrix element specified by calculating a few-body operator. One such example is elastic scattering of a nucleon from a nucleus, in which case calculation of the self-energy of the one-particle Green's function yields the exact optical potential and thus the elastic scattering cross section. In all other cases, rather than address individual S-matrix elements, it appears far more prudent to restrict our attention to mean values of appropriate operators. In heavy-ion collisions, such operators might include the fragment mean proton number, neutron number, and cm momentum or higher moments like the dispersion in these quantities.

2. Hole-line expansion

Suitable resummations of perturbation theory provide the most powerful technique presently available for systematically approximating expectation values of few-body operators in either finite or infinite systems. Since a detailed treatment of the expansion may be found in recent reviews of nuclear matter theory (Day, 1978; Bethe, 1971), only the essential physical ideas will be summarized here.

One begins with the Goldstone expansion (Goldstone, 1957), in which observables are calculated in terms of a sum of linked time-ordered graphs. In contrast to Feynman diagrams, which sum over all relative time orders, time-ordered Goldstone diagrams retain a fundamental distinction between hole lines, representing propagators for normally occupied single-particle states, and particle lines, representing propagators for normally unoccupied states.

Because of the strong repulsion between nucleons at short distances, the perturbation series is first rewritten in terms of the reaction matrix G, which sums all possible rescattering of two interacting nucleons into unoccupied intermediate states. This ladder sum, represented graphically in Fig. 1, yields the integral equation

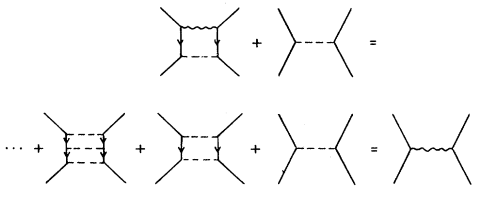

FIG. 1. Sum of two-body ladder diagrams defining the reaction matrix G. Dashed lines represent the two-body potential, solid lines with upward arrows represent particle propagators, and the wavy line denotes G.

$$G = v - v\frac{Q}{e}G \ , \tag{2.1}$$

where Q projects onto unoccupied states and e denotes the energy denominator pertinent to the specific Goldstone graph under consideration.

Physically, defining the correlated wave function ψ in terms of the uncorrelated wave function ϕ,

$$G\phi \equiv v\psi \ , \tag{2.2}$$

the ladder sum builds into ψ the short-range correlations induced by the repulsive core. In free space, G reduces to the familiar T matrix, and ψ simply corresponds to the exact scattering wave function defined by the potential v. The difference between v and G is far from a minor quantitative effect: matrix elements of v and G display enormous qualitative differences. The diagonal matrix elements $\langle \nu_1\nu_2 \mid v \mid \nu_1\nu_2 - \nu_2\nu_1 \rangle$ which occur in the Hartree-Fock approximation to the energy, where the ν's denote occupied states, are strongly repulsive for realistic repulsive core potentials and would never lend to binding. In contrast, the corresponding matrix elements in the resummed theory, $\langle \nu_1\nu_2 \mid G \mid \nu_1\nu_2 - \nu_2\nu_1 \rangle$, are attractive and yield roughly the required nuclear binding.

Having rewritten the Goldstone expansion in terms of G matrices, the next resummation is effected by summing all ladders in which three particles rescatter from each other via G matrices any number of times into unoccupied states. This ladder sum is represented graphically in Fig. 2 and yields the three-body Fadeev equations

$$T^{(3)} = G_{12} - G_{12}\frac{Q}{e}(T^{(1)} + T^{(2)}) \ , \tag{2.3}$$

where the full three-body amplitude is defined

$$T = T^{(1)} + T^{(2)} + T^{(3)} \ ,$$

and the superscript denotes the particle which is a spectator during the last potential interaction. Just as all Goldstone diagrams containing at most two independent hole lines could be summed in terms of the two-body reaction matrix, so also all three-hole-line contributions are summed via the three-body Faddeev equations. Higher-order approximations are obviously formulated by solving n-body Faddeev equations which sum all n-hole-line diagrams.

A common argument for the grouping of diagrams according to the number of hole-lines is based on the effect of adding an additional G matrix to an arbitrary Goldstone diagram in nuclear matter (Day, 1967). If it is added such that the total number of independent particle lines is increased by one, a simple estimate shows that the ratio of the new diagram to the original one is of the order of unity. If, however, it is added so that an additional independent hole line is generated, then a rough estimate suggests that the ratio of the new diagram to the original diagram is of the order of magnitude of κ, the excitation probability of a pair out of the normally interacting Fermi sea:

$$\kappa = \frac{1}{A}\sum_{\substack{\rho_1\rho_2 \\ \nu_1\nu_2}} |\langle \phi_{\rho_1\rho_2} \mid \psi_{\nu_1\nu_2} \rangle_{AS}|^2$$

$$= \frac{1}{A}\sum_{\nu_1\nu_2} \langle \phi_{\nu_1\nu_2} - \psi_{\nu_1\nu_2} \mid \phi_{\nu_1\nu_2} - \psi_{\nu_1\nu_2} \rangle_{AS} \ . \tag{2.4}$$

In Eq. (2.4), the ν's denote occupied hole states, ρ's indicate unoccupied particle states, and ψ denotes the correlated two-body wave functions, Eq. (2.2). This "wound integral" or pair excitation probability κ is of the order of 15% for the Reid potential at nuclear matter density and allows one to estimate the uncertainty of an n-hole line approximation to the potential energy as

$$\Delta U(n) \sim U(2)\kappa^{n-1} \ , \tag{2.5}$$

where $U(2)$ denotes the two-hole-line approximation.

An alternative physical argument to motivate the hole-line expansion is to recognize that the effect of solving the three-body Faddeev equation is to correct the error from approximating three-body correlations by the iterated products of two-body correlation functions. Since products of two-body correlation functions already exclude three particles from each other's cores, the bulk of the physics has already been accomplished by the G matrix, and the fractional change arising from improving the three-body correlations should be correspondingly smaller. Similarly, it is reasonable to expect that errors induced by differences between exact n-body correlations and products of lower-body correlations will continue to decrease with n and that the parameter characterizing the magnitude of the correction relative to that in the previous order should be something like the dimensionless wound integral κ.

An alternative formalism intimately related to the hole-line expansion is the coupled-cluster expansion (Kümmel, Lührmann, and Zabolitzky, 1978) discussed in Sec. IV. For the present discussion, it is sufficient to note that the nth order approximation includes all n-hole-line diagrams. The fact that certain classes of diagrams including higher numbers of hole lines are also included, such as G matrices with "backward-going" hole-line segments and subsets of RPA ring diagrams, is of technical interest, but does not seriously affect the present considerations.

The crucial question for the intellectual credibility of

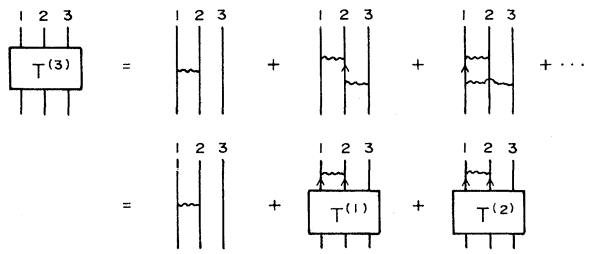

FIG. 2. Sum of three-body ladder diagrams defining the Faddeev amplitude $T = T^{(1)} + T^{(2)} + T^{(3)}$. The wavy lines denote G matrices as defined in Fig. 1.

the theory is the convergence of the hole-line expansion. Aside from apparent numerical convergence, which is a necessary but not sufficient condition, the only other evidence presently available comes from model systems for which independent calculations exist utilizing alternative techniques. For this reason, we now turn to nuclear matter.

3. Nuclear matter

Nuclear matter is a fictitious infinite uniform system comprised of equal densities of neutrons and protons interacting with nuclear forces in the absence of Coulomb interactions. The binding energy per particle of 16 ± 0.5 MeV may be reliably extrapolated from the systematics of nuclear binding energies throughout the Periodic Table. The inferred equilibrium density $\rho_0=0.16\pm0.015$ fm^{-3} corresponding to a Fermi momentum $k_F=1.34$ depends slightly upon our current theoretical understanding of finite nuclei to extrapolate from the interior proton densities measured experimentally in finite nuclei. The theoretical advantage of dealing with nuclear matter arises from two simplifications arising from translation invariance: the single-particle wave functions are plane waves instead of self-consistent Hartree-Fock wave functions, and momentum conservation eliminates whole topologies of diagrams and yields equations which are diagonal in momentum space.

The results of the most extensive nuclear matter calculations to date (Day, 1981a, 1981b) are shown in Fig. 3. The binding energy per particle in the n-hole-line approximation $E(n)$ is denoted by solid lines, and the uncertainty expected from Eq. (2.5) is indicated by error bars for $E(2)$ and $E(3)$. Uncertainties in estimating four-hole-line graphs are denoted by the error bars for $E(4)$, and the extrapolated saturation point is indicated by the shaded region. Salient points relevant to convergence are the facts that changes from one order to the next are rapidly decreasing and that Eq. (2.4) yields an adequate order-of-magnitude error estimate. One should note that the binding energy is a particularly sensitive quantity because of the large cancellation between kinetic and potential energies—the expansion is actually for the potential energy, and the final uncertainty of several MeV out of a total of 40 MeV is quite satisfactory. We will return to the question of the discrepancy with the extrapolated equilibrium density in Sec. II.B.

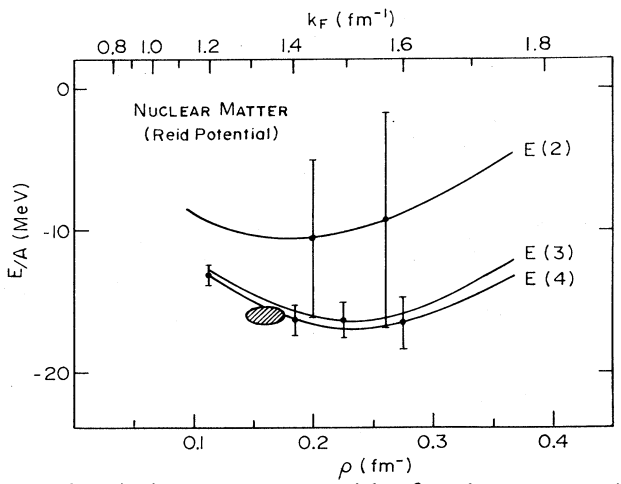

FIG. 3. Binding energy per particle of nuclear matter, with the full Reid potential in the n-hole line approximation, $E(n)$. Error bars for $E(2)$ and $E(3)$ represent the wound integral error estimate, Eq. (2.5), and for $E(4)$ represent conservative estimates of errors in the four-hole-line calculations. The shaded region denotes the saturation point extrapolated from empirical data.

In recent years, a number of comparisons have been made between hole-line results and variational calculations for various model problems. Since a number of reviews are available (Zabolitzky, 1980; Pandharipande and Wiringa, 1979; Negele 1977, 1979), only the results will be summarized here. For central potentials, a Jastrow trial function is used

$$\psi(r_1,r_2\ldots r_n)=\prod_{i,j} f(r_i\ldots r_j)\phi(r_1,r_2\ldots r_n)\,, \qquad (2.6)$$

where ϕ is a Fermi gas determinant or constant for fermions or bosons, respectively, and correspondingly more complicated trial functions are invoked for state-dependent potentials. Two techniques are available for evaluating the expectation value of the Hamiltonian with trial functions of the form (2.6). Whereas the hypernetted-chain expansion is a powerful tool, it invokes truncations with associated convergence ambiguities and thus provides less than compelling evidence concerning convergence of the hole-line expansion. Whatever the brute-force technique of evaluating the energy numerically with Monte Carlo integration may lack in elegance is more than compensated by providing rigorous bounds subject only to controllable statistical sampling errors.

The results of hole-line calculations and variational bounds are shown in Fig. 4 for a "homework potential" defined as a central potential equal to the $^3S_1$ component of the Reid potential (Day, 1981a, 1981b). Here, the two-, three-, and four-hole-line results appear to converge roughly as in the case of the full Reid potential, and the estimated range of error in the four-hole-line result is indicated by the error bars. The two Monte Carlo variational upper bounds, denoted by the points labeled MC, are close to, but safely above the hole-line result (Ceperley, Chester, and Kalos, 1977). Combined with experience for boson systems, in which comparison with exact solutions to the Bose matter problem obtained using the Green's-function Monte Carlo method (Kalos, Levesque, and Verlet, 1974) shows that Jastrow functions yield bounds for hard-core potentials quite close to the exact energy, Fig. 4 constitutes extremely favorable evidence for the validity of the hole-line expansion. With the rapid progress in treating state-dependent model problems and the possibility of utilizing Green's-function Monte Carlo techniques for fermions, even more definitive evidence should be forthcoming in the near future.

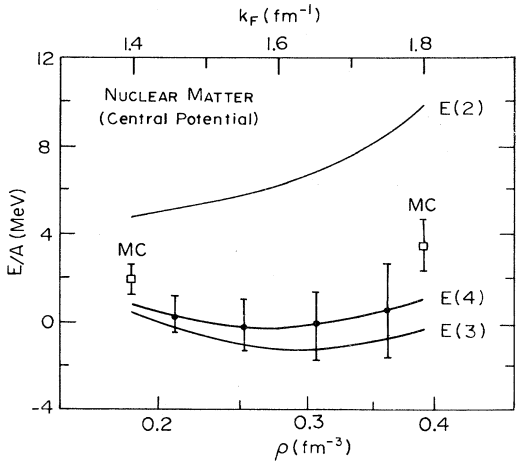

FIG. 4. Binding energy per particle of nuclear matter for the central "homework" potential in the n-hole-line approximation, $E(n)$. Error bars for $E(4)$ represent conservative estimates of errors in the four-hole-line calculation. The two squares labeled MC denote variational bounds using a Jastrow wave function, and the error bars indicate Monte Carlo sampling errors.

4. Finite nuclei and the mean-field approximation

Accepting the premise that the apparent numerical convergence of the hole-line expansion should be taken at face value, we now address finite nuclei.

The only other systems besides nuclear matter for which it is possible to calculate all three-hole-line contributions and estimate four-hole-line diagrams are light nuclei, in which the small number of occupied states contributing in the coupled-cluster formalism compensates the complexities arising from the loss of translation invariance in nuclear matter. Thus, aside from ^{4}He, ^{16}O, and ^{40}Ca, for which coupled-cluster calculations have been performed (Kümmel, Lührmann and Zabolitzky, 1978), and the extrapolation to the large-A limit implied by nuclear matter, the rest of the Periodic Table is inaccessible to such complete calculations. Fortunately, it turns out that most of the essential physics can be included in the mean-field approximation.

A convenient and natural way to define a mean field in the context of the hole-line expansion is to add to and subtract from the Hamiltonian a one-body potential U,

$$H = H_0 + H_1 \ , \tag{2.7a}$$

where

$$H_0 = T + U \tag{2.7b}$$

and

$$H_1 = v - U \ , \tag{2.7c}$$

to develop the perturbation theory in terms of $v-U$, to resum in terms of appropriate G matrices and Faddeev amplitudes, and to define U so as to identically cancel the dominant corrections arising in the expectation value of a one-body operator. The ground-state expectation value of a one-body operator is given by the sum of all Goldstone diagrams containing a single dot, corresponding to that operator, any number of crosses, corresponding to the potential U, and any number of wavy lines, corresponding to G-matrix ladder summations of the bare two-body interaction (Thouless, 1972). Typical low-order contributions containing minimal numbers of hole lines are enumerated in Fig. 5.

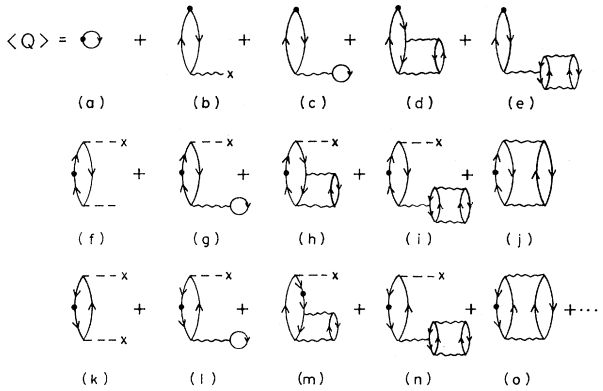

FIG. 5. Some low-order contributions to the ground-state expectation value of a one-body operator, denoted by a solid dot, in terms of the G matrix, denoted by a wavy line, and the potential $(-U)$, denoted by a cross.

The crucial matrix elements of the mean field U in a finite nucleus are those connecting particle and hole states, since particle-particle and hole-hole matrix elements do not alter the determinantal eigenfunctions of H_0 or therefore the leading contribution to $\langle \mathcal{O} \rangle$ [diagram (a) of Fig. 5]. Thus, we shall define the particle-hole matrix elements of U to effect a maximal cancellation of relevant many-body diagrams. Diagrams (c)—(e) enumerate various ways a one-particle, one-hole excitation can be created by the inclusion of additional hole lines. These amplitudes are evidentally precisely cancelled by $-U$ if the matrix elements of U are defined by the diagrams in Fig. 6. The analogous contributions in which diagrams (c)—(e) of Fig. 5 are drawn upside down are obviously also cancelled. Higher classes of diagrams are evidently also cancelled by this definition—for example, diagrams (f)—(i), (k)—(m), and more general contributions in which the upper cross in (f)—(i) and (k)—(m) is replaced by a general particle-hole amplitude.

Contributions to $\langle \mathcal{O} \rangle$ which cannot be cancelled by the definition of Fig. 6 or an appropriate generalization thereof are indicated by the correlation diagrams (j) and (o) of Fig. 5. It is clearly impossible for multiparticle, multihole excitations created prior to the action of $\mathcal{O}$ and annihilated subsequent to its action to be precisely can-

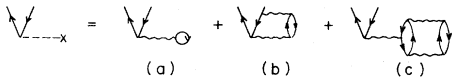

FIG. 6. Diagrammatic definition of the particle-hole matrix elements of the mean field. The mean field U is denoted by a cross, and G matrices are indicated by wavy lines.

celled by the action of any one-body potential U. However, the leading contributions of this type, diagrams (j) and (o) of Fig. 5, yield a total contribution very small compared with that of diagram (a). In the first place, (j) and (o) are each an order of κ smaller than (a). Furthermore, considering their contributions to the one-body density, the probability of depopulating all normally occupied states equals the probability of populating all normally unoccupied states, so the volume integral of diagram (b) is equal and opposite to that of diagram (j). Finally, since the short-range nuclear potential induces high-energy virtual excitations which must be correspondingly short-lived and limited in spatial extent, the correlation range is small compared to the nuclear size and the resulting spatial distributions for diagrams (j) and (o) are necessarily very similar in shape although opposite in sign (Strayer, Bassichis, and Kerman, 1973; Negele 1970a). The net effect of all these considerations is that when diagrams (b)—(i) and (k)—(m) have been eliminated by the appropriate definition of the mean field, diagram (a) yields an excellent first approximation to $\langle \mathcal{O} \rangle$ and correlation diagrams of the forms (j) and (o) constitute small corrections.

The first term in the expansion of the G matrix in Fig. 6(a) yields the Hartree-Fock definition of the potential. Retention of the rest of the series defining the G matrix is essential, as discussed previously, to incorporate the two-body correlations induced by the hard core. Diagrams (b) and (c) are one factor of κ smaller than diagram (a), and thus build in important features from the next order in the hole-line expansion. As is argued in the context of the coupled-cluster expansion (Kümmel, Lührmann, and Zabolitzky 1978), diagram (b) is the leading term in the three-hole line contribution to the particle-hole potential. Diagram (c) is approximately $-\kappa$ times the contribution of diagram (a) and is best interpreted as an occupation probability correction to it. That is, diagram (a) represents the average field arising from interaction with normally occupied states, but roughly 15% of the time, the value of κ in nuclear matter, these states are not occupied, so this fraction of their contribution should be omitted. Ideally, one should also account for the interaction with normally unoccupied states for this 15% of the time, thereby treating particles and holes more symmetrically as argued by Jeukenne, Lejeune, and Mahaux (1976). Physically, we justify the present asymmetric treatment by the fact that matrix elements of the nuclear potential with high-momentum states are on the average much weaker than those with low-momentum hole states, and appeal to the apparent convergence of hole-line and coupled-cluster calculations as evidence that this technically convenient choice is in fact satisfactory.

Retention of the full nonlocality and energy-dependence implied by the diagrammatic definition of the mean field U renders an exact calculation in heavy nuclei even at the mean-field level intractable. A crucial additional simplification, therefore, is to find an accurate approximation to deal with this nonlocality and energy dependence. A useful preliminary step is to note that the diagrammatic definition of U in Fig. 6 is precisely obtained by formal variation of the following approximate expression for the energy (Davies *et al.*, 1974):

$$E=\sum_{\nu}\langle\nu|T|\nu\rangle+\tfrac{1}{2}\sum_{\nu\nu'}\langle\nu\nu'|G(\varepsilon_\nu+\varepsilon_{\nu'})|\nu\nu'-\nu'\nu\rangle, \tag{2.8a}$$

where

$$G(W)=v-vQ\frac{1}{QTQ-W}QG(W), \tag{2.8b}$$

$$\varepsilon_\nu=\langle\nu|T|\nu\rangle+\sum_{\nu'}\langle\nu\nu'|G(\varepsilon_\nu+\varepsilon_{\nu'})|\nu\nu'-\nu'\nu\rangle, \tag{2.8c}$$

the Pauli operator Q is defined

$$Q=\sum_{\rho\rho'}|\rho\rho'\rangle\langle\rho\rho'|, \tag{2.8d}$$

and, as before, ν's and ρ's denote occupied and unoccupied states, respectively. Considering the general infinitesimal variation,

$$|\rho'\rangle=|\rho\rangle-\lambda_{\rho\nu}|\nu\rangle,$$

$$|\nu'\rangle=|\nu\rangle+\lambda_{\rho\nu}|\rho\rangle, \tag{2.9}$$

formal variation of Eq. (2.8a) yields four terms multiplying $\lambda^*_{\rho\nu}$: the trivial kinetic terms from varying the ket in the kinetic energy; diagram (6a) from varying ν or ν' in the ket of the G matrix; diagram (6b) from varying the matrix element of G with respect to the projector Q, which depends on $\lambda_{\rho\nu}$ through Eq. (2.8d); and diagram (6c) from varying the matrix element of G with respect to the energies $(\varepsilon_\nu+\varepsilon_{\nu'})$, which in turn depend on $\lambda_{\rho\nu}$ through Eq. (2.8c). It should be emphasized that we are in no way appealing to the Ritz variational principle, since Eq. (2.8a) is not the expectation value of the Hamiltonian with respect to any trial function, but rather are simply noting an expression capable of yielding the desired mean field upon variation. The key elements in generating diagrams (6b) and (6c) are evidently the Pauli operator Q, and self-consistent single-particle energies ε_ν, respectively. One should, in principle, therefore, retain a G matrix which depends not only on the relative coordinates and all spin-isospin variables, but also upon energy and the global Pauli operator.

Fortunately, the dependence on both energy and the Pauli operator may be adequately approximated by dependence on the local density. Defining the one-body density matrix

$$\rho(x,y)=\sum_{\nu}\langle x|\nu\rangle\langle\nu|y\rangle$$

$$=\sum_{\nu}\psi^*_\nu(y)\psi_\nu(x), \tag{2.10}$$

we observe that the (nonantisymmetrized) Pauli operator may be expressed directly in terms of this density matrix:

$$\langle x_1x_2 \mid Q \mid y_1y_2\rangle = \langle x_1x_2 \mid (1-\sum_{\nu} \mid \nu\rangle\langle\nu \mid)(1-\sum_{\nu'} \mid \nu'\rangle\langle\nu' \mid) \mid y_1y_2\rangle$$
$$= [\delta(x_1-y_1)-\rho(x_1,y_1)][\delta(x_2-y_2)-\rho(x_2,y_2)] \ . \tag{2.11}$$

Physically, one expects the off-diagonal density matrix $\rho(R+r/2,R-r/2)$ to tend to zero when the relative coordinate $|r|$ is of the order of π/k_F, where k_F is the local Fermi momentum. Thus, one obtains an excellent approximation to the angle-averaged density matrix by truncating the exact expansion (Negele and Vautherin, 1972)

$$\rho\left[R+\frac{r}{2},R-\frac{r}{2}\right] = \frac{3j_1(k_Fr)}{k_Fr}\rho(R)+\frac{35j_3(k_Fr)}{2k_F^3r}[\tfrac{1}{4}\nabla^2\rho(R)-\tau(R)+\tfrac{3}{5}k_F^2\rho(R)]$$
$$+\sum_{n=2}^{\infty}\frac{1}{k_Fr}(4n+3)j_{2n+1}(k_Fr)\sum_{l=0}^{n}\frac{(4n+2-2l)!}{l!(2n+1-l)!(2n+1-2l)!}$$
$$\times\left[\frac{\nabla_1-\nabla_2}{2k_F}\right]^{2(n-1)}\rho(R_1,R_2)\Big|_{R_1=R_2=R} \ , \tag{2.12a}$$

where

$$\tau(R)=\sum_{\nu} \mid \nabla\psi_\nu(R)\mid^2 \tag{2.12b}$$

and k_F is the Fermi momentum corresponding to the density $\rho(R)$. The first term is just the nuclear matter density matrix at the corresponding density and gives rise to the local density approximation which adequately accounts for the gross behavior of the density matrix, and thus the Pauli operator, within the range of the two-body potential. The small errors in the surface, where the local density approximation slightly overestimates the off-diagonal range of $\rho(R+r/2,R-r/2)$, are well treated perturbatively by use of the second term in Eq. (2.12a). In the same spirit, one may approximate the energy dependence of the G matrix appearing in Eq. (2.8a) by the average single-particle energy of nucleons in nuclear matter and perturbatively correct for the difference (Negele and Vautherin, 1972, 1975). The net result is that in lowest approximation, both the effect of the global Pauli operator and the dependence on single-particle energies have been replaced by dependence on the local density, $\rho[(r_1+r_2)/2]$,

$$G(r_1-r_2,Q,\varepsilon)$$
$$\approx G\{r_1-r_2,Q[\rho((r_1+r_2)/2)],\bar{\varepsilon}[\rho((r_1+r_2)/2)]\} \ . \tag{2.13}$$

Variation of the energy expression (2.8a) evaluated using the local density approximation immediately yields tractable approximations to each of the three terms in Fig. 6. Variation of the kets in the G matrix yields diagram (a), $\partial G/\partial Q\,\partial Q/\partial\psi_\nu^*$ yields diagram (b), and $\partial G/\partial\bar{\varepsilon}\,\partial\bar{\varepsilon}/\partial\psi_\nu^*$ yields diagram (c).

The importance of each of these contributions to the mean field is emphaized in Fig. 7, where the charge density for ^{40}Ca is calculated three different ways. Including only the lowest-order G matrix yields a density which is roughly 50% too high in the interior, a deficiency of the Brueckner-Hartree-Fock approximation which has been recognized for many years (Davies, McCarthy, and Sauer 1972). The combined effect of adding diagrams (b) and (c) resolves roughly two-thirds of the discrepancy with experiment. [The curve corresponding to the combined effect of diagrams (a) and (c) comes from a calculation with several technical differences relative to the other curves utilizing the local density approximation, but should still be representative of the qualitative effect of the diagram.] Thus, we conclude that contributions corresponding to diagrams (b) and (c) of Fig. 6 play an important role and must necessarily be included in a mean-field theory.

Similar conclusions follow in the context of the more complete and systematic coupled-cluster formalism. Unfortunately, due to complicated cancellations, it is difficult to unambiguously assess the role of individual Goldstone diagrams in the n-body coupled-cluster approximation. In the review by Kummel, Lührmann, and Zabolitzky (1978) it is demonstrated in (their) Sec. 4.3 that diagram 6(b) is a leading contribution from the three-body

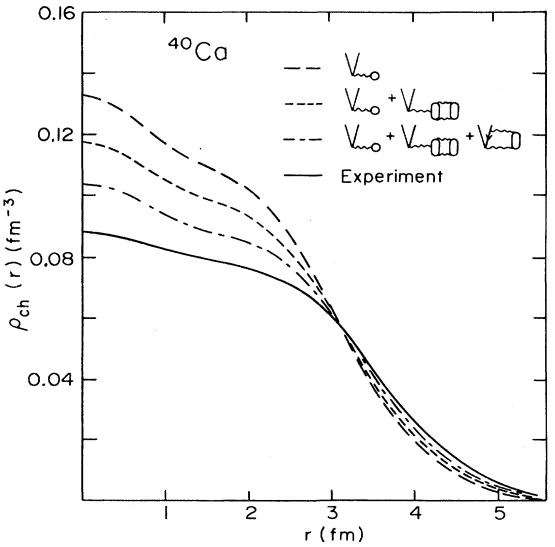

FIG. 7. Charge density of ^{40}Ca calculated using three different combinations of contributions to the mean field. The experimental charge density is shown for comparison.

amplitude and increases the rms radius as in the mean-field theory. In that work, arguments were also presented in connection with Figs. 4—6 suggesting that diagrams 6(c) also significantly increased the radius. Subsequent calculations (Zabolitzky, 1981) have shown that in ^{4}He this effect is cancelled by other higher-order terms, and since the analogous calculations have not been performed in heavier nuclei, the role of this term is presently unclear. At the suggestion of Zabolitzky, coupled-cluster results displayed subsequently in Fig. 8 are for the case in which terms corresponding to diagram 6(c) have been omitted. The final coupled-cluster results for ^{40}Ca with the Reid potential show reasonable evidence for numerical convergence at an interior density which is somewhat higher than experiment and a binding energy several MeV per particle less than experiment, in qualitative agreement with the simple local density approximation results presented here.

Through the use of a mean-field theory utilizing a density-dependent reaction matrix, then, one is able to retain most of the essential features of the hole-line expansion in a theory applicable throughout the Periodic Table.

B. Deficiency of two-body potential theory

Since, primarily for historical reasons, most relevant calculations of finite nuclei and nuclear matter have been performed with the Reid potential, our considerations thus far have been restricted to a single phenomenological potential. To distinguish between the limitations arising from the assumption of a two-body potential and those due to this specific interaction therefore requires a critical look at systematics.

1. Systematics

The essential features of saturation with the Reid potential are as follows. The three-body system may be solved essentially exactly, so the underbinding of 1.5 MeV in ^{3}He (Payne *et al.*, 1980) is a clear deficiency of the Reid potential. The rms radius is 9% high and the second maximum of the form factor at high momentum transfer, even when corrected for meson exchange currents, is significantly lower than experiment. Turning to heavier systems, calculated consistently through the three-hole-line approximation, one observes a smooth systematic behavior in binding and saturation. Light nuclei are somewhat underbound but have roughly the proper spatial extent. The proper rms radius is largely fortuitous, since in light nuclei $\langle r^2\rangle^{1/2}$ is strongly influenced by the exponential decay of the single-particle wave functions, which is, in turn, much too slow due to underbinding. Heavier nuclei attain proportionally more binding energy, but shrink to unphysically high central densities with correspondingly smaller radii. In the limit of nuclear matter, the binding energy per particle is approximately correct, but the density is definitely too high.

Can these systematic deficiencies be remedied by changing the off-shell behavior of the two-body potential while maintaining the on-shell behavior dictated by phase shifts and deuteron properties? Present evidence, summarized in Figs. 8 and 9, indicates that they cannot. The

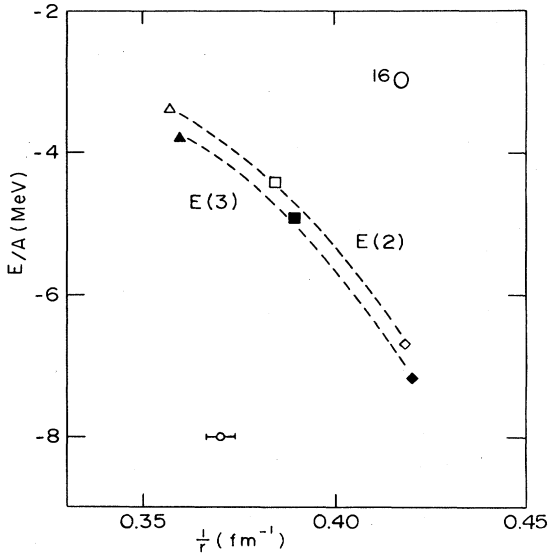

FIG. 8. Binding energy per particle of ^{16}O vs $1/r$ for the Hamada-Johnston potential (triangles), Reid soft core potential (squares), and super-soft core potential (diamonds), calculated in the coupled-cluster approximation. Results including two-body and three-body subsystem amplitudes are denoted by open and solid symbols, respectively, and the dashed lines are to guide the eye. The experimental saturation point is indicated by the error bar.

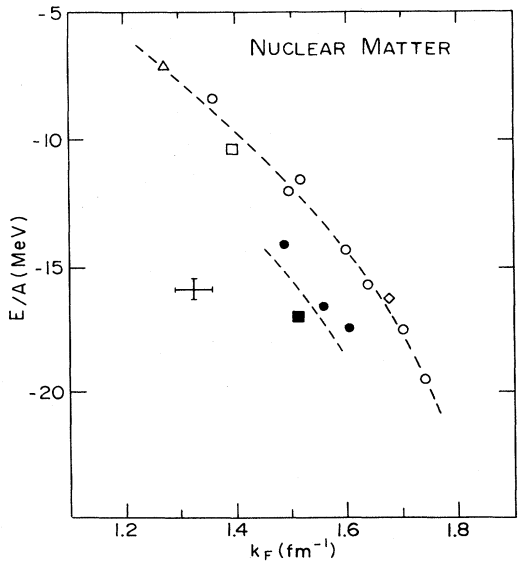

FIG. 9. Binding energy per particle vs k_F for nuclear matter. The polyhedrons denote the same potentials as in Fig. 8, and results for a number of other potentials are indicated by circles. As in Fig. 8, open and solid symbols represent two- and three-hole-line approximations, respectively, the dashed lines are drawn to guide the eye, and the extrapolated saturation point is indicated by the error bar.

scale specifying saturation in finite nuclei, analogous to the Fermi momentum k_F in nuclear matter, is $1/r$, where r denotes the rms radius. Hence, to compare systematic behavior in finite nuclei with that in nuclear matter, Fig. 8 shows results by Kümmel, Lührmann, and Zabolitzky (1978) for E/A versus $1/r$ in ^{16}O using two other potentials which are consistent with scattering data. The Hamada-Johnston (HJ) (1962) potential has an infinitely repulsive core, and the supersoft core (SSC) potential of De Tourreil and Sprung (1973) has an extremely soft repulsive core. At the $E(2)$ level of the coupled-cluster expansion, which corresponds closely to the two-hole-line approximation in nuclear matter, one observes that these three results lie on a smooth curve lying well above and to the right of the experimental result. If one utilizes the off-shell freedom to increase binding, one necessarily at the same time increases the central density. Similar results are obtained for ^{40}Ca. The same behavior is also evident in a corresponding plot of E/A vs k_F for nuclear matter in Fig. 9, where the equilibrium binding energy per particle in the two-hole-line approximation is shown for a much larger variety of potentials (Day, 1981a, 1981b). This clustering of the results of virtually all known potentials in a narrow band, known as the Coester band, suggests there is essentially only one degree of freedom in the off-shell behavior which affects the saturation properties. As in ^{16}O, varying this off-shell behavior dictates correlated changes in energy and density, so that the density is necessarily increased with increasing binding energy.

The $E(3)$ level of the coupled-cluster expansion, which contains all three-hole-line contributions, and which is believed to have essentially converged, displays the same qualitative behavior in Fig. 7 as the $E(2)$ approximation. Since this curve does not pass through the experimental point, we conclude that simply varying the off-shell behavior of the two-body force will not simultaneously yield the correct interior density and binding energy. Similarly, in nuclear matter, the single $E(3)$ results indicate that three-body contributions will not shift the Coester band far enough to become consistent with the extrapolated empirical saturation point of nuclear matter. Hence, at present we are forced to conclude that suppressed degrees of freedom play a non-negligible role, and to include their effect phenomenologically through an effective interaction.

2. Effective interaction

Attempts to date to estimate the effects of many-body forces arising from multiple meson exchange and Δ propagation are schematic but suggestive. They appear to offer the prospect of increasing the ^{3}He binding energy by an MeV, introducing correlations which deplete the central density of ^{3}He, and yield a contribution in nuclear matter which shifts the saturation density to somewhat lower values. Hence, since our goal in constructing a mean-field theory is to accurately describe the mean field in a real nucleus, instead of that in a ficticious system bound by the Reid potential, we shall phenomenologically parametrize such many-body forces so as to reproduce the observed binding and saturation properties of nuclei.

We observe that Δ's may enter in two characteristic ways, both of which may be represented by a short-range density-dependent two-body force. If the nucleon-nucleon potential in free space is defined in terms of all irreducible meson-exchange diagrams including nucleon or Δ intermediate states, then components of the free potential will have nucleon-Δ intermediate states built into them. In nuclear matter, because of the Pauli principle, some of these intermediate states will be blocked, giving rise to density dependence of the potential itself, in addition to the obvious density dependence of the iterated G matrix. Because of the relatively high masses involved, this density dependence is of correspondingly short range. A genuine short-range three-body force, arising, for example, from a virtual isobar connected by mesons to two other nucleons, when evaluated in a nuclear ground state and summed over all occupied orbitals, is also qualitatively similar to a density-dependent two-body force. Thus both effects may be included phenomenologically by adding to the energy expression, Eq. (2.8a), a short-range density-dependent two-body force. Since the saturation of nuclear matter specifies only two conditions, the equilibrium energy and density, essentially only two parameters of the density-dependent force are specified. Because the mean field is dominated by the G matrix, with its spin, isospin, and density dependence dictated by a potential fit to phase shifts, the detailed spin, isospin, and density dependence of the short-range phenomenological force are not quantitatively important as long as the proper saturation conditions are satisfied. The ultimate test of any such phenomenology, of course, is its ability to reproduce systematic properties of nuclei throughout the Periodic Table, and this topic will be considered in Sec. II.C.

Numerous effective interactions have been developed during the last decade following the general philosophy of beginning with a realistic G matrix and adjusting it phenomenologically to obtain the proper saturation properties (Negele, 1970a; Sprung and Banerjee, 1971; Negele and Vautherin, 1972; Campi and Sprung 1972; Fai and Nemeth, 1973; Coon and Kohler, 1974; Gogny, 1975). Of these various forms, the simplest to use in coordinate space calculations is the density matrix expansion (DME) form (Negele and Vautherin, 1972). The energy expression Eq. (2.8) is written for a spin-saturated system in terms of integrals of the G matrix and the one-body density matrix, the density matrix is expanded using Eq. (2.12a), and integrals over relative coordinates are performed. The final result is of the form

$$H = \int d^3R\, H(R)\,, \tag{2.14a}$$

where the Hamiltonian density is a functional of the proton and neutron densities, $\rho_n(R)$ and $\rho_p(R)$, and the kinetic energy densities, $\tau_n(R)$ and $\tau_p(R)$, and thus a particularly simple functional of the single-particle wave functions ψ_ν,

$$H(R)=H[\rho_n,\rho_p,\tau_n,\tau_p]\equiv H[\psi_\nu^*,\psi_\nu]\ . \qquad (2.14b)$$

The DME form of Hamiltonian density is completely analogous to that arising from the purely phenomenological Skyrme force (Vautherin and Brink, 1972). Ignoring spin-orbit and Coulomb terms for the moment, the Skyrme force has five parameters specifying the strength and spin dependence of two- and three-body δ-function potentials, and a zero-range two-body potential with quadratic momentum dependence. Treating this effective interaction as if it were the bare potential, even though it is unrelated to scattering properties, and making the Hartree-Fock approximation yield a Hamiltonian density for spin-saturated systems depending on products of $\rho_q(R)$ and $\tau_q(R)$, where q denotes protons or neutrons. Since values of the parameters obtained phenomenologically by fitting observed nuclear properties are very close to those obtained by linearizing the DME Hamiltonian density about nuclear matter density, one may regard Skyrme forces (at least those having values of effective mass near 0.7) as economical parametrizations of realistic effective interactions. Thus the long sequence of arguments concerning calculations of ladder sums, convergence of the hole-line expansion, and a variational definition of the mean field which includes the dominant diagrams and introduction of a phenomenological three-body or density-dependent two-body force ultimately reduce to an incredibly simple recipe: treat the Skyrme force in the Hartree-Fock approximation or, equivalently, treat the DME Hamiltonian density variationally.

The explicit form of the effective Hamiltonain density commonly used in time-dependent mean-field calculations is given in Sec. VII.

C. Survey of results for finite nuclei

As a prelude to the study of nuclear dynamics, this brief survey of results for finite nuclei has three purposes: to show that two phenomenological parameters produce systematic agreement with experiment throughout the Periodic Table, to give examples of quantitative predictive power, and to set a precedent for the level of quantitative precision one will ultimately hope to achieve in dynamic problems. For consistency and ease of comparison, most results will be quoted for the DME theory.

The general systematics of binding energies and removal energies are well reproduced by most of the effective interactions cited in the last section. The accuracy in binding energy per particle of 0.3 MeV achieved by the DME out of a total potential energy per particle of roughly 40 MeV appears quite reasonable, given the various approximations involved. Introduction of additional parameters in other interactions can reduce this deviation still further.

Similarly, the systematics of rms charge radii are well reproduced and typical DME results are compared with experiment in Table I. For spherical nuclei throughout the Periodic Table, the maximum discrepancy between the DME and the experiment is 0.05 fm, with agreement for good closed-shell nuclei like ^{40}Ca and ^{208}Pb being considerably better. Thus, the fractional error in both the potential energy per particle, as reflected in the binding energy, and the spatial extent, as manifested in the rms radius, are at the level of 1%.

Our most detailed knowledge of the spatial distribution of matter in nuclei arises from precise high-momentum transfer elastic scattering measurements during the last decade. As an example of the predictive power of the DME, the elastic scattering cross sections for ^{208}Pb predicted by the DME (Negele and Vautherin, 1972) are compared in Fig. 10 with the subsequent impressive experimental measurements at Saclay (Frois *et al.*, 1977) spanning 11 orders of magnitude.

A more useful qualitative understanding of the physical content of such high-momentum transfer experiments is provided by inverting the electron data, as well as muonic x-ray transition energies, to obtain an envelope of density distributions which are statistically consistent with the

TABLE I. Comparison of experimental rms radii, in fm, with DME mean-field theory. Experimental charge radii, $\langle r^2\rangle_{ch}^{1/2}$, are taken from the compilation of DeJager, DeVries, and DeVries (1974); and, except where errors are indicated, the experimental uncertainty is less than 0.01 fm. Experimental values for the difference between rms neutron and proton radii, $\langle r^2\rangle_n^{1/2}-\langle r^2\rangle_p^{1/2}$, deduced from high-energy proton scattering are taken from: (a) Chaumeaux, Layly, and Schaeffer (1977); (b) Varma and Zamick (1977); (c) Varma and Zamick (1978); and (d) Ray (1979); and the theoretical uncertainty in the analysis is of the order of ±0.06 fm.

	$\langle r^2\rangle_{ch}^{1/2}$ Theory	$\langle r^2\rangle_{ch}^{1/2}$ Experiment	$\langle r^2\rangle_n^{1/2}-\langle r^2\rangle_p^{1/2}$ Theory	$\langle r^2\rangle_n^{1/2}-\langle r^2\rangle_p^{1/2}$ Experiment
^{16}O	2.79	2.71±0.01	−0.03	0.00 a
^{40}Ca	3.50	3.48	−0.05	−0.03 a −0.04 c
^{48}Ca	3.50	3.47	0.18	0.16 a 0.19 c
^{58}Ni	3.80	3.78	0.00	0.01 d
^{90}Zr	4.29	4.28±0.02	0.07	0.13 b
^{116}Sn	4.63	4.62±0.01	0.12	0.15 d
^{208}Pb	5.49	5.50	0.20	0.21 c 0.16 d

measured cross sections and their experimental uncertainties. Details of the analysis are described in a review article (Friar and Negele, 1975) and error envelopes obtained in this way for a variety of spherical nuclei (Sick, 1974; Sick *et al.*, 1975; Friar and Negele, 1977, Sick *et al.*, 1979) are compared with DME calculations in Fig. 11. Whereas the overall agreement appears quite satisfactory, individual discrepancies between the mean-field theory and experiment are latent with interesting nuclear structure information. For example, whereas Ca and Pb constitute good shell closures, ^{90}Zr is known to have a significant depopulation of the $1p_{1/2}$ and $0f_{5/2}$ orbitals and corresponding occupation of the $0g_{9/2}$ level. A simple schematic calculation based on the pairing theory (Negele, 1971) shows that in ^{90}Zr the correlation correction decreases the interior density in the region of 2 fm by roughly 8%, significantly improving the agreement with experiment. (Analogous pairing calculations in ^{40}Ca and ^{208}Pb yield no change in the density.) The ^{58}Ni nucleus is another special case. When one calculates its energy as a function of deformation, one finds it to be exceedingly soft with respect to quadrupole deformations. Thus the simple static mean-field approximation is inadequate, and one must allow for large amplitude collective motion in the quadrupole degree of freedom. Although the general formalism for large-amplitude collective motion in Sec. V has not yet been applied to this nucleus, one observed that the shapes of the prolate and oblate admixtures in the wave function are sufficiently different that one expects the large-interior density fluctuation to be somewhat diminished (Negele and Rinker, 1977). In all these cases, then, one is led to the conclusion that the mean-field approximation not only describes the systematic behavior of spherical nuclei throughout the Periodic Table, but also serves as a valid starting point for systematic examination of specific structure effects which go beyond the mean field. Thus the phenomenological component of the effective interaction is small enough that it is sensible to evaluate leading corrections to the mean field as if the effective interaction were actually derived from an underlying two-body potential.

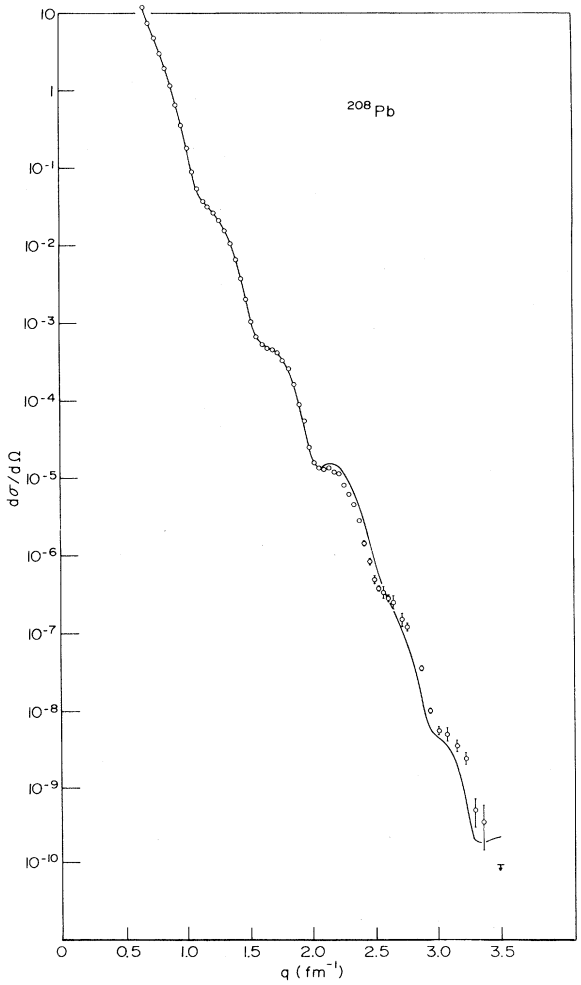

FIG. 10. Cross sections for elastic electron scattering from ^{208}Pb at 502 MeV compared with DME mean-field theory prediction (solid line).

The discussion of the spatial distribution of matter thus far has dealt essentially with protons, since we have only considered the charge scattering of electrons. From a theoretical point of view, given the strong interplay between neutron and proton distributions in the self-consistent mean-field theory, it is difficult to imagine how one could systematically obtain the correct proton distributions throughout the Periodic Table while making significant errors in neutron distributions. Nevertheless, although neutron distributions are much more difficult to measure experimentally and are subject to greater ambiguities of interpretations than protons, it is worthwhile to briefly survey the present status of measurements of neutron distributions.

The least ambiguous probe of neutron distributions is

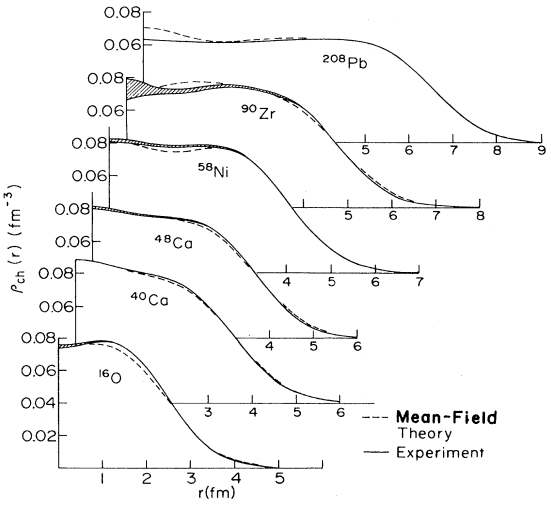

FIG. 11. Comparison of DME mean-field theory charge distributions in spherical nuclei (dashed lines) with empirical charge densities. The solid curves and shaded regions represent the error envelope of densities consistent with the measured cross sections and their experimental uncertainties.

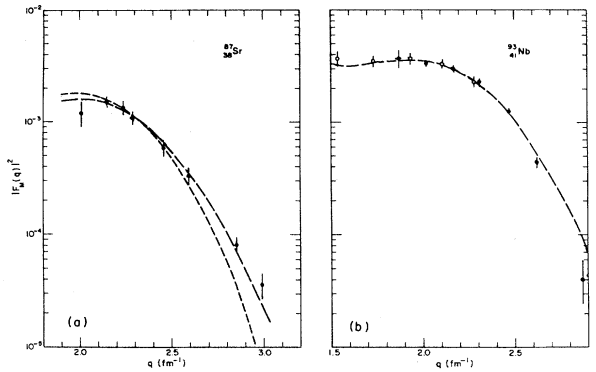

FIG. 12. Comparison of experimental measurements of the magnetic form factor for ^{87}Sr (a) and ^{97}Nb (b) with mean-field theory (long dashed lines). The effect of omitting the contribution of meson exchange currents is indicated by the short dashed curve for ^{87}Sr.

magnetic elastic scattering. Time reversal and parity restrict the transverse electromagnetic current to odd magnetic multipoles, and in nuclei like ^{87}Sr and ^{93}Nb, which have an odd $g_{9/2}$ neutron hole and an odd $g_{9/2}$ proton particle, respectively, the M9 form factor directly measures the spin density of the $g_{9/2}$ orbital. An important feature of the analysis is inclusion of the sizeable contributions of exchange currents (Suzuki, Hyuga, and Arima 1979; Dubach, 1980), and Fig. 12 shows mean-field results by Dechargé and Gogny (1980), including exchange current corrections by Dubach, compared with experimental Saclay results (deWitt Huberts *et al.*, 1971, Sick *et al.*, 1977). Recent calculations by Desplanques and Mathiot (1982) which deemphasize exchange currents and include core polarization contributions to the effective current operator, yield results which are essentially identical to the long dashed curves in Fig. 12. The case of ^{93}Nb is basically a check of the analysis: we already believe on other grounds that mean-field proton distributions are correct and Fig. 12 thus confirms that the exchange current calculations and nuclear structure assumptions are valid. Comparable agreement for ^{87}Sr then implies that the neutrons are indeed where the mean field says they should be.

Since good closed-shell nuclei with odd neutrons in $J=l+\frac{1}{2}$ orbitals are far from copious, evidence for systematics must be gleaned from more ambiguous high-energy proton scattering. Because nuclei are strongly absorptive, the least model-dependent feature of high-energy scattering is the positions of diffraction minima, which reflect the strong absorption radius. In all Glauber theory and optical potential analyses, the mass radii inferred from minima are highly insensitive to theoretical corrections. Furthermore, in mirror nuclei these analyses yield neutron-proton radius differences consistent with the small and reliably calculable Coulomb-induced radius shifts, so these analyses should be believable within uncertainties of the order of 0.06 fm. Table II also shows the results of such analyses for $\langle r_n^2\rangle^{1/2}-\langle r_p^2\rangle^{1/2}$ compared with mean-field predictions. Subject to obvious uncertainties, the tentative conclusion is that mean-field systematics for neutron distributions are essentially as good as for protons.

One of the most important successes of the static mean-field theory from the viewpoint of dynamics is its ability to accurately predict the shapes of deformed nuclei. Viewed as a classical Hamiltonian field theory, as will prove fruitful in the treatment of nuclear dynamics, the Hamiltonian density $H(\psi_\nu^*,\psi_\nu)$ exhibits spontaneous symmetry breaking. That is, some of the static solutions to the variational equations do not possess all the symmetries, such as rotational invariance, of the underlying interactions. Whereas all the exact many-body eigenstates must, of course, be eigenstates of angular momentum, in the case of rotational nuclei in the rare-earth and actinide regions, the mean-field theory yields an excellent approximation to the deformed intrinsic state from which all the states of the ground-state band are generated.

The important feature for our present consideration is the fact that the effective interaction with two phenomenological constants determined by nuclear saturation yields sufficiently accurate energy of deformation surfaces so as to correctly decide between spherical and deformed configurations and to dictate in detail the shapes of intrinsic states. Since the intrinsic state approximation is most accurate for nuclei with the deepest minima in their energy of deformation surfaces and the largest values of $\langle J^2\rangle$, ^{238}U is the best case for which experimental electron scattering data presently exists in which to quantitatively test the mean-field predictions. Figure 13 shows a contour plot of the predicted proton and neutron densities of the axially symmetric intrinsic state of ^{238}U

TABLE II. Parameters of the effective Hamiltonian density Eq. (7.2) for four interactions described in the text.

	Force	SK II	SK III	Local	Zero-range
t_0	(MeV fm^3)	−104.49	−334.47	−497.726	−1099.0
x_0		4.01	1.743	0	0
t_1	(MeV fm^5)	585.6	395.0	0	0
t_2	(MeV fm^5)	−27.1	−95.0	0	0
t_3	(MeV fm^6)	9331.0	14000.0	17270.0	17624.0
v_L	(MeV)	−444.85	−355.79	−363.044	0
v_U	(MeV)	−868.63	−619.60	−363.044	0
μ	(fm^{-1})	2.175	2.175	2.175	
m^*/m		0.58	0.76	1	1

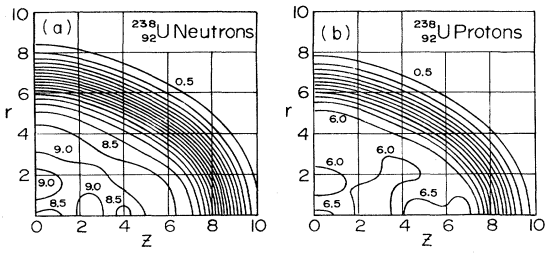

FIG. 13. Proton (a) and neutron (b) density contours of the deformed intrinsic state for ^{238}U calculated in the mean-field approximation. The density contours are in increments of 0.005 fm^{-3}, the labels denote the density multiplied by 100, and the distance z along the symmetry axis and the radial distance r are in fm.

(Negele and Rinker, 1977). In addition to the obvious quadrupole deformation, the intrinsic density also displays nontrivial deformation of higher multipolarity, as well as the usual fluctuations associated with shell structure. In the intrinsic state approximation, the form factor for the transition from the ground state to the J^+ state in the ground-state band determines the Jth multipole in a Legendre expansion of the intrinsic density. The comparison in Fig. 14 between the theoretical DME prediction for the inelastic ground-state band transitions (Negele and Rinker, 1977) and the subsequent experimental data (Creswell *et al.*, 1981) shows that the predictive power for the first four multipoles of the intrinsic state of ^{238}U is comparable to that for spherical nuclei. In lighter nuclei, for which the intrinsic state approximation is expected to be less accurate, some discrepancies do arise in $4^\dagger$ and $6^\dagger$ transitions, but the $0^\dagger$ and $2^\dagger$ form factors are of comparable accuracy to those shown here.

In summary, the mean-field approximation, founded in two levels of phenomenology, yields a very satisfactory understanding of the gross features of finite nuclei. Binding energies, rms proton and neutron radii, the radial distribution of charge in spherical nuclei, and detailed shapes of deformed nuclei are quantitatively reproduced, and, in many cases, even predicted prior to experimental measurement. To the extent that the bulk of the mean field may be understood microscopically in terms of two- and three-body correlations in the many-body medium induced by the strong short-range behavior of the nuclear potential, one may reasonably aspire to attain a comparable understanding of the mean field in dynamical situations. The remaining part of the mean field which presently can only be understood phenomenologically at least yields a systematic description of a wide range of nuclear properties and may plausibly be expected to be equally applicable to low-energy nuclear dynamics. Finally, given the success of purely phenomenological forces of the Skyrme type or of the form presented in Sec. VII when used in the static Hartree-Fock approximation, it is reasonable for one's first explorations of dynamics to simply utilize these forces in the time-dependent Hartree-Fock approximation.

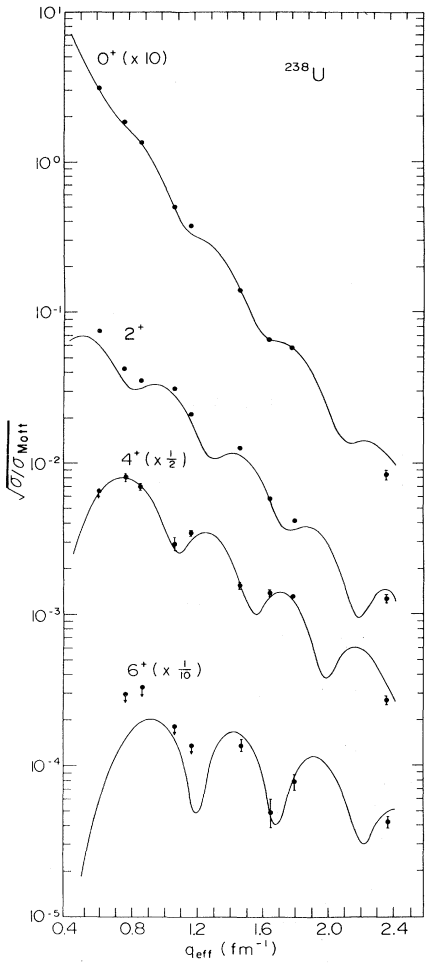

FIG. 14. Cross sections for elastic and inelastic scattering within the ground-state rotational band of ^{238}U compared with the DME mean-field theory predictions (solid line).

III. TIME-DEPENDENT HARTREE-FOCK INITIAL-VALUE PROBLEM

The objective of this section is to review the essential features of the time-dependent Hartree-Fock (TDHF) approximation with a minimum of technical complications. Thus, for the present considerations, the two-body potential shall be assumed to be sufficiently weak that short-range correlations are inessential and the Hartree-Fock term is an adequate approximation to the full mean field. The derivation of systematic hierarchies of successive approximations will be postponed, and here the TDHF approximation will be obtained by application of the time-dependent variational principle to a determinantal trial function. For initial exploratory applications to finite nuclei, one would imagine applying the same theory, including trivial generalizations for three-body or density-dependent forces, using the phenomenological Skyrme-like interaction discussed in the previous section. The ultimate justification, of course, must be founded in the subsequent systematic derivations in Secs. IV and V.

A. Variational derivation

The time-dependent variational principle (Kerman and Koonin, 1976) may be motivated by noting that the full many-body Schrödinger equation follows from varying the action

$$S=\int dt \int dr_1 \ldots dr_n \left[\psi^*(r_1 \ldots r_n,t) \left(i\frac{\partial}{\partial t} - H \right) \times \psi(r_1 \ldots r_n,t) \right] . \tag{3.1}$$

As usual, the result of varying the real and imaginary parts of ψ is reproduced by independent variations with respect to ψ^* and ψ, with the result that ψ must satisfy the Schrödinger equation,

$$i\frac{\partial}{\partial t}\psi(r_1 \ldots r_n,t)=H\psi(r_1 \ldots r_n,t) . \tag{3.2}$$

To obtain the TDHF equations, the many-body wave function is parametrized by a time-dependent Slater determinant,

$$\Psi_{\mathrm{SD}}(r_1 r_2 \ldots r_n,t) = \frac{1}{\sqrt{n!}} \mathrm{Det}[\psi_1(r_1,t),\psi_2(r_2,t) \ldots \psi_n(r_n,t)] , \tag{3.3}$$

where the single-particle wave functions $\psi(r)$ are orthonormal. With this wave function, the action is

$$S[\psi^*,\psi]=\int dt \left\langle \psi_{\mathrm{SD}}(t) \left| i\frac{\partial}{\partial t} - H \right| \psi_{\mathrm{SD}}(t) \right\rangle = \int dt \left[\sum_\nu \int dr\, \psi_\nu^*(r) i\frac{\partial}{\partial t}\psi_\nu(r) - \mathscr{H}(\psi^*,\psi) \right] , \tag{3.4}$$

where

$$\mathscr{H}(\psi^*,\psi)=\sum_\nu \int dr\, \psi_\nu^*(r)K(r)\psi_\nu(r)+\tfrac{1}{2}\sum_{\nu\mu}\int dr_1 dr_2 dr_3 dr_4 \psi_\nu^*(r_1)\psi_\mu^*(r_2)\tilde{V}(r_1,r_2;r_3,r_4)\psi_\mu(r_4)\psi_\nu(r_3) , \tag{3.5}$$

the antisymmetrized potential is defined

$$\tilde{V}(r_1,r_2;r_3,r_4)=\langle r_1 r_2 \mid V \mid r_3 r_4 - r_4 r_3 \rangle , \tag{3.6}$$

and the kinetic energy operator is denoted K. Variation with respect to ψ_ν^* yields the TDHF equation of motion (Dirac, 1930)

$$i\frac{\partial}{\partial t}\psi_\nu(r)=\frac{\partial \mathscr{H}}{\partial \psi_\nu^*(r)}=K(r)\psi_\nu(r)+\sum_\mu \int dr_2 dr_3 dr_4 \psi_\mu^*(r_2)\tilde{V}(r,r_2;r_3,r_4)\psi_\mu(r_4)\psi_\nu(r_3) \equiv (K+W)\psi_\nu , \tag{3.7a}$$

and similarly, variation with respect to ψ_ν yields

$$-i\frac{\partial}{\partial t}\psi_\nu^*(r)=\frac{\partial \mathscr{H}}{\partial \psi_\nu(r)} . \tag{3.7b}$$

The TDHF approximation thus acquires the form of a classical field theory with the Hamiltonian $\mathscr{H}(\psi^*,\psi)$ given in Eq. (3.5) obeying the Hamiltonian equation (3.7) and its complex conjugate. The degrees of freedom of the determinant (3.3) are actually less than specified by the functions $\psi_\mu(r)$, since any unitary transformations among the ψ_μ's yields the same determinant. The field theory is correspondingly gauge invariant with respect to these unitary transformations.

Physically, nuclear dynamics is described in this approximation by the simultaneous evolution of A single-particle wave functions in the nonlocal mean field W. It is an initial-value problem, since the first-order differential equation in time requires specification of the wave function at the initial time. This time-dependent theory exhibits many features which are already familiar in the static HF approximation. In both cases, the structure of linear quantum mechanics is replaced by a system of coupled nonlinear equations. Unavoidable semiclassical features arise in both cases: the localized center-of-mass wave function represents a wave packet of momentum eigenstates and a deformed HF wave function must be understood as a wave packet of angular momentum eigenstates. In neither case is there an obvious way to systematically improve the variational ansatz for the wave function. Hence there is no obvious means in this formulation to derive an appropriate effective interaction.

1. Conservation laws

Several conservation laws follow immediately from the TDHF equations of motion, Eq. (3.7).

The overlap matrix of the single-particle wave functions is a constant of the motion:

$$\frac{d}{dt}\int dr\, \psi_\nu^*(r)\psi_\mu(r)=i\int dr \left[\frac{\partial \mathscr{H}}{\partial \psi_\nu}\psi_\mu - \psi_\nu^* \frac{\partial \mathscr{H}}{\partial \psi_\mu} \right] = i\int dr\, dr' \psi_\nu^*(r)[(K+W)^\dagger - (K+W)]\psi_\mu(r')=0 . \tag{3.8}$$

This conservation law is the Noether theorem associated with the gauge invariance of $\mathscr{H}$ with respect to unitary

transformations among the single-particle wave functions. Given an initial condition in which the determinantal wave function is expressed in terms of orthonormal single-particle wave functions, these wave functions remain orthonormal in time. Clearly, the Pauli principle in this case is implemented through the simultaneous evolution of all A wave functions in the common Hermitian potential W. Two obvious consequences of Eq. (3.8) are conservation of the norm of the TDHF wave function and conservation of the expectation value of the number operator N.

The time dependence of the expectation value of any operator $\mathcal{O}$ having no intrinsic time dependence may be written (Koonin, 1979)

$$i\frac{d}{dt}\langle\psi_{\rm SD}\,|\,\mathcal{O}\,|\,\psi_{\rm SD}\rangle=\sum_\nu\int dr\left[\frac{\delta\langle\mathcal{O}\rangle}{\delta\psi_\nu(r)}i\frac{\partial\psi_\nu(r)}{\partial t}+\frac{\delta\langle\mathcal{O}\rangle}{\delta\psi_\nu^*(r)}i\frac{\partial\psi_\nu^*(r)}{\partial t}\right]$$
$$=\sum_\nu\int dr\left[\frac{\delta\langle\mathcal{O}\rangle}{\delta\psi_\nu(r)}\frac{\delta\mathcal{H}}{\delta\psi_\nu^*(r)}-\frac{\delta\langle\mathcal{O}\rangle}{\delta\psi_\nu^*(r)}\frac{\delta\mathcal{H}}{\delta\psi_\nu(r)}\right]. \tag{3.9}$$

If $\mathcal{O}$ is the Hamiltonian H, then $\langle\mathcal{O}\rangle=\langle H\rangle=\mathcal{H}$ so that the TDHF energy is conserved as expected. What is not so obvious is that the expectation value of any one-body operator which commutes with H is also conserved. In second-quantized notation with the convention that $\alpha,\beta\ldots\varepsilon$ run over all states and ν,μ denote occupied states, we may write

$$\left[\sum_{\alpha\beta}\mathcal{O}_{\alpha\beta}a_\alpha^\dagger a_\beta,\left[\sum_{\gamma\delta}K_{\gamma\delta}a_\gamma^\dagger a_\delta+\tfrac{1}{4}\sum_{\gamma\delta\varepsilon\eta}\tilde{V}_{\gamma\delta\varepsilon\eta}a_\gamma^\dagger a_\delta^\dagger a_\eta a_\varepsilon\right]\right]$$
$$=\sum_{\alpha\beta\gamma}(\mathcal{O}_{\alpha\gamma}K_{\gamma\beta}-K_{\alpha\gamma}\mathcal{O}_{\gamma\beta})a_\alpha^\dagger a_\beta+\tfrac{1}{2}\sum_{\alpha\beta\gamma\delta\varepsilon}(\mathcal{O}_{\alpha\varepsilon}\tilde{V}_{\varepsilon\beta\gamma\delta}-\tilde{V}_{\alpha\beta\gamma\delta}\mathcal{O}_{\varepsilon\delta})a_\alpha^\dagger a_\beta^\dagger a_\delta a_\gamma\,, \tag{3.10}$$

so that the determinantal expectation value is

$$\langle[\mathcal{O},K+v]\rangle=\sum_{\nu\gamma}(\mathcal{O}_{\nu\gamma}K_{\gamma\nu}-K_{\nu\gamma}\mathcal{O}_{\gamma\nu})$$
$$+\sum_{\nu u\varepsilon}(\mathcal{O}_{\nu\varepsilon}\tilde{V}_{\varepsilon u\nu u}-V_{\nu u\nu\varepsilon}\mathcal{O}_{\varepsilon u})\,. \tag{3.11}$$

Rewriting Eq. (3.11) in coordinate representation reproduces the right-hand side of Eq. (3.9), so that $\langle\mathcal{O}\rangle$ is conserved if it commutes with H. Conserved quantities of particular interest in physical applications are the expectation values of the total momentum $\mathbf{P}=\sum_j\mathbf{P}_j$; and the total angular momentum $\mathbf{J}=\sum_j(r_j\times P_j+s_j)$, where s_j denotes the spin operator. By the preceding argument, these are both conserved if the two-body potential is Galilean invariant.

2. Alternative representations

Because of the gauge freedom in writing the TDHF equations of motion in terms of single-particle wave functions, it is useful to reexpress the equations in a representation independent form using the one-body density matrix.

The one-body density matrix is defined in terms of field operators by the relation

$$\rho(x,x';t)\equiv\langle\Psi(t)\,|\,\psi^\dagger(x')\psi(x)\,|\,\Psi(t)\rangle\,. \tag{3.12}$$

The expectation value of a one-body operator may therefore be expressed

$$\langle\Psi(t)\,|\,\mathcal{O}\,|\,\Psi(t)\rangle=\int dr'dr\,\mathcal{O}(r'r)\rho(rr')\equiv\mathrm{tr}\,\mathcal{O}\rho\,. \tag{3.13}$$

For the case in which $\mathcal{O}$ is the number operator, it follows that the trace of ρ is A, the number of particles.

The one-body density matrix can be generated from a determinal wave function of the form Eq. (3.3) if and only if it satisfies the idempotency condition $\rho^2=\rho$; that is,

$$\int dr'\rho(r,r')\rho(r',r'')=\rho(r,r')\,. \tag{3.14}$$

By Eq. (3.12) ρ is Hermitian and by (3.14) it can only have eigenvalues 1 or 0. From the conditions on the trace, A of the eigenvalues must be 1 and in the diagonal representation, the density matrix may therefore be written in the form

$$\rho(x,x')=\sum_{\nu=1}^{A}\psi_\nu^*(x')\psi_\nu(x)\,, \tag{3.15}$$

where the ψ_ν's are orthonormal. This is precisely the form of ρ obtained by substituting the determinantal wave function (3.3) in the definition (3.12). Conversely, given a determinantal wave function, the resulting density matrix, Eq. (3.15), immediately satisfies $\rho^2=\rho$.

The TDHF equation may be expressed in terms of the density matrix as follows. The single particle equation, Eq. (3.7) may be written

$$i\frac{\partial}{\partial t}\psi_\nu(r)=\int dr'h(r,r')\psi_\nu(r')\,, \tag{3.16}$$

where

$$h(r,r')\equiv K(r,r')+W(r,r')\,, \tag{3.17}$$
$$W(r,r')=\int dr_2dr_4\langle rr_2\,|\,V\,|\,r'r_4-r_4r'\rangle\rho(r_4,r_2)\,, \tag{3.18a}$$

and

$$K(r,r')=-\delta(r-r')\frac{1}{2m}\nabla_r^2\,. \tag{3.18b}$$

In the familiar case of a local Galilean invariant potential

$$\langle r_1 r_2 \mid V \mid r_3 r_4 \rangle = \delta(r_1 - r_3)\delta(r_2 - r_4) v(r_1 - r_2) , \tag{3.19}$$

the single-particle Hamiltonian h becomes

$$h(r,r',t) = K(r,r') + \delta(r-r') \int dr_2 \rho(r_2,r_2,t) v(r-r_2) - \rho(r,r';t) v(r-r') . \tag{3.17a}$$

The first potential term is just the Hartree convolution of the diagonal density, $\rho(r) \equiv \rho(r,r)$, with the two-body potential, and the last term is the nonlocal exchange contribution. By Eq. (2.12a), the range of this nonlocality is of the order of π/k_F.

Using Eqs. (3.15) and (3.16) and the Hermiticity of h, one obtains the following equation of motion for the one-body density matrix:

$$i\frac{\partial}{\partial t}\rho(x,x') = \sum_\nu \phi_\nu^*(x') \int dx'' h(x,x'') \phi_\nu(x'') - \sum_\nu \int dx'' \phi_\nu^*(x'') h^*(x',x'') \phi_\nu(x)$$
$$= \int dx'' [h(x,x'')\rho(x'',x') - \rho(x,x'')h(x'',x')] . \tag{3.20}$$

Equations (3.20) and (3.17) may be written more compactly, using an obvious matrix notation, as follows:

$$i\dot{\rho} = [h,\rho] , \tag{3.20a}$$

$$h = K + \mathrm{tr} v\rho . \tag{3.17b}$$

This form of the TDHF equations is illuminating in the sense that one may think in terms of evolution of a one-body density matrix instead of a full many-body wave function. As already emphasized in the preceding section, it is much more reasonable to seek to approximate expectation values of one-body operators than to approximate the full many-body wave function. Although the variational derivation utilized a determinantal many-body wave function, if the TDHF approximation has physical validity, it rests far more in its predictions concerning the one-body density matrix than in its description of a full A-particle wave function. Note further that Eqs. (3.20a) and (3.17b) specify a general initial-value problem for any one-body density matrix, not just an idempotent one satisfying $\rho^2 = \rho$. All these considerations, then, suggest that one profitable approach to generalizing the TDHF approximation would be to generate systematic approximations to the equations of motion of few-body density matrices; this approach will be reviewed in the next section.

A second alternative representation of the TDHF equation is in terms of the Wigner transform of the one-body density matrix (Koonin, 1975, 1979). The Wigner phase-space distribution function is defined as the Fourier transform with respect to the relative coordinate of the one-body density matrix (Wigner, 1930).

$$f(R,p) = \int \frac{d\mathbf{r}}{(2\pi)^3} e^{i(p/\hbar)\cdot r} \rho\left[\mathbf{R} + \frac{\mathbf{r}}{2}, R - \frac{r}{2}\right] . \tag{3.21}$$

In the classical limit f becomes the classical distribution function and aside from lacking positive definiteness, retains quantum mechanically many of the properties of the classical distribution function. As may be verified directly from the definitions,

$$\rho(R) = \int dp\, f(R,p) , \tag{3.22a}$$

$$\rho(p) = \int dR\, f(R,p) , \tag{3.22b}$$

$$\langle \mathbf{J}(R) \rangle = \int dp\, (\mathbf{p}/m) f(R,p) , \tag{3.22c}$$

$$\langle K(R) \rangle = \int dp\, (p^2/2m) f(R,p) , \tag{3.22d}$$

where, of course, quantities like the kinetic energy density are subject to arbitrary integrations by parts. Taking the Wigner transfer of Eq. (3.20), defining transforms of the local Hartree and nonlocal Fock terms of Eq. (3.18) by

$$W^H(R,p) = \int dr\, v(r)\rho(R+r) , \tag{3.23a}$$

$$W^F(R,p) = \int dr\, e^{i(p\cdot r/\hbar)} \rho\left[R + \frac{r}{2}, R - \frac{r}{2}\right] v(r) , \tag{3.23b}$$

and retaining factors of $\hbar$ yields

$$\left[\frac{\partial}{\partial t} + \frac{\mathbf{p}}{m}\cdot\frac{\partial}{\partial R}\right] f(R,p,t) + \frac{2}{\hbar}\sin\left[\frac{\hbar}{2}(\partial_{R_2}\cdot\partial_{p_1} - \partial_{p_2}\partial_{R_1})\right] \{[W^H(R_1p_1) - W^F(R_1p_1)] f(R_2,p_2,t)\} \Big|_{R_1=R_2=R, p_1=p_2=p} = 0 . \tag{3.24}$$

Ignoring the nonlocal Fock term W^F, we note that in the classical limit or the limit of long-wavelength density fluctuations of a uniform medium, only the first term in the expansion of the sine contributes, and the time-dependent Hartree equation becomes the Vlasov equation

$$\left[\frac{\partial}{\partial t} + \frac{p}{m}\cdot\frac{\partial}{\partial R} - \frac{\partial W^H}{\partial R}\frac{\partial}{\partial p}\right] f(R,p,t) = 0 . \tag{3.25}$$

For infinite nuclear matter in the Hartree-Fock approximation, f is a uniform sharp Fermi distribution,

$$f(r,p)=\theta(p_f-|p|)\frac{1}{h^3}\ .$$

Based on results in the hole-line expansion, the exact momentum distribution differs by having on the order of 15% of the probability removed from the Fermi sea and distributed above p_f. For finite systems in the HF approximation there is some diffuseness in the Fermi surface induced by the finite geometry, as well as the familiar diffuseness in the surface in coordinate space. In the crudest approximation, the phase-space distribution is expected to evolve like an incompressible fluid of density $1/\hbar^3$. Explicit calculations of $f(R,p,t)$ will be shown in Sec. VI.

3. Limiting cases

Several limiting forms of the TDHF equations are worthy of note. In the case of stationary states, for which

$$\psi_\nu(x,t)=\psi_\nu^0(x)e^{-i\varepsilon_\nu t}\ ,$$

Eq. (3.16) reduces to the usual static HF equation

$$h\psi_\nu^0(x)=\varepsilon_\nu\psi_\nu^0(x)\ . \tag{3.26}$$

The representation-independent form of the static HF equation

$$[h_0,\rho_0]=0 \tag{3.27}$$

follows immediately upon noting that the time-dependent phase factors cancel out of the density matrix:

$$\begin{aligned}\rho_0(r,r';t)&=\sum_\nu \psi_\nu^{0*}(r')e^{i\varepsilon_\nu t}\psi_\nu^0(r)^{-i\varepsilon_\nu t}\\&=\sum_\nu \psi_\nu^{0*}(r')\psi_\nu^0(r)\ .\end{aligned} \tag{3.28}$$

Any solution to the static HF equations may be boosted with velocity v to obtain a uniformly translating solution to the TDHF equation. It may be verified by substituting in Eqs. (3.16) and (3.20) that the following solutions satisfy the equations of motion:

$$\psi_\nu(x,t)=e^{-i(\varepsilon_\nu+mv^2/2)t}e^{imvx}\psi_\nu^0(x-vt)\ , \tag{3.29a}$$

$$\rho(x,x';t)=e^{imv(x-x')}\rho^0(x-vt,x'-vt)\ , \tag{3.29b}$$

$$W(x,x';t)=e^{imv(x-x')}W^0(x-vt,x'-vt)\ . \tag{3.29c}$$

A second limiting case of TDHF is the random-phase approximation (RPA). Consider a density matrix ρ which differs from the ground-state density matrix ρ_0 by an infinitesimal deviation ρ_1,

$$\rho\equiv\rho_0+\rho_1\ . \tag{3.30}$$

Explicitly displaying the functional dependence of W on ρ,

$$i(\dot\rho_0+\dot\rho_1)=[(T+W[\rho_0]+W[\rho_1]),(\rho_0+\rho_1)]\ . \tag{3.31}$$

Using the fact that ρ_0 satisfies the static equation, and retaining only first-order infinitesimals, the following equation is obtained (Goldstone and Gottfried, 1959):

$$i\dot\rho_1=[W[\rho_1],\rho_0]+[T+W[\rho_0],\rho_1]\ . \tag{3.32}$$

Letting $\alpha,\beta,\gamma,\delta,\xi$ denote occupied or unoccupied orbitals in the HF basis

$$T+W[\rho_0]\,|\,\alpha\rangle=E_\alpha\,|\,\alpha\rangle\ , \tag{3.33}$$

and using (3.18a), $\langle\alpha\,|\,\dot\rho\,|\,\beta\rangle$ is given by

$$\begin{aligned}&\left[i\frac{\partial}{\partial t}-(E_\alpha-E_\beta)\right]\langle\alpha\,|\,\rho\,|\,\beta\rangle\\&\quad=\langle\alpha\,|\,[W[\rho_1],\rho_0]\,|\,\beta\rangle\\&\quad=\sum_{\gamma,\delta,\xi}(\langle\alpha\gamma\,|\,v\,|\,\xi\delta-\delta\xi\rangle\langle\delta\,|\,\rho_1\,|\,\gamma\rangle\langle\xi\,|\,\rho_0\,|\,\beta\rangle\\&\qquad-\langle\alpha\,|\,\rho_0\,|\,\xi\rangle\langle\xi\gamma\,|\,V\,|\,\beta\delta-\delta\beta\rangle\langle\delta\,|\,\rho_1\,|\,\gamma\rangle)\ .\end{aligned} \tag{3.34}$$

Since the most general infinitesimal change from the ground state is given by a superposition of particle-hole excitations, the most general form of infinitesimal deviation in the density matrix with a single frequency ω is

$$\rho_1(t)=\rho_1e^{-i\omega t}+\rho_1^\dagger e^{i\omega t}\ , \tag{3.35}$$

where ρ_1 has only particle-hole matrix elements. Thus, denoting particles and holes by ρ and ν, substituting Eq. (3.35) in Eq. (3.34), and equating terms with the same time dependence yields

$$\begin{aligned}[\omega-(E_\nu-E_\rho)]\langle\nu\,|\,\rho_1\,|\,\rho\rangle&=-\sum_{\gamma\delta}\langle\nu\gamma\,|\,V\,|\,\rho\delta-\delta\rho\rangle\langle\delta\,|\,\rho_1\,|\,\gamma\rangle\\&=\sum_{\nu',\rho'}-\langle\nu\nu'\,|\,V\,|\,\rho\rho'-\rho'\rho\rangle\langle\rho'\,|\,\rho_1\,|\,\nu'\rangle-\langle\nu\rho\,|\,V\,|\,\rho\nu'-\nu'\rho\rangle\langle\nu'\,|\,\rho_1\,|\,\rho'\rangle\\[-\omega-(E_\nu-E_\rho)]\langle\nu\,|\,\rho_1^\dagger\,|\,\rho\rangle&=\sum_{\nu',\rho'}-\langle\nu\nu'\,|\,V\,|\,\rho\rho'-\rho'\rho\rangle\langle\rho'\,|\,\rho_1^\dagger\,|\,\nu'\rangle-\langle\nu\rho'\,|\,V\,|\,\rho\nu'-\nu'\rho\rangle\langle\nu'\,|\,\rho_1^\dagger\,|\,\rho'\rangle\ .\end{aligned} \tag{3.36}$$

The standard form of the RPA equations is obtained with the definitions

$$\begin{aligned} A_{\nu\rho\nu'\rho'} &\equiv (E_\rho - E_\nu)\delta_{\nu\nu'}\delta_{\rho\rho'} + \langle \nu\rho' \mid V \mid \rho\nu' - \nu'\rho \rangle , \\ B_{\nu\rho\nu'\rho'} &\equiv \langle \nu\nu' \mid V \mid \rho\rho' - \rho'\rho \rangle , \\ X_{\nu\rho} &\equiv \langle \nu \mid \rho_1^\dagger \mid \rho \rangle , \\ Y_{\nu\rho} &\equiv \langle \rho \mid \rho_1^\dagger \mid \nu \rangle , \end{aligned} \tag{3.37}$$

in which case, Eq. (3.36) becomes

$$\begin{bmatrix} A & B \\ B^* & A^* \end{bmatrix} \begin{bmatrix} X \\ Y \end{bmatrix} = \omega \begin{bmatrix} X \\ -Y \end{bmatrix} . \tag{3.38}$$

Since the RPA specifies the linear response of the system to arbitrarily weak excitations by an external probe, it provides an ideal first test of the application of the mean-field approximation to dynamics. In the case of inelastic electron scattering, the external field is the transient electromagnetic field of the scattered electron, which is both very weak and accurately known. Just as in the case of elastic electron scattering, high-momentum transfer inelastic form factors have been inverted to specify transition density distributions in coordinate space. Figure 15 compares the experimental transitions densities for the lowest 2^+ and 3^- states in ^{208}Pb with the theoretical RPA predictions based on the Gogny density-dependent effective interaction (Gogny, 1979).

In translationally invariant infinite matter, the RPA mode which approaches zero excitation energy linearly with momentum q is the zero sound mode. One may establish contact with Landau's derivation of zero sound (Landau, 1957) by linearizing the Vlasov equation, Eq. (3.25), with respect to small fluctuations about the nuclear matter distribution function. The solution for the zero sound mode with wave vector $\mathbf{q}$ is then

$$\delta f(\mathbf{R},\mathbf{p},t) = e^{i(\mathbf{q}\cdot\mathbf{r}-\omega t)} \frac{\mathbf{p}\cdot\mathbf{q}\,\delta(\mid p \mid - k_F)}{\omega - \mathbf{p}\cdot\mathbf{q}/m} , \tag{3.39}$$

where the frequency is specified by s defined by

$$\omega = \frac{qk_F}{m} s , \tag{3.40}$$

which satisfies the equation

$$\frac{\pi^2}{2m^* k_F \int dr\, V(r)} = \left[\frac{s}{2} \ln \frac{s+1}{s-1} - 1 \right] . \tag{3.41}$$

For an undamped mode, Eq. (3.41) implies that the volume integral of V must be repulsive and that s, which by Eq. (3.40) is the ratio of the zero sound velocity to the Fermi velocity, must be greater than one.

This simplified treatment of zero sound in the time-dependent Hartree approximation is deficient in two essential respects. The exchange interaction, which was omitted to obtain the Vlasov equation, Eq. (3.25), is in fact stronger than the direct Hartree term. Its inclusion by solving the full RPA equations in an infinite medium is only an additional technical complication. A more serious conceptual problem is that in the HF approximation the same bare potential $V(r)$ is simultaneously required to be strongly attractive, to produce a bound system, and to be repulsive near the Fermi surface to generate isoscalar, spin-scalar zero sound. To resolve this problem, it is essential to derive an effective interaction to replace the bare interaction in the HF energy functional.

For the Skyrme interaction, it is straightforward to derive the parameters F_0 and F_1, which enter into the counterpart to Eq. (3.41), which is derived in Fermi liquid theory (Abrikosov and Khalatnikov, 1959)

$$\frac{1 + \frac{1}{3}F_1}{F_0 + \frac{1}{3}F_0F_1 + F_1 s^2} = \frac{s}{2} \ln \left[\frac{s+1}{s-1} - 1 \right] . \tag{3.41a}$$

Since the Skyrme parametrization can accomplish saturation either through repulsive momentum-dependent terms or a repulsive three-body force, there exists a continuous family of interactions consistent with bulk nuclear properties. A convenient measure of the amount of momentum dependence is the effective mass m^* [which corresponds to a constant k mass in the general treatment of Jeukenne, Leujeune, and Mahaux (1976)]. For $m^* = m$, there is no momentum dependence, and saturation requires strong repulsive density dependence. The second derivative of the energy with respect to density defining the effective interaction in Fermi liquid theory thus strongly amplifies this three-body repulsion and

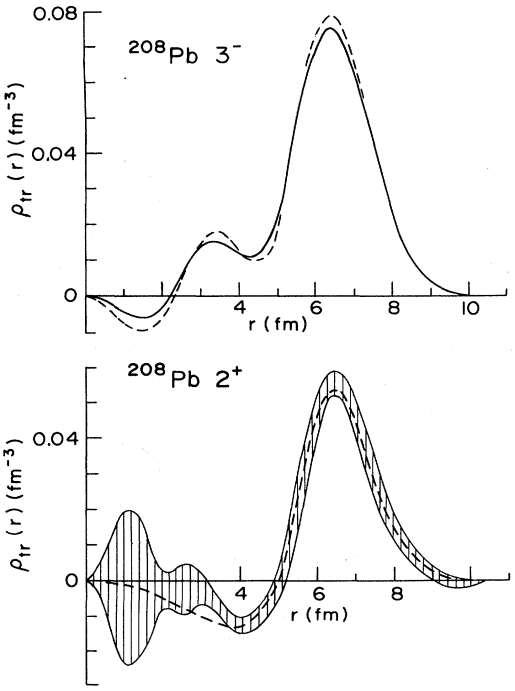

FIG. 15. Comparison of experimental and RPA transition densities for the lowest 3^- and 2^+ states in ^{208}Pb. Error envelopes enclosing transition densities consistent with the measured cross sections and their experimental uncertainties are denoted by the solid curve and shaded region, and the RPA results are denoted by the dashed curves.

yields the Landau parameters $F_0=+0.74$ and $F_1=0$ (Bäckman, Jackson, and Speth, 1975). With $m^*=0.38m$, the Skyrme force saturates with no density dependence, and the resulting values $F_0=-0.45$ and $F_1=-1.9$ imply that the zero sound mode does not propagate. Within the Skyrme parametrization, the F's are monotonic functions of m^*/m and the left-hand side of (3.41a) is positive only for m^*/m greater than 0.85. Since nuclear matter calculations suggest that m^* in the Skyrme force is of the order of $0.7m$ (Negele and Vautherin, 1972), and given the uncertainties in deriving Landau parameters, it is inconclusive whether or not this zero sound mode actually exists. For any of the interactions for which the driving term is positive, the magnitude is sufficiently small that the zero sound velocity implied by Eq. (3.41a) is only slightly greater than the Fermi velocity,

$$v_0 \sim k_F/m = 84 \pm 3 \text{ fm}/10^{-21} \text{ s} . \tag{3.42}$$

This should be compared to the speed of ordinary sound,

$$v_1 = \left[\frac{K}{9m}\right]^{1/2} = 48 \pm 3 \text{ fm}/10^{-21} \text{ s} , \tag{3.43}$$

where we have used the value of the compression modulus $K=220\pm20$ MeV implied by the energy of the isoscalar monopole resonance (Blaizot, 1980). The ratio v_0/v_1 is fortuitously close to the value $\sqrt{3}$ which occurs in the limit of an arbitrarily weakly interacting Fermi liquid. In addition to this sound mode's involving fluctuations in the total density, spin waves, isospin waves, and spin-isospin waves of similar nature are possible, depending upon the spin and isospin structure of the effective interaction.

The final important limit of TDHF is an adiabatic limit (Baranger and Véneroni, 1978). A general density matrix satisfying $\rho^2=\rho$ may be written in the form

$$\rho = e^{i\chi}\rho_0 e^{-i\chi} , \tag{3.44}$$

where ρ_0 is time even and satisfies $\rho_0^2=\rho_0$. If χ is sufficiently small, which implies that all velocities are small, a systematic expansion may be developed in which approximate equations of motion for ρ_0 and χ are determined from the TDHF equation. This formulation provides an elegant and general method for deriving a collective Hamiltonian which contains not only the usual simple potential energy terms, but also the crucial mass parameters associated with each collective variable. Whereas applications of the adiabatic theory to date have been limited, it offers an appealing alternative to the solution of the full TDHF theory in appropriate cases.

4. Semiclassical scattering problem

In the context of the TDHF initial-value problem, collisions of nuclei may be described by an intuitively plausible but nonrigorous semiclassical approximation. For the initial state, an $(A_1+A_2)\times(A_1+A_2)$ determinantal wave function is constructed from the HF ground-state wave functions of nuclei with A_1 and A_2 nucleons, respectively. Denoting the HF single-particle wave functions in the rest frame of the HF potential with A_s particles as $\psi_\nu^{(s)}(x)$, the A_1+A_2 initial wave functions for the system are chosen to be

$$\psi(t_0,x) = e^{i\mathbf{k}_s\cdot\mathbf{x}}\psi_\nu^{(s)}(x-\mathbf{R}_s) . \tag{3.45}$$

As long as the two nuclei are sufficiently separated that the HF potential generated by wave functions in one nucleus has negligible overlap with the wave functions in the other nucleus, each nucleus will translate freely in its HF ground state with momentum $\mathbf{k}_s$ by Eqs. (3.29). Thus one has semiclassically specified both the position R_s and momentum $\mathbf{k}_s$ of each fragment. For a given relative momentum $\mathbf{k}_1-\mathbf{k}_2$, all impact parameters may be explored by varying the initial relative coordinate $\mathbf{R}_1-\mathbf{R}_2$.

Once the nuclei begin to enter each other's Coulomb field, all A_1+A_2 single-particle wave functions are influenced by all others. At large relative separations, the nuclei essentially follow Coulomb trajectories with negligible excitation. As the nuclei approach each other more closely, Coulomb excitation and eventually nuclear excitation will occur. In those cases in which distinct fragments separate after a collision, with cm coordinates denoted R_s', each fragment may, in general, have components from each of the A_1+A_2 single-particle wave functions. In contrast to the special case of the initial state, Eq. (3.45), in general for the final state no unitary transformations will be able to bring the single-particle wave functions into a form in which one subset of wave functions vanishes everywhere except in the region of R_1' and the remaining wave functions vanish everywhere except in the region of R_2'. In terms of the density matrix, the off-diagonal contributions $\rho(R_1+x,R_2+y)$, where x and y are of the order of the size of the nuclei, are defined to vanish for the initial wave function, but in general the corresponding terms $\rho(R_1'+x,R_2'+y)$ are nonzero for the final state. At the level of obtaining approximations to expectation values of one-body operators, the interpretation of these final density matrices introduces no conceptual ambiguities. If one instead attempts to formulate a complete scattering theory, then these so-called "spurious cross-channel correlations" (Griffin *et al.*, 1979) are but one of several shortcomings of the semiclassical TDHF initial-value problem which need to be resolved along the lines reviewed in Sec. V.

At the semiclassical level, it is useful to examine the implications of the wave packet defined by the initial condition in Eq. (3.45). In principle, each fragment should, of course, have a wave function which factorizes into a cm wave function multiplying an intrinsic wave function depending only on relative coordinates

$$\psi_{\mathbf{K}}(r_1\ldots r_n) = \exp\left[i\mathbf{K}\cdot\left[\frac{1}{A}\sum_{j=1}^{A}\mathbf{r}_j\right]\right]\psi_{\text{int}}(x_1^{\text{rel}}\ldots x_{n-1}^{\text{rel}}) . \tag{3.46a}$$

In contrast, the Galilean-invariant initial wave function of Eqs. (3.29a) and (3.45) has the form

$$\psi_{\mathbf{K}}(r_1 \ldots r_n) = \exp\left[i(A\mathbf{k}) \cdot \left[\frac{1}{A} \sum_{j=1}^{A} r_j \right] \right] \psi^{\mathrm{HF}}(r_1 \ldots r_n) \ . \tag{3.46b}$$

Whereas the wave function translates with the proper cm momentum $K = A\mathbf{k}$ and thus has the correct value for $\langle p_{\mathrm{cm}} \rangle$, ψ^{HF} is not a function of relative coordinates, and, in particular, has the feature of vanishing when the cm coordinate is outside the nucleus. Thus one is unavoidably dealing with a localized cm wave packet so that

$$\Delta p_{\mathrm{cm}} > \frac{\hbar}{2 r_0 A^{1/3}} \ , \tag{3.47}$$

and the corresponding fractional spread in beam energy is

$$\frac{\Delta E}{E} = \frac{\hbar}{(2 m E r_0 A^{4/3})^{1/2}} \ , \tag{3.48}$$

where E is the beam energy per particle. For an oxygen nucleus at 2 MeV per particle, Eq. (3.48) implies an 8% spread in beam energy, so for light ions at low energies such considerations begin to become relevant. In terms of the expectation value of operators, one observes that although the initial condition is capable of describing the proper mean value for the momentum $\langle p \rangle$, the TDHF one-body density matrix is incapable of representing the proper dispersion, $\langle (p - \langle p \rangle)^2 \rangle^{1/2}$, even in the initial state.

A final consideration suggesting that it is the expectation values of one-body operators, rather than the full determinantal wave function, which should be taken seriously in the semiclassical scattering problem is the dispersion in particle number for the final-state fragments. To define the number of particles in a final-state fragment, it is convenient to define a number operator which counts particles in an appropriate region of space. For simplicity, consider a binary final state with fragments receding in the positive and negative z directions in the cm frame, so that the particles in the right-hand half space may be counted by the right-hand number operator

$$\hat{N}^R = \sum_{\alpha\beta} N^R_{\alpha\beta} a^\dagger_\alpha a_\beta \ , \tag{3.49}$$

where, in coordinate representation,

$$N^R(\mathbf{r},\mathbf{r}') = \delta(\mathbf{r} - \mathbf{r}')\theta(z) \ . \tag{3.50}$$

Following Bonche, Koonin, and Negle (1976), from the fact that N^R in Eq. (3.50) is a projector one is enabled to write the determinantal expectation value of the dispersion in particle number as

$$\langle (\hat{N}^R - \langle N^R \rangle)^2 \rangle^{1/2} = \left[\sum_\nu N^R_{\nu\nu} - \sum_{\nu\mu} N^R_{\nu\mu} N^R_{\mu\nu} \right]^{1/2} , \tag{3.51}$$

where, as usual, ν and μ denote occupied single-particle wave functions. As observed by Dasso, Døssing, and Pauli (1979), the eigenvalues of the matrix $N^R_{\mu\nu}$ are ≤ 1, so that the dispersion is necessarily less than or equal to $(A/4)^{1/2}$. At the formal level, the observation that the dispersion in fragment particle number is bounded by $(A/4)^{1/2}$ is analogous to the bound on the dispersion in momentum in Eq. (3.47). Physically, it is a much more significant bound, since the experimentally observed dispersion tends to grossly exceed $(A/4)^{1/2}$.

B. Theoretical limitations

Both the formal presentation in the context of the time-dependent variational principle and the discussion of the semiclassical description of scattering have revealed limitations and deficiencies of the TDHF initial-valve problem. As a prelude to generalizations in subsequent sections, it is useful to group these limitations into two broad categories which will ultimately be addressed by different techniques.

1. Correlations and collision terms

One salient limitation in the TDHF approximation is the treatment of the two-body correlations.

Because of the imprecision pervading discussions of the extent to which two-body collisions are included in TDHF, it is useful to rewrite the full time-dependent Schrödinger equation in a basis defined by the complete set of eigenfunctions of the TDHF single-particle Hamiltonian h of Eq. (3.17). Let the full wave function be expanded in determinants of the form Eq. (3.3)

$$\Psi = \sum_{\{n\}} C_{\{n\}}(t) \Psi^{\mathrm{SD}}_{\{n\}}(t) \ , \tag{3.52}$$

where $\Psi^{\mathrm{SD}}_{\{n\}}$ denotes a determinant comprised of time-dependent wave functions satisfying

$$i \frac{\partial}{\partial t} \psi_\alpha = h \psi_\alpha \ , \tag{3.53}$$

where α denotes either occupied or unoccupied single-particle states, and the occupation numbers $\{n\}$ are defined relative to the normally occupied states such that $\{0\}$ denotes the TDHF wave function, $\{\rho,\nu\}$ denotes a particle-hole excitation relative to $\{0\}$ with particle state ρ occupied and hole state ν empty, and similarly for multiparticle, multihole excitations. Differentiation of (3.52) with respect to time, substitution of Eqs. (3.53) and (3.17), and projection onto state $\Psi^*_{\{m\}}$ then yields equations for the time dependence of the $C_{\{n\}}$'s. Of particular interest is the equation of motion for $C_{\{0\}}$:

$$i\dot{C}_{\{0\}} = -\tfrac{1}{2} \sum_{\nu_1\nu_2} \langle \nu_1\nu_2 \,|\, \tilde{V} \,|\, \nu_1\nu_2 \rangle c_{\{0\}} + \sum_{\nu_1\nu_2\rho_1\rho_2} C_{\{\rho_1\rho_2\nu_1\nu_2\}} \langle \rho_1\rho_2 \,|\, \tilde{V} \,|\, \nu_1\nu_2 \rangle \ . \tag{3.54}$$

The first term on the right-hand side of Eq. (3.54) sim-

ply corrects the phase associated with $\psi_{\{0\}}$ which must evolve with the total HF energy instead of the sum of the HF eigenvalues. The only admixtures in the wave function are introduced through the two-particle, two-hole contributions in the last term. Thus we observe that at each instant, all the proper one-particle, one-hole excitations are exactly accounted for by the TDHF equation of motion, and only the two-particle, two-hole excitations must be added. Far from omitting the effect of two-body collisions, the TDHF approximation therefore includes all the forward scattering terms and one-particle, one-hole contributions, and only the two-particle, two-hole amplitudes have been neglected.

In the static case, as discussed in Sec. II, it was crucial to modify the static HF theory by including the two-particle, two-hole excitations contained in the reaction matrix. This same class of diagrams may be approximately included in the time-dependent case by using in the time-dependent problem the density-dependent effective interaction derived for ground states. Although the basic features of the two-body correlations should be included sensibly, the time dependence of these correlations is totally neglected and presumably becomes a serious error in sufficiently high energy reactions. Associated with the fact that the ground-state correlations are frozen into the effective density-dependent interactions is the feature that two-body and higher-body density matrices have no reason to be reliable in the TDHF approximation.

These limitations associated with correlations suggest a natural rationale for a systematic hierarchy of successive approximations. If one is interested in the time evolution of successively higher-body correlation functions, it is reasonable to formulate an exact system of coupled equations for n-body density matrices. In truncating this hierarchy to obtain closed, and therefore solvable, equations, one may be guided by the desire to obtain the TDHF equation, Eq. (3.20a), in lowest order, something like a time-dependent reaction matrix at the next level, and a theory incorporating the physics of a time-dependent Faddeev equation at the following level. Formulation of a theory in terms of density matrices instead of a complete wave function may, in principle, complicate questions concerning interpretation and semiclassical aspects of the theory. However, as long as questions are posed in terms of expectation values of few-body operators, there are no conceptual problems in principle. Although one will never have a full wave function to implement—for example, the boundary conditions for incoming waves—one may at least construct n-body density matrices for the initial conditions which have the proper values for expectation values, dispersion, and up to nth moments of any operators of physical relevance. Since the dynamics of correlations is presumably most important at high energy, emphasis on few-body density matrices instead of on the entire wave function presumably should cause little difficulty. The systematic hierarchy of approximations emerging from this rationale will be reviewed in Sec. IV.

2. Quantum theory

Complementary to the correlation questions which are relevant at high energy are the intrinsically semiclassical aspects of the TDHF initial-value problem at low energy. To calculate any physical observable, the TDHF initial-value problem requires, in addition to the equation of motion, the imposition of some suitable initial condition. In general, there is no systematic procedure by which to derive this initial condition. In cases such as the scattering problem described in Sec. III.A.3, intuitively plausible semiclassical initial conditions can be formulated which, despite conceptual ambiguities, reproduce much of the observed phenomenology. In other applications, such as spontaneous fission or the construction of eigenstates of large amplitude collective motion, no obvious satisfactory initial conditions emerge. For spontaneous fission, the deformed HF minimum for a fissionable nucleus, which might superficially appear to be the physically correct initial condition, is manifestly unsuitable because by Eq. (3.28) the resulting one-body density matrix is time independent. Indeed, for both fission and large-amplitude collective motion, it will be shown in Sec. V that the proper quantum problem is not formulated in terms of an initial condition at all, but rather in terms of a periodic boundary condition.

A related ambiguity concerns quantization of the TDHF equation. Although the TDHF equation of motion reproduces the familiar RPA equations, Eq. (3.38), nowhere does there emerge a natural quantization condition on the amplitude of the excitations, expressed either in terms of ρ [Eq. (3.35)] or of X and Y [Eq. (3.37)]. Even though Eq. (3.7) looks like a classical field theory that might conceivably admit second quantization and it is tempting to apply a standard quantization prescription to the Hamiltonian obtained from the adiabatic reduction in Eq. (3.44), in the present context there is no rigorous justification for such quantization procedures.

The theoretical framework for addressing such quantum-mechanical questions is complementary in many respects to the hierarchy of coupled density-matrix equations designed to address many-body correlations. At the low energies at which such quantal issues are relevant, the dynamics of correlation functions are not crucial and may plausibly be treated by the ground-state effective interaction. Hence the primary emphasis is on writing exact expressions for quantum-mechanical observables and systematically approximating these expressions in such a way as to obtain a quantum mean-field theory in lowest order. A natural formalism for such approximations turns out to be that of functional integrals, and this theory will be developed in detail in Sec. V.

IV. TRUNCATION OF EQUATIONS OF MOTION

The formulation of a systematic microscopic theory of nuclear dynamics ultimately requires at least as careful a

treatment of two-body and higher-body correlations as was necessary for the stationary states reviewed in Sec. II. Ideally, in addressing the problems associated with correlation and collision terms emphasized in Sec. II.A.1, it is desirable to establish contact with, and fully exploit, our present understanding of the time-independent many-body problem.

The approach in this section will be to consider alternative formulations of general hierarchies of equations of motion coupling n-body correlation terms to those involving correlations of $n+1$ bodies. The primary criteria for choosing between alternative formalism will be the economy of representation of the relevant correlation terms and the degree to which the time-dependent theory can be understood as a generalization of the familiar time-independent theory.

A. Density-matrix hierarchies

Exact equations of motion for expectation values of operators may be derived from the Heisenberg equation of motion for the second-quantized field operator

$$\hat{\psi}(x,t)\equiv e^{iHt}\hat{\psi}(x)e^{-iHt} . \tag{4.1}$$

Commutation with the second-quantized Hamiltonian

$$\hat{H}=\int dx_1\hat{\psi}^\dagger(x_1,t)K(x_1)\hat{\psi}(x_1,t) + \tfrac{1}{2}\int dx_1dx_2\hat{\psi}^\dagger(x_1,t)\hat{\psi}^\dagger(x_2,t)v(x_1-x_2) \times\hat{\psi}(x_2,t)\hat{\psi}(x_1,t) \tag{4.2}$$

yields the Heisenberg equation

$$i\frac{\partial}{\partial t}\hat{\psi}(x,t)=[\hat{\psi}(x,t),\hat{H}] = K(x)\hat{\psi}(x,t) + \int dx_1\hat{\psi}^\dagger(x_1,t)v(x-x')\hat{\psi}(x_1,t)\hat{\psi}(x,t) . \tag{4.3}$$

Using Eq. (4.3) and its adjoint, the time derivative of an operator containing products of n creation and n annihilation operators will yield an expression involving at most products of $n+1$ creation and annihilation operators, so that the evolution of expectation values of n-body operators will necessarily be coupled with expectation values of $n+1$ particle operators.

1. Density matrices

A particularly simple hierarchy of equations of motion is obtained in terms of density matrices. The n-body density matrix is defined

$$\rho_n(1,2\ldots n;1'2'\ldots n';t) \equiv\langle\hat{\psi}^\dagger_{1'}(t)\hat{\psi}^\dagger_{2'}\ldots\hat{\psi}^\dagger_{n'}(t)\hat{\psi}_n(t)\ldots\hat{\psi}_2(t)\hat{\psi}_1(t)\rangle . \tag{4.4}$$

By application of Eq. (4.3) and its adjoint n times, the time derivative of the n-body density matrix may be expressed in terms of integrals over n and $n+1$ body density matrices, yielding a hierarchy analogous to the Bogoliubov, Born, Green, Kirkwood, Yvonne hierarchy in classical statistical mechanics. The equation of motion for the one-body density matrix is thus

$$i\frac{d}{dt}\rho_1(x',x;t)=\langle\hat{\psi}^\dagger(x,t)\left[K(x')+\int dx_1\hat{\psi}^\dagger(x_1,t)\hat{\psi}(x_1,t)v(x_1-x') - K(x)-\int dx_1\hat{\psi}^\dagger(x_1,t)\psi(x_1,t)v(x_1-x)\right]\hat{\psi}^\dagger(x',t)\rangle$$
$$=[K(x')-K(x)]\rho_1(x',x;t)+\int dx_1[v(x_1-x')-v(x_1-x)]\rho_2(x',x_1;x,x_1;t) . \tag{4.5}$$

The crucial issue is, of course, truncation. Other than the obvious desire to approximate $\rho_{(n+1)}$ in terms of ρ_n and lower-order terms, in the language of density matrices one has no physical guidance. In lowest order, there is relatively little choice. Expressing ρ_2 as products of ρ_1's and requiring antisymmetry leads to the approximation

$$\rho_2(x_1,x_2;x_1'x_2';t)\approx\rho_1(x_1,x_1';t)\rho_1(x_2,x_2';t) -\rho_1(x_1,x_2';t)\rho_1(x_2,x_1';t) . \tag{4.6}$$

Substitution of Eq. (4.6) in (4.5) immediately reproduces the TDHF equation, Eq. (3.20), with h as defined in Eq. (3.18).

Since the only correlations imposed by the ansatz Eq. (4.6) are the Pauli correlations associated with antisymmetry, it is reasonable that all dynamical correlations associated with the two-body interactions are neglected. However, it is surprising, and symptomatic of the nontransparent nature of implications of truncation prescriptions, that asserting Eq. (4.6) as a strict equality implies that the full wave function may be represented as a determinant. This observation (Koonin, 1979) follows from setting $x_2=x_2'$ and integrating over x_2 in Eq. (4.6). From the defintion, Eq. (4.4),

$$\int dx_2\rho_2(x_1,x_2;x_1',x_2;t)=\langle\psi^\dagger(x_1',t)\mathcal{N}\psi(x_1)\rangle =(A-1)\rho_1(x_1,x_1';t) \tag{4.7a}$$

where $\mathcal{N}$ denotes the number operator, whereas from Eq. (4.6)

$$\int dx_2 \rho_2(x_1,x_2;x_1',x_2;t) = A\rho_1(x_1,x_1';t) - \int dx_2 \rho_1(x_1,x_2;t)\rho_1(x_2,x';t) \ . \quad (4.7b)$$

Equating (4.7a) and (4.7b) implies $\rho^2=\rho$, and hence, as shown in Sec. III, the wave function may be represented as a determinant.

To obtain an equation for $\dot{\rho}_2$, it is necessary to impose an approximation for ρ_3. In this case, there are many possibilities for expressing ρ_3 as products of $\rho_2\rho_1$ or $\rho_1\rho_1\rho_1$ and antisymmetrizing. Unfortunately, there is no obvious way to relate any of these prescriptions to our previous experience with perturbation theory, or even to see in advance whether they are consistent with conservation laws. Hence it is useful to consider an alternative hierarchy based on Green's functions.

2. Green's functions

Instead of the equal-time expectation value of field operators in Eq. (4.4), the n-particle Green's function is defined as the following time-ordered product of field operators:

$$(i)^n G_n(x_1t_1,\ldots,x_nt_n;x_1't_1'\cdots x_n't_n') \equiv \langle T\hat{\psi}(x_1,t_1)\cdots\hat{\psi}(x_n,t_n)\hat{\psi}^\dagger(x_n't_n')\cdots\hat{\psi}^\dagger(x_1't_1')\rangle \ , \quad (4.8)$$

where T denotes the time-ordering operator. Formulation in terms of Green's functions is in general less economical than density matrices, since G_n involves $2n$ time arguments instead of the single time argument of ρ_n. In compensation, however, the time-ordered product enables direct comparison with perturbation theory through application of Wick's theorem.

The hierarchy of coupled equations of motion for Green's functions (Martin and Schwinger, 1959) is obtained by representing the time-ordered product in Eq. (4.8) in terms of theta functions and using the equation of motion, Eq. (4.3):

$$\begin{aligned} i\frac{\partial}{\partial t}G_1(xt,x't') &= \frac{\partial}{\partial t}[\theta(t-t')\langle\psi(x,t)\psi^\dagger(x',t')\rangle - \theta(t'-t)\langle\psi^\dagger(x',t')\psi(x,t)\rangle] \\ &= \delta(t-t')\langle[\psi(x,t),\psi^\dagger(x't')]_+\rangle + \left\langle T\frac{\partial}{\partial t}\psi(x,t)\psi^\dagger(x't')\right\rangle \\ &= \delta(t-t')\delta(x-x') + \frac{1}{i}K(x)\langle T\psi(x,t)\psi^\dagger(x't')\rangle + \frac{l}{i}\int dx''\langle T\hat{\psi}^\dagger(x'',t)v(x,x'')\hat{\psi}(x'',t)\hat{\psi}(x,t)\hat{\psi}^\dagger(x',t')\rangle \ . \end{aligned} \quad (4.9)$$

If we denote a time infinitesimally greater than t by t^+, noting that

$$-i\int dx''v(x,x'')G_2(xt,x''t;x't',x''t^+) = i\int dx''v(x,x'')\langle T\hat{\psi}^\dagger(x'',t)\hat{\psi}(x,t)\hat{\psi}(x'',t)\hat{\psi}^\dagger(x't')\rangle \ , \quad (4.10)$$

and abbreviating the space-time variables (x_nt_n) by (n), the lowest-order equation becomes

$$\left[i\frac{\partial}{\partial t_1}-K(x_1)\right]G_1(1,1') = \delta(1,1') - i\int dx_2 v(x_1-x_2)G_2(1,2;1'2^+)_{t_2=t_1} \ . \quad (4.11)$$

By similar algebra, the general equation in nth order is

$$\begin{aligned} \left[i\frac{\partial}{\partial t_1}-K(x_1)\right]G_n(1,2,\ldots n;1',2'\ldots n') &= \sum_{i=1}^{n}\delta(1,i')(-1)^{i-1}G_{n-1}[2\ldots n;1'\ldots(i-1)',(i+1)'\ldots n'] \\ &\quad - i\int dx_{n+1}v(x_1-x_{n+1})G_{n+1}[1,2,\ldots(n+1);1',2'\ldots(n+1)'^+]_{t_{N=1}=t_n} \ . \end{aligned} \quad (4.12)$$

In general, the time evolution of G_n is coupled to G_{n+1} and G_{n-1}, so as before the hierarchy may be truncated by specifying a physically motivated prescription for approximating some G_{n+1} in terms of G_n and lower-order Green's functions. The TDHF approximation arises from a factorization analogous to Eq. (4.6):

$$G_2(12,1'2') = G_1(11')G_1(22') - G_1(12')G_1(21') \ . \quad (4.13)$$

Thus

$$\left[i\frac{\partial}{\partial t_1}-K(x_1)\right]G_1(1,1') = \delta(1,1') - i\int dx_2 v(x_1-x_2)G_1(1,1')G_1(2,2^+) - G_1(1,2^+)G_1(2,1')_{t_2=t_1} \quad (4.14a)$$

or

$$i\frac{\partial}{\partial t_1}G_1(1,1')=\delta(1,1') + \int dx_3 h(x_1,x_3;t_1)G_1(x_3t_1;x_1't_1') , \tag{4.14b}$$

where $h(x_1,x_3;t_1)$ is given by Eq. (3.18), so that G_1 evolves in the same mean field as the TDHF wave functions. Evaluating the difference between Eq. (4.14b) and the adjoint equation

$$-i\frac{\partial}{\partial t_1'}G_1(1,1')=\delta(1,1') + \int dx_3 G(x_1t_1;x_3t_1')h(x_3,x_1;t_1') \tag{4.14c}$$

for $t_1'=t_1^+$ yields the TDHF equation

$$i\langle\dot{\hat{\psi}}^\dagger(x',t)\hat{\psi}(x,t)+\hat{\psi}^\dagger(x',t)\dot{\hat{\psi}}(x,t)\rangle = i\dot{\rho}(x,x',t) = \int dx_3[h(x,x_3;t)\rho(x_3,x';t)-\rho(x,x_3;t)h(x_3;x';t)] . \tag{4.15}$$

Whereas the Green's-function formulation does not uniquely specify compelling truncation prescriptions in higher orders, known properties of Green's-function approximations provide considerable guidance. For example, simple conditions on G_2 (Baym and Kadanoff, 1961; Baym, 1962) ensure number, momentum, and energy conservation, and can be implemented by generating a truncation by functional differentiation of a set of skeletal diagrams with respect to an external source. Motivated by the role of ladder summations in the perturbation expansion of the ground-state energy, one can also adopt a conserving truncation which sums all two-hole-line ladders in the ground-state energy expansion. As may be straightforwardly verified by expressing the ground-state energy as an integral over the coupling constant of the product of the Green's function and the proper self-energy (Fetter and Walecka, 1971), such a conserving ladder summation is accomplished by replacing Eq. (4.13) by an integral equation for G_2:

$$G_2(12,1'2')=G_1(11')G_1(22')-G_1(12')G_1(21') + i\int dx_3dx_4dt_4G_1(13)G_1(2,4) \times v(x_3-x_4)\delta(t_3-t_4)G_2(34;1'2') . \tag{4.16}$$

Obviously, even more complicated integral equations could be envisioned to effect more complete summations.

Having seen the general structure of density-matrix and Green's-function hierarchies, we can now critically assess the level of complexity required to generalize beyond the TDHF approximation and to understand why the alternative formulation in the next section is preferable. The simplest structure for an equation of motion for $\dot{\rho}_2(x_1,x_2;x_1',x_2';t)$ arises when $\rho_3(t)$ is expressed in terms of spatial integrals over $\rho_1(t)$ and $\rho_2(t)$, in which case a coupled set of equations first order in time for ρ_1 and ρ_2 must be evolved in time. The minimum level of complexity thus involves evolution of a function ρ_2 of four vector spatial variables and one time variable. This same minimum level of complexity arises in the Green's-function formulation only in special cases in which all time arguments are set equal. In these cases, the Green's-function expression reduces to a corresponding density-matrix result, as was the case in Eq. (4.15). In cases for which the Green's-function hierarchy differs from that for density matrices, presumably to accomplish some physical objective such as summing ladder diagrams, evolution of G instead of ρ_2 necessarily involves retention of additional time dependencies and possibly, as in the case of Eq. (4.16), the solution of integrodifferential equations instead of simple first-order differential equations.

Even at the minimum level of complexity, evolution of a function of four vector variables and time appears sufficiently impractical that it is desirable to turn to the coupled-cluster theory which represents two-body correlations in finite systems more efficiently. The alternative of introducing further approximations in the Green's-function formalism is explored in the literature (Wong and Tang, 1978, 1979; Orland and Schaeffer, 1978) and calculations of the effects of collision terms have been reported by Richert, Brink, and Weidenmüller (1979) and Wong and Davies (1980).

B. Coupled-cluster approximation

The formulation which appears most suited to the present problem is a time-dependent generalization of the exp(S) or coupled-cluster approximation pioneered by Coester (1958) (see also Coester and Kümmerl, 1960), and subsequently applied extensively to fermion systems (Kümmel, Lührmann, and Zabolitzky, 1978). In this theory, the full many-body wave function at any time is written in the form

$$\Psi=\exp(S)\Phi , \tag{4.17}$$

where

$$S=\sum_{n=1}^{N}\hat{S}^{(n)} \tag{4.18}$$

and $\hat{S}^{(n)}$ represents the most general n-particle, n-hole operator defined relative to the Slater determinant of occupied states Φ. The time-dependent Schrödinger equation implies a hierarchy of nonlinear, coupled equations for the static or time-dependent n-particle, n-hole ampli-

tudes, which may be truncated in the same manner as a density-matrix or Green's-function hierarchy. However, the n-particle amplitude may be expressed in terms of n spatial coordinates and n occupied state labels ν_i rather than $2n$ coordinates, since $S^{(n)}$ may be written

$$\langle x_1 x_2 \cdots x_n \mid S^{(n)} \mid \nu_1 \nu_2 \cdots \nu_n \rangle \equiv \sum_{\rho_1 \cdots \rho_n} \langle x_1 \mid \rho_1 \rangle \cdots \langle x_n \mid \rho_n \rangle \langle \rho_1 \cdots \rho_n \mid S_n \mid \nu_1 \cdots \nu_n \rangle \, .$$

The economy of dealing with particle-hole amplitudes $S^{(n)}(x_1 \ldots x_n; \nu_1 \ldots \nu_n)$ instead of density matrices $\rho_n(x, \ldots, x_n, x_1', \ldots, x_n')$ is appreciable. For a system of A particles, $S^{(1)}$ is specified by A functions of one vector variable compared with ρ_1, which is a function of two vector variables. Stated differently, evolving ρ_1 instead of S_1 is as inefficient as integrating the TDHF equation for the full one-body density matrix Eq. (3.20), instead of realizing that because $\rho^2=\rho$, one may go to the diagonal representation and simply evolve A single-particle functions according to Eq. (3.16). For n-body amplitudes, this economy is raised to nth power as n vector variables in ρ_n are replaced by n discrete occupied state labels.

Whereas the basic ideas underlying the coupled-cluster hierarchy are very simple, the technical details involved in applying even the time-independent theory to the most general case are somewhat tedious and notationally cumbersome. Therefore, this review will emphasize only the essential features and general structure of the theory. As a preparation for the application to time-dependent problems, the time-independent theory will first be reviewed in the next section. The general time-dependent theory with the simplest truncation procedure will be presented in the following section and truncation for strongly repulsive forces is treated in Sec. IV.B.3.

1. Time-independent coupled-cluster approximation

For stationary states, equations for the n-particle, n-hole amplitudes appearing in Eqs. (4.17)–(4.18) are obtained by projecting the Schrödinger equation

$$e^{-S}\mathrm{H}e^{S} \mid \Phi \rangle = E \mid \Phi \rangle \tag{4.20}$$

onto a complete set of m-particle, m-hole states. Denoting unoccupied states by ρ_i, the following hierarchy of equations arises:

$$\langle \Phi \mid e^{-S}\mathrm{H}e^{S} \mid \Phi \rangle = E \, , \tag{4.21a}$$

$$\langle \Phi \mid \hat{a}_\nu^\dagger \hat{a}_\rho e^{-S}\mathrm{H}e^{S} \mid \Phi \rangle = 0 \, , \tag{4.21b}$$

$$\vdots$$

$$\langle \Phi \mid \hat{a}_{\nu_1}^\dagger \ldots \hat{a}_{\nu_m}^\dagger \hat{a}_{\rho_m} \ldots \hat{a}_{\rho_1} e^{-S}\mathrm{H}e^{S} \mid \Phi \rangle = 0 \, . \tag{4.21c}$$

From the identity

$$e^{-X}\hat{O}e^{X} = \hat{O} + [\hat{O},X] + \frac{1}{2!} \mid [\hat{O},X],X \mid + \cdots \tag{4.22}$$

$$\hat{S}^{(n)} = \frac{1}{(n!)^2} \langle x_1 x_2 \cdots x_n \mid S^{(n)} \mid \nu_1 \nu_2 \cdots \nu_n \rangle \times \hat{\psi}^\dagger(x_1)\hat{\psi}^\dagger(x_2) \cdots \hat{\psi}^\dagger(x_n)\hat{a}_{\nu_n} \cdots \hat{a}_{\nu_2}\hat{a}_{\nu_1} \, , \tag{4.19}$$

where

it is evident that if H contains only one- and two-body operators, repeated commutation with H can remove at most two pairs of creation and annihilation operators from the particle-hole operators $\hat{S}^{(n)}$. Thus, since $e^{-S}\mathrm{H}e^{S} \mid \Phi \rangle$ must connect to $\mid \Phi \rangle$ in Eq. (4.21a) and at most two pairs of particle-hole operators have been contracted, the resulting equation can involve only S_1 and S_2. In fact, for the special case of Eq. (4.21a), the exact equation

$$\langle \Phi \mid H(\hat{S}^{(1)} + \tfrac{1}{2}\hat{S}^{(1)}S^{(1)} + \hat{S}^{(2)}) \mid \Phi \rangle = E \tag{4.23}$$

is trivially obtained by noting $\langle \Phi \mid S = 0$ and expanding e^S. Similarly, Eq. (4.21b) involves amplitudes only through $S^{(3)}$, and in general Eq. (4.21c) includes amplitudes through $S^{(m+2)}$. The explicit form of the general equation is somewhat complicated, but follows straightforwardly from substitution of Eq. (4.22), which terminates after five terms when $\hat{0}=H$, in Eq. (4.21c).

Since the resulting hierarchy of equations for the $S^{(n)}$'s is equivalent to the original Schrödinger equation, physical approximations are introduced by the method of truncation. The simplest truncation prescription, which we shall use in the present section, is to specify that $S^{(n)}=0$ for all $n>m$. This has the effect of treating particle-hole correlations of up to m particles exactly, while retaining only those correlations for more than m particles which arise from products of lower-order amplitudes. In terms of familiar perturbation theory, truncation at $m=2$ sums particle-particle and hole-hole ladders as well as RPA ring diagrams, and this approximation has been shown to be accurate for a single Lipkin model and for systems with long-range forces (Kümmel, Lührmann, and Zabolitzky, 1978). For potentials which are infinitely repulsive at short distances, it is inconsistent to define the higher $S(n)$'s to be zero, and instead one must impose a prescription which makes the wave function vanish when n particles are within a hard-core radius. For finite but strongly repulsive cores, a similar condition is physically reasonable, and this truncation procedure will be addressed subsequently in Sec. IV.B.3.

Retaining only m nonzero amplitudes yields m equations of the form (4.21c) in m unknowns which completely specify the $S^{(n)}$'s. With these amplitudes, Eq. (2.21) yields an mth order approximation to the energy which is distinct from the expectation value of H with the wave function

$$\psi^{(m)} \equiv \exp(\hat{S}^{(1)} + \hat{S}^{(2)} + \cdots + \hat{S}^{(m)}) \mid \Phi \rangle$$

since $-\hat{S}\neq\hat{S}^\dagger$. Truncation at $m=1$ yields the Hartree-Fock approximation, which is most obvious by noting that the most general determinant may be written $\exp(S^{(1)})\,|\,\Phi\rangle$ by Thouless' theorem (Thouless, 1972). In general, one always has the freedom to specify $S^{(1)}\equiv 0$ and to solve an equation for the single-particle wave functions comprising the determinant $|\,\Phi\rangle$.

2. Time-dependent coupled-cluster approximation

The time-dependent coupled-cluster theory (Monkhorst, 1977; Hoodbhoy and Negele, 1978, 1979; Schonhammer and Gunnarson, 1978) is obtained analogously by projecting the time-dependent Schrödinger equation,

$$e^{-\hat{S}}\mathrm{H}e^{\hat{S}}\,|\,\Phi\rangle = ie^{-\hat{S}}\frac{\partial}{\partial t}e^{\hat{S}}\,|\,\Phi\rangle\ , \tag{4.24}$$

onto n-particle, n-hole states:

$$\langle\Phi\,|\,e^{-\hat{S}}\mathrm{H}e^{\hat{S}}\,|\,\Phi\rangle = i\langle\Phi\,|\,e^{-\hat{S}}\frac{\partial}{\partial t}e^{\hat{S}}\,|\,\Phi\rangle\ , \tag{4.25a}$$

$$\langle\Phi\,|\,\hat{a}_\nu^\dagger\hat{a}_\rho e^{-\hat{S}}\mathrm{H}e^{\hat{S}}\,|\,\Phi\rangle = i\langle\Phi\,|\,\hat{a}_\nu^\dagger\hat{a}_\rho e^{-\hat{S}}\frac{\partial}{\partial t}e^{S}\,|\,\Phi\rangle\ , \tag{4.25b}$$

$$\langle\Phi\,|\,\hat{a}_{\nu_1}^\dagger\ldots\hat{a}_{\nu_m}^\dagger\hat{a}_{\rho_m}\ldots\hat{a}_{\rho_1}e^{-\hat{S}}\mathrm{H}e^{\hat{S}}\,|\,\Phi\rangle = i\langle\Phi\,|\,\hat{a}_{\nu_1}^\dagger\ldots\hat{a}_{\nu_m}^\dagger\hat{a}_{\rho_m}\ldots\hat{a}_{\rho_1}e^{-\hat{S}}\frac{\partial}{\partial t}e^{\hat{S}}\,|\,\Phi\rangle\ . \tag{4.25c}$$

The general structure of these equations is observed by noting that

$$e^{-\hat{S}}\frac{\partial}{\partial t}e^{\hat{S}} = \frac{\partial}{\partial t}+\dot{\hat{S}}+\frac{1}{2!}[\dot{\hat{S}},\hat{S}]+\frac{1}{3!}([\dot{\hat{S}},\hat{S}],\hat{S})+\cdots \tag{4.26}$$

and writing $S^{(n)}$ in an arbitrary time-dependent basis,

$$\hat{S}^n(t) = \frac{1}{(n!)^2}\sum_{\rho_i\nu_i}\langle\rho_1\ldots\rho_n\,|\,S^n(t)\,|\,\nu_1\ldots\nu_n\rangle \times\hat{a}_{\rho_1}^\dagger(t)\ldots\hat{a}_{\rho_n}^\dagger(t)\hat{a}_{\nu_n}(t)\ldots\hat{a}_{\nu_1}(t)\ . \tag{4.27}$$

Since

$$\frac{\partial}{\partial t}\hat{a}_\alpha^\dagger = \sum_\beta\langle\beta\,|\,\dot{\alpha}\rangle\hat{a}_\beta^\dagger\ , \tag{4.28}$$

each nonvanishing term on $\dot{S}^{(m)}$ either contains an $\hat{a}_\rho^\dagger$ or $\hat{a}_\nu$ term, for which $[\hat{S}^{(m)},\hat{S}^{(n)}]=0$, or contains at most one $\hat{a}_\nu^\dagger$ or $\hat{a}_\rho$ term, in which case the commutator $[\hat{S}^m,\hat{S}^n]$ contains only $\hat{a}_{\rho_i}^\dagger$ and $\hat{a}_{\nu_i}$ operators. Hence, in any case, the multiple commutator $([\dot{\hat{S}},\hat{S}],\hat{S})$ must vanish and

$$\langle\Phi\,|\,\hat{a}_{\nu_1}^\dagger\ldots\hat{a}_{\nu_m}^\dagger\hat{a}_{\rho_m}\ldots\hat{a}_{\rho_1}e^{-\hat{S}}\frac{\partial}{\partial t}e^{\hat{S}}\,|\,\Phi\rangle = \langle\Phi\,|\,\hat{a}_{\nu_1}\ldots a_{\nu_m}^\dagger\hat{a}_{\rho_m}\ldots\hat{a}_{\rho_1}\left[\frac{\partial}{\partial t}+\dot{\hat{S}}+\frac{1}{2}[\dot{\hat{S}},S]\right]\,|\,\Phi\rangle\ . \tag{4.29}$$

Although Eq. (2.26) yields many terms, the only nonvanishing term involving the time derivative of an $S^{(n)}$ amplitude, as opposed to the derivative of a basis function

$$\langle\beta\,|\,\dot{\alpha}\rangle \text{ is } \frac{d}{dt}\langle\rho_1\ldots\rho_m\,|\,S^m(t)\,|\,\nu_1\ldots\nu_m\rangle\ .$$

Thus, Eq. (4.25) specifies $d/dt\langle\rho\,|\,S^{(1)}(t)\,|\,\nu\rangle$ in terms of known functions at time t, providing a first-order differential equation in time for the one-particle, one-hole amplitudes. In general, Eq. (4.25c) provides a first-order equation for the m-particle, m-hole amplitude, so that given initial conditions at time $t=0$, the amplitudes may be evolved in time by numerically integrating a system of first-order equations. The first equation, Eq. (4.25a), clearly plays no role in the time evolution, since no time derivatives of particle-hole amplitudes survive in the right-hand side. It could be satisfied identically by introducing an appropriate time-dependent phase in the definition of Φ, but since such an overall phase is unobservable, Eq. (4.25a) is devoid of physical content. Formally, it is satisfied identically when the order of truncation, m, equals the number of particles.

Truncation of the time-dependent hierarchy proceeds precisely as in the time-independent theory. In lowest order, setting all $S^{(n)}$'s equal to zero for $n\geq 2$ yields the TDHF approximation, which is again most readily apparent by choosing the basis in which $S^{(1)}$ is identically zero. In this case, Eq. (4.25c) becomes

$$\langle\Phi\,|\,\hat{a}_\nu^\dagger\hat{a}_\rho\left[\hat{H}-i\frac{\partial}{\partial t}\right]\,|\,\Phi\rangle = 0\ , \tag{4.30}$$

which implies the TDHF equation

$$\langle\rho\,|\,i\frac{\partial}{\partial t}\,|\,\nu\rangle = \langle\rho\,|\,h\,|\,\nu\rangle\ , \tag{4.31}$$

with h as defined in Eq. (3.17). Making the usual arbitrary choice for hole-hole matrix elements yields the more familiar form

$$i\frac{\partial}{\partial t}\,|\,\nu\rangle = h\,|\,\nu\rangle\ . \tag{4.32}$$

Truncation at $n=2$ yields two closed coupled equations for $\dot{S}^{(1)}$ and $\dot{S}^{(2)}$ in terms of $S^{(1)}$ and $S^{(2)}$ which describe the time evolution of two-body correlations, and in nth order one obtains m equations for $\dot{S}^{(1)}$ through $\dot{S}^{(m)}$.

A particulary attractive feature of the theory is the fact that solutions to the truncated time-independent equations at any order m are stationary solutions to the truncated time-dependent equations truncated at the same order by virtue of the fact that the left-hand terms of Eqs. (4.21) are identical to those of Eqs. (4.25). Thus

one immediately capitalizes upon knowledge of the perturbation theoretic content and numerical convergence of the time-independent theory. In this sense, the coupled-cluster theory retains the advantages sought in the Green's-function formulation, while retaining the simpler structure of first-order differential equations in time for amplitudes with n spatial variables, n single-particle labels, and one time argument instead of integrodifferential equations for functions with $2m$ spatial variables and up to n time variables. In addition, since the time-dependent equations reduce to the time-independent theory for stationary states, it is immediately evident how to pick initial conditions for scattering problems which are precisely commensurate with the approximations built into the dynamical equations. A final technical point is that just as the HF equations may be efficiently solved by evolution of the TDHF equations in imaginary time (Davies *et al.*, 1980) so the static coupled-cluster equations may be solved by evolving an initial guess for a wave function in imaginary time or by beginning with a solution to a one-body Hamiltonian, $H_0=T+U$, and adiabatically switching on the interaction $H'=V-U$ in the time-dependent theory.

3. Truncation for repulsive-core interactions

Whereas setting all $S^{(n)}=0$ for $n>m$ in the time-dependent coupled-cluster equations of the previous section is the formally simplest truncation procedure and is adequate for the model problem in Sec. VI, it is unsuitable in the presence of potentials with highly repulsive cores. In this section, a truncation suitable for repulsive-core interactions will be motivated physically, and the resulting coupled equations of motion for S_1 and S_2 will be presented (Hoodbhoy and Negele, 1979). Since the essential features of this truncation problem arise already in the static coupled-cluster theory, a more general presentation may be found in the review by Kümmel, Lührmann, and Zabolitzky (1978). Formally, in terms of reduced subsystem amplitudes $\chi_n^{(ij)}$ defined in that work, the general algorithm for truncation at order n is to set $\chi_{m+1}^{(ij)}=\chi_{m+2}^{(ij)}=0$ in all terms containing the two-body potential $V(x_ix_j)$ and to set the particle-hole amplitude $S_{m+1}=0$ in all other terms.

To facilitate the physical discussion of truncation at second order, it is useful to define a subsystem amplitude (Kümmel, 1974) which specifies the amplitude for finding in ψ n particles localized at positions x_1 through x_n and $A-n$ particles in single-particle states ν_{n+1} through ν_A. This subsystem amplitude is defined

$$\begin{aligned}\langle x_1\ldots x_n \mid \psi_n \mid \nu_1\ldots\nu_n\rangle &= \langle\Phi \mid \hat{a}^\dagger_{\nu_1}\ldots\hat{a}^\dagger_{\nu_n}\hat{\psi}(x_n)\ldots\hat{\psi}(x_1)\mid\psi\rangle \\ &= \langle\Phi \mid \hat{a}^\dagger_{\nu_1}\ldots\hat{a}^\dagger_{\nu_n}\hat{\psi}(x_n)\ldots\hat{\psi}(x_1)e^{\Sigma\hat{S}^{(m)}}\mid\Phi\rangle\ , \end{aligned} \tag{4.33}$$

where the particle-hole amplitudes $\hat{S}^m$ are defined in Eqs. (4.17)–(4.19). Expanding out the exponential in the last term of Eq. (4.33), it follows that

$$\langle x_1 \mid \psi_1 \mid \nu_1\rangle = \langle x_1 \mid \nu_1\rangle + \langle x_1 \mid S_1 \mid \nu_1\rangle\ , \tag{4.34a}$$

$$\langle x_1x_2 \mid \psi_2 \mid \nu_1\nu_2\rangle = \langle x_1 \mid \psi_1 \mid \nu_1\rangle\langle x_2 \mid \psi_1 \mid \nu_2\rangle - \langle x_1 \mid \psi_1 \mid \nu_2\rangle\langle x_2 \mid \psi_1 \mid \nu_1\rangle + \langle x_1x_2 \mid S_2 \mid \nu_1\nu_2\rangle\ , \tag{4.34b}$$

$$\begin{aligned}\langle x_1x_2x_3 \mid \psi_3 \mid \nu_1\nu_2\nu_3 = \mathscr{A}_\nu(&\langle x_1 \mid \psi_1 \mid \nu_1\rangle\langle x_2 \mid \psi_1 \mid \nu_2\rangle\langle x_3 \mid \psi_1 \mid \nu_3\rangle + \langle x_1x_2 \mid S_2 \mid \nu_1\nu_2\rangle\langle x_3 \mid \psi_1 \mid \nu_3\rangle \\ &+ \langle x_1x_3 \mid S_2 \mid \nu_1\nu_3\rangle\langle x_2 \mid \psi_1 \mid \nu_2\rangle + \langle x_2x_3 \mid S_1 \mid \nu_2\nu_3\rangle\langle x_1 \mid \psi_1 \mid \nu_1\rangle + \langle x_1x_2x_3 \mid S_3 \mid \nu_1\nu_2\nu_3\rangle)\ , \end{aligned} \tag{4.34c}$$

and so on, when $\mathscr{A}_\nu$ represents antisymmetrization, as in Eq. (4.34b), with respect to all ν's except those within the same S or ψ. In each order, S_n represents that part of ψ_n which cannot be decomposed into antisymmetrized products of lower amplitudes and thus physically corresponds to a correlation amplitude.

When the equations of motion implied by Eqs. (4.25) are worked out in detail, the equation for

$$\frac{d}{dt}\langle x_1\ldots x_n \mid S^n \mid \nu_1\ldots\nu_n\rangle$$

contains higher-order amplitudes involving products of the form

$$V(x,x')\langle xx'y_3\ldots y_{n+1} \mid \psi_{n+1} \mid \nu_1\ldots\nu_{n+1}\rangle\ , \tag{4.35a}$$

$$V(x,x')\langle xx'y_3\ldots y_{n+2} \mid \psi_{n+2} \mid \nu_1\ldots\nu_{n+2}\rangle\ , \tag{4.35b}$$

and

$$\mathscr{O}(x)\langle xy_2\ldots y_{n+1} \mid \psi_{n+1} \mid \nu_1\ldots\nu_{n+1}\rangle\ , \tag{4.36}$$

where $\mathscr{O}(x)$ may be the kinetic energy operator $K(x)$ or the time derivative of a single-particle wave function $\dot{\phi}^*_\nu(x)$. It is the potential terms, Eqs. (4.35), which require a modified truncation procedure in the presence of highly repulsive cores. Clearly, any exact subsystem amplitude, obtained by projecting the exact wave function onto a state localizing particles at x and x', must have the property that it goes to zero as x approaches x'. The product of this amplitude with $v(x-x')$ will then be well behaved and remain finite even when v becomes infinitely repulsive. To obtain a satisfactory truncation, this same property must be built into any approximations for subsystem amplitudes whenever they are multiplied by the two-body potential. Since $\langle xx' \mid \psi_2 \mid \nu\nu'\rangle$ satisfies a two-body equation analogous to the Bethe-Goldstone equation, it necessarily possesses the desired properties for small $(x-x')$. These same properties in $(x-x')$ may be assured in Eqs. (4.35) if one imposes an independent-pair approximation specifying that the two

particles interacting via the potential propagate independently of the others with correlation described by ψ_2. The approximation for $V\psi_3$ is thus

$$V(xx')\langle xx'y \mid \psi_3 \mid \nu_1\nu_2\nu_3\rangle \approx \mathscr{A}_\nu V(xx')\langle xx' \mid \psi_2 \mid \nu_1\nu_2\rangle\langle y \mid \psi_1 \mid \nu_3\rangle \ . \quad (4.37)$$

Comparison with Eq. (4.34c) indicates that this is different from specifying $S_3=0$, since certain products of the form $\langle xy \mid S_2 \mid \nu_i\nu_j\rangle\langle x' \mid \psi_1 \mid \nu_k\rangle$ are also omitted. Whereas antisymmetry is thereby relinquished, just those terms involving products of S's having arguments other than x and x' are dropped, so as to ensure the proper behavior for small $(x-x')$. The analogous truncation for $V\psi_4$ is

$$V(xx')\langle xx'y_1y_2 \mid \psi_4 \mid \nu_1\nu_2\nu_3\nu_4\rangle \approx \mathscr{A}_\nu V(xx')\langle xx' \mid \psi_2 \mid \nu_1\nu_2\rangle\langle y_1y_2 \mid \psi_2 \mid \nu_3\nu_4\rangle \ . \quad (4.38)$$

In contrast to these terms involving the two-body potential, there is no reason for the operator $\mathscr{O}$ in Eq. (4.36) to single out any particular pair of particles or for the behavior of small values of any relative coordinate to be relevant. Thus it is natural to use the familiar totally antisymmetric truncation for Eq. (4.36) obtained by simply specifying $S_{n+1}=0$.

Substitution of these independent-pair truncations for Eqs. (4.35) and totally antisymmetric truncations for Eq. (4.36) into the equations of motion, Eqs. (4.25), and straightforward albeit tedious algebra yield coupled first-order differential equations in time for the evolution of correlation amplitudes S_1 through S_m. The first generalization beyond TDHF arises at $m=2$. In an arbitrary basis of time-dependent orthonormal wave functions, $\phi_\nu(x,t)$, the equation of motion for ψ_1 (and thus S_1) may be written

$$i\frac{\partial}{\partial t}\langle x \mid \psi_1 \mid \nu\rangle = K(x)\langle x \mid \psi_1 \mid \nu\rangle + \sum_{\nu'}\int dx'\phi^*_{\nu'}(x')[K(x')\langle xx' \mid S_2 \mid \nu\nu'\rangle + V(xx')\langle xx' \mid \psi_2 \mid \nu\nu'\rangle] - \sum_{\nu'}\langle x \mid \psi_1 \mid \nu'\rangle h_{\nu\nu'} + i\sum_{\nu'}\int dx'\dot{\phi}^*_{\nu'}(x')(\langle xx' \mid S_2 \mid \nu\nu'\rangle - \langle x' \mid \psi_1 \mid \nu\rangle\langle x \mid \psi_1 \mid \nu'\rangle) \ , \quad (4.39)$$

where

$$h_{\nu_1\nu_2} = \int dx\, \phi_{\nu_1}(x)\left[K(x)\langle x \mid \psi_1 \mid \nu_2\rangle + \sum_\nu \int dx'\phi^*_\nu(x')V(xx')\langle xx' \mid \psi_2 \mid \nu_2\nu\rangle\right] . \quad (4.40)$$

This equation may readily be observed to have the structure of N time-dependent Brueckner-Hartree-Fock equations by considering it in the maximum overlap basis (Coester and Kümmel, 1960), in which, by definition, the $\phi_\nu(x)$'s are defined such that S_1 is identically zero and thus $\langle x \mid \psi_1 \mid \nu\rangle = \phi_\nu(x)$. The amplitude ψ_2 satisfies a time-dependent Bethe-Goldstone equation, so that $v(xx')\langle xx' \mid \psi_2 \mid \nu\nu'\rangle$ corresponds to

$$G[\phi_\nu(x)\phi_\nu(x') - \phi_\nu(x')\phi_\nu(x)] \ ,$$

and thus the second term on the right-hand side of Eq. (4.39) contains essentially the mean field arising from a G matrix. In this basis, the third term is a physically irrelevant unitary transformation among occupied-state wave functions and the last term ensures orthonormality of the time-dependent maximum overlap wave functions. The time-dependent Bethe-Goldstone equation is somewhat more lengthy, but has the structure of expressing the time derivative of S_2 in terms of S_2, S_1, and the basis functions, and thus may straightforwardly be evolved in time. Further discussion of the properties of the repulsive-core coupled-cluster equations, details of the derivations, and the final results may be found in the literature (Hoodbhoy and Negele, 1979).

In summary, the coupled-cluster expansion appears to provide the most promising theory presently available for systematically extending the TDHF approximation to include the effects of collisions and correlations. Since it involves functions with fewer spatial variables and time arguments than alternative Green's-function and density-matrix formulations, it is correspondingly easier to implement numerically. The corresponding theory for stationary states has already been evaluated, retaining amplitudes through S_3 for nuclei as heavy as ^{40}Ca, not only demonstrating satisfactory convergence and adequate treatment of repulsive cores, but also setting a scale for practical calculations. Since iteration of the static problem to self-consistency is computationally analogous to evolution in time for a comparable number of time steps, it is quite reasonable to expect that at the much simpler level of retaining only S_2, calculation of collisions for light systems should be feasible. Model calculations for one-dimensional systems would be even easier and would already begin to resolve many of the open questions concerning collision and correlation terms.

V. FUNCTIONAL INTEGRAL FORMULATION

An alternative generalization of the time-dependent mean-field approximation utilizing a functional integral representation of the many-body evolution operator resolves many of the deficiencies associated with the semiclassical aspects of the TDHF initial-value problem discussed in Sec. III.B.2.

To appreciate the power and conceptual advantages of

this functional integral approach, it is useful to briefly recall the deficiencies of conventional treatments of collective motion in nuclear physics. The first step in conventional theories is the *ad hoc* selection of collective variables, which may well be biased by some combination of technical convenience and prior knowledge of the experimental phenomena one wishes to coax the theory to reproduce. Given some set of coordinates to be imposed upon the system, canonically conjugate momenta are either derived or postulated. The next step is to obtain either by derivation or prescription an adiabatic Hamiltonian involving at most quadratic terms in the momenta and, in general, an inertial tensor and potential depending upon all the coordinates. Finally, a quantization prescription is imposed on the resulting Hamiltonians to arrive at a quantum theory of collective motion, the validity of which is difficult to assess and which is exceedingly difficult to systematically improve.

In the functional integral formulation, in contrast, one writes an exact expression for a quantum observable in terms of a functional integral over a field containing all the degrees of freedom of the one-body density matrix. In particular, the one-body density matrix contains all the shape degrees of freedom one believes to be important from semiclassical intuition, but, in addition, an infinite number of degrees of freedom are equally accessible to the theory with no *a priori* bias. A systematic approximation scheme is then obtained by application of the stationary-phase or saddle-point approximation and subsequent evaluation of higher-order corrections. The lowest-order theory is a time-dependent mean-field theory in which the coordinates, momenta, equations of motion, and quantization conditions have been simultaneously and consistently specified by the underlying Hamiltonian and the specific quantum observable under consideration. Although technical and mathematical problems certainly arise, the functional integral formalism at least offers the potential of extending the quantum theory of collective motion significantly beyond the state of the art obtained with conventional techniques. Certainly the recent achievements using analogous techniques in field theory lend further credence to this promise (Abers and Lee, 1973; Dashen, Hasslacher, and Neveu, 1974a, 1974b; Rajaraman, 1975; Faddeev, 1976; 't Hooft, 1976; Polyakov, 1977; Coleman, 1977).

The emphasis of the functional integral formalism, which develops a consistent quantum-mechanical generalization of the TDHF initial-value problem, is complementary to that of the coupled-cluster expansion, which addressed many-body correlations. Unlike the coupled-cluster theory, the present theory replaces the initial-value problem with a fully specified boundary value problem and, where appropriate, specifies quantization conditions on the dynamical variables. In doing so, however, in lowest order, it sacrifices the general treatment of many-body correlation, which was the primary objective of the coupled-cluster approach. In practical applications, it is generally obvious which of these complementary features is physically most relevant, and it remains a problem for future research to combine both these quantum and correlation reports into a single formalism, as discussed subsequently in Sec. V. H.

A. Overview

Because of the potential importance of functional integral methods, the unfamiliarity of many nuclear physicists with these techniques, and the highly technical nature of the research literature, this section will attempt to provide a detailed and pedagogical review of the functional integral approach to many-body theory. The presentation will necessarily be somewhat parochial, in that there exist a number of technically different alternative formalisms which yield very similar and often identical results. Whereas it is clearly not desirable to display all the technical details of each method, it is at least useful to sketch the essential elements of each approach. A natural compromise is to present in detail a method which makes direct contact with mean-field theory and has been utilized in recent research (Levit, Negele and Paltiel, 1980a, 1980b; Negele 1979), and only briefly to summarize the major features of alternative approaches.

1. Outline of method

The basic approach consists of five main steps. First, one selects a quantum observable to be evaluated. In view of the earlier discussion of approximation of few-body operators versus the full many-body wave function, it appears most prudent in any practical applications where only low orders of corrections to the stationary-phase approximation can realistically be evaluated, to restrict attention to expectation values of few-body operators.

Next, one expresses this observable in terms of the many-body evolution operator. Since the evolution operator contains all the information available from the full many-body Schrödinger equation, this may always be done through evaluation of an appropriate trace or level density, adiabatic switching on of an interaction, preparation of in or out states, or some other suitable construction. An example of considerable generality will be the evaluation of the expectation value of any operator $\mathcal{O}$ in an eigenstate of the many-body Hamiltonian. Following Gutzwiller (1967, 1969, 1970, 1971), one may write

$$\begin{aligned} -i\int dt\, e^{iET}\mathrm{tr}\mathcal{O}U(T,0) &= -i\int dT\, e^{iET}\sum_N \langle N\,|\,\mathcal{O}e^{-iE_NT}\,|\,N\rangle \\ &= \sum_N \frac{\langle N\,|\,\mathcal{O}\,|\,N\rangle}{E-E_N+i\eta}\,, \end{aligned} \tag{5.1}$$

where tr denotes the trace, U is the evolution operator, and $\{\,|\,N\rangle\}$ denotes a complete set of eigenstates. Thus the Fourier transform of the trace of $\mathcal{O}$ times the evolution operator yields a simple pole at each eigenvalue E_N

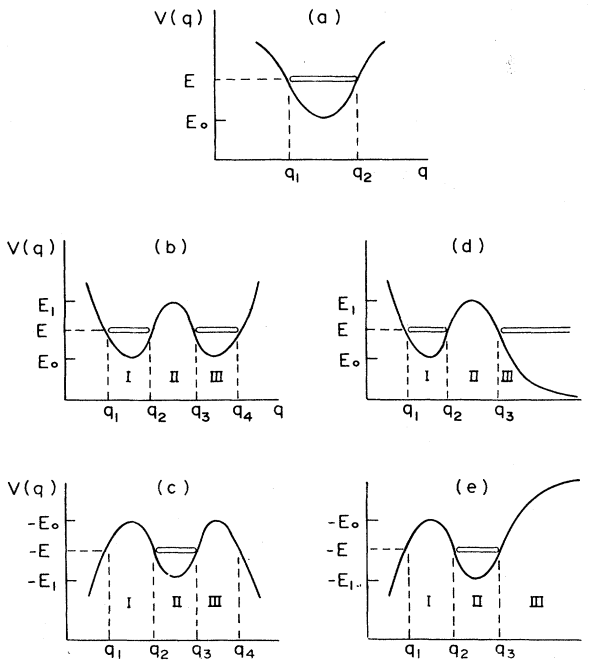

FIG. 16. Sketches of potentials $V(q)$, periodic trajectories, and turning points as discussed in the text.

with a residue equal to the expectation value of $\mathcal{O}$ in that state. For evaluation of the spectrum, $\mathcal{O}$ may simply be taken as unity.

The third step is to write a functional integral representation for the evolution operator $U(T,0)$. At this stage, the theory is formally exact, and one still has the quantum mechanics of the full many-body problem.

The fourth step, which yields the lowest-order approximation, is to apply the stationary-phase approximation (SPA) to the functional integral appearing in U, as well as to any other integrals which cannot be performed analytically, such as the time integral in Eq. (5.1). Of the infinite number of fields occurring in the exact functional integral for U, the SPA selects one or more distinct fields which render the action stationary and thus constitute the "best" fields with which to obtain a leading-order approximation to the observable of interest. In all the alternative functional integral formulations, these stationary solutions will have the physical interpretations of a mean-field theory, and the formalism presented subsequently in detail renders this mean-field physics particularly transparent. Ambiguities concerning initial conditions have no opportunity to arise in this theory, since the SPA specifies the boundary conditions as well as equations of motion for the mean field. Also, since application of the method to different problems will yield different functionals to be approximated in the SPA, each problem will give rise to a different mean-field theory.

The final step in the method is to systematically evaluate the corrections to the SPA. Formally, for problems with time-independent mean fields, one may obtain various familiar forms of perturbation expansions. A particularly interesting one is the loop expansion which provides the diagram rules for expanding the energy or expectation value of any operator in terms of fermion propagators and RPA phonon propagators. Analogous expansions exist for time-dependent problems but are sufficiently complicated that explicit numerical calculations are presently impractical.

2. Example with one degree of freedom

Before embarking on the solution of the many-body problem, it is useful to illustrate the salient elements of the method by applying it to the trivial problem of one-dimensional quantum mechanics in the potentials sketched in Fig. 16 (Levit, Negele, and Paltiel, 1980b).

To find the eigenstates in a potential $V(q)$, we set $\mathcal{O}=1$ in Eq. (5.1), evaluate the trace by integrating over a complete set of coordinate states $|q\rangle$, and utilize the Feynman path integral representation for the evolution operator (Dirac, 1933; Feynman and Hibbs, 1965; Reed and Simon, 1972) to obtain

$$\begin{aligned}\mathrm{tr}\frac{1}{E-H+i\eta} &= -i\int_0^\infty dT\, e^{iET}\int dq\langle q\,|\,e^{-iHT}\,|\,q\rangle \\ &= -i\int_0^\infty dt\, e^{iET} \\ &\quad\times\int dq\int D[q(t)]e^{iS[q(t)]}\,,\end{aligned} \tag{5.2}$$

where

$$S[q(t)]=\int_0^T dt\{\tfrac{1}{2}m\dot{q}(t)^2-V[q(t)]\} \tag{5.3}$$

is the classical action for a trajectory $q(t)$ satisfying the boundary conditions

$$q(0)=q(t)=q\ . \tag{5.4}$$

Application of the SPA to the functional integral over $q(t)$ yields

$$\langle q\,|\,e^{iS[q(t)]}\,|\,q\rangle \sim Ae^{iS[q_0(t)]}\,, \tag{5.5}$$

where q_0 is the stationary solution to the classical Euler-Lagrange equation arising from $\delta S=0$. That is, $q_0(t)$ satisfies

$$m\frac{d^2}{dt^2}q_0=-\nabla V(q_0)\,, \tag{5.6}$$

subject to the boundary condition Eq. (5.4). The factor A is the result of performing the Gaussian integral for quadratic fluctuation about $q_0(t)$, and its explicit form is immaterial to the present argument.

To apply the SPA to the integral over q in Eq. (5.2), we note that $S[q_0]$ in Eq. (5.5) depends upon q through the end points of $q_0(t)$. Since the derivative of the action with respect to the end point yields the momentum, stationarity of $S[q_0]$ requires

$$0=\frac{\partial S[q_0]}{\partial q}=\frac{\partial S[q_0]}{\partial q(t)}+\frac{\partial S[q_0]}{\partial q(0)}=p(t)-p(0)\ . \tag{5.7}$$

Thus Eq. (5.2) becomes

$$\mathrm{Tr}\frac{1}{E-H+i\eta}\approx -iA'\int_0^\infty dT\, e^{iET+S(T)} \equiv -iA'\int_0^\infty dT\, e^{iW(T)}\ , \tag{5.8}$$

where $S(T)$ is the classical action for a classical trajectory which is periodic both in coordinate q and momentum p with period T, and where an additional quadratic fluctuation factor is included in A'.

Noting that the derivative of the action with respect to the final time yields the negative of the energy, application of the SPA to the T integral in Eq. (5.8) leads to the condition

$$E=-\frac{\partial S(T)}{\partial T}=E(T)\ , \tag{5.9}$$

where $E(T)$ is the energy of a classical periodic orbit of period T. The final SPA result obtained by summing over all periods T_m which satisfy the stationarity condition Eq. (5.9) is

$$\mathrm{Tr}\frac{1}{E-H+i\eta}\approx -iA'\sum_m f_m e^{iW(T_m)}\ , \tag{5.10}$$

where f_m denotes the factor obtained by integrating the quadratic fluctuations around the stationary point T_m.

The structure of the final result, Eq. (5.10), is particularly simple for the case of a potential $V(q)$ with a single minimum as sketched in Fig. 16(a). The classical periodic trajectory may be visualized in terms of the motion of a particle constrained to move on a surface the shape of $V(q)$ in a uniform gravitational field. When it is released from position q, it executes periodic classical motion with energy E and fundamental period

$$T(E)=2\int_{q_1}^{q_2}\left[\frac{m}{2[E-V(q)]}\right]^{1/2}dq\ . \tag{5.11}$$

Clearly, any integer multiple of $T(E)$ satisfies the stationarity condition, so that $T_m=mT(E)$. Noting that the exponent in Eq. (5.10) may be written

$$W(T_m)=ET_m+\int_0^{T_m}(p\dot{q}-H)\equiv mW[T(E)]\ , \tag{5.12}$$

where

$$W[T(E)]=\int_0^{T(E)}p\dot{q}\,dt=\oint p\,dq =2\int_{q_1}^{q_2}\{2m[E-V(q)]\}^{1/2}dq\ , \tag{5.13}$$

and ignoring the factor f_n, Eq. (5.10) yields the following series:

$$\mathrm{Tr}\frac{1}{E-H+i\eta}=-iA'\sum_m (e^{i\oint W[T(E)]})^m =\frac{-iA'e^{iW[T(E)]}}{1-e^{iW[T(E)]}}\ , \tag{5.14}$$

which has poles for all energies satisfying the quantization condition

$$n\,2\pi=W[T(E)]=\oint p\,dq\ . \tag{5.15}$$

The factors f_m turn out to contribute the same magnitude for each m and a phase of $\pi/2$ for each classical turning point (Gutzwiller, 1967), so their inclusion simply changes the minus sign in the denominator of Eq. (5.14) to a plus and thereby yields the correct Bohr-Sommerfeld quantization rule (Kramers, 1926)

$$(2n+1)\pi=W(T(E))=\oint p\,dq\ . \tag{5.16}$$

The lowest state in the well thus acquires its proper zero-point energy in this approximation.

An interesting and important new feature arises in the analogous treatment of the double-well potential in Fig. 16(b). For energies between E_0 and E_1, classical periodic solutions of the form discussed above exist separately in regions I and III. The fundamental period T_{I} and reduced action W_{I} in region I are given by Eqs. (5.11) and (5.13), respectively, and the analogous expressions for region III are obtained by the appropriate change of limits. Since the SPA for the time integral in Eq. (5.8) requires summation over all the isolated stationary points in the complex T plane, in addition to all integral multiples of the real periods T_{I} and T_{III}, integral multiples of classical periodic trajectories with complex periods must also be included.

For the potential of Fig. 16(b), the existence of a classical periodic solution with purely imaginary period may be easily understood by considering the continuation of the classical equation of motion, Eq. (5.6), to imaginary time. Replacing *(it)* by τ, Eq. (5.6) may be written

$$m\frac{\partial^2}{\partial\tau^2}q_0=-\nabla[-V(q_0)]\ , \tag{5.17}$$

so that the effect of continuation to imaginary time is to replace the original classical problem by the analogous problem in the inverted potential shown in Fig. 16(c). Calculation of the stationary solution in region II corresponding to one classical oscillation from q_2 to q_3 and back and repetition of the steps performed above for real solutions gives rise to the period

$$T_{\mathrm{II}}(E)=i\,2\int_{q_2}^{q_3}\left[\frac{m}{2[V(q)-E]}\right]^{1/2}dq \tag{5.18}$$

and a contribution to the trace of $e^{-W_{\mathrm{II}}}$, where

$$W_{\mathrm{II}}=2\int_{q_2}^{q_3}\{2m[V(q)-E]\}^{1/2}dq\ . \tag{5.19}$$

A general periodic trajectory in the double well of Fig. 16(b) is thus comprised of any number of closed orbits in

each of the three regions connected in any order, so that the SPA approximation Eq. (5.10) is generalized to

$$\mathrm{Tr}\frac{1}{E-H+i\eta}\approx -iA'\sum_{klm} f_{klm} e^{ikW_{\mathrm{I}}(E)} e^{-lW_{\mathrm{II}}(E)} e^{imW_{\mathrm{III}}(E)} . \tag{5.20}$$

The technical question of phases in the quadratic correction factor f_{klm} is addressed by Bender *et al.* (1978), with the result that f_{klm} is a constant times $(-1)^{k+l+m}$. Calculating the sum over all trajectories beginning in any of the three regions and containing all combinations of cycles in each region yields

$$\begin{aligned}\mathrm{Tr}\frac{1}{E-H+i\eta} \propto & \sum_{n=1}^{\infty}\left[-e^{iW_{\mathrm{I}}}\sum_{m=0}^{\infty}\left[-e^{-W_{\mathrm{II}}}\sum_{l=0}^{\infty}(-e^{iW_{\mathrm{III}}})^l\right]^m\right]^n + \sum_{m=1}^{\infty}\left[\sum_{n=0}^{\infty}(-e^{iW_{\mathrm{I}}})^n(-e^{-W_{\mathrm{II}}})\sum_{l=0}^{\infty}(-e^{iW_{\mathrm{III}}})^l\right]^m \\ & + \sum_{n=1}^{\infty}\left[-e^{iW_{\mathrm{III}}}\sum_{m=0}^{\infty}\left[-e^{-W_{\mathrm{II}}}\sum_{l=0}^{\infty}(-e^{iW_{\mathrm{III}}})^l\right]^m\right]^n \\ = & \frac{-2e^{i(W_{\mathrm{I}}+W_{\mathrm{III}})}-e^{iW_{\mathrm{I}}}-e^{-W_{\mathrm{II}}}-e^{iW_{\mathrm{III}}}}{(1+e^{iW_{\mathrm{I}}})(1+e^{iW_{\mathrm{III}}})+e^{-W_{\mathrm{II}}}} .\end{aligned} \tag{5.21}$$

Two special cases of the general double-well problem are of particular interest. For the symmetric double well, $W_{\mathrm{II}}=W_{\mathrm{III}}$ and we may recover the familiar WKB expression for the splitting of the nearly degenerate even- and odd-parity states. In lowest approximation, if the central barrier were very high, the problem of Fig. 16(b) would reduce to a degenerate pair of single-well problems, yielding degenerate solutions satisfying Eq. (5.16):

$$W_{\mathrm{I}}(E_n^{(0)})=(2n+1)\pi , \tag{5.22}$$

where $E_n^{(0)}$ denotes the zeroth approximation to the nth eigenstate. This result follows immediately from the SPA result, Eq. (2.21), since in the case of a high barrier, W_{II} is very large, rendering $e^{-W_{\mathrm{II}}}$ exponentially small, and the denominator reduces to double poles at energy $E_n^{(0)}$. In next approximation, we may write $E_n=E_n^0+\Delta E_n$ and expand the condition for a pole in Eq. (5.21),

$$(1+e^{iW_{\mathrm{I}}(E_n^0+\Delta E_n)})^2=-e^{-W_{\mathrm{II}}(E_n^0+\Delta E_n)} , \tag{5.23}$$

to first order in E_n. Using Eq. (5.22), noting from Eqs. (5.11) and (5.13) that

$$\frac{\partial W(E)}{\partial E}=T=\frac{2\pi}{\omega} ,$$

and observing that $e^{-W_{\mathrm{II}}(E_n^0)}\Delta E_n$ is second-order small, we obtain

$$\left[\frac{\partial W_1}{\partial E}\Delta E_n\right]^2\approx e^{-W_2(E_n^0)} , \tag{5.24}$$

which yields the familiar WKB result for the energy splitting

$$E_n\approx E_n^0\pm\frac{\omega}{2\pi}e^{-W_2(E_n^0)/2} . \tag{5.25}$$

Thus, in this application, the dominant quantum effects in the classically forbidden region, region II, have been reproduced in the SPA through the periodic stationary solutions corresponding to imaginary time.

A second application, closer in spirit to our subsequent treatment of tunneling decay, is obtained by distorting the right-hand well to extend to the edge of an arbitrarily large normalization box, yielding the potential for a metastable state sketched in Fig. 16(d) (Levit, Negele, and Paltiel, 1980b; Patrascioiu, 1981; Lapedes and Mottola, 1982). The lifetime is obtained by evaluating the smoothed level density, defined as the imaginary part of Eq. (5.2) with the infinitesimal η replaced by a finite width γ, such that γ is smaller than any physical width but larger than the level spacing in the normalization box. In this case, we obtain periodic stationary solutions in region I as before, and in lowest approximation these yield the result Eq. (5.22) for the energies of the quasistable states. Also, as in the case of the symmetric potential, periodic imaginary-time trajectories are obtained in region II, corresponding to solution of the classical equations of motion in the inverted potential sketched in Fig. 16(e). The role of periodic solutions in region III is quite different in the present problem, and one may show that $e^{iW_{\mathrm{III}}}$ yields negligibly small contributions.

Thus the smoothed density of states has poles at complex energies $E_n^0+\Delta E_n$ satisfying

$$1+e^{iW_{\mathrm{I}}(E_n^0+\Delta E_n)}=e^{-W_{\mathrm{II}}(E_n^0+\Delta E_n)} , \tag{5.26}$$

and expansion to first order in ΔE_n as before yields

$$\Delta E_n=-\frac{i\Gamma_n}{2} , \tag{5.27}$$

where

$$\Gamma_n=2\frac{\omega(E_n)}{2\pi}e^{-W_2(E_n)} . \tag{5.28}$$

Near E_n, the level density is therefore proportional to

$$\left[(E-E_n)^2+\left[\frac{\Gamma_n}{2}\right]^2\right]^{-1} ,$$

so that Γ_n is the inverse lifetime of the metastable state. To within the factor of 2, which is presumably corrected by a careful evaluation of all corrections to the SPA, Eq. (5.28) is recognized as the familiar WKB formula for tunneling decay of a metastable state.

This simple example from one-dimensional quantum mechanics, which of course could be solved much more easily by conventional techniques, turns out to embody all the essential features of our subsequent treatment of the eigenstates of large-amplitude collective motion and tunneling decay of quantum many-body systems. In particular, application of the basic steps in our systematic procedure yields periodic equations of motion evolving in either real or imaginary time. Calculation of an appropriate action specified in terms of these stationary solutions then provides the necessary information to extract the leading approximation to the spectrum of bound states, and energies and lifetime of quasistable states.

3. Limitations

Whereas the functional integral formulation offers the compelling conceptual advantages emphasized above, it is not without its own problems and limitations.

The most salient problem of physical concern is the absence, except in specifically constructed models, of an explicit small parameter in which to generate an asymptotic expansion. For purposes of discussion, it is useful to consider the familiar Laplace method for generating an asymptotic expansion for the integral

$$I(\varepsilon)=\int dx\, g(x)e^{-(1/\varepsilon)f(x)} . \tag{5.29}$$

Expanding $f(x)$ and $g(x)$ about the point x_0 at which $f(x)$ is a minimum, expanding all terms other than $f''(x)$ in the resulting exponent, and integrating the resulting products of polynomials multipled by a Gaussian yield the series

$$\begin{aligned} I(\varepsilon)\approx & g(x_0)e^{-f(x_0)/\varepsilon}\left[\frac{2\pi\varepsilon}{f''(x_0)}\right]^{1/2} \\ & \times\left[1+\varepsilon\left[\frac{g''(x_0)}{2g(x_0)f''(x_0)}-\frac{f''''(x_0)}{8[f''(x_0)]^2}\right.\right. \\ & \left.\left.-\frac{g'(x_0)f'''(x_0)}{2g(x_0)[f''(x_0)]^2}+\frac{5[f'''(x_0)]^2}{24[f''(x_0)]^3}\right]+\mathcal{O}\varepsilon^2\right] . \end{aligned} \tag{5.30}$$

It is clearly desirable for the functional integrals we utilize to have a form analogous to Eq. (5.29) with an explicit parameter corresponding to ε. One such alternative is a semiclassical expansion in powers of $\hbar$. The example in the last section of one-dimensional quantum mechanics was such an expansion. Explicitly including the factors of $\hbar$ normally suppressed for economy, the functional integral $\int D[q]e^{i/\hbar S(q)}$ is directly analogous to Eq. (5.30), with $\hbar$ playing the role of the expansion parameter ε. Unfortunately, although the exponents of the many-body functional integrals may be written explicitly to contain a multiplicative factor of $1/\hbar$, they will also contain additional $\hbar$ dependence, rendering a strict semiclassical expansion impossible.

A second alternative would be to generate a $1/N$ expansion. One may imagine a class of theories which differ from one another both by their interaction strength and the spin degeneracy N in some spin degrees of freedom. In certain special cases, requiring that the class of theories has a sensible limit for large N specifies the N dependence of the interaction strength and allows one to rescale the integration variables such that an explicit factor of N will multiply the action. The resulting formal expansion in powers of $1/N$ may then be useful if the physical Hamiltonian embodies a sufficiently high spin degeneracy. The question thus arises whether in nuclear physics one might attempt to formulate such an argument on the basis of the spin-isospin degeneracy of four. Unfortunately, when such a $1/N$ expansion is carried out, the leading contribution to the potential energy, the direct Hartree potential, is considerably weaker than the Fock exchange term, which formally should be a factor of $1/N$ smaller. Although we will later examine a model in Sec. VI which does admit a $1/N$ expansion, there appears no way, at present, to motivate a $1/N$ expansion for a realistic nuclear Hamiltonian.

The lack of an explicit expansion parameter does not necessarily preclude application of the SPA or saddle-point approximation. Indeed, the functional integrals we evaluate may well possess saddle points with very large second derivatives in the directions of steepest descent, giving rise to useful and accurate low-order approximations. For example, in the case of very collective states, it seems physically plausible that many particles participate in motion characterized by the appropriate collective variable, and that the action for this variable is thus multiplied by a suitably large constant reflecting this collectivity. However, in this case, there is as yet no quantitative measure of the accuracy of the expansion.

A second aspect associated with the lack of expansion parameter is the freedom to write a variety of different exact expressions, each of which yields a different SPA lowest-order approximation. For example, in Eq. (5.29), if we set $\varepsilon=1$, there is no criterion by which to decide that f belongs in the exponent instead of $f\ln(g)$ or any other arbitrary decomposition of the integrand. Much more freedom exists in the many-body case, as we shall see below, with the result that we can arrange for the SPA to yield a mean field of the Hartree, Fock, or pairing form, as well as any reasonable or even unreasonable combinations of these forms. Pragmatically, one may be guided by physical arguments and the minimization of corrections to the SPA, but formally the theory suffers from the lack of an explicit expansion parameter.

In addition to these formal considerations, there are serious practical limitations associated with evaluating

even the Gaussian integrals arising in the SPA. As we shall see in the next section, generalization of Eq. (5.30) to many degrees of freedom replaces $f''(x_0)$ by the determinant of the second functional derivative of the action. In a problem involving only one nontrivial space-time dimension, whether the functional depends upon functions of time, functions of one spatial dimension, or functions of one variable parametrizing symmetric behavior in space and time, simple techniques exist for evaluation of the resulting determinants (Coleman, 1977). In a time-independent application with three spatial degrees of freedom, however, the problem is equivalent to solution for all the eigenvalues of the random-phase approximation (RPA). Including time dependence further complicates the problem to a four-dimensional generalization of the familiar RPA problem.

Thus, although it is straightforward to generate formal expressions corresponding to the multidimensional generalization of the term

$$\left[\frac{2\pi\varepsilon}{f''(x_0)}\right]^{1/2} g(x_0)e^{-f(x_0)/\varepsilon}$$

in Eq. (5.30), it is usually practical to explicitly calculate only the stationary contribution $g(x_0)e^{-f(x_0)/\varepsilon}$. The significance of omitting the Gaussian integral may be seen by rearranging Eq. (5.30) to obtain the logarithm of $I(\varepsilon)$:

$$\ln I(\varepsilon)\approx\frac{1}{\varepsilon}[-f(x_0)]+\frac{1}{2}\ln\left[\frac{2\pi g^2(x_0)\varepsilon}{f''(x_0)}\right]+\varepsilon A+\mathcal{O}\varepsilon^2\,, \tag{5.31}$$

where A denotes the coefficient of ε in Eq. (5.30). Thus the stationary contribution yields the correct $1/\varepsilon$ leading behavior $\ln I(\varepsilon)$, and evaluation of the Gaussian integral includes corrections which are formally of order $\ln\varepsilon$. In a departure from the usual mathematical usage, we shall refer to evaluation of the stationary contribution $g(x_0)e^{-f(x_0)/\varepsilon}$ as the SPA, and refer to the factor $[2\pi\varepsilon/f''(x_0)]$ as the quadratic correction. In this terminology, then, the SPA yields the dominant $1/\varepsilon$ behavior of $\ln I(\varepsilon)$, the quadratic correction yields the $\ln\varepsilon$ correction, and higher-order corrections yield terms of order ε and higher. We have already seen in the example in the last section that the simple SPA yielded a meaningful first approximation. For example, the SPA quantization condition Eq. (5.15) yielded the same structure and qualitative behavior as the quadratically corrected expression Eq. (5.16). It is reasonable to expect, therefore, that in subsequent applications, omission of multiplicative determinantal factors which are impractical to evaluate still yields a meaningful first approximation. This expectation is further strengthened by the fact that the resulting theory reduces to well-known useful approximations in certain limits. In any event, for the pedagogical purposes of this review, it does not appear worthwhile to become excessively mired in the technical details of evaluation of quadratic corrections; and for these specialized details, the reader is referred to the original literature.

A final limitation to bear in mind is the problem of the effective interaction. Since, as demonstrated below, the SPA and its systematic corrections generate the full perturbation expansion, the method in principle includes all the two-body ladders and higher correlations wihch are to be included in the effective interaction. Although formal methods to treat these higher-order terms are discussed, no practical calculation has yet been implemented, so the pragmatic approximation adapted at present is to utilize the effective Skyrme-like interactions motivated by our present understanding of the ground-state problem. Although the aesthetic deficiencies of this approximation are all too obvious, as discussed previously, there are strong physical grounds for expecting the effective interaction for low-energy dynamics to be very well approximated by that derived for the nuclear ground state.

B. The auxiliary field

To obtain a functional integral representation of the many-body evolution operator, it will prove useful to rearrange the nuclear Hamiltonian as follows:

$$\begin{aligned} H&=\sum_{\alpha\beta}T_{\alpha\beta}\hat{a}_\alpha^+\hat{a}_\beta+\tfrac{1}{2}\sum_{\alpha\beta\gamma\delta}v_{\alpha\beta\gamma\delta}\hat{a}_\alpha^+\hat{a}_\beta^+\hat{a}_\delta\hat{a}_\gamma \\ &\equiv\sum_{\alpha\beta}K_{\alpha\beta}\hat{\rho}_{\alpha\beta}+\tfrac{1}{2}\sum_{\alpha\beta\gamma\delta}v_{\alpha\beta\gamma\delta}\hat{\rho}_{\alpha\gamma}\hat{\rho}_{\beta\delta}\,, \end{aligned} \tag{5.32}$$

where

$$\hat{\rho}_{\alpha\gamma}\equiv\hat{a}_\alpha^+\hat{a}_\gamma \tag{5.33}$$

and

$$K_{\alpha\delta}\equiv T_{\alpha\delta}-\tfrac{1}{2}\sum_\beta v_{\alpha\beta\beta\delta}\,. \tag{5.34}$$

The unphysical self-interaction term arising from anticommuting the annihilation operators in the normal-ordered two-body interaction which has formally been grouped with the kinetic energy in K will ultimately be removed from the theory. Transforming to the interaction representation by defining time-dependent operators which include evolution under the one-body operator $\hat{K}\equiv\sum_{\alpha\beta}K_{\alpha\beta}\hat{\rho}_{\alpha\beta}$, the density operator becomes

$$\hat{\rho}_{\alpha\beta}(t)\equiv e^{i\hat{K}t}\hat{\rho}_{\alpha\beta}e^{-i\hat{K}t}\,, \tag{5.35}$$

and the full many-body evolution operator in the interaction representation may be written

$$U_I(t_f,t_i)=T_t\exp\left[-\frac{i}{2}\int_{t_i}^{t_f}dt\sum_{\alpha\beta\gamma\delta}\hat{\rho}_{\alpha\gamma}(t)v_{\alpha\beta\gamma\delta}\hat{\rho}_{\beta\delta}(t)\right]. \tag{5.36}$$

To avoid notational confusion, in this section I shall affix a subscript to the time ordering operator T_t to indicate the variable with respect to which operators are ordered, denote the kinetic energy operator as $\hat{T}$, its matrix elements as $T_{\alpha\beta}$ or $T(x)$, and reserve the symbol T for the period of a periodic solution.

The problem of evaluating the trace of the evolution

operator involving the exponential of a two-body operator is structurally analogous to calculation of the partition function of a system containing two-body interactions. Thus it is useful to utilize a technique first introduced by Stratonovich (1957) and Hubbard (1959) for the case of statistical mechanics and recently applied to the nuclear many-body problem by Kleinert (1977, 1978) and by Levit (1980). These authors introduce an integral over an auxiliary field to reduce the exponential of a two-body operator to a functional integral over an infinite set of exponentials of one-body operators. The advantage of this transformation is that the trace of the exponential of one-body operators may be evaluated easily, and the resulting functional integral may be approximated utilizing the SPA.

The introduction of the auxiliary field is based on the familiar Gaussian integrals for the exponential of a quadratic form specified by a real symmetric matrix $A_{mn'}$

$$\int \prod_m \frac{d\sigma_m}{(2\pi i)^{1/2}} \exp\left[\frac{i}{2}\sum_{mm'}\sigma_m A_{mm'}\sigma_{m'}\right]\begin{Bmatrix}1\\ \sigma_i\sigma_j\end{Bmatrix} = (\det A)^{-1/2}\begin{Bmatrix}1\\ iA^{-1}_{ij}\end{Bmatrix}. \quad (5.37a,b)$$

These identities follow immediately from performing an orthogonal transformation to bring A into diagonal form, noting that its Jacobian is unity, and performing the independent Gaussian integrals to obtain the product of the inverses of the square roots of the eigenvalues, which yields $(\det A)^{1/2}$. Shifting each variable of integration σ_m by the constant ρ_m and rearranging Eq. (5.37a) yields

$$\exp\left[-\frac{i}{2}\sum_{mm'}\rho_m A_{mm'}\rho_{m'}\right] = (\det A)^{1/2}\int\prod_m\frac{d\sigma_m}{(2\pi i)^{1/2}}\exp\left[\frac{i}{2}\sum_{mm'}\sigma_m A_{mm'}\sigma_{m'}\right]\exp\left[-i\sum_{mm'}\sigma_m A_{mm'}\rho_{m'}\right]. \quad (5.38)$$

For noncommuting operators $\hat{\rho}$, an analogous result may by obtained to leading order in Δt, where $A_{mm'}\equiv V_{mm'}\Delta t$, by expanding the exponential $\exp(-i\Delta t\sum_{mn}\sigma_m V_{mn}\hat{\rho}_n)$ and performing the Gaussian integrals using Eqs. (5.37). Noting that only even powers of σ are nonvanishing and retaining all factors of Δt yields

$$\begin{aligned}
&\int\prod_m\frac{d\sigma_m}{(2\pi i)^{1/2}}\exp\left[\frac{i}{2}\Delta t\sum_{mn}\sigma_m V_{mn}\sigma_n\right]\exp\left[-i\Delta t\sum_{mn}\sigma_m V_{mn}\hat{\rho}_n\right]\\
&\quad=\int\prod_m\frac{d\sigma_m}{(2\pi i)^{1/2}}\exp\left[\frac{i}{2}\Delta t\sum_{mn}\sigma_m V_{mn}\sigma_m\right]\left[1+\frac{1}{2}\left[i\Delta t\sum_{mn}\sigma_m V_{mn}\hat{\rho}_n\right]^2+\mathcal{O}(\Delta t^4)\right]\\
&\quad=\det(\Delta t V)^{-1/2}\left[1-\frac{i}{2}\sum_{\substack{mm'\\nn'}}(\Delta t V)^{-1}_{mm'}\Delta t V_{mn}\hat{\rho}_n\Delta t V_{m'n'}\hat{\rho}_{n'}+\mathcal{O}(\Delta t^2)\right]\\
&\quad=\det(\Delta t V)^{1/2}\left[\exp\left[-\frac{i}{2}\Delta t\sum_{nn'}\hat{\rho}_n V_{nn'}\hat{\rho}_{n'}\right]+\mathcal{O}(\Delta t)^2\right], \quad (5.39)
\end{aligned}$$

which is equivalent to Eq. (5.38) to leading order. To recover the evolution operator U_I the time interval is broken up into small discrete steps such that $t_l = l\Delta t$ and a time-ordered product of identities of the form (5.39) is constructed. Letting the index m denote α, β, and t_l, where α and β represent a complete set of spin, isospin, and spatial quantum labels, the following notation is convenient for the continuum limit:

$$\begin{aligned}
&\sigma_m\to\sigma_{\alpha\beta}(t_l),\\
&\hat{\rho}_m\to\hat{\rho}_{\alpha\beta}(t_l), \quad (5.40)\\
&A_{mm'}\to A_{\alpha\beta;\alpha'\beta'}(t_l,t_{l'})(\Delta t)^2,
\end{aligned}$$

and

$$\sum_l \Delta t f(t_l)\to\int dt\, f(t). \quad (5.41)$$

Taking the continuum limit, which is discussed in detail by Kerman, Levit, and Troudet (1982), yields the result

$$U_I(t_f,t_i)\equiv T_t\exp\left[-\frac{i}{2}\int_{t_i}^{t_f}dt\{\hat{\rho}(t)v\hat{\rho}(t)\}\right] = \int D[\sigma]\exp\left[\frac{i}{2}\int_{t_i}^{t_f}dt\{\sigma(t)v\sigma(t)\}U^{\sigma}_I(t_f,t_i)\right], \quad (5.42)$$

where

$$U^{\sigma}_I(t_f,t_i)\equiv T_t\exp\left[-i\int_{t_i}^{t_f}dt\{\sigma(t)v\hat{\rho}(t)\}\right], \quad (5.43)$$

the measure is defined

$$\int D[\sigma]\equiv\det[v\delta]\prod_{\alpha\beta l}\int\left[\frac{\Delta t\, d\sigma_{\alpha\beta}(t_l)}{(2\pi i)^{1/2}}\right], \quad (5.44)$$

and the curly brackets denote matrix sums of the form

$$\{\hat{\rho}(t)v\hat{\rho}(t)\}\equiv\sum_{\alpha\beta\alpha'\beta'}\hat{\rho}_{\alpha\beta}(t)v_{\alpha\alpha'\beta\beta'}\hat{\rho}_{\alpha'\beta'}(t). \quad (5.45)$$

Although the interaction representation was useful in deriving the functional integral representation, Eq. (5.43), it will be convenient in evaluation of the trace in Eq. (5.1) and for obtaining equations of motion for wave functions to transform back to the Schrödinger representation:

$$U_s(t_f,t_i)=\int D[\sigma]\exp\left[\frac{i}{2}\int_{t_i}^{t_f}dt\{\sigma(t)v\sigma(t)\}\right]U_s^{\sigma}(t_f,t_i)\ , \tag{5.46}$$

where

$$U_S^{\sigma}(t_f,t_i)=T_t\exp\left[-i\int_{t_i}^{t_f}dt\,\hat{h}_{\sigma}(t)\right] \tag{5.47}$$

and

$$\hat{h}_{\sigma}(t)=\sum_{\alpha\beta}\left[\hat{K}_{\alpha\beta}+\sum_{\alpha'\beta'}\sigma_{\alpha'\beta'}(t)v_{\alpha'\alpha\beta'\beta}\right]\hat{a}_{\alpha}^{\dagger}\hat{a}_{\beta}\ . \tag{5.48}$$

In addition to Eq. (5.42), a second useful relation follows from Eq. (5.38). For a general matrix A, which is not necessarily diagonal in time, setting $\rho_m=0$, taking the continuum limit, and using the fact that the measure in (5.44) is defined relative to $v\delta$, Eq. (5.38) yields

$$\int d[\sigma]\exp\left[i/2\int dt\,dt'\sum_{\alpha\beta\alpha'\beta'}\sigma_{\alpha\beta}(t)A_{\alpha\beta,\alpha'\beta'}(t,t')\sigma_{\alpha'\beta'}(t')\right]=\left[\frac{\det(v\delta)}{\det A}\right]^{1/2}\ . \tag{5.49}$$

This result will be useful in evaluating quadratic corrections to the SPA.

It is important that the significance of Eq. (5.46) not be overlooked in the proliferation of new notation and definitions. The evolution operator U_s^{σ} describes the evolution with respect to a one-body time-dependent Hamiltonian $\hat{h}_{\sigma}$ parametrized by the auxiliary field $\sigma(t)$. Equation (5.46) simply states that the exact evolution operator is obtained by multiplying U_S^{σ} by a functional of $\sigma(t)$ and integrating over all σ. Thus, as desired, evolution under the influence of a two-body potential has been reduced to a functional integral over evolution operators involving only a one-body potential.

Evaluation of the trace of U_s requires calculating matrix elements of Eq. (5.46) for a complete set of states $|\psi_n\rangle$. Applying the SPA separately to each matrix element yields

$$\mathrm{Tr}U_S(t_f,t_i)\approx\sum_N\int D[\sigma]\exp\left[i\left[S_N[\sigma^0]+\int dt\int dt'\sum_{\alpha\beta\alpha'\beta'}\frac{\delta^2S_N}{\delta\sigma_{\alpha\beta}(t)\delta\sigma_{\alpha'\beta'}(t')}(\sigma_{\alpha\beta}(t)-\sigma^0_{\alpha\beta}(t))[\sigma_{\alpha'\beta'}(t')-\sigma^0_{\alpha'\beta'}(t')]\right]\right]$$

$$=\sum_N\left[\frac{\det(v\delta)}{\det\dfrac{\delta^2S_N}{\delta\sigma\,\delta\sigma}}\right]^{1/2}e^{iS_N[\sigma^0]}\ , \tag{5.50}$$

where

$$S_N[\sigma]\equiv\tfrac{1}{2}\int dt\{\sigma(t)v\sigma(t)\}-i\ln\left\langle\Psi_N\left|T_t\exp\left[-i\int_{t_i}^{t_f}dt\,h_{\sigma}(t)\right]\right|\Psi_N\right\rangle \tag{5.51}$$

and σ^0 satisfies the condition $\delta S_n[\sigma]/\delta\sigma=0$. Utilizing the definition Eq. (5.48), stationarity of Eq. (5.48) yields the result

$$\sigma^0_{\alpha\beta}(t)=\frac{\left\langle\Psi_N\left|T_t\hat{\rho}_{\alpha\beta}(t)\exp\left[-i\int_{t_i}^{t_f}dt\,\hat{h}_{\sigma}(t)\right]\right|\Psi_N\right\rangle}{\left\langle\Psi_N\left|T_t\exp\left[-i\int_{t_i}^{t_f}dt\,\hat{h}_{\sigma}(t)\right]\right|\Psi_N\right\rangle}\ . \tag{5.52}$$

Although in the Schrödinger representation $\hat{\rho}_{\alpha\beta}\equiv a_{\alpha}^{\dagger}a_{\beta}$ has no explicit time dependence, a time parameter is introduced in Eq. (5.52) so that the time-ordering operator T_t places $\hat{\rho}_{\alpha\beta}(t)$ at the correct position t in the h_{σ} integral. Choosing the basis $|\Psi_n\rangle$ to be a set of determinants of eigenfunctions ψ of $U_s^{\sigma^0}$, as will be constructed explicitly below, the stationary solution of σ^0 is the one-body density matrix

$$\sigma^0_{\alpha\beta}(t)=\rho_{\beta\alpha}(t)=\sum_j\psi_j^*(\alpha,t)\psi_j(\beta,t)\ . \tag{5.53}$$

Using this expression for σ^0, we note from Eqs. (5.47) and (5.48) that the evolution operator for the stationary solution, $U_s^{\sigma^0}$, describes evolution in the one-body potential

$$W_{\alpha'\beta'}(t)=\sum_{\alpha\beta}v_{\alpha\alpha'\beta\beta'}\rho_{\beta\alpha}(t)\ . \tag{5.54}$$

Comparison with Eq. (3.18a) indicates this is just the direct term of the familiar TDHF mean field. Thus, at the level of the SPA, the approximate evolution operator is directly related to the familiar mean-field theory. Of all the σ's which in principle must be included to obtain the exact evolution operator, the most important one, in the SPA sense, is the self-consistent one-body density matrix specified by the eigenfunctions of U^{σ^0}. The potential defining U^{σ^0}, in turn, is the direct Hartree contribution, Eq. (5.52), defined by this same one-body density matrix.

Thus far, at the expense of rather cumbersome notation, the full generality of the spatial, spin, and isospin dependence of the one-body density operator $\hat{\rho}_{\alpha\beta}(t)$ has been retained. Except for the subsequent presentation in Sec. V.D of how to obtian the Hartree-Fock approximation instead of the present Hartree theory, this generality is superfluous and provides a significant impediment to displaying the essential structure of the theory. Hence, it is useful to suppress spin and isospin variables, specialize to the case of a local potential specified by Eq. (3.17), and use coordinate representation. In this case, the labels α and β associated with $\hat{\rho}_{\alpha\beta}(t)$ may be replaced by a single spatial coordinate r so that only the diagonal density operator $\hat{\rho}(r)=\psi^{\dagger}(r)\psi(r)$ and a local field, $\sigma(r,t)$, contribute. Equation (5.45) is replaced by

$$[\hat{\rho}(t)v\hat{\rho}(t)]\equiv\int d^3r\,d^3r'\hat{\rho}(r,t)v(r-r')\hat{\rho}(r',t)\ , \tag{5.55}$$

the mean field, Eq. (5.54) becomes

$$W(r,t)=\int d^3r'v(r-r')\rho(r',t)\ , \tag{5.56}$$

and the single particle Hamiltonian becomes

$$\hat{h}_{\sigma}(t)=\hat{T}+\int d^3r\left[-\frac{1}{2}v(0)+\int d^3r'\sigma(r',t)v(r-r')\right]\times\psi^{*}(x)\psi(x)\ . \tag{5.57}$$

The operator $\hat{h}_0(t)$ in Eq. (5.57) is the second quantized representation of the one-body operator

$$\hat{h}_{\sigma}(t)=\sum_i h_{\sigma}(r_i,t)\ , \tag{5.58}$$

where $h_{\sigma}(r_i,t)$ is the one-body Hamiltonian

$$h_{\sigma}(r,t)=-\frac{1}{2m}\nabla_r^2-\frac{1}{2}V(0)+\int d^3r'\sigma(r',t)v(r-r')\ . \tag{5.59}$$

In the subsequent presentation, both the context and the distinction between curly brackets in Eq. (5.45) and square brackets in Eq. (5.55) should distinguish the simple Hartree equations from the general case.

C. Calculation of quantum eigenstates

We are now prepared to approximate eigenstates of a quantum many-body system in a manner analogous to that in Sec. V.A.2 for a system having one degree of freedom.

1. Periodic solutions

It is convenient to write the trace in Eq. (5.50) in the Schrödinger representation for a symmetric time interval

$$\mathrm{Tr}U(T/2,-T/2)=\sum_N\int d[\sigma]\exp\left[\frac{i}{2}\int_{-T/2}^{T/2}dt[\sigma(t)v\sigma(t)]\right]\left\langle\Psi_N\left|T_t\exp\left[-i\int_{-T/2}^{T/2}dt\,\hat{h}_{\sigma}(t)\right]\right|\Psi_N\right\rangle \tag{5.60}$$

and to define single-particle wave functions which evolve with the single-particle Hamiltonian, Eq. (5.59):

$$\psi_k(r,t)\equiv U_s^{\sigma}(t,-T/2)\psi_k(r,-T/2)\equiv T_t\exp\left[-i\int_{-T/2}^{t}dt'h(r,t')\right]\psi_k(r,-T/2)\ . \tag{5.61}$$

The trace in Eq. (5.60) is conveniently evaluated by defining the states $|\Psi_N\rangle$ to be determinants comprised of the eigenfunctions of the single-particle evolution operator on the interval $(+T/2,-T/2)$

$$T_t e^{-i\int_{-T/2}^{T/2}dt'h_{\sigma}(r,t')}\psi_k(r,-T/2)=e^{-i\alpha_k(\sigma,T)}\psi_k(r,-T/2)\ , \tag{5.62}$$

where α is real, since the single-particle evolution operator is unitary. Letting $\{n\}$ denote the occupation numbers of the single-particle wave functions included in the determinant Ψ_N, Eq. (5.60) may be written

$$\mathrm{Tr}U(T/2,-T/2)=\sum_{\{n\}}\int D[\sigma]\exp\left[\frac{i}{2}\int_{-T/2}^{T/2}dt[\sigma(t)v\sigma(t)]-i\sum_{k\epsilon\{n\}}\alpha_k(\sigma,T)\right]\ . \tag{5.63}$$

Equations (5.61) and (5.62) are equivalent to the boundary-value problem

$$i\frac{\partial}{\partial t}\psi_k(r,t)=h_{\sigma}(t)\psi_k(r,t)\ , \tag{5.64}$$

with the boundary condition

$$\psi_k(r,T/2)=e^{-i\alpha(\sigma,T)}\psi_k(r,-T/2)\ . \tag{5.65}$$

Defining new single-particle functions with a phase factor removed,

$$\phi_k(r,t)\equiv e^{i\alpha_k(\sigma,T)(t/T)}\psi_k(r,t)\ , \tag{5.66}$$

one obtains the equivalent boundary-value problem

$$\left[i\frac{\partial}{\partial t}-h_{\sigma}(t)\right]\phi_k(r,t)=\frac{\alpha_k(\sigma,T)}{T}\phi_k(r,t)\ , \tag{5.67}$$

with the periodic boundary condition

$$\phi_k(r,T/2)=\phi_k(r,-T/2)\ . \tag{5.68}$$

At this point, the stationary sigma field σ^0 may be obtained from Eq. (5.52), as in the last section, or equivalently from variation of the exponent of Eq. (5.63)

$$S_{\{n\}}[\sigma]\equiv\tfrac{1}{2}\int_{-T/2}^{T/2}dt[\sigma(t)v\sigma(t)]-\sum_{k\epsilon\{n\}}\alpha_k(\sigma,T)\ . \tag{5.69}$$

This latter expression is particularly useful in setting the stage for continuation to imaginary time and for subsequent variation with respect to the period. The functional derivative of $\alpha_k(\sigma,t)$ with respect to σ may be computed by multiplying (5.67) for a solution $\phi^{(1)}(r,t)$ in a field $\sigma^{(1)}$ by $\phi^{(2)}(r,t^*)^*$, subtracting the complex conjugate of the analogous equation for $\phi^{(2)}(r,t^*)$ multiplied by $\phi^{(1)}(r,t)$, and integrating over r and t. Assuming, for the moment, that

$$\sigma(r,t^*)^*=\sigma(r,t)\ . \tag{5.70}$$

noting that the equation of motion, Eq. (5.67) implies

$$\frac{d}{dt}\int dr\,\phi_j(r,t^*)^*\phi_k(r,t)=0 \tag{5.71}$$

so that the normalization may be defined

$$\int dr\,\phi_j(r,t^*)^*\phi_k(r,t)=\delta_{jk}\ , \tag{5.72}$$

and taking the limit as $\sigma^{(2)}$ approaches $\sigma^{(1)}$ yields

$$\frac{\delta\alpha(\sigma,t)}{\delta\sigma}=\int\int\int dr\,dr'dt\,\delta\sigma(r',t)v(r-r')\times\phi_k(r,t^*)^*\phi_k(r,t)\ . \tag{5.73}$$

Hence, stationarity of $S_{\{n\}}[\sigma]$ in Eq. (5.69) yields

$$\sigma^0(r,t)=\sum_{k\varepsilon\{n\}}\phi_k(r,t^*)^*\phi_k(r,t)\ , \tag{5.74}$$

which is consistent with the assumption Eq. (5.6) and which agrees with Eq. (5.50) for real time.

The self-consistent set of equations (5.67), (5.68), and (5.74) merit several comments. Clearly, this set of equations is the many-fermion counterpart of the periodic classical solutions to Eq. (5.6) for one degree of freedom. Since the ϕ's are periodic, $\sigma^0(r,t)$ is necessarily periodic. The form of solution $\psi=e^{-i\alpha t/T}\phi$, with ϕ periodic, then follows from Floquet's theorem, and as in the analogous case of Bloch's theorem for crystals, in which periodic functions are multiplied by exponentials containing a quasimomentum, the quantity α/T has the physical interpretation of quasienergy. For real time, these equations reduce to the self-consistent coupled equations

$$\left[-i\frac{\partial}{\partial t}-\frac{1}{2m}\nabla_r^2-\frac{1}{2}V(0)+\int dr'v(r-r')\sum_k\phi_k^*(r,t)\phi_k(r,t)\right]\phi_k(r,t)=\frac{\alpha_k}{T}\phi_k(r,t) \tag{5.75}$$

with the boundary conditions that ϕ vanish on the spatial boundaries and be periodic with period T. As a four-dimensional generalization of the three-dimensional Hartree equations, one straightforward and successful means of solution is to specify an initial function $\sigma(r,t)$, solve the eigenvalue problem Eq. (5.75) for the resulting ϕ's in this potential, calculate the corresponding σ, and iterate to self-consistency.

Just as the classical equation, Eq. (5.6), when continued to purely imaginary time, admitted periodic solutions which described tunneling in the classically forbidden region, so also Eqs. (5.67), (5.68), and (5.74) yield periodic solutions when continued to imaginary time which we will subsequently utilize to understand spontaneous fission. For purely imaginary time, we define $(it)\equiv\tau$ and let $\tilde{\phi}_k(r,\tau)\equiv\phi_k(r,\tau/i)$ be a real solution to the equations obtained by replacing (it) in Eq. (5.67) by τ. It follows that $\phi_k[r,(\tau/i)^*]^*=\tilde{\phi}_k(r,-\tau)$, so that the self-consistent coupled equations in imaginary time are

$$\left[\frac{\partial}{\partial t}-\frac{1}{2m}\nabla_r^2-\frac{1}{2}V(0)+\int dr'v(r-r')\sum_l\tilde{\phi}(r,-\tau)\tilde{\phi}(r,\tau)\right]\tilde{\phi}_k(r,\tau)=\frac{\tilde{\alpha}_k}{T}\tilde{\phi}_k(r,t)\ . \tag{5.76}$$

Solutions to Eqs. (5.76) may be found by the same iterative method as for Eqs. (5.75) and will be discussed more fully in Sec. V.D.

Returning to real time, a particular class of solutions to Eq. (5.75) is those with no time dependence, in which case the SPA simply reproduces the static Hartree equations. Multiplication of Eq. (5.75) by $\phi_k^*(r)$ and integration over d^3r yields the familiar Hartree single-particle energy

$$\frac{\alpha_k}{T}=\langle k\,|\,K\,|\,k\rangle+\sum_{l\varepsilon\{n\}}\langle kl\,|\,v\,|\,kl\rangle\ , \tag{5.77}$$

where, in an obvious notation, the kets denote single-particle states. If we recognize that

$$\int_{-T/2}^{T/2}dt(\sigma^0v\sigma^0)$$

may be written as $T\sum_{k,l\varepsilon\{n\}}\langle kl\,|\,v\,|\,kl\rangle$, Eq. (5.69) yields

$$S_{\{n\}}[\sigma^0]=-TE_H\ , \tag{5.78}$$

where

$$E_H=\left[\sum_{k\varepsilon\{n\}}\langle k\,|\,K\,|\,k\rangle+\tfrac{1}{2}\sum_{kl\varepsilon\{n\}}\langle kl\,|\,v\,|\,kl\rangle\right] \tag{5.79}$$

and thus

$$\mathrm{Tr}U(T/2,-T/2)\approx\sum_{\{n\}}e^{-iTE_H}\left[\frac{\det(v\delta)}{\det\left[\dfrac{\delta^2S^{\{n\}}}{\delta\sigma\,\delta\sigma}\right]}\right]^{1/2}\ . \tag{5.80}$$

The quantity E_H is the familiar Hartree approximation to the total energy, and arises from the fact that the factor $\frac{1}{2}\int dt[\sigma^0v\sigma^0]$ properly corrected the overcounting of the potential energy which occurred in the sum of Hartree eigenvalues. Deferring to the next section con-

sideration of the quadratic corrections reflected in the determinant in Eq. (5.80), the Fourier transform of the leading contributions to $\mathrm{tr}U(T/2,-T/2)$ in Eq. (5.80) thus has a pole at the Hartree energy for each set of occupation numbers $\{n\}$ yielding sensible physical approximation for one class of eigenstates.

2. Quantization conditions for time-dependent solutions

In the general case of time-dependent solutions to Eqs. (5.75), ignoring quadratic corrections as before, eigenstates are specified by poles of the following Fourier transform:

$$\mathrm{tr}\frac{i}{E-H+i\eta}=\int_0^\infty dT\, e^{iET}\mathrm{tr}U(T/2,-T/2)$$
$$\approx\sum_{\{n\}}\int_0^\infty dT\, e^{i(ET+S_{\{n\}}[\sigma^0,T])}\ , \quad (5.81)$$

where $S_{\{n\}}[\sigma^0,T]$ is given by Eq. (5.69). For notational simplicity, it is useful to restrict our attention to the partial trace associated with one particular set of occupation numbers, to suppress $\{n\}$ from the notation, and to adopt the convention that sums over single-particle state labels are restricted to this set. Once one specifies occupation numbers and the period T, the self-consistent periodic time-dependent Hartree equations specify σ^0 and the associated α's. Hence σ^0 and the α's depend parametrically upon T, and $S[\sigma^0]$ is a function of T, which we emphasize by writing

$$S(T)\equiv\tfrac{1}{2}\int_{-T/2}^{T/2}dt[\sigma^0(t)\upsilon\sigma^0(t)]-\sum_k\alpha_k(\sigma^0,T)\ , \quad (5.82)$$

and the partial trace associated with occupation numbers $\{n\}$ is

$$U(E)\equiv\int_0^\infty dt\, e^{i[ET+S(T)]}\equiv\int_0^\infty dt\, e^{iW(T)}\ . \quad (5.83)$$

The formal similarity between this problem and the one-dimensional example, Eq. (5.8), is now explicit. Whereas in that one-dimensional example stationarity of $ET+S(T)$ led to the condition that E be the energy of the classical solution, in the many-body case stationarity implies that E is the Hartree energy of the self-consistent periodic solution:

$$E=-\frac{dS}{dT}=\frac{1}{T}\int_{-T/2}^{T/2}dt\,\mathscr{H}(\phi_k^*,\phi_k)\ , \quad (5.84)$$

where the Hartree energy functional is defined by Eq. (3.5) with the exchange terms omitted. Since the ϕ's are related by a phase factor, Eq. (5.66), to the ψ's which satisfy a time-dependent Hartree equation, $H(\phi_\mu^*,\phi_\mu)$ is time independent by Eq. (3.8). Equation (5.84) is derived by rewriting Eq. (5.75) in terms of a scaled time variable $\eta=t/T$, noting that T then appears as an explicit parameter, calculating the variation of the eigenvalue $\partial\alpha/\partial T$ as in the steps leading to Eq. (5.73) and noting that $\int dt[\sigma^0\upsilon\sigma^0]$ removes the potential overcounting terms. With this expression for E, one may then observe that in $W(T)$, defined in Eq. (5.83), ET cancels all the terms in $S(T)$ except those involving the time derivatives of single-particle wave functions, with the result

$$W(T)=i\int_{-T/2}^{T/2}dt\int dr\sum_k\phi_k^*(r,t)\frac{\partial}{\partial t}\phi_k(r,t)\ . \quad (5.85)$$

From this point on, derivation of the quantization condition follows precisely as in the one-dimensional example, Eqs. (5.10)–(5.15). Denoting $T(E)$ as the fundamental period which gives rise to periodic time-dependent Hartree solutions with energy E, stationary points in Eq. (5.83) are obtained for all integral multiples, $mT(E)$, with reduced action $W[mT(E)]=mW[T(E)]$. The same geometric series, Eq. (5.14), arises, yielding the quantization condition

$$n2\pi=W[T(E)]$$
$$=i\int_{-T(E)/2}^{T(E)/2}dt\int dr\sum_k\phi_k^*(r,t)\frac{\partial}{\partial t}\phi_k(r,t)\ . \quad (5.86)$$

The structural similarity of Eqs. (5.86) and (5.15) is even more evident if one notes from the Hamiltonian equations of motion, Eqs. (3.7), that the momentum conjugate to the field $\psi(r,t)$ is $\pi(r,t)=i\psi^*(r,t)$, so that to within terms involving α's, Eq. (5.86) is essentially of the form $\oint dr\,\pi\,d\psi$, which is the natural multidimensional generalization of $\oint p\,dq$.

At the SPA level, quantum states of large-amplitude collective motion are fully specified by the self-consistent equations for periodic time-dependent Hartree solutions, Eqs. (5.75), and the quantization condition, Eq. (5.86). In general, Eqs. (5.75) specify time-dependent oscillations having amplitudes which depend continuously upon T, and the quantization condition singles out a discrete set of amplitudes and energies corresponding to quantum eigenstates. The theory represents the simplest available approximation that has all the physical elements of a fundamental theory of quantum collective motion. All the degrees of freedom of the one-body density are accessible, and the dynamical equations and quantization conditions arise with no further prescriptions concerning collective variables, inertial parameters, or quantization procedure. Furthermore, as discussed in the next section, corrections to the SPA may in principle be systematically evaluated.

Two special limits of these time-dependent equations should be noted. Time-independent solutions to Eqs. (5.75) correspond to $n=0$ in Eq. (5.86), so the static Hartree states discussed previously are automatically included. For infinitesimal periodic fluctuations about the static Hartree solutions, the time-dependent quantized theory reduces to the familiar random-phase approximation (RPA). Omitting technical details, which are given by Levit, Negele, and Paltiel (1980a), linearization of Eq. (5.75) yields the RPA equations, Eqs. (3.38), where A and B now include only the direct Hartree matrix elements,

and periodicity of the single-particle wave functions requires that the period be $2\pi/\omega_\nu$ for some RPA eigenvalue ω_ν. The quantization condition reproduces the normalization condition

$$\sum_{\mu\rho}\left[|X^{(\nu)}_{\mu\rho}|^2-|Y^{(\nu)}_{\mu\rho}|^2\right]=m\ , \tag{5.87}$$

where X and Y are defined in Eq. (3.37), and the energy of the state is

$$E=E_H+m\omega_\nu\ , \tag{5.88}$$

where E_H is the Hartree energy, Eq. (5.79). Recovery of the well-known RPA in the infinitesimal limit thus lends further credence to the general theory for finite amplitude quantized vibrations.

D. Corrections to the stationary-phase approximation

Since corrections to the SPA for the many-body problem involve considerable technical complications and since the results are generally not amenable to analytical or numerical evaluation, several comments are warranted to place this present section in proper perspective.

A primary motivation for the consideration of corrections, of course, is to establish that one is dealing with a systematic, consistent theory. In addition, insight into the structure and physical significance of various corrections may be obtained by establishing contact with existing theory in appropriate limits. Even in cases for which explicit calculations are impractical, there is considerable practical value in identifying how to utilize the freedom in writing different exact functional integral expressions to minimize the leading corrections. In particular, such arguments will subsequently be presented to obtain the Hartree-Fock and Hartree-Fock-Bogoliubov approximations.

For these reasons, the objective of this section is to sketch the essential ideas and results, with no attempt to be technically complete. References for details include Rajaraman (1975), Coleman (1977), Negele (1979), Levit, Negele, and Paltiel (1980a, 1980b), and Reinhardt (1980, 1981). For readers who wish to skip this section entirely, no loss of continuity will arise in subsequent sections if one accepts the assertion that the self-consistent, periodic, time-dependent Hartree problem, Eq. (5.75), may be replaced by the analogous TDHF equation with the exchange term properly included and $1/2V(0)$ removed.

One of the arbitrary choices to be made in application of the SPA is whether to apply it separately to each state in the sum over N in Eq. (5.50) or to apply it to the full trace, in which case each matrix element $\langle\psi_N|U|\psi_N\rangle$ would be replaced by a trace. The effect of treating each state separately is seen by considering the result of replacing the trace in Eq. (5.1) by a matrix element in a single state $|\phi\rangle$ and, for simplicity, treating the usual case in which the operator $\mathcal{O}$ commutes with the Hamiltonian:

$$-i\int dT\, e^{iET}\langle\phi|\mathcal{O}U(T,0)|\phi\rangle = \sum_N \frac{|\langle\phi|N\rangle|^2\langle N|\mathcal{O}|N\rangle}{E-E_N+\eta}\ . \tag{5.89}$$

Thus a single state $|\phi\rangle$ yields poles at the energies of all the eigenstates which are not orthogonal to $|\phi\rangle$ and residues equal to the expectation value of $\mathcal{O}$ multiplied by the probability $|\langle\phi|N\rangle|^2$. Exact evaluation of any term in Eq. (5.50) therefore yields the spectrum of all eigenstates having nonzero overlap with $|\psi_N\rangle$, and the SPA may be expected to yield a useful approximation to the state with maximum overlap.

Although application of the SPA to each set of occupation numbers separately is thus adequate for evaluating the spectrum and will be presented in detail below, there are situations in which it is necessary to evaluate corrections to the full trace. One obvious case is calculation of the expectation value $\langle N|0|N\rangle$ without the additional overlap probability $|\langle N|\phi|\rangle^2$. Other applications include the treatment of systems at finite temperature, such as neutron star matter, and evaluation of the nuclear partition function. Utilizing the complete set of eigenfunctions of $U_s(T/2,-T/2)$ defined in Eq. (5.62), when the single-matrix element in Eq. (5.60) is replaced by a trace, one obtains (Reinhardt, 1981; Kerman and Levit, 1981)

$$\begin{aligned}\mathrm{Tr}U(T/2,-T/2)&=\int D[\sigma]e^{(i/2)\int dt[\sigma v\sigma]}\mathrm{tr}U^\sigma_s(T/2,-T/2)\\&=\int D[\sigma]e^{(i/2)\int dt[\sigma v\sigma]}\prod_k(1+e^{-i\alpha_k})\ .\end{aligned} \tag{5.90}$$

Equation (5.69) is then replaced by

$$S[\sigma]\equiv\tfrac{1}{2}\int dt[\sigma v\sigma]-i\sum_k\ln(1+e^{-i\alpha_k})\ , \tag{5.91}$$

so that stationarity generalizes Eq. (5.74) to

$$\sigma^0(r,t)=\sum_k f_k\phi_k(r,t^*)^*\phi_k(r,t)\ , \tag{5.92a}$$

where

$$f_k\equiv(1+e^{i\alpha_k})^{-1}\ . \tag{5.92b}$$

Thus, the sum over n states with unit occupation is replaced by a sum over all states with occupation numbers f_k. Projection onto definite particle number may be accomplished in the usual way by introduction of a chemical potential, and recalling from Eq. (5.76) that for static solutions α_k/T plays the role of the single-particle energy ε_k, one notes that when $iT\to\tau$, f_k becomes the familiar Fermi function, $(1+e^{\varepsilon\tau})^{-1}$.

From the pedagogical point of view of extracting the physical essence with a minimum of technical complications, however, separate approximation of each term in the trace, as in Eqs. (5.50)–(5.52), yields somewhat more transparent results. A useful condition in implementing this approch is to define the basis as the eigenstates of a definite σ_0 rather than as a functional of σ. By choosing

σ_0 to be the self-consistent solution for a particular set of occupation numbers $\{n\}$, one retains the results obtained previously in the SPA for that $\{n\}$. As long as we are interested in changes in the position of the pole for this set $\{n\}$, it is immaterial that the basis is not optimal for calculating poles associated with other sets of occupation numbers. A simple way to understand the rationale for a fixed basis, rather than one functionally dependent upon σ, is to consider the possible terms arising from variation of $S_n[\sigma]$ in Eq. (5.48). If $|\psi_n\rangle$ is independent of σ, the only possible variations are those of σ's in the exponent, so the formal structure of the nth functional derivative is identical to that in which the expectation value with respect to $|\psi_N\rangle$ is replaced by a full trace. In contrast, if $|\psi_N\rangle$ also depends implicitly on σ (instead of σ_0), in addition to the derivatives of the exponents, a whole new class of derivatives of the wave function arises, which ruins the simple formal structure of the first class of terms. Guided by this observation that evaluation of a single term with a fixed basis yields the same formal structure and physical results as the more complicated alternative of using the full trace, I will proceed with the evaluation of corrections for a single term in a fixed basis.

1. RPA correlation energy

The first objective is to correct the leading order SPA results of Sec. V.C by evaluating the quadratic corrections specified by the factor

$$\left[\frac{\det(v\delta)}{\det\dfrac{\delta^2 S_n}{\delta_\sigma \delta_\sigma}}\right]^{1/2}$$

in Eq. (5.50). The second variation of $S_n[\sigma]$, Eq. (5.51), in a fixed basis is

$$\frac{\delta^2 S_n[\sigma]}{\delta\sigma_{\alpha\gamma}(t)\delta\sigma_{\alpha'\gamma'}(t')} = \int dt'' \sum_{\beta\delta} V_{\alpha\beta\gamma\delta}\delta(t-t'')\left[\delta(t''-t')\delta_{\beta\alpha'}\delta_{\delta\gamma'} - \int dt''' \sum_{\beta'\delta'}\delta(t'''-t')V_{\alpha'\beta'\gamma'\delta'}D^0_{\beta\delta\beta'\delta'}(t'',t''')\right]$$
$$\equiv (v\delta)[1-D^0(v\delta)]\,, \tag{5.93}$$

where

$$iD^0_{\beta\delta\beta'\delta'}(t,t') \equiv \langle T_t \hat{\rho}_{\beta\delta}(t)\hat{\rho}_{\beta'\delta'}(t')\rangle - \langle\hat{\rho}_{\beta\delta}(t)\rangle\langle\hat{\rho}_{\beta'\delta'}(t')\rangle\,, \tag{5.94a}$$

$$\langle T_t \mathcal{O}(t)\mathcal{O}'(t')\rangle \equiv \frac{\langle\Psi_n | T_t \mathcal{O}(t)\mathcal{O}'(t') e^{-i\int_{t_i}^{t_f} h_\sigma(t)} | \Psi_n\rangle}{\langle\Psi_n | T_t e^{-i\int_{t_i}^{t_f} h_\sigma(t)} | \psi_n\rangle}\,, \tag{5.94b}$$

and where, as noted after Eq. (5.52), the time labels t and t' on the Schrödinger representation operators are introduced for proper positioning by the time-ordering operator.

Using the symbolic matrix notation in the last line of Eq. (5.93), cancelling out the singular factors $\det(v\delta)$, and using the identity $\det A = \exp(\mathrm{tr}\ln A)$, the quadratic correction factor becomes

$$\left[\frac{\det(V\delta)}{\det\dfrac{\delta^2 S}{\delta\sigma\,\delta\sigma}}\right]^{1/2} = \det[1-D(v\delta)]^{-1/2}$$
$$= e^{-(1/2)\mathrm{tr}\ln[1-D^0(v\delta)]}$$
$$= \exp\left[\frac{1}{2}\sum_{n=1}^{\infty}\frac{1}{n}\mathrm{tr}[D^0(v\delta)]^n\right]. \tag{5.95}$$

To understand the physical content of this result, note first that iD^0 is a simple time-dependent generalization of the familiar density-density correlation function or polarization propagator. When σ is time-independent and Ψ_n is an eigenstate of h_σ, expectation values such as those occurring in Eq. (5.94) may be expressed directly in terms of Green's functions in the one-body field h_σ. From Eq. (5.94b),

$$\langle\mathcal{O}(t)\mathcal{O}'(t')\rangle = \frac{\langle\Psi_n | T_t(e^{ih_\sigma t}\mathcal{O}e^{-ih_\sigma t})(e^{ih_\sigma t'}\mathcal{O}'e^{-ih_\sigma t'}) | \Psi_n\rangle}{\langle\Psi_n|\Psi_n\rangle}\,. \tag{5.96}$$

Expressing $\mathcal{O}$ and $\mathcal{O}'$ in terms of field operators directly yields a Green's function which may be represented in terms of Feynman diagrams. The quantity iD^0 in Eq. (5.94a) is thus a product of two one-body Green's functions starting at t and t' and terminating at t' and t, respectively, so that it represents a particle-hole bubble. Had we dealt with the trace instead of a single ψ_n, the zero-temperature Green's functions would be replaced by their finite temperature counterparts.

With this direct correspondence to Feynman diagrams for time-independent solutions, we are now in a position to examine the quadratic corrections to the Hartree energy, Eq. (5.79). The term $[D^0(v\delta)]^n$ appearing in the exponent of Eq. (5.95) is a matrix product describing an n-term chain of particle-hole bubbles connected by direct instantaneous matrix elements of v. The trace connects the

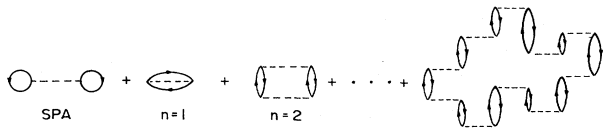

FIG. 17. Feynman diagrams contributing to the ground-state energy, including the SPA and quadratic corrections.

chain back on itself, creating a direct RPA ring diagram as shown by the last term in Fig. 17, and the $1/n$ factor corrects for the n different ways one could pick the top of the ring.

The $n=1$ term involves two density operators at equal times and requires separate consideration. Specializing to a local interaction and dropping spin-isospin indices as before

$$\begin{aligned}\tfrac{1}{2}\mathrm{Tr}D^0v\delta &= -\frac{i}{2}dr\,dr'\int_{-T/2}^{T/2}dt[\langle\hat{\psi}^\dagger(r)\hat{\psi}(r)\psi^\dagger(r')\hat{\psi}(r')\rangle-\langle\psi^\dagger(r)\psi(r)\rangle\langle\psi^\dagger(r')\psi(r')\rangle]v(r-r')\\ &= -\frac{i}{2}T\int dr\,dr'\left[\delta(r-r')\rho(r)-\sum_{kl}\psi_k^*(r)\psi_l^*(r')\psi_k(r')\psi_l(r)\right]v(r-r')\\ &= -\frac{iT}{2}\left[NV(0)-\sum_{kl}\langle kl\mid v\mid lk\rangle\right].\end{aligned} \tag{5.97}$$

Collecting terms in the exponent of Eq. (5.80), from Eqs. (5.79) and (5.97), we thus obtain

$$\begin{aligned}&\mathrm{tr}U(T/2,-T2)\\ &\approx\exp\left[-iT\left[\sum_k\langle k\mid\hat{T}\mid k\rangle\right.\right.\\ &\qquad\left.\left.+\tfrac{1}{2}\sum_{kl}\langle kl\mid v\mid kl-lk\rangle+E_{\mathrm{RPA}}\right]\right],\end{aligned} \tag{5.98}$$

where E_{RPA} represents the terms in the sum for $n>1$ in Eq. (5.95). Although the correlation energy E_{RPA} agrees with the standard Green's-function result derived for homogeneous systems (Fetter and Walecka, 1971), the present derivation is applicable to inhomogeneous systems.

Since the coefficient of T in the exponent of (5.98) is the energy, it is evident that the quadratic corrections produced three significant improvements. The annoying self-energy term $\frac{1}{2}v(0)$ ever present in the one-body operator $\hat{K}$ was exactly cancelled by a compensating term in $\frac{1}{2}\mathrm{Tr}D^0v\delta$, the Fock exchange term was included, and the sum of all direct ring diagrams was generated. Feynman diagrams for the energy at this level of approximation are displayed in Fig. 17, and it is straightforward to verify that all combinatorial factors are correct. Although a general discussion of corrections for time dependent h_σ is deferred to Sec. VD.4, one may immediately note that the structure of the $\frac{1}{2}\mathrm{Tr}D^0v\delta$ term will be identical in the time-dependent case, and thus generate self-energy and exchange terms.

2. The Hartree-Fock and Hartree-Fock-Bogoliubov approximations

Although the energy in Eq. (5.98) is the correct HF energy, the single-particle wave functions defining the matrix elements in that equation are generated by a Hartree single-particle Hamiltonian, Eq. (5.59), and the theory as it stands falls short of a self-consistent HF theory.

That we obtained a Hartree, rather than Fock or Hartree-Fock mean field, is associated with the fact that we applied the SPA to one particular choice from a large class of formally exact functional integral representations of the evolution operator. The theory was essentially restricted to a local mean field by applying the Hubbard-Stratonovich transformation to the Hamiltonian written in the form Eq. (5.32). Diagonality in the indices $\alpha\gamma$ and $\beta\delta$ implies that only the diagonal density instead of density matrix appears in the subsequent equations and that σ^0 defined in Eq. (5.49) must necessarily also be local. To appreciate the freedom available in writing different exact functional integral expressions, note that it was an arbitrary choice in Eq. (5.32) to group $a_\alpha^\dagger$ with a_γ and $a_\beta^\dagger$ with a_δ. One could just as well have grouped $a_\alpha^\dagger$ with a_δ and $a_\beta^\dagger$ with a_γ, obtaining a different but correct expression. A simple formal manipulation to effect this interchange is to note, by antisymmetry, the identity

$$\tfrac{1}{2}\sum_{\alpha\beta\gamma\delta}V_{\alpha\beta\gamma\delta}a_\alpha^\dagger a_\beta^\dagger a_\delta a_\gamma=-\tfrac{1}{2}\sum_{\alpha\beta\gamma\delta}V_{\alpha\beta\delta\gamma}a_\alpha^\dagger a_\beta^\dagger a_\delta a_\gamma\,, \tag{5.99}$$

so that all the exact functional integral expressions must remain correct if $V_{\alpha\beta\gamma\delta}$ is systematically replaced by $-V_{\alpha\beta\delta\gamma}$ in the preceding derivation. This seemingly trivial change in the exact expression yields nontrivial changes in the SPA result. Specializing to a local spin-isospin independent potential and denoting spin and isospin states by s_α and τ_α, respectively, one may substitute in Eq. (5.45) and elsewhere the expression

$$\begin{aligned}V_{\alpha\beta\gamma\delta}=&-\delta(r_\alpha-r_\delta)\delta_{s_\alpha s_\delta}\delta_{\tau_\alpha\tau_\delta}\delta(r_\beta-r_\gamma)\\ &\times\delta_{s_\beta s_\gamma}\delta_{\tau_\beta\tau_\gamma}V(r_\alpha-r_\beta)\,.\end{aligned} \tag{5.100}$$

In contrast to the Hartree expression, Eq. (5.53), one now obtains from Eq. (5.45) the result

$$\begin{aligned}\{\hat{\rho}(t)v\hat{\rho}(t)\}\rightarrow&-\sum_{ss'\tau\tau'}\int d^3r\,d^3r'\hat{\rho}_{s\tau,s'\tau'}(r,r',t)v(r-r')\\ &\times\hat{\rho}_{s'\tau',s\tau}(r',r,t)\,.\end{aligned} \tag{5.101}$$

For spin-isospin saturated nuclei, the resulting mean field from Eq. (5.74) is diagonal in spin-isospin, with the form

$$\sigma^0_{s\tau s'\tau'}(r,r')=\delta_{ss'}\delta_{\tau\tau'}\sum_n \phi^*_n(r)\phi_n(r') , \tag{5.102}$$

where the ϕ's are now eigenfunctions of Eq. (5.67) with h_σ defined by

$$h_\sigma(r,r';t)_{s\tau s'\tau'}=\delta_{ss'}\delta_{\tau\tau'}\left[\delta(r-r')\left[-\frac{1}{2m}\nabla_r^2-\frac{1}{2}\mathrm{SE}\right]-v(r-r')\sum_n \psi^*_n(r')\psi_n(r)\right] \tag{5.103}$$

instead of the Hartree Hamiltonian in (5.57), and where SE denotes the self-energy term arising from $-\frac{1}{2}\sum_\gamma V_{\alpha\gamma\gamma\beta}a^\dagger_\alpha a_\beta$ in Eq. (5.34).

Comparison with the HF single-particle Hamiltonian, Eq. (3.18), indicates that Eq. (5.103) precisely includes the Fock exchange term, completely omits the Hartree direct term, and in addition has a different spurious self-energy term. Repetition of the calculations leading to Eq. (5.98) with the form of V in Eq. (5.100) shows that the SPA yields the proper kinetic energy plus Fock exchange term plus a spurious self-energy, that the $n=1$ quadratic correction in Eq. (5.96) exactly removes the self-energy and inserts the proper Hartree term, and that the $n>1$ terms include exchange RPA ring diagrams.

The purely Fock SPA theory obtained above is no more satisfying than the previous Hartree theory, but is indicative of the freedom available by writing alternative exact expressions, and suggests that a proper HF theory should be attainable by an appropriate representation of the two-body potential. The naive guess of writing the interaction in the antisymmetrized form

$$\tfrac{1}{2}\sum_{\alpha\beta\gamma\delta} V_{\alpha\beta\gamma\delta}a^\dagger_\alpha a^\dagger_\beta a_\delta a_\gamma=\tfrac{1}{2}\sum_{\alpha\beta\gamma\delta}(\tfrac{1}{2}V_{\alpha\beta\gamma\delta}-\tfrac{1}{2}V_{\alpha\beta\delta\gamma})a^\dagger_\alpha a^\dagger_\beta a_\delta a_\gamma \tag{5.104}$$

is clearly unsatisfactory, with repetition of the preceding analysis yielding a mean field equal to one-half of the HF mean field, an SPA energy including only one-half of the HF potential energy, and with the other half of the HF potential energy coming from the $n=1$ term of the quadratic corrections. It is a curious fact, as will become evident in Sec. V.G, that in many other functional integral approaches, as well, formulation in terms of antisymmetrized matrix elements of v generally gives a mean field containing only half of the HF potential.

The appropriate decomposition to obtain the full HF field may be motivated by the fact that application of analogous functional integral techniques to a field theory of nucleons coupled to mesons yields direct and exchange terms in the fermion potential arising from the classical fields of distinct mesons. Thus in a static potential theory one may decompose the interaction into two terms:

$$\hat{v}\equiv\hat{v}^D+\hat{v}^E \tag{5.105}$$

such that v^D will generate the direct Hartree potential and v^E will generate the exchange Fock potential. To effect this decomposition, a sufficient condition is to require that the direct Hartree potential of $\hat{v}^E$ and the exchange Fock potential of $\hat{v}^D$ vanish in the state $|\Psi_n\rangle$, that is

$$\sum_{kl}\langle kl\,|\,v^D\,|\,lk\rangle=\sum_{kl}\langle kl\,|\,v^E\,|\,kl\rangle=0 . \tag{5.106a}$$

Although this condition may be enforced in an arbitrary system, and the derivation is by no means limited to closed shells or nuclei with at most one particle or hole relative to a closed shell, these latter systems are particularly simple to treat by the requirement that the following spin sums vanish:

$$\sum_s v^D_{ss's's}=\sum_s v^E_{ss'ss'}=0 . \tag{5.106b}$$

Equation (5.106b) may be implemented easily by spin algebra, as suggested by the example of the one-pion potential. Since it contains $\boldsymbol{\sigma}_1\cdot\boldsymbol{\sigma}_2\boldsymbol{\tau}_1\cdot\boldsymbol{\tau}_1$, the spin (or isospin) trace vanishes and it automatically represents a component of $\hat{V}^E$.

Finally, using the antisymmetrization freedom in Eq. (5.97), the interaction may be written in the form

$$\tfrac{1}{2}\sum_{\alpha\beta\gamma\delta} v_{\alpha\beta\gamma\delta}a^\dagger_\alpha a^\dagger_\beta a_\delta a_\gamma=\tfrac{1}{2}\sum_{\alpha\beta\gamma\delta}(v^D_{\alpha\beta\gamma\delta}-v^E_{\alpha\beta\delta\gamma})a^\dagger_\alpha a^\dagger_\beta a_\delta a_\gamma . \tag{5.107}$$

By virtue of Eq. (5.105) and our previous arguments, one obtains an exact evolution operator if one systematically replaces $v_{\alpha\beta\gamma\delta}$ by the expression $(v^D_{\alpha\beta\gamma\delta}-v^E_{\alpha\beta\delta\gamma})$. The result of such a substitution with a local potential is evident from preceding arguments. The potential v^D will generate the terms of the preceding Hartree theory except that, by Eq. (5.106), the self-energy term vanishes and the Fock term in the $n=1$ quadratic correction vanishes. Similarly, v^E will yield the preceding Fock theory, except that the self-energy is again zero and the Hartree term in the $n=1$ quadratic correction again vanishes. The net result is that the SPA yields an h_σ which contains the proper HF mean field and the correct HF total energy and that the $n=1$ Gaussian correction vanishes identically. As remarked earlier, these conclusions pertain to time-dependent, as well as time-independent solutions.

The observation that the leading quadratic correction vanishes provides the best justification for selecting this particular decomposition of the interaction. In the absence of a formal expansion parameter, it is clearly desirable to force as much of the physics as possible into the stationary contribution. An obvious criterion for selection between alternative exact functional integral expressions is that the saddlepoint be as steep as possible, or equivalently, that the quadratic corrections be minimal. Since the leading quadratic correction is proportional to $\mathrm{tr}(v\delta D)$, it is clear by construction that condition (5.107) will make it vanish, so one is led naturally to the same HF decomposition from the viewpoint of minimizing the leading correction.

Condition (5.106), to obtain the HF decomposition, may be implemented in a variety of ways. As a prelude to

the Hartree-Fock-Bogoliubov theory, it is useful to consider the special case of a central potential and a closed-shell nucleus and to note that the following decomposition satisfies condition (5.107) and thus Eq. (5.106):

$$v^D=(1-\tfrac{1}{3}\boldsymbol{\sigma}_1\cdot\boldsymbol{\sigma}_2)v(r_1-r_2)\ ,$$
$$v^E=(\tfrac{1}{3}\boldsymbol{\sigma}_1\cdot\boldsymbol{\sigma}_2)v(r_1-r_2)\ . \tag{5.108}$$

When the potential is written in this form, it becomes clear that the one-body density matrix, and thus σ, may be thought of as four independent spatial functions

$$\sigma(r_1\sigma_1;r_2\sigma_2)=\sigma_0(r_1r_2)+\sum_{i=1}^{3}(\sigma_2\,|\,\boldsymbol{\sigma}_i\,|\,\sigma_1)\sigma_i(r_1,r_2)\ . \tag{5.109}$$

Writing v^D and v^E as in Eq. (5.108) yields identical equations of motion for the three spatial components, so in fact only two independent σ fields are actually utilized in the functional integral. Two linear combinations of these independent σ fields ultimately generate the direct and exchange components of the HF mean field. Thus, in exploring the freedom to write alternative functional integral representations, we were led from the Hartree and Fock theories which each utilized a single σ field, to the HF approximation which utilized two independent fields. Since there are four fields available for a system with spin and sixteen available for nucleons with spin and isospin, it is clear that there is still a great deal of additional freedom in the functional integral representation which, in principle, could be used to advantage.

Since Hartree and Fock mean fields arise from application of the Hubbard- Stratonovich transformation to the alternative groupings of creation and annihilation operators in Eq. (5.32), it is natural that the pairing field should arise from grouping the creation operators together and the annihilation operators together. Thus, following Hubbard (1959), one may introduce a complex field $\chi_{\alpha\beta}$, define the operators

$$\hat{\eta}_{\gamma\delta}\equiv\hat{a}_\gamma\hat{a}_\delta \tag{5.110}$$
$$\hat{\eta}^\dagger_{\gamma\delta}=\hat{a}^\dagger_\delta\hat{a}^\dagger_\gamma\ ,$$

and obtain the following alternative to Eq. (5.42) for the interaction representation evolution operator:

$$T_t\exp\left[-\frac{i}{2}\int dt\,\eta^\dagger_{\alpha\beta}(t)V_{\alpha\beta\gamma\delta}\eta_{\gamma\delta}(t)\right]=D[\chi^*,\chi]\exp\left[\frac{i}{2}\int dt\,\chi^*_{\alpha\beta}(t)V_{\alpha\beta\gamma\delta}\chi_{\gamma\delta}(t)\right]T_t\exp\left[-\frac{i}{2}\int dt\,V_{\alpha\beta\gamma\delta}[\chi^*_{\alpha\beta}\eta_{\gamma\delta}+\eta^*_{\alpha\beta}\chi_{\gamma\delta}]\right]\ , \tag{5.111}$$

where $\int D[\chi^*,\chi]$ indicates independent integration over the real and imaginary parts of χ. Repetition of the steps which led to Eq. (5.52) yields

$$\chi^0_{\alpha\beta}t=\frac{\left\langle\Psi_n\left|T_t\hat{\eta}_{\alpha\beta}(t)\exp(-i\int dt\,\hat{h}_\chi(t)dt)\right|\Psi_n\right\rangle}{\left\langle\psi_n\left|T_t\exp\left[-i\int dt\,\hat{h}_\chi(t)dt\right]\right|\psi_n\right\rangle} \tag{5.112}$$

where the mean field appearing in the single-particle Hamiltonian is now the pairing field:

$$\hat{h}_\chi(t)=\hat{T}+\tfrac{1}{2}\sum_{\alpha\beta\gamma\delta}V_{\alpha\beta\gamma\delta}[\chi^*_{\alpha\beta}(t)\eta_{\gamma\delta}+\eta^\dagger_{\alpha\beta}\chi_{\gamma\delta}(t)]\ . \tag{5.113}$$

To combine Hartree, Fock, and pairing fields in the same theory requires a generalization of the decomposition, Eq. (5.105):

$$\hat{v}=\hat{v}^D+\hat{v}^E+\hat{v}^P\ , \tag{5.114a}$$

where the exchange and pairing matrix elements of $\hat{v}^D$ vanish, the direct and pairing matrix elements of $\hat{v}^E$ vanish, and the direct and exchange matrix elelents of $\hat{v}^P$ vanish. For a central potential and a closed-shell nucleus, these conditions are satisfied by the following generalization of Eq. (5.108):

$$\hat{v}^D=(1-\sigma^1_y\sigma^2_y)v(r_1-r_2)\ ,$$
$$\hat{v}^E=\tfrac{1}{2}(\sigma^1_y\sigma^2_y+\sigma^1_z\sigma^2_z)v(r_1-r_2)\ ,$$
$$\hat{v}^P=\tfrac{1}{2}(\sigma^1_y\sigma^2_y-\sigma^1_z\sigma^2_z)v(r_1-r_2)\ . \tag{5.114b}$$

The total mean field in this case is

$$\hat{h}(t)=\hat{T}+\sum_{\alpha\beta\gamma\delta}\{\sigma_{\alpha\gamma}(t)(V^D_{\alpha\beta\gamma\delta}-V^E_{\alpha\beta\delta\gamma})\hat{\rho}_{\beta\delta}+\tfrac{1}{2}V^P_{\alpha\beta\gamma\delta}[\chi^*_{\alpha\beta}(t)\hat{\eta}_{\gamma\delta}+\hat{\eta}^\dagger_{\alpha\beta}\chi_{\gamma\delta}(t)]\}\ , \tag{5.115}$$

with σ and χ specified by equations of the form (5.52) and (5.112), but with h_σ and h_χ replaced by the total mean field $\hat{h}(t)$. Instead of defining $|\psi_n\rangle$ in Eqs. (5.57) and (5.112) to be a Slater determinant, the self-consistent problem is much simpler if $|\psi_n\rangle$ is chosen to be a BCS wave function, in which case the periodic self-consistent HF equations are replaced by self-consistent Hartree-Fock-Bogoliubov equations. Introduction of the pairing field has also been treated recently by Kleinert (1978) and by Tomoda and Sevgen (1982).

Several other alternatives to the decomposition (5.105) may be used to generate a Hartree-Fock rather than a Hartree mean field. Writing the Hamiltonian in terms of antisymmetrized matrix elements $\bar{V}_{\alpha\beta\gamma\delta}\equiv V_{\alpha\beta\gamma\delta}-V_{\alpha\beta\delta\gamma}$, one may arbitrarily decompose the evolution operator in the form

$$\exp\{-i[-\lambda\hat{\rho}_{\alpha\gamma}\bar{V}_{\alpha\beta\gamma\delta}\hat{\rho}_{\beta\delta}+K+(\tfrac{1}{4}+\lambda)\hat{\rho}_{\alpha\gamma}\bar{V}_{\alpha\beta\gamma\delta}\hat{\rho}_{\beta\delta}]\}\ .$$

The density operators $\hat{\rho}$ in the first term may be removed by replacing them by derivatives with respect to external sources, as in Eq. (5.124) below, and the second term may

be linearized with an auxiliary field. Since the first term deliberately has been made independent of the auxiliary field, application of the SPA yields a stationary field which is any desired multiple of the density and thus, as utilized by Reinhardt (1980) for $\lambda=\frac{1}{4}$ one obtains the HF mean field. In addition to the usual class of SPA corrections, one also has an infinite set of perturbation corrections arising from the derivatives with respect to the external source. Since this method effectively removes part of the potential energy term from the variation with respect to the auxiliary field, an equivalent result may be obtained by arbitrarily requiring that a factor $e^{i\lambda\sigma\bar{V}\sigma}$ not be varied in the SPA, corresponding to g in Eq. (5.29), and that the remaining factor $e^{-i(1/4+\lambda)\sigma\bar{V}\sigma}$ be varied in the usual way, corresponding to f in Eq. (5.29). Again, adjustment of λ yields any desired multiple of the density and the HF field arises for $\lambda=-\frac{1}{8}$. Systematic corrections for any choice of λ are given by Eq. (5.30). Yet a final method by Kerman, Levit, and Troudet (1982) utilizes the fact discussed in connection with Eq. (5.39) that the odd terms in σ in the expansion

$$\int d\sigma\, e^{i(\varepsilon/2)\sigma v\sigma} e^{-i\varepsilon\sigma v\rho} = \int d\sigma\, e^{i(\varepsilon/2)\sigma v\sigma}\left[1-i\varepsilon\sigma v\rho-\frac{\varepsilon^2}{2}(\sigma v\rho^2)+\cdots\right] \tag{5.116}$$

do not contribute to the exact integral and that therefore the linear term may be modified at will. Since it does contribute to the SPA, it may be adjusted to yield the HF field or a number nonconserving part may be added to obtain the Hartree-Fock-Bogoliubov field (Troudet, 1982). The special cases of Hartree, Fock, and one-half Hartree-Fock discussed above arise in this method for the three choices of the arbitrary linear term which may be resummed to order ε^2 as an exponential.

In all these methods, the key question is how to justify a particular value of an arbitrarily introduced parameter. Although ideally one would like to demonstrate that a particular parameter optimizes convergence, in practice one must settle for more limited arguments. One possibility is to minimize a particular correction which is believed to be of leading order. In very special cases one may use the parameter to minimize the sum of all corrections to a given approximation. Since the exact evaluation of the functional integral is independent of the parameter, the sum of all corrections to an approximation is stationary with respect to variation of the parameter when the approximation is stationary. Thus, in any case for which the approximate expression is also a bound on the exact result, the corrections are minimized by requiring that the bound be stationary with respect to variation of the parameter. This situation occurs, for example, in evaluating the SPA plus the $n=1$ quadratic corrections for the ground-state energy, in which case the energy is the expectation value of H in a determinant of eigenfunctions of the mean field. By the Ritz variational principle, this determinantal trial function yields an upper bound, and if some value of the arbitrary parameter governing the mean field is capable of generating the HF field, minimization of the energy will necessarily specify that value. Whereas this argument provides a rationale for the HF choice in this particular case, it is clearly of very limited applicability.

3. The loop expansion

Thus far, only quadratic corrections to the SPA in Eq. (5.50) have been evaluated, yielding RPA ground-state correlation corrections in the case of a time-independent mean field. In this section, a perturbation series is obtained by expanding the functional integral

$$\int D[\sigma]e^{-S[\sigma]}=\int D[\eta]\exp\left[i\left[S[\sigma_0]+\tfrac{1}{2}\int dx_1dx_2\frac{\delta^2S[\sigma_0]}{\delta\sigma(x_1)\delta\sigma(x_2)}\eta(x_1)\eta(x_2)+\sum_{n=3}^{\infty}\frac{1}{n!}\prod_{s=1}^{n}\int dx_s\eta(x_s)\frac{\delta^nS[\sigma_0]}{\delta\sigma(x_1)\cdots\delta\sigma(x_n)}\right]\right], \tag{5.117}$$

where σ_0 is a stationary time-independent solution, $S[\sigma]$ is given by Eq. (5.51) with a fixed basis of eigenstates generated by σ_0, $\eta=\sigma-\sigma_0$, and x_s denotes the space-time coordinates $(\mathbf{x}_s,t_s)$. The resulting expansion is closely analogous to the loop expansion in field theory (Bender, Cooper, and Guralnik, 1977), with meson propagators being replaced by RPA phonons. One thus obtains a derivation of the diagram rules for expressing the energy of a nuclear eigenstate in terms of fermion and RPA phonon propagators (Reinhardt, 1978). For notational clarity, the expansion will be written for the simple Hartree form of the auxiliary field.

The evaluation of Eq. (5.117) proceeds in two steps. We shall first calculate the general functional derivative

$$\frac{\delta^nS[\sigma_0]}{\delta\sigma(x_1)\cdots\delta\sigma(x_n)},$$

and then address the functional integral over η. The second derivative of S has already been calculated in Eq. (5.93) to obtain $(v\delta)[1-D^0(v\delta)]$. Noting that the first term in Eq. (5.51) will not contribute to higher derivatives, we need only consider the term

$$i\tilde{S}[\sigma]\equiv\ln\langle\Psi\,|\,T_te^{-i\int h_\sigma}\,|\,\Psi\rangle\,, \tag{5.118}$$

where, for convenience we write

$$-i\int h_\sigma \equiv -i\int dt\, K + \int dx\, \sigma(x)\hat{f}(x) \tag{5.119}$$

with

$$\hat{f}(x)\equiv -i\int dx' V(x-x')\hat{\rho}(x') \tag{5.120}$$

and

$$V(x-x')\equiv v(x-x')\delta(t-t')\ . \tag{5.121}$$

A general derivative of $i\tilde{S}$ evaluated at σ_0 is calculated as follows:

$$\begin{aligned} e^{i(\tilde{S}[\sigma_0+\eta]-\tilde{S}[\sigma_0])} &= \frac{\left\langle \Psi \left| T_t \exp\left[\int \eta(x)\hat{f}(x)\right] \exp\left[-i\int h_\sigma\right] \right| \Psi \right\rangle}{\langle \Psi \mid T_t \exp\left[-i\int h_\sigma\right] \mid \Psi\rangle} \\ &= \sum_n \frac{1}{n!}\int dx_1 \ldots dx_n \eta(x_1)\ldots\eta(x_n)\langle T_t \hat{f}(x_1)\ldots\hat{f}(x_n)\rangle \\ &= \exp\left[\sum_n \frac{1}{n!}\int dx_1\ldots dx_n \eta(x_1)\ldots\eta(x_n)\langle T_t\hat{f}(x_1)\ldots f(x_n)\rangle_{\text{LINKED}}\right]\ . \end{aligned} \tag{5.122}$$

The second line in Eq. (5.122), which arises from expanding the exponential $e^{\int \eta(x)\hat{f}(x)}$ and using the definition (5.94b), may be directly interpreted in terms of diagrams. Using the argument subsequent to Eq. (5.96), and applying Wick's theorem, $\langle T_t\rho(x_1')\ldots\rho(x_n')\rangle$ generates the set of all linked and unlinked diagrams connecting the points $x_1\ldots x_n$ with oriented lines from x_i to x_j corresponding to the propagator $\langle T_t\psi(x_j)\psi^\dagger(x_i)\rangle$ such that each point has one incoming and one outgoing line. Diagrams for $\langle T_t f(x_1)\ldots f(x_n)\rangle$ differ only trivially in that point x_i is linked by a potential interaction to x_i' which in turn has incoming and outgoing fermion propagators. The last line in Eq. (5.122) follows from the fact that all diagrams are generated by the exponential of the sum of all linked diagrams. Hence

$$\begin{aligned} i\frac{\delta^n\tilde{S}[\sigma_0]}{\delta\sigma(x_1)\ldots\delta\sigma(x_n)} &= \frac{\delta^n}{\delta\eta(x_1)\ldots\delta\eta(x_n)}\left[\sum_m \frac{1}{m!}\int dx_1\ldots dx_m \eta(x_1)\ldots\eta(x_m)\langle T_t\hat{f}(x_1)\ldots\hat{f}(x_m)\rangle_{\text{LINKED}}\right]_{\eta=0} \\ &= \langle T_t\hat{f}(x_1)\ldots\hat{f}(x_n)\rangle_{\text{LINKED}} \\ &= (-i)^n\int dx_1'\ldots dx_n' V(x_1-x_1')\ldots V(x_n-x_n')\langle T_t\hat{\rho}(x_1')\ldots\hat{\rho}(x_n')\rangle_{\text{LINKED}}\ . \end{aligned} \tag{5.123}$$

As a check, we note that $\delta^2\tilde{S}/\delta\sigma(x_1)\delta_\sigma(x_2)$ correctly reproduces the term $-V\langle T_t\hat{\rho}\hat{\rho}\rangle_{\text{LINKED}}V\equiv -(v\delta)D^0(v\delta)$ in Eq. (5.93).

Turning now to the η integral in Eq. (5.117), it is convenient to introduce a source term $e^{-i\int dx\lambda(x)\eta(x)}$, replace $\eta(x_s)$ by $i[\partial/\partial\lambda(x_s)]$ in the terms with $n>3$, and evaluate the resulting Gaussian integral over η as follows:

$$\begin{aligned} \int D[\sigma]e^{iS[\sigma]} &= \exp\left[iS[\sigma_0]+\sum_{n=3}^{\infty}\frac{i}{n!}\prod_{s=1}^{n}\int dx_s i\frac{\partial}{\partial\lambda(x_s)}\frac{\delta^n S[\sigma_0]}{\delta\sigma(x_1)\ldots\delta\sigma(x_n)}\right] \\ &\quad\times\int D[\eta]\exp\left[\frac{i}{2}\int dx_1dx_2\frac{\delta^2S[\sigma_0]}{\delta\sigma(x_1)\delta\sigma(x_2)}\eta(x_1)\eta(x_2)-i\int dx\,\lambda(x)\eta(x)\right]_{\lambda=0} \\ &= e^{iS[\sigma_0]}\left[\frac{\det V}{\det\frac{\delta^2S}{\delta\sigma\,\delta\sigma}}\right]^{1/2} \\ &\quad\times\exp\left[\sum_{n=3}^{\infty}\frac{1}{n!}\int dx_1\ldots dx_n\int dx_1'\ldots dx_n' V(x_1-x_1')\ldots V(x_n-x_n')\right. \\ &\qquad\left.\times\langle T_t\hat{\rho}(x_1')\ldots\hat{\rho}(x_n')\rangle_{\text{LINKED}}\frac{\partial}{\partial\lambda(x_1)}\cdots\frac{\partial}{\partial\lambda(x_n)}\right] \\ &\quad\times\exp\left[-\frac{i}{2}\int dx\,dy\lambda(x)\left[\frac{\delta^2S}{\delta\sigma\,\delta\sigma}\right]^{-1}_{(x,y)}\lambda(y)\right]\Bigg|_{\lambda=0} \end{aligned} \tag{5.124}$$

To understand Eq. (3.94) in terms of diagrams, first note that repeated differentiation of the Gaussian in λ brings down successive factors of $(\delta^2 S/\delta\sigma\delta\sigma)^{-1}_{(x,y)}$ and that only those terms in which both λ's associated with a given $\delta^2 S^{-1}/\delta\sigma\,\delta\sigma$ have been differentiated survive in the limit $\lambda=0$. The exponential in Eq. (5.124) containing the $\partial/\partial\lambda$ derivatives generates products of closed fermion propagator loops. In each loop, fermion propagators connect three or more points x'_1 through x'_n, and each point x'_j is connected in turn to the factor $iV(x'_j-x_j)\delta/\delta\lambda x_j$. Hence one obtains all diagrams in which the points in the various closed fermion loops are connected in all possible ways by the quantity $-(i/2)V(\delta^2 S/\delta\sigma\,\delta\sigma)^{-1}V$. By Eq. (5.93), recalling that V defined in Eq. (5.121) includes a δ function in time,

$$V\left[\frac{\delta^2 S}{\delta\sigma\,\delta\sigma}\right]^{-1}V=V[V(1-D_0V)]^{-1}V$$
$$=\sum_{n=0}^{\infty}V[D_0V]^n \qquad (5.125)$$

yielding the RPA phonon propagator shown in Fig. 18 which sums all chains of interactions connected by particle-hole bubbles. Rewriting Eq. (5.124) in the abbreviated form

$$\int D[\sigma]e^{iS[\sigma]}=e^{iS[\sigma_0]}\left[\frac{\det V}{\det\dfrac{\sigma^2 S}{\delta\sigma\,\delta\sigma}}\right]^{1/2}X$$
$$\equiv e^{iS[\sigma_0]-1/2\,\mathrm{tr}\ln(1-D_0V)+Y}, \qquad (5.126)$$

the preceding argument shows that X is the sum of all diagrams, both linked and unlinked, comprised of any number of closed fermion loops connected in all possible ways with RPA phonons such that at least three phonon vertices connect to each fermion loop. By the linked-cluster theorem, the quantity Y in the last line of Eq. (5.126) is then the sum of all such diagrams which are completely linked. These linked diagrams constitute the higher-order corrections to the HF plus the RPA correlation energy represented by the first two terms in the exponent. To establish contact with the loop expansion in field theory, note that the number of loops refers to the number of RPA phonons, not the number of fermion loops. In this language, the $\frac{1}{2}\mathrm{tr}\ln(1-D_0V)$ term graphed in Fig. 17 is the one-loop correction, since it consists of a single RPA propagator connected to a closed fermion propagator. This term cannot be generated again in Y because of the requirement that each fermion loop contain at least three phonon vertices. The general two-loop connections are graphed in Fig. 19, as well as typical terms arising from expansion of the RPA phonons. Whereas for terseness

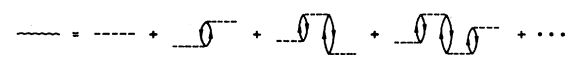

FIG. 18. The RPA phonon corresponding to Eq. (5.125).

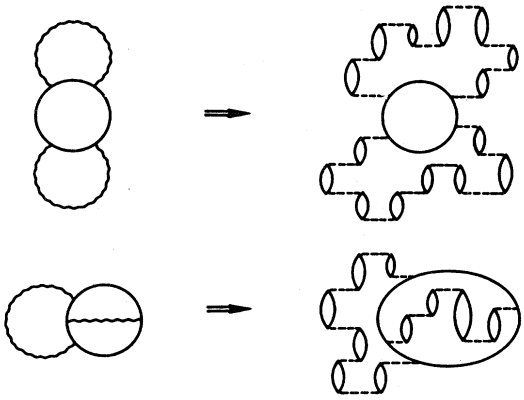

FIG. 19. The general form of the two-loop corrections.

the preceding derivation has ignored signs and factors, it is straightforward to verify that the signs and factors agree with the first few orders of standard perturbation theory (Negele, 1979).

4. Time-dependent generalization

In the last section, the structure of the corrections to the SPA was displayed in the special case of a time-independent mean field $\sigma_0(x)$. Infinitesimal fluctuations about σ_0 corresponded to RPA phonons, and systematically summing these RPA fluctuations reproduced standard results familiar from diagrammatic perturbation theory. For a time-dependent stationary solution $\sigma_0(x,t)$, the structure of the corrections is analogous, except that the fluctuations have nontrivial temporal as well as spatial dependence. Treatment of these fluctuation corrections is more difficult due to the emergence of technical complications, the unfamiliarity of diagram expansions for time-dependent potentials, and the lack of any relevant analytic or numerical solutions for such time-dependent problems.

One technical difficulty ignored thus far arises from invariance with respect to translations in space and time. If $\sigma_0(x,t)$ is a periodic stationary solution

$$\frac{\delta S}{\delta\sigma}[\sigma_0(x,t)]=0\,, \qquad (5.127a)$$

then another solution is obtained by shifting the time origin

$$\frac{\delta S}{\delta\sigma}[\sigma_0(x,t-t_0)]=0\,. \qquad (5.127b)$$

Naive application of the SPA by integrating over all values of t_0 and evaluating $(\det\delta^2 S/\delta\sigma\,\delta\sigma)^{-1/2}$ commits two related errors. By Eqs. (5.127) for infinitesimal t_0,

$$\int dx\,dt\frac{\delta^2 S}{\delta\sigma(x't')\delta\sigma(x,t)}\frac{\partial}{\partial t}\sigma_0(x,t)=0\,, \qquad (5.128)$$

so that $(\partial/\partial t)\sigma_0$ is an eigenfunction with zero eigenvalue. The resulting divergence in $(\det\delta^2 S/\delta\sigma\,\delta\sigma)^{-1/2}$ reflects the fact that in some direction the integrand, which was

assumed to be Gaussian, in fact has infinite extent. This direction corresponds to displacements in time origin t_0, which have already been treated explicitly by integration over t_0 and are thus being double counted. Thus the correct quadratic correction factor becomes (Coleman, 1977)

$$\left[\det\frac{\delta^2 S}{\delta\sigma\,\delta\sigma}\right]^{-1/2}\rightarrow a\int dt_0\left[\det'\frac{\delta^2 S}{\delta\sigma\,\delta\sigma}\right]^{-1/2}, \tag{5.129}$$

where det' denotes the determinant evaluated in the space orthogonal to $(\partial/\partial t)\sigma_0(x,t)$ and a is a calculable constant. The zero eigenvalue arising from invariance with respect to spatial translation is treated analogously.

The details of the explicit evaluation of $\det'(\delta^2 S/\delta\sigma\,\delta\sigma)=\det'(V-VD^0V)$ are presented by Reinhardt (1981a, 1981b). The calculation is simplified by writing D^0 in the basis of eigenfunctions σ_α of the periodic mean field, Eq. (5.67). Since

$$\begin{aligned} iD^0(x_1y_1t_1;x_2y_2t_2) &= \sum_{\alpha\beta} n_\beta(1-n_\alpha)[\theta(t_1-t_2)\psi^*_\beta(x_1t_1)\psi_\alpha(y_1t_1)\\ &\quad\times\psi^*_\alpha(x_2t_2)\psi_\beta(y_2t_2)\\ &\quad+\theta(t_2-t_1)\psi^*_\beta(x_2t_2)\psi_\alpha(y_2t_2)\\ &\quad\times\psi^*_\alpha(x_1t_1)\psi_\beta(y_1t_2)], \end{aligned} \tag{5.130}$$

where n_β is an occupation number which is 1 if β is occupied and 0 of it is unoccupied and the ψ's are defined by Eqs. (5.64) and (5.65), it follows that in the ϕ basis, D^0 satisfies the equation

$$\left[i\frac{\partial}{\partial t_1}-\frac{\alpha_\beta-\alpha_\alpha}{T}\right][D^0_{\alpha\beta\gamma\delta}(t_1t_2)] =\delta_{\alpha\delta}\delta_{\beta\gamma}\delta(t_1-t_2)(n_\alpha-n_\beta). \tag{5.131}$$

Noting that D^2 is defined only in the particle-hole space, we may write schematically

$$\begin{aligned} \frac{\mathrm{Det}'\left[\frac{\delta^2 S}{\delta\sigma\,\delta\sigma}\right]}{\mathrm{Det}V} &= \mathrm{Det}'[D_0(D_0^{-1}-V)]=\frac{\mathrm{Det}'(D_0^{-1}-V)}{\mathrm{Det}D_0^{-1}}\\ &=\frac{\mathrm{Det}'\left[i\frac{\partial}{\partial t}-\frac{\alpha_\beta-\alpha_\alpha}{T}-V\right]}{\mathrm{Det}\left[i\frac{\partial}{\partial t}-\frac{\alpha_\beta-\alpha_\alpha}{T}\right]}. \end{aligned} \tag{5.132}$$

The matrix in the numerator of Eq. (5.132) is a time-dependent generalization of the RPA matrix, Eq. (3.38). Reinhardt (1981) and Kerman and Levit (1981) show how the ratio of the determinants in Eq. (5.132) can finally be expressed in terms of the sum of the generalized RPA eigenvalues minus the sum of the particle-hole energies $(\alpha_\beta-\alpha_\alpha)/\tau$. In the general time-dependent case, these fluctuation terms modify both the energy condition, Eq. (5.84), and the quantization condition, Eq. (5.86). In the special case of a time-independent σ_0, for the ground state this correction reduces to the RPA correlation energy, thereby reproducing the previous time-independent result obtained diagrammatically. In addition to the ground state, however, one also obtains an infinite sequence of excited states corresponding to all possible occupation numbers for RPA phonons built on the ground state. For these states, the quantization condition, Eq. (5.86), is unchanged, while the energy, Eq. (5.89), is shifted from the HF energy by the RPA ground-state correlation energy plus the sum of the RPA energies of all the occupied phonon modes.

Thus the formal structure of the fluctuation corrections corresponds to a natural and physically understandable generalization of the time-independent RPA. Since the generalized RPA equations depend upon time as well as spatial coordinates, explicit calculation of these effects is presently computationally impractical.

E. Barrier penetration and spontaneous fission

In the example of quantum mechanics with one degree of freedom in Sec. V.A.2, evolution in classically forbidden regions was described by complex stationary points in the application of the SPA to the time integral in Eq. (5.2). In particular, for the classically forbidden region II of Fig. 16(d), stationary solutions with purely imaginary period corresponded to classical solutions in the inverted potential of Fig. 16(e). The action calculated for these periodic solutions in imaginary time then yielded the familiar WKB penetrability for the decay width, Eq. (5.28). In this section, we shall therefore examine the analogous continuation of the many-fermion evolution operator to imaginary time to obtain a quantum mean-field theory of spontaneous fission.

One possible approach to the spontaneous fission problem is to evaluate the imaginary-time behavior of the evolution operator

$$\langle\Psi\,|\,e^{-H\tau}\,|\,\Psi\rangle=\int D[\sigma]e^{iS[\sigma]} \tag{5.133}$$

(Negele, Levit, and Paltiel, 1979; Negele, 1979; Reinhardt, 1981), following the treatment of Coleman (1977) for spontaneous decay in field theory. In the limit of large τ, the lowest state dominates Eq. (5.133) and application of the SPA yields a set of solutions analogous to the instantons or pseudoparticles arising in field theory. An infinite set of these solutions may be approximately summed, yielding an imaginary part to the energy which is interpreted as the lifetime. This approximation yields the same penetrability as derived below from the density of states, as well as an explicit premultiplying factor arising from the quadratic corrections. The validity of this premultiplying factor, however, is now suspect as a result of a calculation by Patrascioiu (1981) showing that it yields the incorrect result in a one-dimensional example.

An alternative approach, presented here, extends the calculation of the level density, Eq. (5.21), to the many-fermion problem (Levit, Negele, and Paltiel, 1980b). Generalization of the treatment of one-dimensional quantum mechanics involves two principal components. First, it is necessary to continue the mean-field equations to imaginary time and to understand how replacing (it) by τ inverts the analog of the potential in Fig. 16 (d). Secondly, it is necessary to sum the appropriate stationary solutions in classically allowed and forbidden regions, joining them properly at turning points, and including all relevant decay modes.

The continuation to imaginary time has been performed in Eqs. (5.71), (5.74), and (5.76). Specializing to the Hartree case and omitting self-energies for simplicity, the self-consistent mean-field equation in a classically forbidden region, Eq. (5.76), is

$$\left[\frac{\partial}{\partial\tau}-\frac{1}{2m}\nabla_r^2+\int dr' v(r-r')\sum_l \tilde{\phi}_l(r,-\tau)\tilde{\phi}_l(r,\tau)\right]\tilde{\phi}_k(r,\tau) = \frac{\tilde{\alpha}_k}{T}\tilde{\phi}_k(r,\tau), \quad (5.134)$$

with $\tilde{\phi}_k(r,\tau)$ satisfying the periodic condition

$$\tilde{\phi}_k\left[r,\frac{T}{2}\right]=\tilde{\phi}_k\left[r,-\frac{T}{2}\right], \quad (5.135)$$

and the orthonormality relation

$$\int dr\,\tilde{\phi}_j(r,-\tau)\phi_k(r,\tau)=\delta_{jk}\ , \quad (5.136)$$

Although the self-consistent eigenvalue problem, Eq. (5.134), is not Hermitian, it has a set of real solutions with real eigenvalues, and general solutions differ from these real solutions by the trivial phase factors $e^{i(2\pi n/T)t}$ and eigenvalue shifts $i(2\pi n/T)$, where n is any integer.

Written in terms of $\tilde{\phi}(\tau)$ and $\tilde{\phi}(-\tau)$, it is not evident that continuation from (it) to τ has reversed the sign of the effective potential energy as in the one-dimensional example. This sign reversal is manifest if one performs a canonical transformation in the action, Eq. (3.4) (Levit, Negele, and Paltiel, 1980b). Choosing the time origin at a classical turning point, the periodic real-time dependent solutions to Eq. (5.75) may be written

$$\phi_k(r,t)\equiv[\rho(r,t)]^{1/2}e^{i\chi(r,t)}\ , \quad (5.137)$$

where ρ, analogous to a coordinate, is real and time even

$$\rho(r,t)=\rho(r,-t)\equiv g(r,t^2)\ , \quad (5.138)$$

and χ, corresponding to a momentum, is real and time odd

$$\chi(r,t)=-\chi(r,-t)\equiv t f(r,t^2)\ . \quad (5.139)$$

Transforming the Hartree action expressed in terms of ϕ and ϕ^* to these new variables yields

$$S=\int dt\left\langle\Psi\left|i\frac{\partial}{\partial t}-H\right|\Psi\right\rangle = \int dt\left[\int dr\sum_k\left[\chi_k\frac{d}{dt}\rho_k+\frac{1}{2m}\rho_k(\nabla\chi_k)^2\right]+V(\rho)\right], \quad (5.140)$$

where

$$V(\rho)=\int dr\sum_k\left[\frac{1}{8m}\frac{(\nabla\rho_k)^2}{\rho_k}+\tfrac{1}{2}\int dr'\sum_j\rho_k(r,t)v(r-r')\rho_j(r',t)\right]. \quad (5.141)$$

The potential $V(\rho)$ depends upon all the degrees of freedom in the one-body density (and in the general HF case, the one-body density matrix) and by Eq. (3.137) is just the expectation value of the HF energy for a time-even determinant. A convenient way to appreciate its gross features is to evaluate the constrained energy of deformation surface defined by minimizing $V(\rho)$ with respect to all determinants satisfying one or more constraints. A familiar example with one constraint relevant to fission is the energy as a function of quadrupole moment, as sketched in Fig. 20. The point Q_1 is the relative minimum corresponding to the HF ground state of the parent nucleus, and Q_2 is the fission saddle point. Introducing more constraints would generalize Fig. 20 to a surface representing more of the shape degrees of freedom of the one-body density matrix.

Continuing to imaginary time by replacing (it) by τ as in Eq. (5.76) yields

$$\tilde{\rho}(r,\tau)\equiv\rho\left[r,\frac{\tau}{i}\right]=g(r,-\tau^2)=\tilde{\rho}(r,-\tau) \quad (5.142)$$

and

$$\tilde{\chi}(r,\tau)\equiv i\chi\left[r,\frac{\tau}{i}\right]=\tau f(r,-\tau^2)=-\tilde{\chi}(r,-\tau)\ , \quad (5.143)$$

so that

$$\tilde{\phi}(r,\tau)=[\tilde{\rho}(r,\tau]^{1/2}e^{\tilde{\chi}(r,\tau)}\ . \quad (5.144)$$

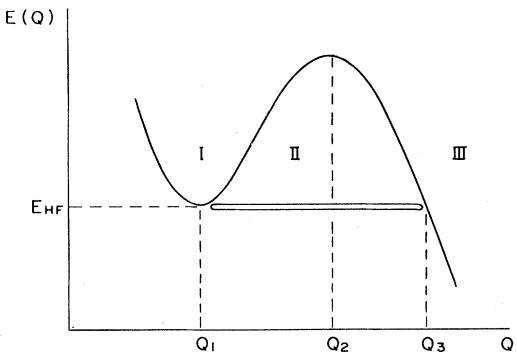

FIG. 20. Sketch of the constrained Hartree-Fock energy $E(Q)$ as a function of quadrupole moment Q for a fissile nucleus. At any value of Q, $E(Q)$ is defined as a minimum of the HF energy, Eq. (3.4) or (3.141), in the space of time-even determinants having quadrupole moment Q.

The imaginary-time action becomes

$$\tilde{S}=\int d\tau\left\langle\tilde{\Psi}\left|-\frac{\partial}{\partial\tau}-H\right|\tilde{\Psi}\right\rangle$$
$$=\int d\tau\left[\int dr\sum_k\left[\tilde{\chi}_k\frac{d}{d\tau}\tilde{\rho}_k-\frac{1}{2m}\tilde{\rho}_k(\nabla\tilde{\chi}_k)^2\right]+V(\tilde{\rho})\right], \tag{5.145}$$

and one notes that the sign of the second term in Eq. (5.145) has changed relative to Eq. (5.140). Finally, making use of the arbitrariness in the definition of the sign of $\tilde{\chi}$, the variable change $\tilde{\chi}_k\rightarrow-\tilde{\chi}_k$ in Eq. (5.145) yields Euler-Lagrange equations for $\tilde{\chi}(r,\tau),\tilde{\rho}(r,\tau)$ identical in form to those for $\chi(r,t),\rho(r,t)$, except that $V(\rho)$ and $V(\tilde{\rho})$ enter with opposite signs. Thus the multidimensional generalization of Fig. 20 is indeed inverted, and the periodic, self-consistent solutions to Eqs. (5.134) are therefore precisely analogous to periodic solutions to the real-time equations, Eqs. (5.75), in a region surrounding a local minimum in $V(\rho)$.

Several new features arise in summing stationary trajectories in the many-fermion problem. In the one-dimensional quantum-mechanical example in Figs. 16(b) and 16(c), a general periodic trajectory could always be decomposed into a sequence of periodic trajectories within each of the regions I, II, and III. It was this decomposition which allowed one to express the sum of all possible trajectories in terms of a multiple geometric series involving one single periodic solution in each of the three regions, Eq. (5.21). In the analogous many-body problem, however, to decompose a trajectory involving two regions into periodic solutions for each separate region, the determinant of single-particle wave functions ϕ_k satisfying the real-time self-consistent eigenvalue problem, Eq. (5.75) must equal the determinant of functions $\tilde{\phi}_k$ satisfying the imaginary-time equations Eq. (5.76) at the corresponding turning points. In general, for an arbitrary energy, there is no reason why periodic solutions in classically allowed and forbidden regions should join, and there is therefore no practical way to sum all periodic trajectories. As argued in Sec. V.A.2, the case of tunneling decay is simpler than the general double-well problem because trajectories in the exterior region III of Fig. 16(d) do not contribute to the smoothed level density from which the decay width is calculated (Appendix A of Levit, Negele, and Paltiel, 1980b). Thus in the nuclear fission problem one is faced with summing all trajectories in regions I and II of the multidimensional analog of Fig. 20.

In the limit of infinite period, stationary solutions to Eq. (5.76) in the classically forbidden region II of Fig. 20 have the static HF energy and exactly join the static HF solution of region I at the turning point Q_1. In general, there are several distinct, well-separated solutions in region II, corresponding to symmetric fission, asymmetric fission, and alpha decay, as well as more complicated many-body breakup. Each such solution evolves from the HF ground state at Q_1 through a saddle point to some distinct configuration at the boundary of the classically allowed regime, and all solutions involving any combination of these trajectories should be summed in the SPA. Denoting the reduced action, Eq. (5.86), in region I by $W_{\rm I}$ and defining its imaginary-time counterpart in a specific decay channel (a) by

$$W_{\rm II}^a=\int_{-T/2}^{T/2}d\tau\,dr\sum_k\tilde{\phi}_k^{(a)}(r,-\tau)\frac{d}{d\tau}\tilde{\phi}_k^{(a)}(r,\tau)\ . \tag{5.146}$$

the contribution of all stationary solutions to the trace is

$$\frac{i}{E-H+i_k}=\sum_{k=1}^{\infty}\left[e^{iW_{\rm I}}\sum_{n=0}^{\infty}\left[\sum_a e^{-W_{\rm II}^{(a)}}\right]^n\right]^k$$
$$+\sum_{k=1}^{\infty}\left[\sum_a e^{-W_{\rm II}^{(a)}}\sum_{n=0}^{\infty}\left[e^{iW_{\rm I}}\right]^n\right]^k$$
$$=\frac{1}{1-e^{iW_{\rm I}}-\sum_a e^{-W_{\rm II}^{(a)}}}-1\ . \tag{5.147}$$

If analogous solutions in regions I and II could be joined infinitesimally above $E_{\rm HF}$, then by the arguments leading to Eq. (5.28) one would obtain the total width as a sum of partial decay widths

$$\Gamma=\sum_a\Gamma^{(a)}\ , \tag{5.148}$$

where

$$\Gamma^{(a)}=2\left[\frac{\partial W_{\rm I}}{\partial E}\right]^{-1}e^{-W_{\rm II}^{(a)}}\ . \tag{5.149}$$

Since the joining problem has been solved only at the HF energy, the present treatment yields only the penetrability $e^{-W_{\rm II}^{(a)}}$, and the appropriate premultiplying factor has not yet been derived.

The theory of spontaneous decay arising from self-consistent solutions to the imaginary-time mean-field equation, Eq. (5.76), appears to embody the essential physics of the fission problem. Single-particle behavior, through the evolution of a determinantal wave function as well as all the relevant collective degrees of freedom, are consistently combined in a microscopic quantum theory. The competition between alternative decay modes is manifest in the distinct solutions governing each partial width. Thus it is reasonable to expect that appropriate numerical solution of the mean-field equations can provide a quantitative understanding of fission lifetime systematics, including such details as shell effects and the competition between symmetric and asymmetric fission.

F. Scattering

In principle, the general program outlined above may be applied to scattering theory by writing exact functional integral expressions for observables and systematically applying the SPA. In practice, significant problems arise in the scattering problem which were not present in the simpler case of the evaluation of the trace of the evolution operator for quantum eigenstates and spontaneous decay.

One serious problem concerns the feasibility of adequately approximating the S matrix in the SPA. Although the S matrix is a natural quantity to utilize in formal scattering theory the fact that it ultimately corresponds to the overlap of many-body initial and final states renders it as difficult to calculate in principle as the ground-state wave function discussed in Sec. II.A.1. Whereas the initial efforts in scattering theory reviewed below deal directly with S matrix elements, the validity of the theory for individual amplitudes is presently uncertain. Either proof is required that commensurate approximations to in and out states yield overlaps much more favorable than those between model states and eigenstates, or the theory should ultimately be formulated in terms of expectation values of few-body operators rather than S-matrix elements.

Additional technical complications arise in scattering theory as a result of the need to define reaction channels and to project onto states of well-defined cm momentum. Hence, instead of addressing the full scattering problem, it is valuable to begin with the simpler case of excitation by an external one-body potential.

1. Response to an external potential

The problem of the response of a many-fermion system to an external potential has been addressed by Alhassid and Koonin (1981). The S matrix is given by the limit of the following evolution operator:

$$S=\lim_{T\to\infty} U_0(0,T)U(T,-T)U_0(-T,0)\ , \tag{5.150}$$

where U_0 denotes evolution under the many-body Hamiltonian, Eq. (5.32), and U denotes evolution under the many-body Hamiltonian plus an external field $V(r,t)$. As in Eq. (5.46), each evolution operator may be written in terms of a functional integral with respect to an auxiliary field, with the result

$$\langle\beta'\,|\,S\,|\,\beta\rangle=\lim_{T\to\infty}\int\int\int D[\sigma_f]D[\sigma]D[\sigma_i]\exp\left[\frac{i}{2}\left[\int_T^0 dt(\sigma_f v\sigma_f)+\int_{-T}^{T}dt(\sigma v\sigma)+\int_0^{-T}dt(\sigma_i v\sigma_i)\right]\right]$$
$$\times\langle\beta'\,|\,U^{\sigma_f}(0,T)U^{\sigma}(T,-T)U^{\sigma_i}(-T,0)\,|\,\beta\rangle\ , \tag{5.151a}$$

where, as in Eq. (5.47),

$$U^{\sigma_{f,i}}(t',t)\equiv T_t e^{-i\int_t^{t'}dt[\hat{K}+(\sigma_{f,i}v\hat{\rho})]}\ , \tag{5.151b}$$

$$U^{\sigma}(t',t)\equiv T_t e^{-i\int_t^{t'}dt[\hat{K}+\hat{V}(r,t)+(\sigma v\hat{\rho})]}\ , \tag{5.151c}$$

the quantities $(\sigma v\sigma)$ and $(\sigma v\hat{\rho})$ are defined in Eq. (2.55), and $|\beta\rangle$ and $|\beta'\rangle$ denote initial and final states. The distinction of these separate auxiliary fields is artificial, although useful, and one could view Eq. (5.151a) as the evolution in a single time variable which runs from 0 to $-T$ without any external field, from $-T$ to $+T$ in the presence of the external field, and from T to 0 without the external field. The SPA is applied in each of the three time intervals, assuming that the modulus of $\langle\beta'\,|\,U^{\sigma_f}U^{\sigma}U^{\sigma_i}\,|\,\beta\rangle$ is slowly varying and thus requiring stationarity of the argument of $\langle\beta'\,|\,U^{\sigma_f}U^{\sigma}U^{\sigma_i}\,|\,\beta\rangle$ plus the exponential in Eq. (3.151a). The stationary solution, analogous to Eq. (5.52), is

$$\sigma_l^0(t)=\mathrm{Re}\frac{\langle\beta'\,|\,\tilde{T}_t\hat{\rho}U^{\sigma_f^0}U^{\sigma^0}U^{\sigma_i^0}\,|\,\beta\rangle}{\langle\beta'\,|\,U^{\sigma_f^0}U^{\sigma^0}U^{\sigma_i^0}\,|\,\beta\rangle}\ , \tag{5.152}$$

where σ_l denotes any one of σ_f, σ, or σ_i and $\tilde{T}_t$ inserts $\hat{\rho}$ into the corresponding interval $(0,T)$, $(T,-T)$, or $(-T,0)$, respectively, at time t.

As shown by Alhassid and Koonin (1981), Eqs. (5.151) and (5.152) possess several desirable properties. For times $-\tau$ prior to the interaction period, $\sigma_i^0(-\tau)=\sigma^0(-\tau)$ and similarly for τ subsequent to the interaction period $\sigma_f^0(\tau)=\sigma^0(\tau)$. Since the evolution by U^{σ_i} prior to the interaction time is precisely compensated by U^{σ} and similarly for the evolution subsequent to the interaction time, it therefore follows that the SPA approximant to the S matrix, obtained by substituting the stationary solution σ^0 in Eq. (5.151a), is independent of T once T exceeds the interaction period. The limit in Eq. (3.151a) thus exists in the SPA, and in contrast to the treatment of Griffin *et al.* (1979), there is no need to introduce any *ad hoc* time averages. A second desirable property is that if $V(r,t)$ has time-reversal symmetry, the SPA approximant to Eq. (3.151a) also displays time-reversal symmetry. In general, however, the present approximation is not unitary. Applications of this theory to a solvable model is reviewed in Sec. VI.B.

2. Expectation values of one- and two-body operators

The problem of calculating the time evolution of one- and two-body operators has also been addressed by Alhassid, Müller, and Koonin (1981). Introducing auxiliary fields in the usual way, according to Eq. (5.46), one gets an exact expression for the evolution of the one-body density,

$$\langle\hat{\rho}(T)\rangle=\langle\beta\,|\,U(0,T)\hat{\rho}(T)U(T,0)\,|\,\beta\rangle$$
$$=\int D[\sigma_1]D[\sigma_2]\exp\left[\frac{i}{2}\left[\int_T^0 dt(\sigma_1 v\sigma_1)+\int_0^T dt(\sigma_2 v\sigma_2)\right]\right]\langle\beta\,|\,U^{\sigma_1}(0,T)\hat{\rho}(T)U^{\sigma_2}(T,0)\,|\,\beta\rangle\ . \tag{5.153}$$

By changing the variable of integration in the Gaussian integral over the auxiliary field at a specific time, the following identity may be verified:

$$\int D[\sigma]\sigma e^{i[1/2(\sigma v\sigma)-(\sigma v\hat{\rho})]}=\int D[\sigma]\hat{\rho}e^{i[1/2(\sigma v\sigma)-(\sigma v\hat{\rho})]}\ , \tag{5.154}$$

so (5.153) may be rewritten

$$\langle\hat{\rho}(T)\rangle=\int D[\sigma_1]D[\sigma_2]\sigma(T)\exp\left[\frac{i}{2}\left[\int_T^0 dt(\sigma_1 v\sigma_1)+\int_0^T dt(\sigma_2 v\sigma_2)\right]\right]\langle\beta\,|\,U^{\sigma_1}(0,T)U^{\sigma_1}(T,0)\,|\,\beta\rangle\ . \tag{5.155}$$

Applying the SPA, assuming $\sigma(t)$ is slowly varying and thus requiring stationarity of the exponent in Eq. (3.155) plus ln $\langle\beta\,|\,U_{\sigma_1}U_{\sigma_2}\,|\,\beta\rangle$, yields the stationary solutions

$$\sigma_2^0(t)=\frac{\langle\beta\,|\,U^{\sigma_1^0}(0,t)U^{\sigma_1^0}(t,T)U^{\sigma_2^0}(T,t)\hat{\rho}U^{\sigma_2^0}(t,0)\,|\,\beta\rangle}{\langle\beta\,|\,U^{\sigma_1^0}(0,T)U^{\sigma_2^0}(T,0)\,|\,\beta\rangle} \tag{5.156a}$$

and

$$\sigma_1^0(t)=\frac{\langle\beta\,|\,U^{\sigma_1^0}(0,t)\hat{\rho}U^{\sigma_1^0}(t,T)U^{\sigma_2^0}(T,t)U^{\sigma_2^0}(t,0)\,|\,\beta\rangle}{\langle\beta\,|\,U^{\sigma_1^0}(0,T)U^{\sigma_2^0}(T,0)\,|\,\beta\rangle}\ . \tag{5.156b}$$

A self-consistent solution to Eqs. (5.156) is $\sigma_1^0(t)=\sigma_2^0(t)\equiv\sigma^0(t)$, since in this case $U^{\sigma^0}(t,T)U^{\sigma^0}(T,t)=1$, rendering Eqs. (5.156a) and (5.156b) identical. For a general state β,

$$\sigma^0(t)=\frac{\langle\beta\,|\,U^{\sigma^0}(0,t)\hat{\rho}U^{\sigma^0}(t,0)\,|\,\beta\rangle}{\langle\beta\,|\,\beta\rangle}\ , \tag{5.157a}$$

and in the special case in which $|\,\beta\rangle$ is a single Slater determinant comprised of single-particle wave functions $\Psi_k(r,0)$,

$$\sigma^0(r,t)=\sum_k \Psi_k^*(r,t)\Psi_k(r,t)\ , \tag{5.157b}$$

where $\Psi_k(r,t)$ is the solution to the TDHF equation, (5.64), with the initial condition $\Psi_k(r,0)$.

This derivation may be extended in two simple ways. Whereas, as usual, the Hartree case has been treated for simplicity, following the treatment in Sec. V.D.2, introduction of a nonlocal auxiliary field $\sigma(r,r',t)$ yields the analogous result for the one-body density matrix and thus any one-body operator. In addition, the identity (5.154) may be applied to both σ_1 and σ_2, so that $\langle\hat{\rho}(r_1r_2,t)\hat{\rho}(r_3r_4,t)\rangle$ may be evaluated in the same way, yielding an analogous result for the expectation value of a two-body operator.

The final result is that a first approximation to the time evolution of the expectation value of any one- or two-body operator is given by Eqs. (5.157a) and (5.157b). In the case in which $|\,\beta\rangle$ is a single Slater determinant, this derivation both justifies the TDHF initial-value prescription and, through corrections to the SPA, provides a formulation for calculating systematic corrections.

3. Asymptotic states

A primary difficulty in the scattering problem is to find a tractable approximation for the asymptotic in and out states which is commensurate with the approximations made to the evolution operator.

One possible method of generating a compatible approximation for channel eigenstates is by adiabatically switching on the two-body interaction:

$$|\,\beta\rangle=\lim_{T\to\infty}\frac{U_\lambda(0,-T)\,|\,\beta_0\rangle}{\langle\beta_0\,|\,U_\lambda(0,-T)\,|\,\beta_0\rangle}\ , \tag{5.158}$$

where U_λ is the evolution operator with respect to the Hamiltonian

$$H_\lambda=\hat{K}+\lambda\tfrac{1}{2}\hat{\rho}v\hat{\rho}+(1-\lambda)U\hat{\rho}\ , \tag{5.159}$$

$\lambda(t)$ is adiabatically switched on from 0 to 1, U is a convenient one-body potential, such as the self-consistent HF potential, and $|\,\beta_0\rangle$ is an eigenstate of $\hat{K}+U\hat{\rho}$. As in Eq. (5.151), a functional integral representation for an S-matrix element may be obtained by introducing auxiliary fields for each of the five evolution operators in the matrix element

$$\langle\beta'\,|\,s\,|\,\beta\rangle=\lim_{\substack{T\to\infty\\T'\to\infty}}\langle\,\beta_0'\,|\,U_\lambda(T',0)U_0(0,T)U(T,-T)\times U_0(-T,0)U_\lambda(0,T')\,|\,\beta_0'\rangle\ , \tag{5.160}$$

and appreciable simplifcations ensue at the SPA level if U in Eq. (5.159) is chosen as the HF potential. An alternative method of implementing commensurate approximations on the evolution operator and asymptotic states utilizes the coherent-state representation of Sec. V.G (Levit, Negele, and Orland, 1981).

The treatment thus far has ignored the need for constructing eigenstates of cm momentum. Formally, a state of definite momentum may be constructed by projection

$$\Psi_{\mathbf{P}}=\int ds\, e^{-i\mathbf{P}\cdot\mathbf{s}}\Psi(r_1+s,\ldots r_n+s)=\int ds\, e^{-i(\mathbf{P}-\hat{P})\cdot\mathbf{s}}\Psi(r_1,\ldots r_n)\ , \tag{5.161}$$

where $\hat{P}$ is the one-body momentum operator. Application of the SPA to a matrix element of the form

$$S_{P_1P_2}=\int ds_1ds_2\langle\beta\,|\,e^{i(P_1-\hat{P})\cdot s}Ue^{-i(P_2-\hat{P})\cdot s}\,|\,\beta\rangle \tag{5.162}$$

yields the stationary solutions

$$P_1=\frac{\langle\beta\,|\,e^{-i\hat{P}\cdot S_1^0}\hat{P}Ue^{i\hat{P}\cdot S_2^0}\,|\,\beta\rangle}{\langle\beta\,|\,e^{-i\hat{P}\cdot S_1^0}Ue^{i\hat{P}\cdot S_2^0}\,|\,\beta\rangle} \tag{5.163a}$$

and

$$P_2=\frac{\langle\beta|e^{-i\hat{P}\cdot S_1^0}U\hat{P}e^{i\hat{P}\cdot S_2^0}|\beta\rangle}{\langle\beta|e^{-i\hat{P}\cdot S_1^0}Ue^{i\hat{P}\cdot S_2^0}|\beta\rangle}\ . \tag{5.163b}$$

These self-consistent equations are analogous to Eqs. (5.152) and (5.156) in the sense that P_i is required to equal an expectation value of $\hat{P}$ at an appropriate time in the evolution. They differ because P_1 and P_2 are implicit functions of the positions S_1^0 and S_2^0 at which the final and initial states are localized by the SPA. Many of the technical details of the construction of asymptotic states, projection, and self-consistency conditions arising from application of the SPA may be found in a recent paper on scattering theory by Reinhardt (1982).

In conclusion, the formal elements of scattering theory are now developed to the point that one may begin to address the fundamental conceptual questions raised at the beginning of this section. The most essential problem is to determine which scattering observables may be legitimately approximated by the SPA. In sufficiently simple models, such as the one-dimensional delta-function problem discussed in Sec. VI.A, the existence of an explicit expansion parameter should allow one to calculate the full S matrix in appropriate limits. Physically, it is also plausible that one may treat sufficiently simple excitations in realistic systems, such as transitions induced by an external field between different RPA vibrations built upon the same intrinsic state of a closed-shell nucleus. In this case, it is reasonable to expect that the poor overlap with the exact intrinsic state will be irrelevant to the transition amplitude and that the collective excitation of vibrational modes will be adequately described. There is much less reason for optimism, however, for S-matrix elements between in- and out-channel states differing essentially in structure, in which case wave-function overlap becomes crucial. In these more complicated cases, it will be necessary to focus attention on suitably defined inclusive observables, rather than individual S-matrix elements. Even when these conceptual issues are resolved, it is clear that significant technical and practical problems need to be overcome before calculations of nuclear collisions are feasible.

G. Alternative formulations

A variety of alternative functional integral representations exist for the many-fermion evolution operator, each of which yields its own technology for obtaining a mean-field theory and systematic corrections. The essential features of these alternative approaches are reviewed in this section, and technical details may be found in the referenced literature.

A useful method for generating functional integrals for the many-body problem is to use overcomplete sets of states (Orland, 1980; Blaizot and Orland, 1980b). Let $|\mathbf{Z}\rangle$ be an overcomplete set of vectors in a Hilbert space parametrized by a continuous family of parameters $\mathbf{Z}\equiv Z_\alpha=\{Z_1,Z_2\ldots\}$ and having a measure $d\mu(\mathbf{Z})$ such that the unit operator in the Hilbert space may be written

$$\int d\mu(\mathbf{Z})\,|\mathbf{Z}\rangle\langle\mathbf{Z}|=1\ . \tag{5.164}$$

Breaking the evolution from t_i to t_f in the full space into N steps of time duration $\varepsilon=(t_f-t_i)/N$ and inserting the unit operator, Eq. (5.164), between each step, a matrix element of the evolution operator between states $|\mathbf{Z}_i\rangle$ and $\langle\mathbf{Z}_f|$ may be written

$$\langle\mathbf{Z}_f|e^{-iH(t_f-t_0)}|\mathbf{Z}_i\rangle=\int d\mu(\mathbf{Z}_{N-1})\int d\mu(\mathbf{Z}_{N-2})\cdots\int d\mu(\mathbf{Z}_1)\langle\mathbf{Z}_f|e^{-iH\varepsilon}|\mathbf{Z}_{N-1}\rangle\langle\mathbf{Z}_{N-1}|e^{-iH\varepsilon}|\mathbf{Z}_{N-2}\rangle$$
$$\times\langle\mathbf{Z}_{N-2}|\cdots|\mathbf{Z}_1\rangle\langle\mathbf{Z}_1|e^{-iH\varepsilon}|\mathbf{Z}_i\rangle\ . \tag{5.165}$$

In the large-N limit, assuming piecewise continuity in $\mathbf{Z}$ as a function of time and retaining terms of leading order in ε,

$$\langle\mathbf{Z}_n|e^{-iH\varepsilon}|\mathbf{Z}_{n-1}\rangle\approx\langle Z_n|(1-iH\varepsilon)\left[|\mathbf{Z}_n\rangle-\varepsilon\left[\frac{|\mathbf{Z}_n\rangle-|\mathbf{Z}_{n-1}\rangle}{\varepsilon}\right]\right]$$
$$\approx\langle\mathbf{Z}_n|\mathbf{Z}_n\rangle\exp\left[\frac{i\varepsilon\left\langle\mathbf{Z}_n\left|i\frac{\partial}{\partial t}-H\right|\mathbf{Z}_n\right\rangle}{\langle\mathbf{Z}_n|\mathbf{Z}_n\rangle}\right], \tag{5.166}$$

so that

$$\langle\mathbf{Z}_f|e^{-iH(t_f-t_i)}|\mathbf{Z}_i\rangle=\int_{|\mathbf{Z}(t_i)\rangle=|\mathbf{Z}_i\rangle}^{\langle\mathbf{Z}(t_f)|=\langle\mathbf{Z}_f|}\mathscr{D}[\mathbf{Z}]\exp\left[i\int_{t_i}^{t_f}dt\frac{\left\langle\mathbf{Z}(t)\left|i\frac{\partial}{\partial t}-H\right|\mathbf{Z}(t)\right\rangle}{\langle\mathbf{Z}(t)|\mathbf{Z}(t)\rangle}+\ln\langle\mathbf{Z}_f|\mathbf{Z}(t_f)\rangle\right], \tag{5.167a}$$

where the measure is defined

$$\mathscr{D}[\mathbf{Z}]\equiv\prod_{t_f<t<t_i}d\mu[\mathbf{Z}(t)]\langle\mathbf{Z}(t)|\mathbf{Z}(t)\rangle\ . \tag{5.167b}$$

Several alternative functional integral expressions may be obtained straightforwardly by different choices for the overcomplete set $|\mathbf{Z}\rangle$.

1. Boson coherent states

For a system of bosons with creation operators $c_\alpha^\dagger$, coherent states are defined

$$|\mathbf{Z}\rangle \equiv e^{\sum_\alpha Z_\alpha c_\alpha^\dagger}|0\rangle , \tag{5.168}$$

where $|0\rangle$ denotes the vacuum. Using the properties of eigenfunctions of the number operator, it is elementary to prove that the overlap of two coherent states is

$$\langle \mathbf{Z}|\mathbf{Z}'\rangle = e^{\sum_\alpha Z_\alpha^* Z'_\alpha} \tag{5.169}$$

and that the matrix element of a normal-ordered operator is

$$\langle \mathbf{Z}|NA(\mathbf{c}^\dagger,\mathbf{c})|\mathbf{Z}'\rangle = e^{\sum_\alpha Z_\alpha^* Z'_\alpha} A(\mathbf{Z}^*,\mathbf{Z}') . \tag{5.170}$$

The closure relation (Bargmann, 1961) is

$$\prod_\alpha \frac{1}{2\pi i}\int dZ_\alpha^* \int dZ_\alpha e^{-\sum_\alpha Z_\alpha^* Z_\alpha}|\mathbf{Z}\rangle\langle\mathbf{Z}| = 1 , \tag{5.171}$$

where the real and imaginary parts of Z_α must be integrated independently. This result may be verified straightforwardly in polar coordinates.

To obtain a functional integral for a many-boson system, Eqs. (5.169)–(5.171) are substituted into Eq. (5.167). The measure is simplified by the fact that the exponential factor in the overlap, Eq. (5.169), cancels the negative exponential in Eq. (5.171). Transforming from number representation $Z_\alpha(t)$ to coordinate representation $\phi(x,t)$, a matrix element of the many-boson evolution operator becomes

$$\langle \phi_f|\exp[-iH(t_f-t_i)]|\phi_i\rangle = \int_{\phi(x,t_i)=\phi_i(x)}^{\phi^*(x,t_f)=\phi_f^*(x)} \mathscr{D}(\phi^*,\phi)\exp\left[i\int_{t_i}^{t_f} dt \int dx\, \phi^*(x,t) \times \left[i\frac{d}{dt} + \frac{\hbar}{2m}\nabla^2 - \tfrac{1}{2}\int dx'\phi^*(x',t)\phi(x',t)v(x-x') \right]\phi(x,t) + \int dx\, \phi_f^*(x)\phi(x,t_f) \right] . \tag{5.172}$$

The corresponding formula for the trace is further simplified by the fact that integration over a complete set of states has a factor analogous to the exponential in Eq. (5.171), which removes the final logarithm in Eq. (5.172), and one obtains periodic boundary conditions on $\int \mathscr{D}(\phi^*\phi)$. Application of the SPA to Eq. (5.172) by independently varying the real and imaginary parts of ϕ, or equivalently ϕ and ϕ^* in the exponent, immediately yields the time-dependent Hartree equation

$$i\frac{d}{dt}\phi(x,t) = \left[-\frac{\hbar^2}{2m}\nabla^2 + \tfrac{1}{2}\int dx'\phi^*(x',t)\phi(x',t) \times\sigma(x-x') \right]\phi(x,t) . \tag{5.173}$$

For a general matrix element, as in Sec. V.F, the function ϕ^* satisfying the boundary condition ϕ_f^* at t_f need not be the complex conjugate of the function ϕ satisfying the boundary condition ϕ_i at t_i, but in the physically important case of the trace, in this and subsequent formulas, ϕ and ϕ^* are complex conjugates. Thus one has described the dynamics of the many-boson system in terms of the evolution of a single condensate wave function $\phi(x,t)$ for the macroscopically occupied Bose condensate, and it is physically reasonable that the direct Hartree field should define the potential.

One way to obtain a functional integral for the N-fermion problem is to embed the fermion space in a much larger boson Fock space defined as a direct product of N boson spaces (Blaizot and Orland, 1980a, 1980b), where an additional label, denoting the boson space, is affixed to all operators and variables of integration, $\phi_i^*(x,t)$, appearing in the functional integrals. To project into the fermion space, it is necessary to antisymmetrize with respect to the labels (i). If one thinks of the additional label as a color quantum number, then one is projecting onto a color singlet. Since the overall boson wave function is totally symmetric, and the color singlet is totally antisymmetric, the remaining portion of the wave function is antisymmetric and thus correctly describes a fermion. Defining a Hamiltonian $\tilde{H}$ in the direct product Boson space

$$\tilde{H} = \sum_{i=1}^N \int dx\, \hat{\phi}_i^\dagger(x)\left[-\frac{\hbar^2}{2m}\nabla^2 \right]\hat{\phi}_i(x) + \tfrac{1}{2}\sum_{i,j=1}^N \int dx\, dx' \hat{\phi}_i^\dagger(x)\hat{\phi}_j^\dagger(x')\sigma(x-z)\hat{\phi}_j(x')\hat{\phi}_i(x) , \tag{5.174}$$

where $\hat{\phi}_i^\dagger$ and $\hat{\phi}_i$ are creation and annihilation operators in the ith Boson space, it may be verified that $\tilde{H}$ has the same matrix elements in the antisymmetric (singlet) subspace as H has in the fermion space and that $\tilde{H}$ commutes with the projector P which projects onto the singlet space. It follows that if the initial state is defined as the singlet projection of the direct product of N coherent states

$$|\Phi_i\rangle = P\exp\left[\sum_{k=1}^{N}\int dx\,\phi_k(x)\hat{\phi}_k^\dagger(x)\right]|0\rangle \tag{5.175}$$

and similarly for $\langle\Phi_f|$, then the matrix elements of the many-fermion evolution operator are given by

$$\langle\Phi_f|e^{-iH(t_f-t_i)}|\Phi_i\rangle = \int \mathscr{D}(\phi_1^*\ldots\phi_N^*,\phi_1\ldots\phi_N) \times\exp\left[i\int_{t_i}^{t_f}dt\int dx\sum_k\phi_k^*(x,t)\left[i\frac{d}{dt}+\frac{\hbar^2}{2m}\nabla^2 -\tfrac{1}{2}\int dx'\sum_j\phi_j^*(x',t)\phi_j(x',t)v(x-x')\right]\phi_k(x,t)\right], \tag{5.176}$$

where, for simplicity, the boundary conditions and overlap at the final time have been omitted. As was the case with Eq. (5.172), application of the SPA to Eq. (5.176) yields time-dependent Hartree, rather than time-dependent Hartree-Fock equations for the ϕ_j's. Given that the N-fermion problem was embedded in a many-boson space, it is not surprising that one obtains an approximation equivalent to the evolution of N independent boson condensates. [That the functions must be independent follows from the fact that the singlet projector yields zero in Eq. (3.175) unless the functions ϕ_k are linearly independent.] If one formally replaced V in Eqs. (5.175) and (5.176) by one-half of the antisymmetrized potential, the matrix elements of $\tilde{H}$ would still be correct, but the Hartree potential in the SPA would be replaced by one-half of the correct Hartree-Fock potential, a fact reminiscent of the discussion subsequent to Eq. (5.109).

2. Slater determinants

In terms of an overcomplete set of Slater determinants, a convenient expression for the unit operator (Blaizot and Orland, 1980, 1981) is

$$\prod_{k,j}\int\mathscr{D}[\phi_k^*(x),\phi_j(x)]\delta\left[\int dx\phi_k^*(x)\phi_j(x)-\delta_{kj}\right] \times\mathscr{N}|\phi_1\phi_2\ldots\phi_N\rangle\langle\phi_1\phi_2\ldots\phi_N| = 1, \tag{5.177}$$

where $\mathscr{N}$ is a normalization constant, $|\phi_1\phi_2\ldots\phi_N\rangle$ denotes a determinant comprised of the single-particle wave functions $\phi_1,\phi_2\ldots\phi_n$, and the real and imaginary parts of ϕ and ϕ^* are integrated independently. This result may be verified directly, obtained from Schur's lemma, or derived by applying singlet projectors to the left and right of Eq. (5.171). By virtue of the δ function in Eq. (5.177), the overlap factor in the general equation (5.167b) is a constant, and to within an irrelevant multiplicative constant, the many-fermion evolution operator between initial and final determinantal wave functions $|\Phi_i\rangle$ and $|\Phi_f\rangle$ is

$$\langle\Phi_f|e^{-iH(t_f-t_i)}|\Phi_i\rangle = \int\mathscr{D}(\phi_1^*\cdots\phi_N^*,\phi_1\cdots\phi_N)\prod_{k,j}\delta\left[\int dx\,\phi_k^*(x,t)\phi_j(x,t)-\delta_{kj}\right] \times\exp\left\{i\int_{t_i}^{t_f}dt\left[\int dx\sum_k\phi_k^*(x,t)\left[i\frac{d}{dt}+\frac{\hbar^2}{2m}\nabla^2\right]\phi_k(x,t) -\int\int dx\,dx'\sum_{kj}\phi_k^*(x,t)\phi_j^*(x',t)v(x-x') \times[\phi_k(x,t)\phi_j(x',t)-\phi_j(x,t)\phi_k(x',t)]\right]\right\}. \tag{5.178}$$

Two salient differences relative to Eq. (5.176) are the explicit appearance of exchange terms in the exponential, arising from the fact that the expectation value of H in Eq. (5.167) is evaluated between determinants instead of between products of coherent states, and the δ function restriction to integration over orthonormal functions. Application of the SPA to Eq. (5.178) immediately yields the TDHF equation, Eq. (3.7a), rather than the time-dependent Hartree equation, and the required orthonormality at all times follows automatically from Eq. (3.8).

The SPA equations for quantized eigenstates may be seen to be equivalent to the self-consistent periodic eigenvalue problem, Eq. (5.75), except of course for the additional Fock exchange term, as follows. Evaluation of the

trace, as in the boson case, imposes a periodic boundary condition. Variation of the exponent in Eq. (3.178) subject to the constraints of orthonormality and periodicity may be accomplished by introduction of the Lagrange multipliers

$$\sum_{kj}\int dt\,\tilde{\alpha}_{kj}(t)\int dx\,\phi_k^*(x,t)\phi_j(x,t)$$

with the result

$$\left[-i\frac{\partial}{\partial t}-\frac{\hbar^2}{2m}\nabla_r^2+\int dx'v(x-x')\sum_j\phi_j^*(x',t)\phi_j(x',t)\right]\phi_k(x,t)$$
$$-\int dx\,dx'v(x-x')\sum_j\phi_j^*(x',t)\phi_j(x,t)\phi_k(x',t)=\sum_j\tilde{\alpha}_{kj}(t)\phi_j(x,t)\ . \quad (5.179)$$

By an appropriate transformation, $\tilde{\alpha}$ may be diagonalized. The periodicity condition is satisfied by any function of time, $\alpha_k(t)$, such that

$$\int_0^T dt\,\tilde{\alpha}_k(t)=\alpha_k\ , \quad (5.180)$$

where α_k is defined by Eq. (5.75). The solutions to Eq. (5.179), with diagonal $\tilde{\alpha}_k$ satisfying (5.180), are gauge-equivalent to the solutions of (5.75) and thus yield the same SPA result for eigenstates. Although this method thus provides an economical derivation of the previous SPA results, nontrivial technical problems arise in evaluating corrections to the SPA (Blaizot and Orland, 1980b).

An alternative, but equivalent, treatment of determinants (Kuratsuji and Suzuki, 1980; Blaizot and Orland 1980b) is formulated in terms of the Thouless parametrization of a determinant

$$|\mathbf{S}\rangle\equiv e^{\sum_{\rho\nu}S_{\rho\nu}\hat{a}_\rho^\dagger\hat{a}_\nu}|0\rangle\ , \quad (5.181)$$

where $S_{\rho\nu}$ is a particle-hole amplitude in the notation of Sec. IV.B. Resolution of the unit operator is accomplished by finding the invariant measure for the group of unitary transformations among the determinants, Eq. (5.181), with the result

$$\int\prod_{\rho\nu}\frac{dS_{\rho\nu}^*\,dS_{\rho\nu}}{2\pi i}\mathrm{Det}\left[1+\sum_\rho S_{\rho\nu}^\dagger S_{\rho\nu'}\right]^{-N}|\mathbf{S}\rangle\langle\mathbf{S}|=1\ , \quad (5.182)$$

where N is the sum of the dimension of the particle and hole spaces. Blaizot and Orland (1980b) demonstrate in an appendix the equivalence of Eqs. (5.182) and (5.177).

3. Grassman variables

A final functional integral which may be used to generate representations for the many-fermion evolution operator is provided by coherent states utilizing Grassman variables. Whereas this approach involves considerably more formal apparatus than in alternative methods, it is extensively utilized in analogous field theory problems and an understanding of at least its basic elements is therefore crucial for reading the relevant literature. An extensive treatment of Grassman variables is provided by Berezin (1966), and a detailed derivation of fermion coherent states is given by Ohnuki and Kashiwa (1978).

The boson coherent states, Eq. (5.168), may be modified to treat fermions by replacing the ordinary variables Z_α by Grassman variables ζ_α which anticommute with each other and with fermion creation and annihilation operators $\hat{a}_\alpha^\dagger,\hat{a}_\alpha$. By virtue of this anticommutation, $\zeta_\alpha^2=0$ and the most general functions of Grassman variables are monomials. Elementary functions are defined by their Taylor-series expansions, which terminate after the linear term. To obtain a resolution of unity analogous to Eq. (5.171), the definite integral of a function of Grassman variables is defined by the relations

$$\int d\zeta_\alpha=0\ , \quad (5.183a)$$

$$\int d\zeta_\alpha\zeta_\alpha=1\ , \quad (5.183b)$$

and involution is defined such that

$$(\zeta_\alpha^*)^*=\zeta_\alpha \quad (5.184a)$$

and

$$(\zeta_\alpha\zeta_\beta)^*=\zeta_\beta^*\zeta_\alpha^*\ . \quad (5.184b)$$

It then follows that a Gaussian integral for Grassman variables is given by

$$\int d\zeta\,d\zeta^*e^{-\zeta^*a\zeta}=\int d\zeta\int d\zeta^*(1-\zeta^*a\zeta)=\int d\zeta\left[-\int\zeta\,d\zeta\right]^*a\zeta=a\ , \quad (5.185)$$

so that by diagonalization, as in Eq. (5.37),

$$\int\prod_\alpha d\zeta_\alpha d\zeta_\alpha^*e^{-\sum_{\alpha\beta}\zeta_\alpha^*A_{\alpha\beta}\zeta_\beta}=\det A=e^{\mathrm{tr}\ln A}\ . \quad (5.186)$$

This result differs from the corresponding integral over ordinary variables, appropriate for bosons,

$$\int\prod_\alpha\left[\frac{dZ_\alpha dZ_\alpha^*}{2\pi i}\right]e^{-\sum_{\alpha\beta}Z_\alpha^*A_{\alpha\beta}Z_\beta}=[\det A]^{-1}=e^{-\mathrm{tr}\ln A}\ , \quad (5.187)$$

only in the sign of the exponent, suggesting how the Grassman formalism eventually generates the appropriate relative signs in fermion and boson many-body theory.

Fermion coherent states analogous to Eq. (5.168) are defined by

$$|\zeta\rangle\equiv e^{-\sum_\alpha\zeta_\alpha a_\alpha^\dagger}|0\rangle=|0\rangle-\sum_\alpha\zeta_\alpha|\alpha\rangle\ . \quad (5.188)$$

Using this definition and the preceding relations for Grassman variables, it follows that the overlap of two coherent states is

$$\langle \zeta \mid \zeta' \rangle = e^{\sum_\alpha \zeta_\alpha^* \zeta_\alpha'} , \tag{5.189}$$

the matrix element of a normal-ordered fermion operator is

$$\langle \zeta \mid NA(\mathbf{a}^\dagger, \mathbf{a}) \mid \zeta' \rangle = e^{\sum_\alpha \zeta_\alpha^* \zeta_\alpha'} A(\zeta^*, \zeta') , \tag{5.190}$$

and the closure relation is

$$\prod_\alpha \left[\int d\zeta_\alpha d\zeta_\alpha^* \right] e^{-\sum \zeta_\alpha^* \zeta_\alpha'} \mid \zeta \rangle \langle \zeta \mid = 1 . \tag{5.191}$$

Since these relations are precisely analogous to Eqs. (5.169)–(5.171), the matrix element of the many-fermion evolution operator may be written

$$\langle \zeta_f \mid e^{-iH(t_f - t_i)} \mid \zeta_i \rangle = \int_{\zeta(x,t_i)=\zeta_i(x)}^{\zeta^*(x,t_f)=\zeta_f^*(x)} \mathscr{D}(\zeta^*, \zeta) \times \exp\left[i \int_{t_i}^{t_f} dt \int dx\, \zeta^*(x,t) \left[i\frac{d}{dt} + \frac{\hbar^2}{2m}\nabla^2 - \tfrac{1}{2} \int dx' \zeta^*(x',t)\zeta(x',t) v(x-x') \right] \zeta(x,t) + \int dx\, \zeta_f^*(x)\zeta(x,t)_f \right] , \tag{5.192}$$

which differs from Eq. (5.172) only in the replacement of the variables ϕ by Grassman variables ζ. Because of anticommutation of the ζ variables, the expression for the trace has an additional minus sign relative to Eq. (5.191),

$$\prod_\alpha \left[\int d\zeta_\alpha d\zeta_\alpha^* \right] e^{-\sum \zeta_\alpha^* \zeta_\alpha} \langle -\zeta \mid F \mid \zeta \rangle = \mathrm{tr} F , \tag{5.193}$$

so that the final overlap factor in Eq. (5.192) is removed in the trace or partition function as for bosons, but the resulting functional integral is over antiperiodic rather than periodic functions. The periodicity and antiperiodicity for bosons and fermions, respectively, ultimately specifies the proper boundary conditions for Green's functions and yields the proper boson and fermion occupation number.

Whereas the parallel between fermions and bosons has thus far been complete, there is no direct way to apply the SPA to Eq. (5.192) to obtain a Fermion time-dependent Hartree equation corresponding to Eq. (5.173). Thus, at this point, the only way to proceed further is to remove the Grassman variables from the problem completely. Indeed, the most unsatisfactory feature of the formalism is the fact that having gone to the effort of expressing the evolution operator in terms of Grassman variables, one must ultimately remove them from the problem and introduce auxiliary fields, which we have already seen could have been done directly without such a digression.

Introducing an auxiliary field in Eq. (5.192), as in Eq. (5.38), to reduce the exponential of a quadratic form in $\zeta^*\zeta$ to an integral over exponentials linear in $\zeta^*\zeta$ and schematically indicating the x,t dependence by an obvious matrix notation,

$$\int \mathscr{D}(\zeta^*\zeta) e^{i\zeta_\alpha^*[i(\partial/\partial t) - K]_{\alpha\beta}\zeta_\beta - (i/2)\zeta_\alpha^*\zeta_\gamma v_{\alpha\beta\gamma\delta}\zeta_\beta^*\zeta_\delta} = \int \mathscr{D}(\sigma)\mathscr{D}(\zeta^*\zeta) e^{(i/2)\sigma_{\alpha\gamma} v_{\alpha\beta\gamma\delta}\sigma_{\beta\delta}} e^{i\zeta_\alpha^*[i(\partial/\partial t) - K - v_{\alpha\beta\gamma\delta}\sigma_{\beta\delta}]\zeta_\gamma} = \int \mathscr{D}(\sigma) e^{(i/2)\sigma_{\alpha\gamma} v_{\alpha\beta\gamma\delta}\sigma_{\beta\delta} + \ln \mathrm{Det}[(\partial/\partial t) + iK + iv_{\alpha\beta\gamma\delta}\sigma_{\beta\delta}]} , \tag{5.194}$$

where the last line follows from Eq. (5.187). Using the relation

$$\frac{\delta}{\delta A_{ij}} \mathrm{Det} A = A_{ji}^{-1} \mathrm{Det} A , \tag{5.195}$$

and Eqs. (4.8) and (4.11), stationarity of the exponent in Eq. (5.194) yields

$$\sigma(x',t;x,t) = -i \left[i\frac{\partial}{\partial t} - K - v\sigma \right]^{-1} = -iG(x,t,x't^\dagger) = \rho(x',x) . \tag{5.196}$$

Thus, the Green's function evolves in the Hartree mean field $v_{\alpha\beta\gamma\delta}\sigma_{\beta\delta}$, where σ is just the one-body density matrix, and by the arguments in Sec. IV.A.2, the SPA is equivalent to the time-dependent Hartree approximation. Clearly, the derivation in Eqs. (5.194)–(5.196) applies equally well to boson coherent states, with two additional minus signs in the Gaussian integral, and in the relation between the density and the Green's function yielding the same time-dependent Hartree equation. Because of its ultimate reliance upon the introduction of an auxiliary field, this formalism yields a Hartree theory unless one of the techniques discussed in Sec. V.D.2 is utilized to generate a Hartree-Fock or Hartree-Fock-Bogoliubov mean field. Details of the application of this formalism to the calculation of quantized eigenstates and spontaneous fission are presented by Reinhardt (1981a, 1981b).

H. Two-body correlations

The functional integral methods presented in this section are strictly applicable only to two-body potentials which are sufficiently weak that the Hartree-Fock mean

field is a sensible starting point for a systematic expansion. Unfortunately, there is, at present, a major conceptual gap in developing a functional integral formalism utilizing many-body techniques comparable to those described in Secs. II.A. and IV.B for treating strong short-range repulsion. Therefore, in this concluding section it is possible only to sketch several alternative approaches which may eventually be used to develop a theory suitable for nuclear forces. Given the practical difficulties of solving self-consistent time-dependent mean-field equations and the additional complexity involved in any explicit treatment of two-body correlations, it is clear that in the short term practical calculation will be forced to utilize effective interactions. Ultimately, however, one may hope either that the insight from a proper formal treatment of correlations will provide a more satisfactory definition and justification of the effective interaction or that new and tractable approximation techniques will be developed.

One alternative, implicit in the original work of Hubbard (1959), is to sum the quadratic corrections to the functional integral over the complex pairing field in Eq. (5.111). Just as the quadratic corrections for the Hartree or Hartree-Fock mean field in Secs. V.D.1 and V.D.2 summed direct or exchange particle-hole ladders, or RPA diagrams, the quadratic corrections to Eq. (5.111) sum particle-particle and hole-hole ladders. Thus, in the evaluation of the energy, the matrix element of the bare v is essentially replaced by a G matrix.

One major problem with this theory is the fact that the mean field does not contain the ladder sums [and unless the decomposition (5.114) is utilized, contains only the pairing field]. In addition, there is no obvious way to systematically sum three-body and higher-order Faddeev ladders. Finally, from our physical understanding of the quadratic corrections to the Hartree or Hartree-Fock mean field as the collective RPA vibrations, the essential physics of the corrections to Eq. (5.111) should be the physics of collective pairing vibrations rather than short-range Brueckner correlations.

A closely related alternative is to add and subtract a term formally in the functional integral, Eq. (5.111), as at the end of Sec. V.D.2. Defining a new variable

$$\sigma_{\alpha\beta}\equiv V_{\alpha\beta\gamma\delta}\chi_{\gamma\delta}\ , \tag{5.197}$$

and using an obvious matrix notation, Eq. (5.111) becomes

$$T_t e^{-(i/2)\eta^\dagger V\eta}=\int \mathscr{D}[\sigma^*,\sigma]e^{(i/2)\sigma^* V^{-1}\sigma}e^{-(i/2)(\sigma^*\eta+\sigma\eta^\dagger)}\ . \tag{5.198}$$

We now seek to define the mean field in terms of the solution to an integral equation

$$G=v-vPG\ , \tag{5.199}$$

which corresponds to the familiar G matrix, Eq. (2.1), if the propagator P is chosen to be Q/e and the T matrix if the propagator is $1/e$. Solving Eq. (5.199) for G^{-1}, Eq. (5.198) may be rewritten

$$T_t e^{-(i/2)\eta^\dagger V\eta}=\int \mathscr{D}[\sigma^*\sigma]e^{(i/2)\sigma^* P\sigma}e^{(i/2)\sigma^* G^{-1}\sigma} \times e^{-(i/2)(\sigma^*\eta+\sigma\eta^\dagger)}\ , \tag{5.200}$$

thereby reformulating the theory in terms of G. Application of the SPA assuming the first term is slowly varying then yields a mean field in terms of G plus systematic corrections. Although this manipulation allows one to express the formalism in terms of a G matrix instead of a T matrix, there is no indication that this is optimal. Orland (1981) has shown, using Grassman variables to calculate the trace of the evolution operator, that the quadratic term in the exponent is of precisely the form $e^{-(i/2)\sigma^* P\sigma}$ required to yield the T matrix. This is consistent with the preceding observation that the quadratic corrections sum particle-particle ladder diagrams.

A final alternative is close in spirit to the coupled-cluster approximation of Sec. IV.B. At each point in Eq. (5.165) at which a complete set of states is inserted, one is free to insert instead

$$\int d\mu(Z)e^{-S}|\,\mathbf{Z}\rangle\langle\,\mathbf{Z}|\,e^{S}=1\ , \tag{5.201}$$

where S is any operator. Allowing S to be time dependent but continuous, repeating the steps which led to Eq. (5.167a), and specifying the states $|\,\mathbf{Z}\rangle$ to be determinants yield

$$\langle\phi_f|\,e^{-iH(t_f-t_i)}\,|\phi_i\rangle = \int \mathscr{D}(\phi_1^*\ldots\phi_N^*,\phi_1\ldots\phi_N) \times\prod_{k,j}\delta\left[\int dx\,\phi_k^*(x,t)\phi_j(x,t)-\delta_{jk}\right] \times e^{iA(\phi_1^*\ldots\phi_N)}\ , \tag{5.202a}$$

where

$$A(\phi_1^*\ldots\phi_N)\equiv\int dt\left\langle\phi_1\ldots\phi_N\left|e^{-S}\left[i\frac{\partial}{\partial t}-H\right]e^{S}\right|\phi_1\ldots\phi_N\right\rangle\ . \tag{5.202b}$$

To establish contact with the coupled-cluster approximation, S must be restricted to be a sum of n-particle, n-hole operators. Whereas this restriction is impossible relative to all determinants sampled in the functional integral, the S's at each time may be defined to contain only particle-hole operators relative to the stationary determinant satisfying the SPA equation at that time. Fluctuations relative to the stationary determinant may be parametrized by the Thouless form, Eq. (5.181), so that in the infinitesimal limit, stationarity of A, Eq. (5.202b) requires

$$\int dt \sum_{\rho\nu} \left[\delta Z^*_{\rho\nu} \left\langle \phi_1 \cdots \phi_N \left| a^\dagger_\nu a_\rho e^{-S} \left[i\frac{\partial}{\partial t} - H \right] e^S \right| \phi_1 \cdots \phi_N \right\rangle \right.$$
$$\left. + \delta Z_{\rho\nu} \left\langle \phi_1 \cdots \phi_N \left| e^{-S} \left[i\frac{\partial}{\partial t} - H \right] e^S a^\dagger_\rho a_\nu \right| \phi_1 \cdots \phi_N \right\rangle \right] = 0 . \tag{5.203}$$

Stationarity with respect to $\delta Z^*_{\rho\nu}$ yields precisely the coupled-cluster equation (4.25b) defining the evolution of $S^{(1)}$, and stationarity with respect to $\delta Z_{\rho\nu}$ yields a TDHF-like equation for the evolution of ϕ_ν. For the stationary solutions, the exponent (5.202b) may be written

$$A[\phi_1 \cdots \phi_N] = \int dt \left[\sum_{r=1}^{N} \left\langle \phi_\nu \left| \left[i\frac{\partial}{\partial t} - T \right] \psi_1 \right| \phi_\nu \right\rangle + \tfrac{1}{2} \sum_{\nu\nu'=1}^{N} \langle \phi_\nu \phi_{\nu'} \mid v\psi_2 \mid \phi_\nu \phi_{\nu'} - \phi_{\nu'} \phi_\nu \rangle \right] ,$$

where ψ_1 and ψ_2 are defined in Eqs. (4.34), the potential term thus having the form of an effective interaction $v\psi_2$. Although, at present, the details of the theory have not been worked out, and the quadratic corrections subject to the constraint in Eq. (5.202) have not been evaluated, this approach has many appealing features and merits further investigation.

In summary, the functional integral formulation provides an elegant, powerful, and general technique for addressing a wide variety of static and dynamic problems in many-body theory. Although significant progress has been made recently in the conceptual understanding of long-standing problems in the quantum theory of collective motion and spontaneous decay, substantial formal problems still remain, especially in scattering theory and dealing with short-range correlations. In addition, immense practical problems arise in attempting to apply the functional integral formalism to realistic systems, even at the level of the mean-field approximation using simple effective interactions. Indeed, the decisive factor in determining whether these new ideas ultimately have significant impact on nuclear physics will be the ingenuity and energy devoted to solving these practical problems. This is an appropriate point, then, to shift from the primarily formal emphasis of the last five chapters to address specific applications to model and physical systems.

VI. APPLICATION TO SIMPLE, IDEALIZED SYSTEMS

Application of the mean-field theory developed in the preceding sections to simplified model problems serves several useful functions. For analytically solvable problems, it provides both a quantitative test of the theory and insight into how the mean field describes many-body dynamics. Realistically, of course, just those features of a simplified model which make it solvable also render it unrepresentative of the general many-body problem. Thus, in this section, two very different solvable models are explored, the first having nontrivial spatial dependence but a very sparse S matrix and the second having a more interesting S matrix but no meaningful spatial dependence.

As emphasized in Sec. II, a crucial feature of nuclear many-body systems which should be embodied in models is nuclear saturation. This saturation implies that both the density and mean field in finite nuclei are approximately constant in the interior and that they approach zero rapidly in the surface. Since no analytically solvable saturating models have been discovered, numerical solutions for two simplified saturating models are presented and discussed in detail. Both models have nontrivial spatial dependence in only one dimension and employ density-dependent effective interactions. The virtue of one-dimensional spatial dependence is twofold. The resulting numerical simplifications allow broad exploration of a large class of applications, and the essence of the results may conveniently be displayed graphically. As will become evident subsequently, the collisions treated in Sec. VI.D manifest virtually all the relevant physical features of more realistic applications in two- and three-dimensional geometry.

A. One-dimensional system with attractive delta-function interactions

Consider a system of N particles in one spatial dimension governed by the Hamiltonian

$$H = -\tfrac{1}{2} \sum_{i=1}^{N} \frac{d^2}{dx^2} - g \sum_{i<j=1}^{N} \delta(x_i - x_j) , \tag{6.1}$$

where, for convenience, energy units are defined such that $\hbar^2/m = 1$. (The interaction strength g may also be removed from the problem by measuring length in units of $\hbar^2/2mg$ and energy in units of $2mg^2/\hbar^2$, so the only meaningful parameter in the model is N, the number of particles.)

This Hamiltonian has spatially symmetric bound states of the form (Bethe, 1931)

$$\psi = \exp\left[-\frac{g}{2} \sum_{i<j=1}^{N} | x_i - x_j | \right] . \tag{6.2}$$

A wave function which is antisymmetric with respect to interchange of two variables loses the benefit of one of the delta-function interactions and is unstable with respect to

break-up into two subsystems. Thus, to obtain stable N-particle bound states one must either consider bosons or a system of fermions having an additional color quantum number with degeneracy $2S+1=N$, allowing the wave function to be antisymmetric in color and symmetric in space. The boson case will be treated here for simplicity, but the results may be generalized straightforwardly to the fermion case with the additional color degree of freedom.

1. Bound states

Exact bound-state solutions have been obtained by McGuire (1965) and have been compared with mean-field approximations by Calogero and Degasperis (1975), Nohl (1976), and Yoon and Negele (1977).

A system of N bosons interacting with the Hamiltonian (6.1) has a single N-particle bound state

$$\psi_N = N![(N-1)!g^{N-1}]^{1/2}\exp\left[-\frac{g}{2}\sum_{i<j=1}|x_i-x_j|\right], \tag{6.3}$$

with energy

$$E_N = -\frac{N(N^2-1)g^2}{24} \tag{6.4}$$

and density

$$\rho_N(x) = \int dx_1\ldots dx_N\,\delta\left[\frac{1}{N}\sum_{i=1}^{N}x_i\right]|\psi_N|^2\delta(x_1-x)$$
$$= g(N!)^2\sum_{n=1}^{N-1}(-1)^{n+1}\frac{n\exp(-gnN|x|)}{(N+n-1)!(N-n-1)!}. \tag{6.5}$$

In the large-N limit

$$\rho_N(x)\underset{N\to\infty}{\to}\frac{N^2g}{4\cosh^2\left[\frac{Ngx}{2}\right]}\left\{1+\mathcal{O}\frac{1}{N}\right\}. \tag{6.6}$$

The mean-field approximation is obtained by choosing the trial wave function,

$$\psi_N^H = \sqrt{N}\prod_{i=1}^{N}\phi_b(x_i), \tag{6.7}$$

and minimizing $\langle H\rangle$ with respect to the normalized single-particle wave function, $\phi_b(x)$. The resulting single-particle equation

$$\left\{-\frac{1}{2}\frac{d^2}{dx^2}-g(N-1)|\phi_b(x)|^2-\varepsilon\right\}\phi_b(x)=0 \tag{6.8}$$

has one bound-state solution

$$\phi_b(x) = \frac{[(N-1)g]^{1/2}}{2\cosh\frac{(N-1)gx}{2}} \tag{6.9}$$

with energy eigenvalue

$$\varepsilon_b = \frac{-(N-1)^2g^2}{8}. \tag{6.10}$$

The resulting Hartree energy

$$E_N^H = \frac{-N(N-1)^2g^2}{24} \tag{6.11}$$

and Hartree density

$$\rho_N^H(x) = \frac{N(N-1)g}{4\cosh^2\left\{\frac{(N-1)gx}{2}\right\}} \tag{6.12}$$

agree with the exact results, Eqs. (6.4) and (6.6), to leading order in N.

As usual in the mean-field theory, errors of order $1/N$ relative to the leading contribution arise from the spurious cm motion. Minimization of $\langle H-H_{\rm cm}\rangle$, where $H_{\rm cm}=\frac{1}{2}(\sum_i P_i)^2$, yields the Hartree energy

$$\tilde{E}_N^H = -\frac{N^2(N-1)}{24}g^2, \tag{6.13}$$

thus eliminating half of the order N^2 discrepancy between Eq. (6.4) and (6.11).

The Hartree results (6.11) and (6.12) suggest that the mean-field theory yields an asymptotic expansion in $1/N$, the particle number N being the only parameter in the model after appropriate scaling to remove the mass and coupling constant. Additional insight into the theory may be obtained by examination of the systematic corrections to the mean-field result. The $1/N$ expansion may be obtained straightforwardly either by perturbation theory or by examination of the appropriate functional integral.

The perturbation series for fermions is obtained directly from the Goldstone expansion. For bosons, the same result is straightforwardly obtained by assigning a color quantum number with degeneracy $(2S+1)=N$, adiabatically switching on from an unperturbed color singlet, and disregarding the unphysical singlet color component of the wave function. Any linked graph in the Goldstone expansion for the energy has I interactions and C closed loops. Every interaction contributes a factor of $(N-1)^2$ which arises from the normalization of the particle and hole eigenfunctions of the Hartree potential and a factor of $(N-1)^{-1}$, which arises from the integration over spatial variables. This latter factor may be extracted only because all the wave functions are functions of $(N-1)x$ and the interaction is zero range, allowing the removal of all N dependence from the integrand by change of variables. Every closed loop contributes a factor of N arising from the sum over color states. For every graph, there are $I-1$ energy denominators, each of which contributes a factor of $(N-1)^{-2}$. Hence the overall N dependence of any Goldstone diagram in the energy expansion is $(N-1)^{2-I}N^C\sim N^{C-I+2}$. A similar argument shows that the N dependence for the expansion of the one-body density is N^{C-I+1}.

This analysis yields an unambiguous accounting of the asymptotic dependence of individual graphs on the particle number. The only energy diagram which contributes

in order N^3 is the Hartree diagram, shown as the SPA term in Fig. 17, which has $C=2$ and $I=1$.

Since the fermion propagators are defined as eigenfunctions of the Hartree potential, they sum to all orders Hartree self-energy insertions which have $C=1$ and $I=1$ and are thus independent of N.

Energy diagrams of order N^2 must have equal numbers of interactions and closed loops, and thus are restricted to the exchange diagram, labeled $n=1$ in Fig. 17, and the RPA ring diagrams also shown in Fig. 17. The energy, Eq. (6.13), includes the diagrams labeled SPA and $n=1$ in Fig. 17 plus the cm energy correction, so the remaining error of order N^2 arises from the RPA diagrams of Fig. 17 with $n\geq 2$. The $n=2$ diagram yields (Yoon and Negele, 1977)

$$\Delta E=-0.9956N(N-1)\frac{g^2}{24}\ , \tag{6.14}$$

thus removing all but $\frac{1}{2}\%$ of the N^2 discrepancy with the exact result.

An alternative approach to the $1/N$ expansion utilizes the functional integral expressions (5.192) or (5.199) for bosons or fermions, respectively. Denoting color variables for fermions by Greek subscripts, utilizing an auxiliary field in the usual way, and introducing new scaled variables $g'\equiv gN$ and $\sigma'=(1/N)\sigma$, the functional integral for the time of the evolution operator becomes

$$\begin{aligned}
&\int \mathscr{D}(\xi^*_\alpha\xi_\alpha)\exp\left[i\int dt\,dx\sum_\alpha \xi^*_\alpha(x,t)\left[i\frac{\partial}{\partial t}+\frac{1}{2}\frac{d^2}{dx^2}-\frac{1}{2}g\sum_\beta \xi^*_\beta(x,t)\xi_\beta(x,t)\right]\xi_\alpha(x,t)\right]\\
&=\int \mathscr{D}(\xi^*_\alpha\xi_\alpha)\int \mathscr{D}(\sigma)\exp\left[i\int dt\,dx\sum_\alpha \xi^*_\alpha(x,t)\left[i\frac{\partial}{\partial t}+\frac{1}{2}\frac{d^2}{dx^2}-g\sigma(x,t)\right]\xi_\alpha(x,t)\right]\exp\left[\frac{i}{2}\int dt\,dx\,\sigma^2(x,t)g\right]\\
&=\int \mathscr{D}(\sigma)\exp\left\{N\ln\mathrm{Det}\left[\frac{\partial}{\partial t}-i\left[\frac{1}{2}\frac{d^2}{dx^2}-g\sigma\right]\right]\right\}\exp\left[\frac{i}{2}\int dt\,dx\,g[\sigma(x,t)]^2\right]\\
&=\int \mathscr{D}(\sigma')\exp\left[N\left\{\ln\mathrm{Det}\left[\frac{\partial}{\partial t}-i\left[\frac{1}{2}\frac{d^2}{dx^2}-g'\sigma'\right]\right]+\frac{i}{2}\int dt\,dx\,g'[\sigma'(x,t)]^2\right\}\right].
\end{aligned} \tag{6.15}$$

By virtue of the explicit factor of N in the exponent of (6.15) and the removal of all other N dependence, application of the SPA to Eq. (6.15) yields an asymptotic expansion in $1/N$. The leading term is then the SPA result in Fig. 17, with the quadratic corrections yielding the exchange and RPA diagrams of next order in $1/N$ in agreement with the preceding perturbation analysis. The fact that diagrams are classified according to N^{C-I} follows immediately from the scaling requirement that the coupling constant scale as N^{-1} and that the Green's function, which by Eq. (5.196) equals σ, scale as N.

Although the manipulations in Eq. (6.15) could have been carried out for a general finite-range potential, the $1/N$ expansion hinged crucially upon the fact that the interaction was a delta function and thus had no length scale. For a general potential, the transformation $v_{\alpha\beta\gamma\delta}\equiv v_{\alpha\beta\gamma\delta}N$ would change the Hamiltonian, requiring one to consider a hypothetical class of theories in which the interaction strength varies with N as discussed in Sec. V.A.3.

Similar functional integral techniques have been utilized by Nohl (1976) to calculate bound-state energies for bosons and fermions. In this work, a bare mass term in the nonlinear Schrödinger equation is adjusted to reproduce the proper energy of a one-particle state so that evaluation of quadratic fluctuations yields not only the correct N^3 and N^2 dependence of the energy, but also the correct N dependence. An additional result is the interpretation of ϕ_b, the solution to the mean-field equation (3.31), as the expectation value of a field operator evaluated between eigenstates, Eq. (6.3), for N and $N+1$ particle systems.

2. Scattering

The complete scattering matrix for distinguishable particles has been derived by Yang (1967), utilizing the Bethe ansatz, and the most salient feature is that only elastic scattering occurs in the model. Using this method for the scattering of two N-boson bound states, Yoon and Negele (1977) derived the phase shift from which the following time delay is obtained:

$$\begin{aligned}
\Delta t&\equiv\frac{1}{Nk}\frac{d}{dk}\delta(k)\\
&=-\frac{4g}{Nk}\sum_{m=1}^{N-1}\frac{m}{4k^2+m^2g^2}-\frac{g}{k(4k^2+N^2g^2)}\ ,
\end{aligned} \tag{6.16}$$

where k is the initial cm momentum.

The time-dependent Hartree initial-value problem for the collision of two N-boson states is specified by the equation

$$i\frac{\partial}{\partial t}+\frac{1}{2}\frac{d^2}{dx^2}+(2N-1)g\,|\,\phi(x,t)\,|^2\phi(x,t)=0 \quad (6.17a)$$

with the initial condition

$$\psi_{2N}(x_1,x_2\cdots x_{2N},t_0)=\prod_{i=1}^{2N}\left[\frac{1}{\sqrt{2}}e^{ikx_i}\phi_b(x_i+R)+\frac{1}{\sqrt{2}}e^{-ikx_i}\phi_b(x_i-R)\right], \quad (6.17b)$$

where ϕ_b denotes the N-particle bound-state Hartree wave function of (6.09). Although, as discussed in Sec. II.A.4, the initial condition does not correspond to two intrinsic wave functions multiplied by a cm momentum eigenfunction, the separated fragments do evolve like freely translating ground states and have the correct expectation value of the cm momentum. The cubic Schrödinger equation, Eq. (6.17a), may be solved using the inverse scattering technique of Zakharov and Shabot (1972), and the two-soliton solution satisfying the initial condition (6.17b) is (Dolan, 1976)

$$\begin{aligned}\phi(x,t)=&\sqrt{a}\,e^{-(i/2)(k^2-a^2)t}\\&\times\left[e^{ikx}\left[e^{-a(x-kt)}+\frac{k^2}{(k-ia)^2}e^{-a(3x+kt)}\right]+e^{ikx}\left[e^{-a(x+kt)}+\frac{k^2}{(k+ia)^2}e^{-a(3x-kt)}\right]\right]\\&\times\left[1+2e^{-2ax}\cosh(2akt)-8a^2e^{-2ax}\mathrm{Re}\left[\frac{e^{2ikx}}{4(k+ia)^2}\right]+\frac{k^2}{(k^2+a^2)}e^{-4ax}\right]^{-1},\end{aligned} \quad (6.18)$$

where $a\equiv(2N-1)g/4$ and k is the cm momentum. This solution describes the transmission of two solitons through each other with a time delay but with asymptotic shape after the collision identical to the initial shape prior to the collision. Thus, the most salient feature of the exact solution, restriction to purely elastic scattering, is exactly manifested in the soliton behavior of the mean-field solutions. The time delay defined by Eq. (6.18) is

$$\Delta t^H=\frac{-4}{(2N-1)gk}\ln\left[1+\frac{(2N-1)^2g^2}{16k^2}\right]\underset{n\to\infty}{\approx}-\frac{4}{Ngk}[\ln N+\mathcal{O}(1)] \quad (6.19)$$

and agrees with the exact result, Eq. (6.16), to leading order in $1/N$. This same result is also obtained by Reinhardt (1982) in his formulation of mean-field reaction theory. In view of the generality of the functional integral derivation of the $1/N$ expansion, Eq. (6.15), one could, in principle, calculate systematic corrections to the phase shift and thus the time delay.

The one-dimensional delta-function problem thus provides a model system in which the mean-field theory yields an excellent, controlled approximation for bound states and scattering. The general considerations concerning evaluation of few-body operators instead of wave functions are borne out concretely. The binding energy, one-body density, and time delay (which may be defined in terms of the center of mass of the separating fragments) are all calculable with errors of order $1/N$ despite the fact that overlaps between exact and mean-field wave functions are exponentially small. Similarly, it provides a pedagogical counterexample to criteria which have been suggested for the validity of the time-dependent mean-field theory based on the lifetime of a determinant (Lichtner and Griffin, 1976), since in this model the lifetime estimate would erroneously imply validity for only infinitesimally short time intervals. The chief limitation of the model is the unrealistically sparse S matrix manifesting neither rearrangement nor inelastic scattering, and this deficiency motivates the complementary investigation of the Lipkin model in Sec. VI.B.

3. The sigma model in one spatial dimension

Whereas semiclassical and mean-field approximations to field theories lie beyond the purview of this work, the semiclassical approximation to the sigma model is so intrinsically related to the one-dimensional delta-function model that a terse review is appropriate. The sigma model is a simple field theory in which fermions are coupled to a single scalar field, and may be regarded as a schematic model of nuclei bound by a meson field instead of instantaneous potential interactions. The theory and its semiclassical approximation are treated in detail by Campbell (1978) and Campbell and Liao (1976), and the resulting semiclassical equations may be written

$$\left[i\gamma_0\frac{\partial}{\partial t}+i\gamma_1\frac{\partial}{\partial x}-m-g\phi\right]\psi_i(x)=0 \quad (6.20a)$$

and

$$\left[\frac{\partial^2}{\partial t^2}-\frac{\partial^2}{\partial x^2}+m_\sigma^2+\frac{3m_\sigma^2}{2f}+\frac{m_\sigma^2}{2f^2}\phi^2\right]\phi=gn_0\sum_i\psi_i^\dagger\gamma_0\psi_i\,, \quad (6.20b)$$

where the Dirac matrices in one dimension may be defined $\gamma_0=\sigma_3$ and $\gamma_1=i\sigma_1$, ψ is a two-component Dirac spinor for the nucleon, n_0 denotes the number of nucleons in each positive-energy orbital, and nucleon and meson masses are m and m_σ, respectively. Since two of the four parameters appearing in Eq. (6.20) may be removed by appropriate definition of the length and time scales, it is convenient to characterize the theory in terms of the two

parameters

$$\delta \equiv \frac{m_\sigma^2}{m^2} \tag{6.21a}$$

and

$$\gamma \equiv \frac{n_0}{f_0} \ . \tag{6.21b}$$

In this approximation, a pion corresponds to a periodic, self-consistent solution to Eq. (6.20b) in the absence of a nucleon source, an isobar is a periodic solution coupled to a single nucleon, and a nucleus is an assembly of static solutions to Eq. (6.20) in which nucleons are bound in the mean field ϕ, which in turn is generated by the nucleon source. Thus the model, in principle, affords a laboratory in which to extend classical nonrelativistic nuclear physics based on potential interactions to a field theory allowing for explicit treatment of mesons and isobars.

A remarkable feature of the model is that for $\delta=4$, that is, for a meson twice as massive as the nucleon, the coupled equations (6.20) are analytically solvable and yield several classes of localized soliton solutions, one class of which corresponds to finite nuclei (Campbell and Liao, 1976).

A second interesting feature is that the nonrelativistic reduction, which requires $(\gamma/\delta)^2 \ll 1$ and $\gamma^2/\delta^3 \ll 1$, yields the nonlinear Schrödinger equation (6.17a) (Campbell, 1979). This follows directly from Eqs. (6.20), since in the nonrelativistic limit, the upper component of ψ satisfies a Schrödinger equation in the potential $g\phi$, and in the appropriate limit all the terms on the left-hand side of Eq. (6.20b) are negligible except m_σ^2, so that ϕ is proportional to the square of the wave function. Since the nonrelativistic limit may be attained for the analytically solvable case of $\delta=4$ by decreasing γ, the analytic soliton solutions to the one-dimensional delta-function problem are a special case of the general solutions to the $\delta=4$ sigma model.

Finally, it is useful to note that whereas the $\delta=4$ and nonrelativistic limits of the theory do not yield saturating solutions for finite nuclei, the general model possesses sufficient flexibility to produce saturation. From the fact that the one-dimensional delta-function potential does not saturate, it is evident that the ratios γ^2/δ^2 and γ^2/δ^3 cannot simultaneously be small for a saturating system. However, when γ^2/δ exceeds the order of unity, the mean field becomes so large that a different instability arises and a nucleuslike solution is unstable with respect to breakup into kink-antikink solutions which have no counterpart in nonrelativistic nuclear physics. Thus, for a meson mass significantly lighter than the nucleon mass, as is the case for pions and nucleons which correspond to $\delta=\frac{1}{50}$, there is a large window between the nonrelativistic nonsaturating region and the kink-antikink instability. Numerical solutions of the sigma model (Campbell and Negele, 1981) for $\delta=\frac{1}{50}$ and $\gamma=\frac{1}{225}$ are qualitatively similar to those of the saturating model discussed below in Sec. VI.C.

As this brief survey suggests, the one-dimensional sigma model thus provides the opportunity to investigate a number of interesting aspects of the generalization of nonrelativistic many-body theory to a tractable field theory. Many more details may be found in the cited literature.

B. The two-level Lipkin model

A solvable many-body Hamiltonian, commonly referred to as the Lipkin model, is defined by the Hamiltonian (Lipkin, Meshkov, and Glick, 1965)

$$H = \frac{\varepsilon}{2} \sum_{\substack{p=1,N \\ s=\pm 1}} s \hat{a}_{ps}^\dagger \hat{a}_{ps} + \frac{V}{2} \sum_{p,p',s} \hat{a}_{ps}^\dagger \hat{a}_{p's}^\dagger \hat{a}_{p'-s} \hat{a}_{p-s} \ . \tag{6.22}$$

This Hamiltonian describes two levels separated in energy by ε and having equal matrix elements for raising or lowering a pair of particles. The eigenfunctions and eigenvalues are easily found by introducing quasispin operators obeying angular momentum commutation relations

$$\hat{J}_{\{x\}} \equiv \frac{1}{2} \begin{Bmatrix} 1 \\ -i \end{Bmatrix} \sum_{p=1}^{N} \left[\hat{a}_{p+1}^\dagger \hat{a}_{p-1} \begin{Bmatrix} + \\ - \end{Bmatrix} \hat{a}_{p-1}^\dagger \hat{a}_{p+1} \right]$$
$$\hat{J}_z \equiv \tfrac{1}{2} \sum_{\substack{p=1,N \\ s=1}} s \hat{a}_{ps}^\dagger \hat{a}_{ps} \tag{6.23}$$

in terms of which H may be written

$$H = \varepsilon \hat{J}_z + V(\hat{J}_x^2 - \hat{J}_y^2) \ . \tag{6.24}$$

The Hamiltonian commutes with the total quasispin

$$J^2 = J_x^2 + J_y^2 + J_z^2 \ , \tag{6.25}$$

the number operator

$$\hat{n}_p = \sum_s \hat{a}_{ps}^\dagger \hat{a}_{ps} \ , \tag{6.26}$$

and the parity operator

$$\hat{\pi} = e^{i\pi \hat{J}_x} \ . \tag{6.27}$$

The eigenstates may be found by diagonalization within each subspace of definite J, making use of the fact that since $\hat{\Pi}$ commutes with H, even and odd M may be diagonalized separately. Since H and the external potentials considered in this section commute with J^2, we shall restrict our consideration to the ground-state multiplet, $J=N/2$.

1. Eigenstates

The spectrum of H in the ground-state multiplet for a 14-particle system obtained by diagonalization is shown as a function of effective coupling strength by the crosses in Fig. 21. Only half the spectrum is considered, since eigenvalues come in pairs of opposite sign by virtue of the fact that H changes sign under rotation through 180°

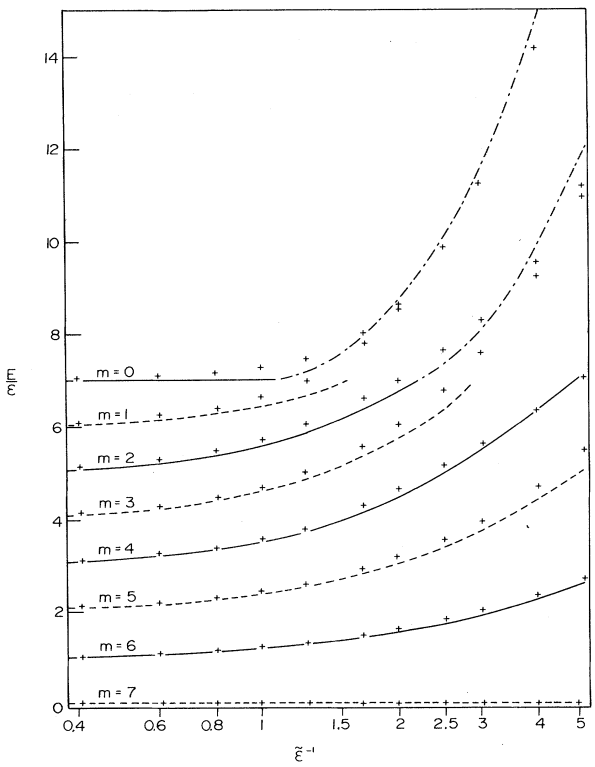

FIG. 21. Comparison of approximate and exact eigenvalues E/ε of a 14-particle Lipkin system for the ground-state multiplet as a function of the effective coupling strength $\chi^{-1}=NV/\varepsilon$. Crosses denote exact eigenvalues, solid and dashed lines denote approximate levels for even and odd m, respectively, in the unbroken symmetry region, and dot-dashed lines denote doubly degenerate solutions in the region of spontaneous symmetry breaking. A logarithmic scale for the coupling strength is used for compactness.

about the $x=y$ axis.

The Hartree-Fock approximation, obtained by minimizing the expectation value of H with respect to a variational wave function which is a product of N identical single-particle wave functions, yields two distinct solutions, depending on the strength of the potential (Agassi, Lipkin, and Meshkov, 1966). A dimensionless parameter characterizing the strength of the interaction is defined by

$$\chi\equiv(N-1)V/\varepsilon\ . \tag{6.28}$$

For weak coupling, $\chi<1$, the HF ground state is the unperturbed ground state with all the particles in the lower level

$$|\psi_{\rm HF}\rangle=\prod_p \hat{a}^\dagger_{p-1}|0\rangle\ , \tag{6.29a}$$

with energy

$$E_{\rm HF}=-\frac{\varepsilon N}{2}\ . \tag{6.29b}$$

Note that since only positive energies are shown in Fig. 21, the ground state corresponds to the negative of the highest state in the figure. For strong coupling, $\chi>1$, the parity symmetry is spontaneously broken and there are two degenerate HF states

$$|\pm\psi_{\rm HF}\rangle=e^{\mp i\alpha J_y}\prod_p|\hat{a}^\dagger_{p-1}|0\rangle\ , \tag{6.30a}$$

where

$$\cos\alpha=\frac{1}{\chi}\ , \tag{6.30b}$$

having energies

$$E_{\rm HF}=\frac{\varepsilon N}{4}\left[\frac{1}{\chi}+\chi\right]\ , \tag{6.30c}$$

where χ is defined in Eq. (6.28).

The degeneracy may be removed by taking linear combinations of the degenerate solutions, giving rise to parity doublets in the strong-coupling regime. The solid and dashed lines labeled $m=0$ in Fig. 21 denote the weak and strong coupling energies, respectively, and indicate that the mean field yields a useful first approximation for the ground state.

A comparable description of the complete spectrum of the ground-state multiplet is provided by the SPA approximation to the functional integral formulation of Sec. V.C (Levit, Negele, and Paltiel, 1980a). Introduction of an auxiliary field for the Hamiltonian, Eq. (6.24), as in Eq. (5.46), yields the trace

$$\begin{aligned}\int_0^\infty dT\,e^{iET}{\rm tr}e^{-iHT}&=\int_0^\infty dT\,e^{iET}\int\mathscr{D}(\sigma_x,\sigma_y)e^{iV\int_0^T(\sigma_x^2-\sigma_y^2)}\\&\quad\times{\rm tr}\left(T_t e^{-i\int_0^T dt[\varepsilon J_z+2V(\sigma_x J_x-\sigma_y J_y)]}\right)\ .\end{aligned} \tag{6.31}$$

A useful parametrization for product wave functions for subsequent developments is provided by the unitary transformation

$$\begin{bmatrix}\hat{\gamma}^\dagger_{p+1}\\ \hat{\gamma}^\dagger_{p-1}\end{bmatrix}=\begin{bmatrix}\cos\left[\frac{\alpha_p(t)}{2}\right]&-i\sin\left[\frac{\alpha_p(t)}{2}\right]e^{i\psi_p(t)}\\ -i\sin\frac{\alpha_p(t)}{2}e^{-i\psi_p(t)}&\cos\left[\frac{\alpha_p(t)}{2}\right]\end{bmatrix}\begin{bmatrix}\hat{a}^\dagger_{p+1}\\ \hat{a}^\dagger_{p-1}\end{bmatrix}\ , \tag{6.32}$$

in terms of which a general product state may be written

$$|\phi(t)\rangle=\prod_p\hat{\gamma}^\dagger_{p-1}(t)e^{-i\chi_p(t)}|0\rangle\ . \tag{6.33}$$

In the special case $\chi_P=\psi_P=0$, this reduces to the result Eq. (6.30a). As in Eq. (5.52) or (5.75), application of the SPA to the σ integrals in Eq. (6.31) yields

$$\sigma_{\{x\}}(t)=\sum_{p=1}^N\sigma^{(p)}_{\{x\}}(t)=\sum_{p=1}^N\langle 0|\gamma_{p-1}J_{\{x\}}\gamma^\dagger_{p-1}|0\rangle\ . \tag{6.34}$$

Observing that for the relevant stationary solutions the

single-particle states are identical for all p's, using the equation of energy conservation and performing some algebra, the quantization condition, Eq. (5.86) becomes

$$N\int \cos^2\left[\frac{\alpha}{2}\right]d\psi = m\,2\pi\ , \tag{6.35}$$

where $\cos^2(\alpha/2)$ as a function of ψ is defined by the equation

$$\cos^2\left[\frac{\alpha}{2}\right]=\frac{1}{2}\left[1-\frac{\tilde{\varepsilon}}{x}\pm\frac{1}{x}(\tilde{\varepsilon}^2+x^2-4\tilde{E}x)^{1/2}\right]\ , \tag{6.36}$$

where $\tilde{\varepsilon}=\varepsilon/NV$, $\tilde{E}=E/N^2V$, and $x=\cos 2\psi$. Evaluation of (6.35) for all the physical branches of (6.36) yields the nondegenerate solutions denoted by solid and dashed lines in Fig. 21 and the doubly degenerate solutions indicated by dashed-dot lines. The ground-state result agrees with Eq. (6.30b), except that the factors $(N-1)$ are replaced by N, because the Hartree mean field in (6.31) does not include the exchange terms at the SPA level.

As evidenced in Fig. 21, the qualitative features of the full spectrum are well reproduced in the mean-field approximation. In particular, the grouping of exact eigenstates into nearly degenerate pairs in the spontaneously broken symmetry region of $E/\varepsilon > N/2$ is reflected at the SPA level in the occurrence of doubly degenerate mean-field solutions. The nonlinear self-consistent mean-field equations for quantum eigenstates are evidently much superior to the RPA, which would necessarily predict uniform level spacings.

Using arguments based on gauge invariance and the time-dependent variational principle, Kan, *et al.* (1979) obtain the same quantization condition and results as obtained above for the Lipkin model. A subsequent improvement was introduced by Kan (1980) by replacing the wave function (6.33) by a parity projected ansatz

$$|\phi_\pm(t)\rangle=(1\pm\hat{\pi})\,|\phi(t)\rangle\ . \tag{6.37}$$

Instead of yielding doubly degenerate solutions in the region of spontaneously broken symmetry, the projected theory produces separated, nearly degenerate doublets which join continuously to the weak-coupling solutions. Thus the projected theory yields a much more accurate description of the transition region.

Higher-order corrections to the mean-field energies have been calculated using perturbation theory (Lipkin, Meshkov, and Glick, 1965), linearized equations of motion (Meshkov, Glick, and Lipkin, 1965), diagram summations (Glick, Lipkin, and Meshkov, 1965), and the coupled-cluster approximation (Lührmann, 1977; Hoodbhoy and Negele, 1978). As a prelude to the subsequent treatment of the time-dependent coupled-cluster theory, it is interesting to examine the $S^{(2)}$ corrections in the static coupled-cluster approximation. Quasispin operators $\hat{I}$ may be defined in terms of the γ's defined in Eq. (6.32) analogous to the operator $\hat{J}$ defined in terms of a's, and it is now convenient to use raising the lowering operators instead of x and y components:

$$\begin{aligned}\hat{I}_+ &\equiv \sum_{P=1}^{N}\hat{\gamma}^\dagger_{p+1}\hat{\gamma}_{p-1}\ ,\\ \hat{I}_- &\equiv \hat{I}^\dagger_+\ ,\\ \hat{I}_z &\equiv \tfrac{1}{2}\sum_{\substack{p=1,N\\ s=\pm1}} s\hat{\gamma}^\dagger_{ps}\hat{\gamma}_{ps}\ .\end{aligned} \tag{6.38}$$

The uncorrelated wave function in the coupled-cluster expansion is $|\phi(t)\rangle$ defined in Eq. (6.33) and the parameters α and ψ are determined to make $S^{(1)}$ vanish identically. By the symmetry in particle labels, $\hat{S}^{(2)}$ is characterized by a single parameter and may be expressed in terms of $\hat{I}_+$:

$$\hat{S}^{(2)}=\tfrac{1}{2}S^{(2)}\hat{I}^2_+\ . \tag{6.39}$$

Hence the static coupled cluster equations, Eq. (4.21), truncated to include only $S^{(2)}$ may be written

$$\langle\phi\,|\,He^{\hat{S}^{(2)}}\,|\,\phi\rangle=E\ , \tag{6.40a}$$

$$\langle\phi\,|\,I_-e^{-\hat{S}^{(2)}}He^{\hat{S}^{(2)}}\,|\,\phi\rangle=0\ , \tag{6.40b}$$

$$\langle\phi\,|\,I^2_-e^{-\hat{S}^{(2)}}He^{\hat{S}^{(2)}}\,|\,\phi\rangle=0\ , \tag{6.40c}$$

and after suitable angular momentum algebra yields the results (Hoodbhoy and Negele, 1978)

$$\begin{aligned}E=-\tfrac{1}{4}\varepsilon N[\,&\chi(1-S^{(2)})\\ &-\chi\cos^2\alpha(1+S^{(2)})+\cos\alpha]\ ,\end{aligned} \tag{6.41a}$$

where

$$\cos\alpha=\frac{1-(N-1)S^{(2)}}{[1-(N-3)S^{(2)}]\chi} \tag{6.41b}$$

and

$$\begin{aligned}&(N^2-7N+9)(1+\cos^2\alpha)\chi(S^{(2)})^2\\ &\quad+[6\chi(N-2)(1-\cos^2\alpha)+4(N-1)\cos\alpha]S^{(2)}\\ &\qquad=-(1+\cos^2\alpha)\chi\ ,\end{aligned} \tag{6.41c}$$

where χ is defined in Eq. (6.28). In the approximation $S^{(2)}=0$, Eqs. (6.41) reduce to Eqs. (6.29) and (6.30) in the weak- and strong-coupling regimes, respectively. The exact energy E for a 14-particle system and the deviation between truncated approximations and the exact energy are shown in Fig. 22 as a function of interaction strength V. The discrepancy between the Hartree-Fock approximations and the exact result, which was barely visible in Fig. 21, is clearly seen to increase in the strong-coupling regime. Including $S^{(2)}$ not only significantly diminishes the error at the transition point between the weak- and strong-coupling regimes, $V_T=\varepsilon/N-1\sim 0.077$, but also greatly improves the approximation throughout the entire strong-coupling regime.

2. Response to an external potential

Alhassid and Koonin (1981) have applied the functional integral formalism of Sec. V.F.1 to the response of a

Lipkin model system to an external perturbation of the form

$$V(t)=\mathbf{f}(t)\cdot\mathbf{J}\ . \tag{6.42}$$

As in Eq. (6.31), auxiliary fields σ_x and σ_y are introduced, which at the SPA level in the simplest case considered here are identical for each particle label p. The SPA for the S matrix, Eq. (5.15a) thus becomes

$$\langle\beta'|S|\beta\rangle\sim\exp\left[iN(N-1)V\left[\int_T^0 dt(\sigma_{f_x}^2-\sigma_{f_y}^2)+\int_{-T}^{T}dt(\sigma_x^2-\sigma_y^2)+\int_0^{-T}dt(\sigma_{ix}^2-\sigma_{iy}^2)\right]\right]$$
$$\times\langle\beta'|U^{\sigma_f}(0,T)U^{\sigma}(T,-T)U^{\sigma_i}(-T,0)|\beta\rangle\ , \tag{6.43a}$$

where

$$U^{\sigma_l}(t',t)=T_t\exp\left[-i\int_t^{t'}dt[\varepsilon\hat{J}_z+\delta_{l0}\mathbf{f}(t)\cdot\mathbf{J}+2(N-1)V(\sigma_{lx}\hat{J}_x-\sigma_{ly}\hat{J}_y)]\right]\ , \tag{6.43b}$$

$$\sigma_{l\{\substack{x\\y}\}}(t)=\mathrm{Re}\frac{\langle\beta'|\tilde{T}_t\hat{J}_{\{\substack{x\\y}\}}U^{\sigma_f}U^{\sigma}U^{\sigma_i}|\beta\rangle}{\langle\beta'|U^{\sigma_f}U^{\sigma}U^{\sigma_i}|\beta\rangle}\ , \tag{6.43c}$$

where σ_l denotes any one of σ_f, σ, or σ_i, $\tilde{T}_t$ inserts $\tilde{J}$ into the corresponding interval $(0,T)$, $(T,-T)$, or $(-T,0)$ at time t, and δ_{l0} indicates that the external source only contributes to U^{σ}.

In the self-consistent equations (6.43) the states $|\beta\rangle$ and $|\beta'\rangle$ are not restricted to determinants, so instead of parametrizing a general time-dependent determinant, it is useful to parametrize an arbitrary evolution operator in group-parameter space. Any sequence of evolution operators is a unitary operator and thus may be expressed in the form

$$U^{\sigma_f}(t,T)U^{\sigma}(T,-T)U^{\sigma_i}(-T,0)\equiv e^{-2i\boldsymbol{\alpha}_f\cdot\mathbf{J}}\ , \tag{6.44}$$

and similarly the products $U^{\sigma}U^{\sigma_i}$ and U^{σ_i} are expressed in terms of $\boldsymbol{\alpha}$ and $\boldsymbol{\alpha}_i$. The equations of motion for the parameters $\boldsymbol{\alpha}$ are obtained from the equation of motion for the evolution operator yielding nonlinear self-consistent first-order equations for $\boldsymbol{\alpha}$ which may be solved numerically. The exact evolution of the system, for comparison with the mean-field theory, is obtained by expanding the wave function in eigenstates of the ground-state multiplet, yielding a first-order equation to be integrated numerically for the time-dependent expansion coefficients.

Typical numerical results for a Gaussian external field, $V(t)\propto e^{-(\varepsilon t)^2}(J_x+J_y+J_z)$, in the weak-coupling regime, $\chi=0.5$, are shown in Fig. 23. The modulus of the amplitude to excite the nth eigenstate from the ground state $|S_{n_0}|$ is shown for three values of the particle number N. The qualitative behavior of the mean-field amplitude is

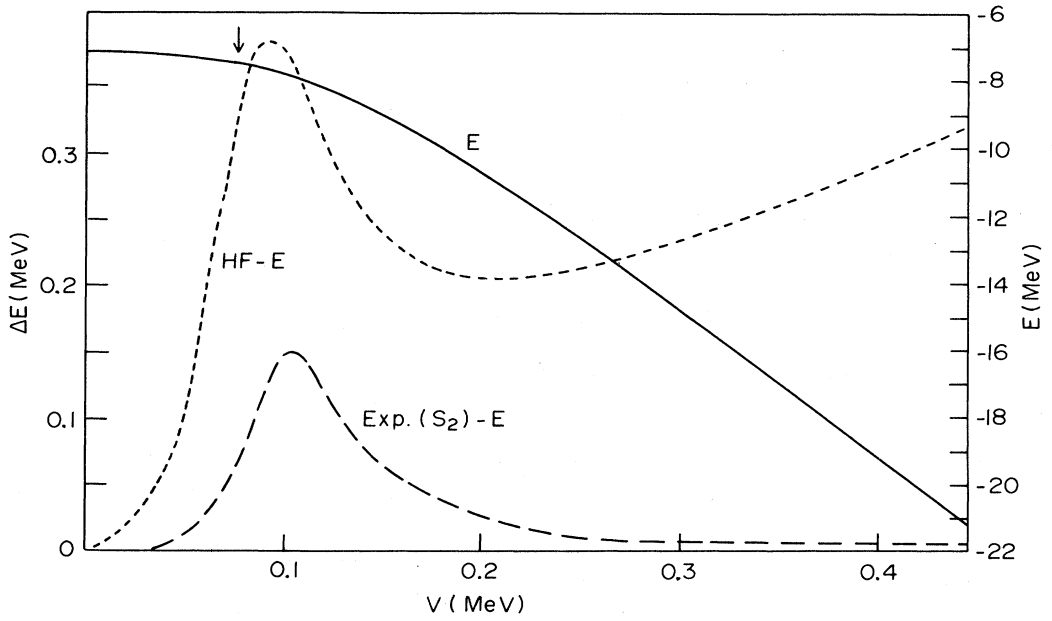

FIG. 22. The exact ground-state energy E (solid line), deviations from E of the HF energy (short dashes), and deviations from E of the coupled-cluster energy including $S^{(2)}$ (long dashes). Note that E is referred to the scale at the right and that the energy deviations use the scale at the left.

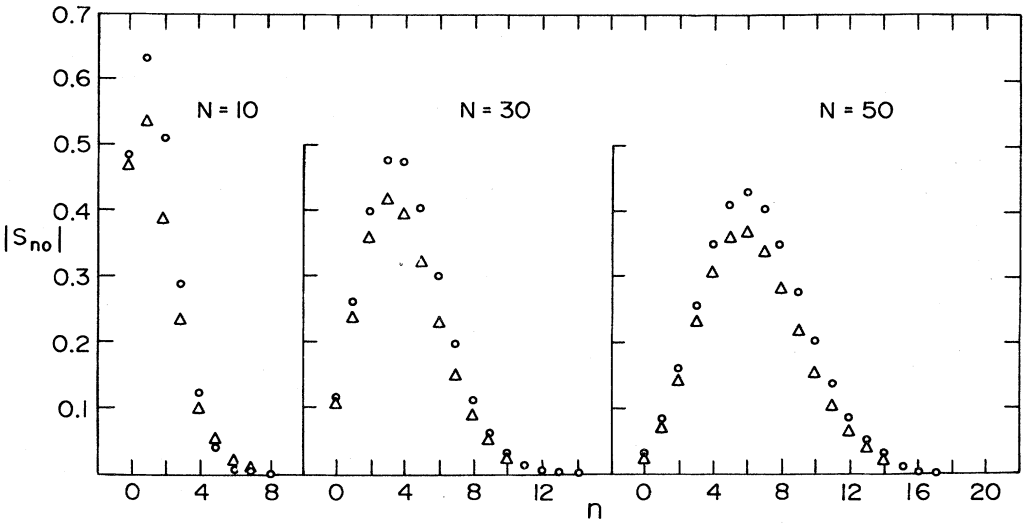

FIG. 23. Modulus of the amplitude $|S_{n0}|$ to excite the nth excited state of the Lipkin model with a Gaussian time-dependent external field. Circles and triangles denote exact and mean-field amplitudes, respectively.

good, although the amplitudes in the regimes of strongest excitation are systematically underestimated and the violation of unitarity is non-negligible. Although the theory does not yield a strict $1/N$ expansion, the agreement appears to improve with increasing N.

3. Interaction of two systems

An extreme caricature of a nuclear collision is provided by two interacting N-particle Lipkin systems. Initially, like two distantly approaching nuclei, particles in each isolated system interact only among themselves, and each system evolves in its respective ground state. At time $t=0$, all $2N$ particles interact with each other, analogous to two overlapping nuclei. Finally, after some interaction time T, the two systems again separate, and each particle is again restricted to interacting with particles within its own system. Since at every time the evolution of the system is exactly solvable in terms of eigenstates of an N- or $2N$-particle Lipkin model, it is straightforward to obtain the exact solution for the wave function and any observables of interest.

The derivation of the time-dependent coupled-cluster equations follows that of Eqs. (6.40), with the exception that separate operators $\hat{I}_1$ and $\hat{I}_2$ must be defined as in Eq. (6.38) for the two N-body systems and Eq. (6.39) must be replaced by the general form for S

$$\hat{S}^{(2)}(t)=\tfrac{1}{2}S_1^{(2)}(t)\hat{I}_{1+}^2+\tfrac{1}{2}S_2^{(2)}(t)\hat{I}_{2+}^2+S_{12}^{(2)}(t)\hat{I}_{1+}\hat{I}_{2+}\ . \tag{6.45}$$

The coupled-cluster equations for the parameters $\alpha_i(t)$ and $\psi_i(t)$ appearing in $\hat{I}_i$, which define the single-particle wave functions, and for the correlation amplitudes S_i and S_{12} are obtained by projection as before:

$$\left\langle\phi\left|\hat{\mathcal{O}}e^{-\hat{S}^{(2)}(t)}\left[H-i\frac{\partial}{\partial t}\right]e^{\hat{S}^{(2)}(t)}\right|\phi\right\rangle=0\ , \tag{6.46}$$

where $\mathcal{O}$ denotes I_{i-}, $(I_{i-})^2$, or $I_{i-}I_{i+}$ and the subscript (i) represents either of the two systems. Algebraic details are given by Hoodbhoy and Negele (1978), and only a few representative results are summarized here.

If $S^{(2)}$ is set to zero, Eqs. (6.46) yield TDHF equations of motion for α_i and ψ_i parameterizing the uncorrelated wave functions, with the results shown in Figs. 24 and 25. A convenient representation of the wave function is provided by quasispin eigenstates with $J=N/2$ and spin projection M, corresponding to $N/2-M$ particles in the lower level and $M-N/2$ in the upper state. The even-odd staggering of the exact results in Fig. 24 reflects the parity symmetry of the Hamiltonian. Prior to the interac-

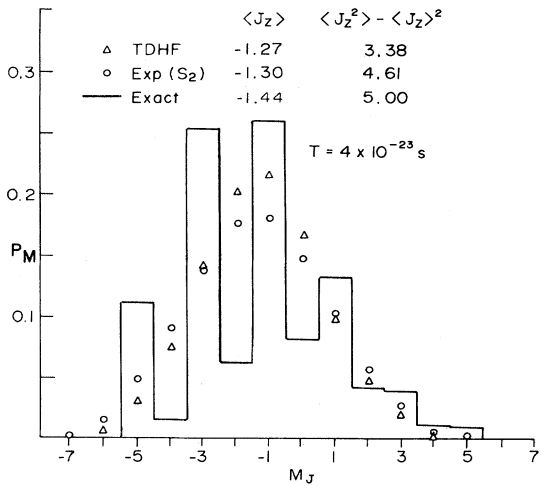

FIG. 24. The probability P for obtaining 7-M_J particles in the lower level of a 14-particle Lipkin system after interaction with a second 14-particle system. Exact, TDHF, and coupled-cluster results are denoted by solid lines, triangles, and circles, respectively, the Lipkin parameters are $\varepsilon=1$ MeV and $NV=5$ MeV, and the interaction time is 4×10^{-23} s.

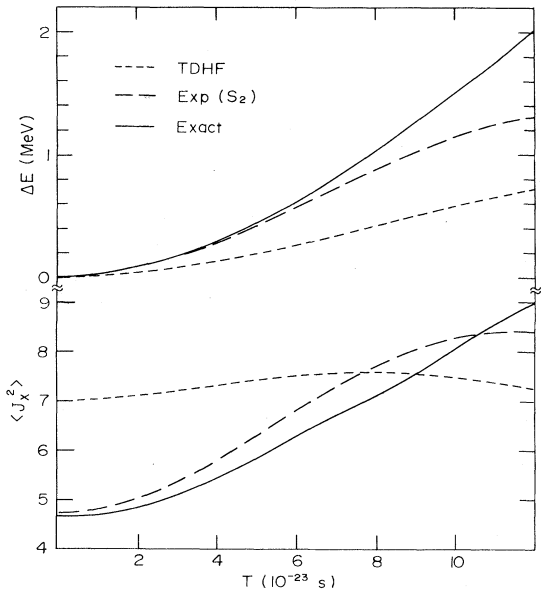

FIG. 25. Excitation energy ΔE and mean value of J_x^2 as a function of interaction time for the system treated in Fig. 24, using exact (solid lines), TDHF (short dashed lines), and coupled-cluster wave functions (long dashed lines).

tion, only pairs of particles can be removed from the ground state, so only components with even numbers of particles in the lower state (odd M_J) are nonvanishing. Interactions between one particle in one system and one in the other introduce components with odd population of the lower state, as well, but for the short interaction time shown in Fig. 24, the correlation is still quite strong. Unless parity projections are explicitly imposed, no approximation with fewer than 14 particle correlations can possibly represent the individual amplitudes, so it is only reasonable to seek to reproduce expectation values of few-body operators. As seen in Fig. 24, $\langle J_z \rangle$, and thus the mean number of particles in the lower state, is well reproduced by the mean-field theory, whereas the dispersion of occupation of the lower state, specified by $\langle J_z^2 \rangle - \langle J_z \rangle^2$, is poorly represented. Introduction of two-body correlations in the coupled-cluster expansion not only further improves $\langle J_z \rangle$, but, more important, yields a reasonable value for the dispersion. Similar results occur in Fig. 24, where the expectation value of two two-body operators, $\langle J_x^2 \rangle$ and the excitation energy, are shown as a function of the interaction time T. Again one observes that qualitatively incorrect behavior of two-body operators in the mean-field theory is dramatically improved by inclusion of two-particle correlations in the coupled-cluster approximation.

Although two interacting Lipkin systems constitute a crude representation of a scattering problem, the success of the mean-field theory in representing expectation values of one-body operators and the necessity of including two-particle, two-hole amplitudes to treat two-body operators certainly suggest that similar features may arise in nucleus-nucleus scattering.

C. One-dimensional saturating system

The preceding solvable models fail to address the crucial feature of saturation in finite nuclei. The eigenstates of the one-dimensional delta-function potential shrink in spatial extent instead of increasing with the number of particles, and the Lipkin model has no spatial degrees of freedom. Thus, to begin to explore mean-field dynamics in a saturating system, it is useful to define a simple model system in one spatial dimension which is constructed to produce saturation.

A simple one-dimensional saturating model is specified by the following Hamiltonian density (Levit, Negele, and Paltiel, 1980b):

$$H(\bar{\psi},\psi) = -M \sum_\alpha \bar{\psi}_\alpha(x,t) \frac{\partial^2}{\partial x^2} \psi_\alpha(x,t) + \tfrac{1}{2} \int dx' \rho(x,t) V(x-x') \rho(x',t) + \tfrac{1}{3} V_3 \rho^3(x,t) , \tag{6.47a}$$

where

$$\rho(x,t) = M \sum_\alpha \bar{\psi}_\alpha(x,t) \psi_\alpha(x,t) ; \tag{6.47b}$$

$\bar{\psi}_\alpha(x,t)$ denotes $\psi_\alpha^*(x,t)$ or $\psi_\alpha(x,-t)$ for real or imaginary time, respectively, V is the sum of a short-range attractive Gaussian and a long-range repulsive Gaussian, energies are measured in units of $E_0 = \hbar^2/2ml_0^2$, time is measured in units of $t_0 = \hbar/E_0$, and the length scale l_0 is defined as the reciprocal of the saturation density. Saturation is achieved by virtue of the repulsive three-body force, the relative strengths of the attractive two-body and repulsive three-body forces are chosen to reproduce the ratio of Fermi kinetic energy to potential energy in nuclear matter, the range of the attractive Yukawa is chosen to be half the mean distance between particles, and the spin-isospin degeneracy M is 4. The long-range repulsive Gaussian force is introduced to mock up the effect of Coulomb repulsion and produce fission of sufficiently large systems, and its strength is defined to render a 16-particle system unstable with respect to breakup into two eight-particle fission fragments, which in turn are stable with respect to further decay. Removing a multiplicative factor as in Eq. (5.66), the periodic mean-field equations for this Hamiltonian density are

$$\left[-i \frac{\partial}{\partial t} + h[\rho] \right] \phi_\alpha(x,t) = \lambda_\alpha \phi_\alpha(x,t) \tag{6.48a}$$

for real time and

$$\left[\frac{\partial}{\partial t} + h[\rho] \right] \phi_\alpha(x,\tau) = \lambda_\alpha \phi_\alpha(x,\tau) \tag{6.48b}$$

for imaginary time, where

$$h[\rho] = -\frac{\partial^2}{\partial x^2} + \int dx' \rho(x,t) V(x-x') + V_3 \rho^2(x,t) . \tag{6.48c}$$

Static solutions to these equations yield the Hartree-Fock ground-state density distributions shown in Fig. 26. The salient result in this figure is the fact that behavior as a function of x for this one-dimensional model faithfully reproduces the behavior of physical nuclear densities as a function of radius r. The surface thickness is essentially independent of particle number, and the interior density displays small quantum density fluctuations around a constant value displaced slightly below the value which would obtain in infinite matter in the absence of a Coulomb-like force. Thus, it is reasonable to expect vibrational states to reflect the behavior of monopole modes in spherical nuclei and fission dynamics to be relevant to neck formation in finite nuclei.

1. Periodic solutions

To appreciate the methods available for solving Eqs. (6.48), it is useful to consider the structure of the real and imaginary time eigenvalue problems. There is no known method for finding all the periodic solutions to these nonlinear, self-consistent equations of motion, and as in the static Hartree problem one must iteratively refine an initial guess for either the potential or the wave functions. Selecting the time origin to coincide with a classical turning point so that the density is time even, one may show that for a specified density $\rho(t)$ the evolution operator

$$U(x,T/2;x',-T/2)\equiv T_t\exp\left[-i\int_{-T/2}^{T/2}dt'h[\rho(t')]\right] \tag{6.49a}$$

and the corresponding operator in imaginary time are symmetric. For imaginary time, since U is real, one may solve the Hermitian eigenvalue problem

$$U(T/2,-T/2)\phi_\alpha(x,-T/2)=e^{-\lambda_\alpha}\phi_\alpha(x,-T/2) \tag{6.49b}$$

for $\phi_\alpha(x,-T/2)$ at the initial time and use this initial condition in the first-order equation (6.48b) to obtain $\phi_\alpha(x,t)$. For real time, using the facts that $U^\dagger=U^{-1}$ and $U^T=U$, the eigenvalue problem

$$U(T/2,-T/2)\phi_\alpha(x,-T/2)=e^{-i\lambda_\alpha}\phi_\alpha(x,-T/2) \tag{6.49c}$$

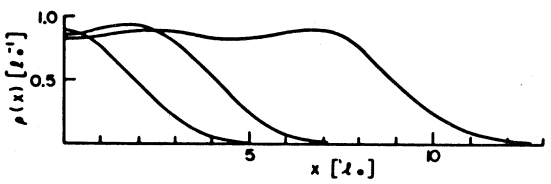

FIG. 26. Ground-state HF density distributions for 4-, 8-, and 16-particle systems. The length scale l_0 is defined such that saturation density for a uniform medium without the repulsive Coulomb-like force is 1.0, and because of reflection symmetry, distributions are shown only for positive x.

may be expressed in the more convenient Hermitian form

$$(U+U^\dagger)\phi_\alpha(x,-T/2)=(e^{-i\lambda_\alpha}+e^{i\lambda_\alpha})\phi_\alpha(x,-T/2)\ , \tag{6.49d}$$

from which $\phi_\alpha(x,t)$ may be obtained as in the imaginary time case. The self-consistency condition on the density may be fulfilled by iteration, and in this approach each iteration requires the diagonalization of a dense $M_x\times M_x$ matrix, where M_x denotes the number of spatial mesh points (or terms in an expansion in a complete set of functions).

In addition to the M_x orthogonal eigenvectors defined above, each of these eigenfunctions may be multiplied by a phase factor $e^{i(2\pi n/T)t}$ to obtain new solutions to Eqs. (6.48). For real time, the resulting eigenvalues are unbounded, and may be written

$$\lambda_{n\alpha}=\lambda_\alpha+\frac{2\pi}{T}n\ , \tag{6.50a}$$

where n may be positive or negative, whereas for imaginary times the additional eigenvalues with $n\neq 0$ are necessarily complex:

$$\lambda_{n\alpha}=\lambda_\alpha+i\frac{2\pi}{T}n\ . \tag{6.50b}$$

For imaginary time, an alternative iterative method may be implemented by calculating

$$\chi_\alpha^{N+1}(x,\tau)=\exp\left[-\beta\left[\frac{\partial}{\partial\tau}+h[\rho]\right]\right]\psi_\alpha^N(x,\tau) \tag{6.51}$$

and defining $\{\psi^{N+1}(x,\tau)\}$ to be orthonormal linear combinations of $\{\chi^{N+1}(x,\tau)\}$ with respect to the norm

$$\int dx\,d\tau\,\psi_\alpha(x,-\tau)\psi_\beta(x,\tau)=\delta_{\alpha\beta}\ . \tag{6.52}$$

If the initial ψ_α are chosen purely real and are sufficiently close to a self-consistent solution, one can show that each application of Eq. (6.51) amplifies eigenfunctions with the largest values of λ_α and that the set of wave functions converges to a self-consistent solution to Eq. (6.48b). This method is completely analogous to solution of the static Hartree-Fock problem by evolution in imaginary time (Davies, *et al.*, 1980). If the time interval is discretized into N_T time steps and the exponential in Eq. (6.51) is expanded in a power series, a sequence of multiplications by a sparse $(N_T\times M_x)^2$ matrix rather than diagonalization of a dense $M_x\times M_x$ matrix is required. The same method, unfortunately is inappropriate to the real time problem because the spectrum, Eq. (6.50a), is unbounded. An alternative iteration procedure is given by

$$\chi_\alpha^{N+1}(x,t)=P\left[\beta\left[-i\frac{\partial}{\partial t}+h(\rho)-\bar{\lambda}_\alpha^N\right]^2\right]\psi_\alpha^N(x,t)\ , \tag{6.53}$$

where P is a polynomial defined to peak sharply at the

origin, $\bar{\lambda}_\alpha$ is the expectation value of $[-i(\partial/\partial t)+h]$ in the state ψ_α^N, and the χ's are orthogonalized appropriately. In the present one-dimensional example, both diagonalization of the evolution operator and the iterative methods in Eqs. (6.51) and (6.53) have been successfully implemented (Levit, Negele, and Paltiel, 1980b; Negele, Serr, and Vichniac, 1982). The development of the latter techniques, however, is absolutely crucial to treatment of higher dimensions, where the diagonalization of a dense matrix of dimension corresponding to the total number of spatial points is totally impractical.

In addition to technical questions of methods to solve Eqs. (6.48), there is the problem of the stability of solutions which are stationary points rather than relative minima. One class of static Hartree-Fock solutions corresponds to relative minima in the space of Slater determinants, and the only practical problem in numerical calculations is to find an initial guess which evolves into the desired minimum. Other interesting stationary points, such as the fission saddle-point configuration, have one or more directions in which the energy decreases; and iterative solutions for these configurations require the imposition of an external constraint to obtain a stable solution. Analogous constraints are required for Eqs. (6.48) and are discussed in the references cited above.

Even with a constraint, the initial guess must be close in some sense to a periodic solution, or else iteration will evolve it into an uninteresting solution, usually a static Hartree-Fock solution. An adequate strategy for finding eigenstates of large-amplitude collective motion is first to solve the RPA equations for infinitesimal vibrations. Starting with the time-dependent wave functions for a sigle mode, a series of sequential self-consistent calculations may be performed gradually increasing the period from the RPA value $T_0=2\pi/\omega$. By continuity, the initial wave function for each new period may thus be made sufficiently close to an exact solution that convergence for an entire family of solutions of increasing amplitude may be assured. The quantum eigenstates correspond to those members of the family which satisfy the quantization conditions Eqs. (5.86). For solutions in imaginary time the same approach may be taken in the inverted well, Fig. 16(e), and as the period is increased to infinity, the solution approaches the bounce described in Sec. V.E.

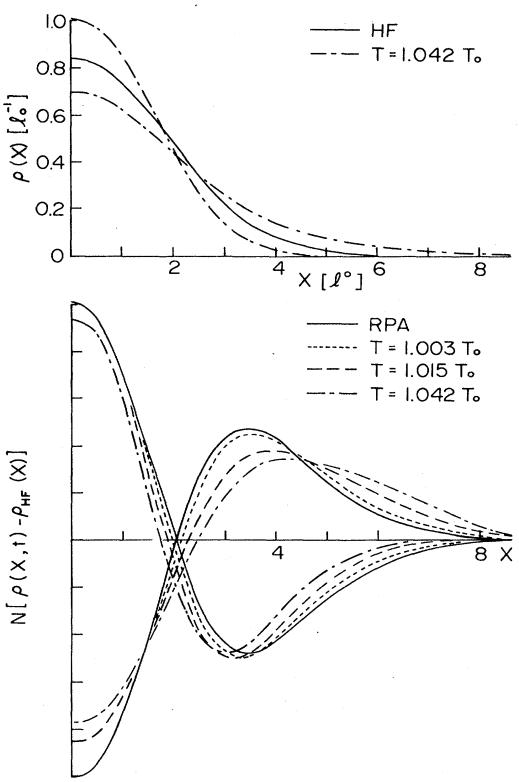

FIG. 27. Large-amplitude vibrations for a four-particle saturating system. The upper graph compares the static HF density (solid curve) with the densities at the classical turning points, $\rho(x,-T/2)$ and $\rho(x,0)$, for the periodic solution with period $T=1.042T_0$ (dot-dash curve). The deviation of the density at the classical turning points from the HF density, normalized as described in the text, is shown in the lower graph. An infinitesimal RPA vibration, corresponding to period T_0, is denoted by the solid lines. Vibrations with successively larger amplitudes and longer periods are indicated by short dashes, long dashes, and the dot-dash curves.

The nonlinearity of the vibrations is shown in the lower graph. For infinitesimal vibrations, the deviation

$$[\rho(x,t)-\rho_{\rm HF}(x)]\Big/\left[\int_0^T dt\int dx\, x^2\cos\left[\frac{2\pi t}{T}\right]\times[\rho(x,t)-\rho_{\rm HF}(x)]\right] \tag{6.54}$$

is independent of the amplitude and equals the RPA transition density denoted by the solid lines. As the period increases and nonlinearities become non-negligible, the deviation at the turning points begins to differ from the RPA result. For the largest amplitude, the shape deviates significantly from the RPA transition density, particularly in the surface, where the vibrations above and below equilibrium density necessarily became quite asymmetric.

The four-particle system is so small that even the largest amplitude vibration is insufficient to satisfy the

2. Large-amplitude vibrations

Solutions to Eq. (6.48a) for large-amplitude vibrations of a four-particle system are shown in Fig. 27. Three periods, 0.34%, 1.49%, and 4.23% larger than the RPA period T_0 are considered, yielding fluctuations in the central density of 5%, 11%, and 18%, respectively. The range of shapes attained for the largest-amplitude case is indicated in the upper graph, which compares the spatial density distributions at the classical turning points of the vibration with the static Hartree-Fock density.

quantization condition for the first quantized excited state. For larger systems, however, vibrations with physically reasonable amplitudes will satisfy the quantization condition and will be of physical relevance to monopole vibrations in nuclei.

3. Spontaneous fission

Solutions to Eqs. (6.48b) for the spontaneous fission of a 16-particle system into two eight-particle fragments are shown in Figs. 28 and 29. The sequence of density profiles in Fig. 28 exhibits the essential features of the bounce solutions to the tunneling equations. At large negative times, the density is indistinguishable from the HF ground state, and the deformation to the scission configuration is localized in a time interval around $\tau=0$. Further increase in the period induces negligible changes in the density in the vicinity of $\tau=0$ and the total energy and simply introduces an arbitrarily long initial period during which the solution is indistinguishable from the static HF solution.

The extent to which the configuration at $\tau=0$ approximates two nearly separated eight-particle fragments is indicated in Fig. 29, in which the four distinct single-particle wave functions are shown at $\tau=-T/2$ and $\tau=0$. At time $\tau=-T/2$, the wave functions are simply the zero-, one-, two-, and three-node eigenfunctions of the static HF potential. The elongation to form a neck at the origin at $\tau=0$ changes the structure, so that the first two wave functions resemble even and odd combinations of nodeless wave functions localized on separate sides of the origin and the last two correspond to even and odd combinations of wave functions localized on each side of the origin containing a single node. Hence a more illuminating representation would be states corresponding to sums and differences of the first two and last two wave functions, in which the total wave function would approximately factorize into two nearly separated subsystems. Whereas the fission lifetime of this one-dimensional model has no direct physical relevance, the dynamics of the neck formation and structure of the periodic self-consistent tunneling solutions are quite similar to those arising in the three-dimensional calculation in Sec. VII.

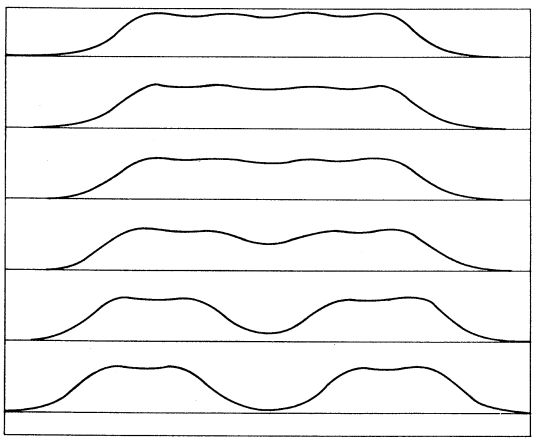

FIG. 28. Density profiles for a 16-particle system undergoing fission into two eight-particle fragments, at evenly spaced intervals from $t=-T/2$ to $t=0$ in time increments of $20t_0$.

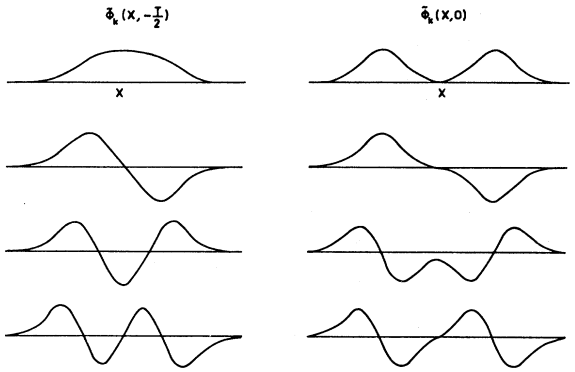

FIG. 29. Normalized self-consistent fission wave functions at times $\tau=-T/2$ and $\tau=0$ for the solution shown in Fig. 28.

Two obvious shortcomings of the one-dimensional model treated in this section are the ambiguities in defining an effective Hamiltonian in one dimension which is genuinely analogous to one in three dimensions and the possibility that phase-space differences between one and three dimensions will significantly alter the qualitative behavior. For these reasons, it is valuable to consider semi-infinite slab geometry in the next section.

D. Semi-infinite slabs

The simplicity of one-dimensional dynamics may be retained in three-dimensional phase space utilizing a realistic effective interaction by considering semi-infinite slabs of matter in which the transverse degrees of freedom are completely decoupled from the longitudinal dynamics (Bonche, Koonin, and Negele, 1976). Since a primary feature of TDHF dynamics in unrestricted geometry is the weak coupling to transverse degrees of freedom, slab collisions illustrate the dominant longitudinal equilibration with a minimum of extraneous complications and clearly display the essential features of realistic three-dimensional collisions.

1. Slab geometry

Semi-infinite slabs of spin-isospin symmetric matter are considered which are translationally invariant in the two transverse directions. The general form of single-particle wave functions for such geometry is

$$\psi_{n,\mathbf{k}_\perp}(\mathbf{r})=\frac{1}{\sqrt{\Omega}}e^{i\mathbf{k}_\perp\cdot\mathbf{r}_\perp}\phi_{n,\mathbf{k}_\perp}(z,t)\ , \tag{6.55}$$

where $\mathbf{r}_\perp\equiv(x,y)$, $\mathbf{k}_\perp\equiv(k_x,k_y)$, and Ω is a transverse normalization area. For the most general interaction, ϕ is a function of three continuous variables, z, k_x, and k_y, and no particular simplification ensues. However, for the ef-

fective interaction

$$v(r,r')=t_0\delta(r-r')+\frac{t_3}{6}\delta(r-r')\rho(r) + V_0\frac{e^{-|r-r'|/a}}{|r-r'|/a}\left[\frac{16}{15}+\frac{4}{15}P_x\right], \quad (6.56)$$

where P_x denotes the space exchange operator, the mean-field appearing in the single-particle equation Eq. (3.7a) is

$$W(z)=\frac{3}{4}t_0\rho(z)+\frac{3}{16}t_3\rho^2(z) + 2\pi a^3 V_0\int_{-\infty}^{\infty}dz'\rho(z')e^{-|z-z'|/a}, \quad (6.57)$$

and the HF equations are thereby separable. The interaction of (6.56) is closely related to the Skyrme forces discussed in Sec. II.B.2 except that one combination of the quadratically momentum-dependent terms is replaced by a more physical finite-range force, and the other combination is constrained to be zero so that the HF equation is separable. The specific combination $4+P_x$ in the finite-range force is necessary to eliminate the spatial exchange term, which would otherwise destroy separability. This interaction, which is a special case of Eq. (7.2) discussed subsequently, is adjusted to yield a nuclear matter binding energy of 15.77 MeV per particle at a saturation density of $\rho=0.145$ fm^{-2}, corresponding to $k_F=1.29$ fm^{-1}.

The static HF problem is solved by spatial wave functions of the form

$$\psi^{(\mathbf{r})}_{n\mathbf{k}_\perp}=\frac{1}{\sqrt{\Omega}}e^{i\mathbf{k}_\perp\cdot\mathbf{r}_\perp}\phi_n^{\mathrm{HF}}(z)\chi_{\tau\sigma}, \quad (6.58)$$

where n denotes the spatial quantum numbers, χ is a spin-isospin spinor, and $\phi_n^{\mathrm{HF}}(z)$ satisfies

$$\left[-\frac{1}{2m}\frac{d^2}{dz^2}+W(z)\right]\phi_n^{\mathrm{HF}}(z)=e_n\phi_n^{\mathrm{HF}}(z). \quad (6.59)$$

The resulting density, obtained by filling all states below the Fermi energy ε_f, is

$$\rho(z)=4\sum_n\sum_{|k|\le 2m(\varepsilon_f-e_n)}|\psi_{nk}|^2 = \sum_n\frac{2m}{\pi}(\varepsilon_f-e_n)|\phi_n^{\mathrm{HF}}(z)|^2 \equiv\sum_n A_n|\phi_n^{\mathrm{HF}}(z)|^2. \quad (6.60)$$

From Eq. (6.60) it is evident that the transverse wave functions play a completely passive role, simply determining the relative weighting of the various longitudinal wave functions $\phi_n^{\mathrm{HF}}(z)$.

Similarly, the TDHF problem is solved by spatial wave functions of the form

$$\psi^{(\mathbf{r},t)}_{n\mathbf{k}_\perp}=\frac{1}{\sqrt{\Omega}}e^{-i(k_\perp^2t/2m)}e^{i\mathbf{k}_\perp\cdot\mathbf{r}_\perp}\phi_n(z,t), \quad (6.61)$$

where $\phi_n(z,t)$ satisfies

$$i\dot{\phi}_n(z,t)=\left[-\frac{1}{2m}\frac{\partial^2}{\partial z^2}+W(z,t)\right]\phi_n(z,t). \quad (6.62)$$

The phase factor $e^{-ik_\perp^2t/2m}$ never contributes to any observables, so, as in the static case, the transverse wave functions play a completely passive role. A different set of transverse wave functions is associated with each longitudinal wave function through the factor A_n when the initial conditions are established, and simply remains attached to that wave function for all subsequent times.

2. Initial states and TDHF evolution

The static HF equations, Eq. (6.59), may be solved for any specified integrated slab thickness, $\mathscr{A}=\int dz\,\rho(z)$. Hence ε_F and the number of occupied states are implicit functions of $\mathscr{A}$. Slab density profiles are shown in Fig. 30 for slab thicknesses corresponding to the integrated density occurring in typical nuclei. These slabs contain from four to seven different z wave functions and are qualitatively very similar in shape to the ^{208}Pb HF density distribution displayed in the upper right portion of the figure.

The TDHF equations, Eq. (6.62), may be evolved in time by the Crank-Nicholson algorithm, used in the original work of Bonche, Koonin, and Negele (1976), or by expanding an exponential approximation to the evolution operator as described in Sec. VII.A. The two most crucial technical points in the evolution are to utilize a unitary approximation, which guarantees stability and orthonormality, and to avoid spurious dissipation by defining the evolution from t_n to $t_n+\Delta t$ by the potential at $t_n+\Delta t/2$. As discussed in Secs. II.A.3 and II.A.4, the initial conditions for a scattering problem are specified by preparing two slab ground states in relative translational motion towards each other by multiplying static HF wave functions by the phase factor $e^{\pm ik\cdot z}$, Eq. (3.45). For simplicity, most of the examples in this section are for symmetric collisions, which are displayed in the cm system and specified by the cm energy per particle. The energy per particle of the projectile in the lab is four times the quoted cm energy per particle. Asymmetric collisions exhibit the same qualitative behavior as shown in these examples.

3. Single-particle propagation in the mean field

The essential physics of the TDHF approximation is most evident if one thinks about each single-particle wave function's evolving independently in the time-dependent mean field. Of course, all the occupied orbitals must be evolved together to construct the mean field, but given the resulting time-dependent potential, $W(z,t)$, it is true that each single-particle wave function simply satisfies the one-body Schrödinger equation, (6.62), in that well. Thus, all intuition regarding wave packets in one-dimensional potential wells is immediately applicable to TDHF evolution. Although keeping track of indivi-

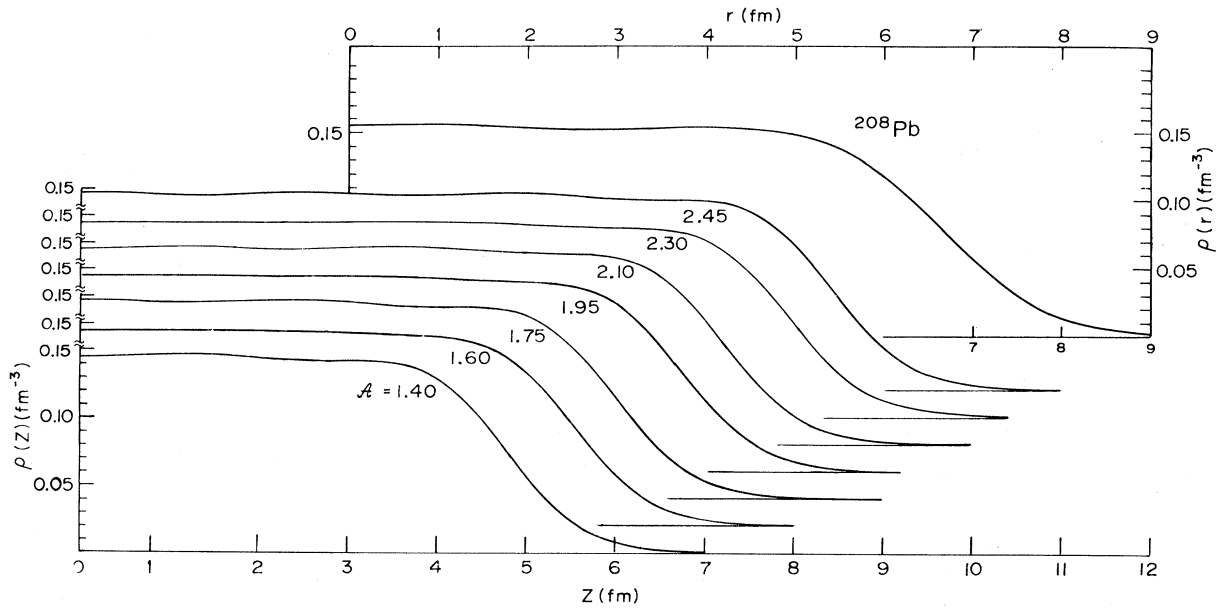

FIG. 30. Density profiles for static slabs. Shown for comparison is the HF density distribution for ^{208}Pb.

dual wave functions is of pedagogical value in understanding the dynamics, one must ultimately bear in mind that there is no physical significance to any particular decomposition of the determinant into single-particle wave functions and no observable operator distinguishes contributions from single-particle orbitals originating in one particular slab.

Figures 31 and 32 display the total density and the contributions to the density from the first and third orbitals of the left-hand slab at successive times for an initial cm energy of 3.5 MeV per particle. The second and fourth orbitals are also shown at the final time in Fig. 32. Because of the Yukawa interaction, even when the density fluctuates, the mean field is quite smooth, so the single-particle orbitals essentially propagate in a smooth 50 MeV well and are reflected from the well edges. The lump at the edge at $t=0.32\times10^{-21}$ s evidently arises from the reflection of the third orbital rather than from any sort of Benard instability in fluid mechanics and is chiefly responsible for beginning to move the edge of the well back to the right. At this energy, when scission occurs, most of the orbitals which began on the left are trapped on the right, but are significantly distorted from their original shape, giving rise to the high excitation energy and conspicuous density fluctuations in the emerging fragments. The slabs have thus essentially passed through each other, dissipating much of their translational kinetic energy in the process, and this behavior persists at all higher bombarding energies.

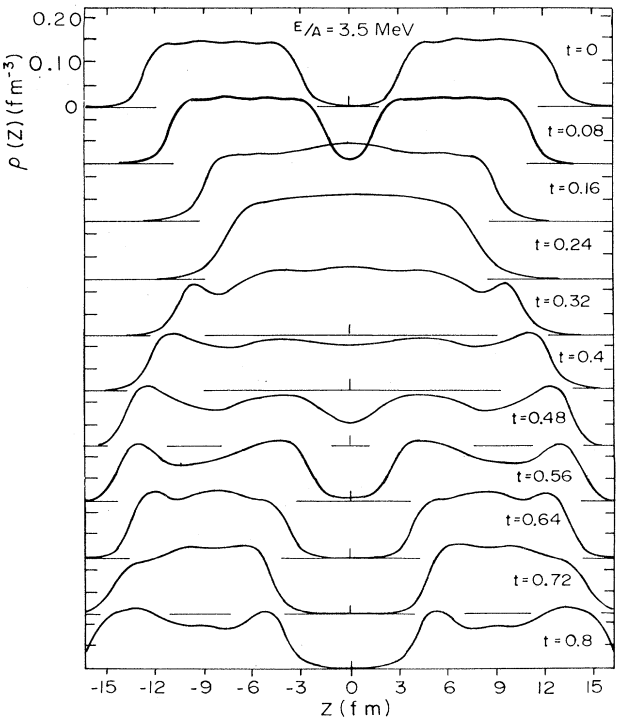

FIG. 31. Density profiles $\rho(z,t)$ at sequential times t, specified in units of 10^{-21} s, for a cm energy $E/A=3.5$ MeV.

Qualitatively different behavior occurs at a cm energy of 1.5 MeV per particle, for which the corresponding density profiles are shown in Fig. 33. In contrast to the higher-energy case, after having elongated at time $t=0.625\times10^{-21}$ s, the compound system contracts and only scissions after a second elongation.

At still lower energies, the repeated multiple reflections of single-particle wave functions from the well edges completely equilibrate the original collective translational kinetic energy into single-particle excitation, forming an oscillating compound slab.

4. Dissipation and fusion

Many essential features of TDHF dynamics are summarized in Fig. 34, which displays the ratio of final to

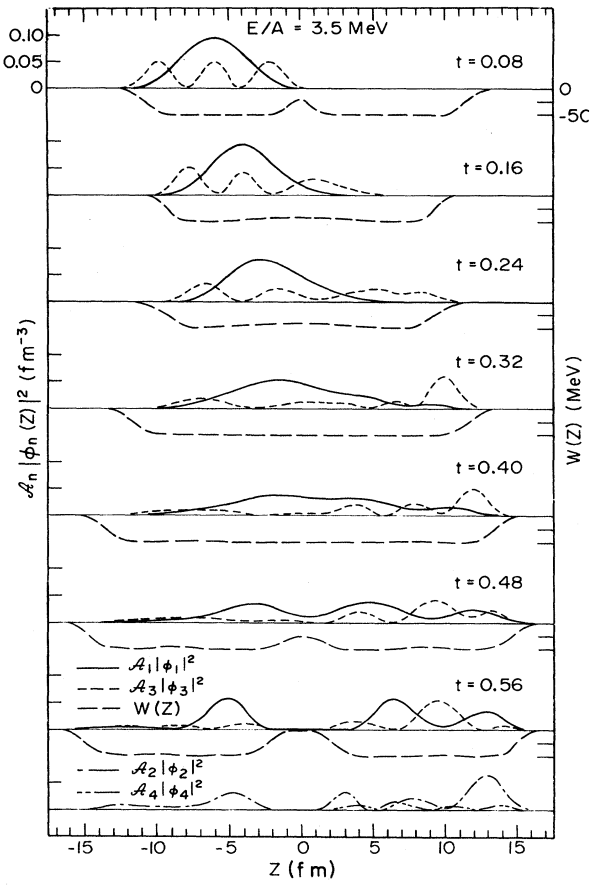

FIG. 32. Contributions of individual single-particle wave functions for the collision shown in Fig. 31. In the upper graphs, the mean field is denoted by the long-dashed line, with the scale shown to the right. The contributions to the density of the lowest orbital and third orbital originating in the left slab are indicated by the solid and short-dashed lines, respectively. The bottom graph displays the contributions of the second and fourth orbital at the final time.

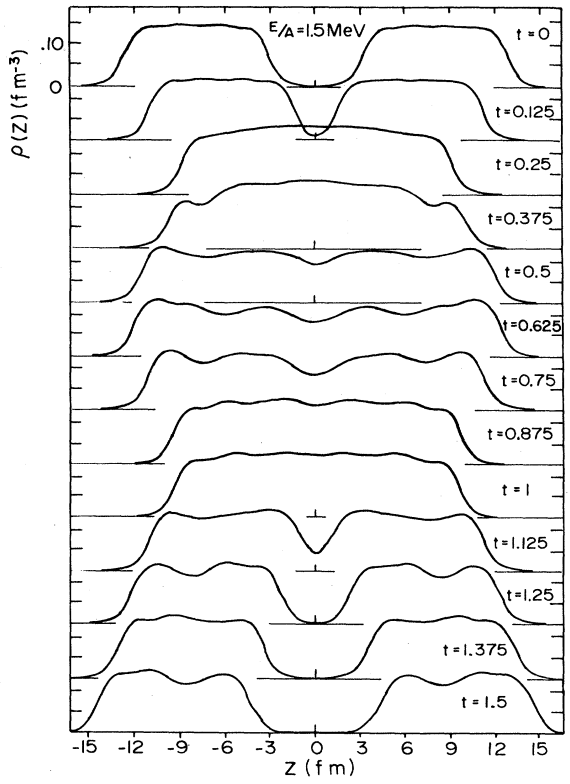

FIG. 33. Density profiles as in Fig. 1 for cm energy $E/A = 1.5$ MeV.

incident translational kinetic energy for symmetric collisions of $\mathscr{A} = 1.4$ fm^{-2} slabs as a function of bombarding energy. Two qualitatively distinct regimes are observed in this figure. Above a cm energy of 2 MeV per particle, corresponding to a lab bombarding energy of 8 MeV per particle, slabs always pass through each other dissipating on the order of 90% of their collective translational energy into internal excitation energy. As observed in the case shown in Fig. 31, in this regime the single-particle wave functions beginning on the left emerge in the right-hand fragment, with the drastic modification of their nodal structure reflecting the collective energy that has been dissipated into internal excitation. The transition at a cm energy of 2 MeV per particle is of wider generality than the specific choice of target and projectile slab thicknesses considered here and is discussed by Bertsch and Mundinger (1978).

Qualitatively different behavior occurs below 2 MeV per particle, where sufficient dissipation occurs to render fusion possible. At these low energies, if scission does not occur within the first few oscillations, further equilibration from subsequent reflections makes it highly unlikely later. Thus the question of whether scission occurs at a particular energy is very delicate, depending crucially upon whether the single-particle orbitals conspire to create a relative maximum or minimum in the neck region as the compound slab reaches its point of maximum stretching. A tiny change in initial conditions modifies the arrangement of single-particle oribtals in an essential way and thus qualitatively affects the final out-

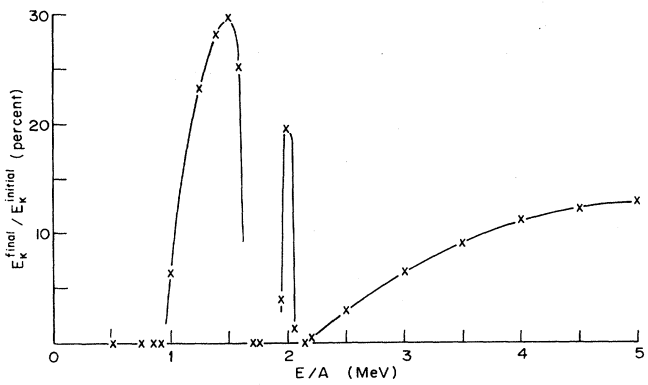

FIG. 34. Ratio of final to incident translational kinetic energy as a function of cm incident energy for symmetric slab collisions.

come of the reaction. The resulting resonance behavior is clearly demonstrated in Fig. 34. Below 2 MeV, complicated multiple reflections occur, giving rise to compound slabs which undergo length oscillations without scissioning (plotted as a ratio of 0 in Fig. 34), as well as resonances in which the slabs separate on the second or subsequent oscillation.

Two essential features of TDHF dynamics seen in these slab collisions are relevant to heavy-ion experiments. One feature is very strong damping in which initial translational kinetic energy is transferred into other degrees of freedom. In realistic geometry, this approximately accounts for both the observed fusion cross sections and the strong dissipation observed in deep inelastic collisions. The second feature is the presence of pronounced single-particle resonances, arising from the fact that one or several single-particle orbitals in the neck region can play a decisive role in determining whether or not fusion occurs. These resonances are extremely suggestive of the resonances in fusion cross sections observed in $^{12}C+{}^{12}C$ and $^{16}O+{}^{12}C$ reactions (Sperr, Vigdor *et al.*, 1976; Sperr, Braid *et al.*, 1976). Unfortunately, ambiguities in the TDHF calculation of fusion cross sections and technical limitations which preclude inclusion of the spin-orbit force have rendered it impractical to perform definitive three-dimensional calculations to verify the presence of oscillations in reactions of ^{12}C and ^{16}O with ^{12}C and the absence in reactions of ^{18}O and ^{19}F on ^{12}C.

5. Particle emission

Two physical mechanisms exist in the mean-field theory for particle emission. Considering the target nucleus in the Fermi gas approximation, the criterion for escape of a particle introduced into the system with momentum k is

$$\frac{k^2}{2m} > \frac{k_F^2}{2m} + \mu \ , \tag{6.63}$$

where μ is the nucleon separation energy. From the rest frame of the target, the projectile appears to be a Fermi gas displaced in momentum space by the projectile momentum, and thus may possess momentum components exceeding the escape criterion, Eq. (6.63). To the extent to which the far surface of the target nucleus is not altered by the projectile, those projectile momentum components satisfying the escape condition will propagate through the target and emerge in the forward direction. As the projectile energy increases, the fraction of the projectile particles fulfilling the emission condition increases and is easily evaluated in the Fermi gas approximation. A second emission mechanism is the generation of high-momentum components in both the target and the projectile by the motion of the surfaces of the single-particle potential.

Although this particle emission expected on very general grounds is present in the collisions shown in Figs. 31—33, the amplitude is so low that it is not evident on linear density plots. Hence density profiles for two separating slabs are shown on a logarithmic plot in Fig. 35, along with the velocity distribution (Negele, 1977). For a static slab in its ground state, the densty distribution at the left surface would be purely exponential. The shoulder in the distribution at roughly one percent of saturation density indicates the high momentum components which are beginning to emerge. For this collision with $E/A=2.4$ MeV, the initial velocity of each slab is $v/c=0.07$, and the maximum velocity component in the Fermi gas model would be $v/c=0.34$. As observed in the lower part of Fig. 35, the velocity distribution at the leading edge shows this range expected in the Fermi gas limit, as well as extending somewhat beyond due to high-momentum components induced by the surface.

Physically, it is reasonable to expect this mean-field particle emission mechanism to be one source of the promptly emitted particles in heavy-ion collisions. An approximate mean-field calculation for ^{24}N on ^{16}O was performed by Bertsch (1977b) and the simple Fermi gas estimate discussed above has been applied to realistic geometries by Bondorf *et al.* (1979, 1980). Realistic TDHF calculations of particle emission are discussed in Sec. VII.B. Clearly, another physical mechanism for particle emission is short-range nucleon-nucleon collisions for which some kinematically allowed final states are no longer blocked by the Pauli principle. A complete theory of particle emission must provide a unified treatment of both mean-field and two-body processes.

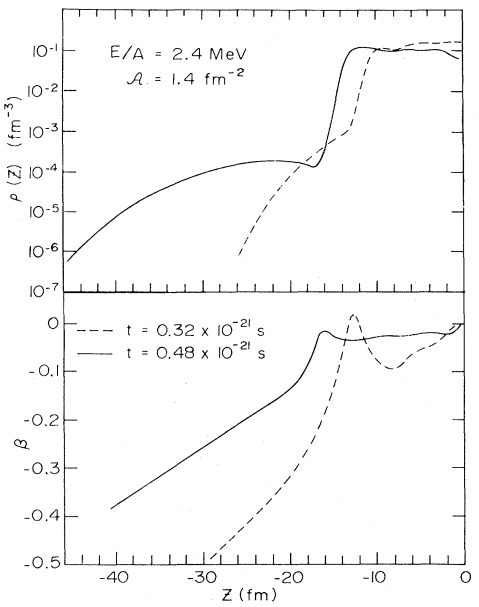

FIG. 35. Density profiles and velocity distributions for separating slabs showing particle emission. In contrast to Figs. 31—33, only the left half-plane is shown for this symmetric collision at a cm energy of 2.4 MeV/A. The velocity is specified by $\beta=v/c$.

6. The Wigner distribution

The Wigner distribution $f(R,p)$ defined in Eq. (3.21), is particularly easy to visualize in slab geometry and has been calculated by Köhler and Flocard (1979). As discussed in Sec. III.A.2, this distribution function possesses most of the features of the familiar classical distribution function with the exception that it is not positive definite. Whereas the general Wigner function in three dimensions is a complicated function of six variables possessing very large, often negative, fluctuations about its average semiclassical value, the average of $f(\mathbf{R},\mathbf{p})$ over the perpendicular momentum components has relatively smooth behavior and provides additional insight into the dynamics of slab collisions.

Using the interaction specified by Eq. (6.56), Köhler and Flocard consider the collision of a finite slab projectile with a stationary infinite slab, with the results for a collision of projectile energy $E/A=2$ MeV shown in Figs. 36 and 37. Note that this is a somewhat lower incident energy than the collision depicted in Fig. 33, since the 1.5 meV A^{-1} cm energy for a symmetric collision corresponds to a lab energy of 6 MeV A^{-1}. Figure 36 displays the total density at a sequence of times, as well as the contribution to the density arising from the projectile orbitals. Figure 37 presents the Wigner function integrated with respect to the transverse components of the momentum

$$F(z,k_z)=\int dk_x dk_y f(\mathbf{x},\mathbf{k})$$
$$=\frac{1}{4\pi^2}\int_0^{k_f} 2m(\varepsilon_F-\varepsilon_k)\phi_k\left[z+\frac{s}{2}\right]\phi_k^*\left[z-\frac{s}{2}\right]$$
$$\times e^{ik_z s}ds\,dk_z\,, \tag{6.64}$$

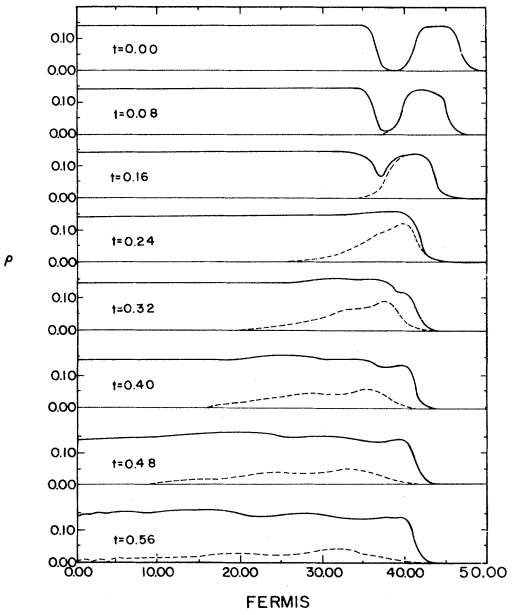

FIG. 36. Density profiles $\rho(z,t)$ at sequential times t, specified in units of 10^{-21} s. The energy of the incident slab is 2 MeV/A and the density is plotted in units of fm^{-3}. The solid lines denote the total density and the dashed lines indicate the density arising from orbitals originating in the right-hand slab.

where k, replacing n in Eq. (6.61), denotes either a continuum state in the infinite slab or a discrete state in the finite slab and f is independent of y and z by translation invariance. The analogous function F in a Fermi gas would be a parabola proportional to $k_F^2-k_z^2$ extending from $-k_F$ to k_F.

As seen in Fig. 37, prior to the collision the target and projectile distributions correspond closely to the parabol-

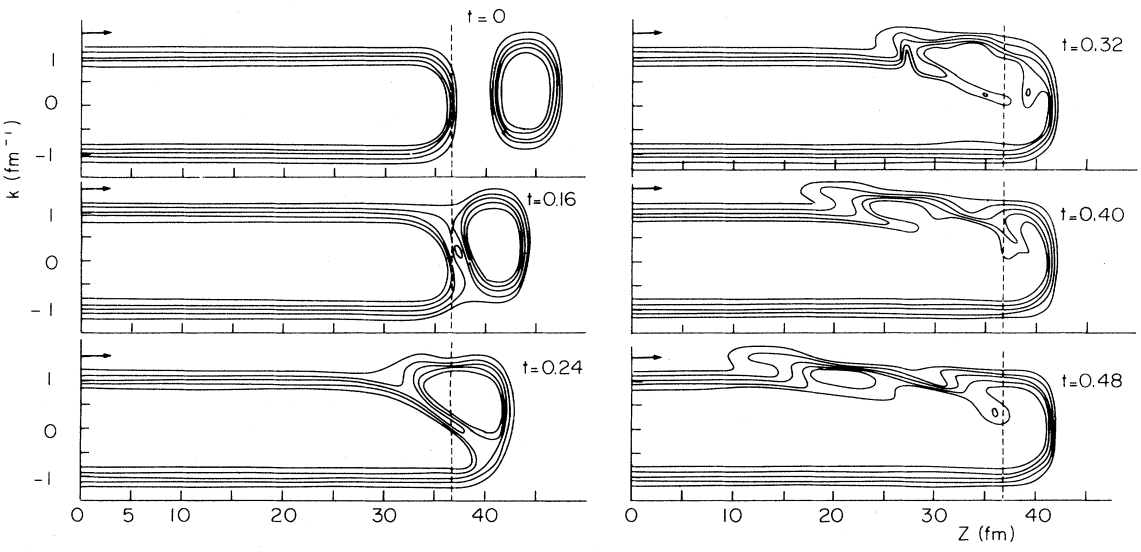

FIG. 37. The Wigner distribution integrated with respect to transverse momentum $F(z,k_z)$, defined in Eq. (6.63), for the collision shown in Fig. 36. Contours of the distributions are plotted at 20, 30, 40, 50, and 60% of the maximum phase-space density. Note that the ordinate k is the negative of k_z, so that the slab displaced to positive values of k propagates in the negative z direction. The arrow denotes the maximum momentum present in a Fermi gas boosted to an energy of 2 MeV/A.

ic momentum distribution expected from a Fermi gas, with minor modifications induced by the spatial surfaces. As the slabs merge, producing a single essentially uniform potential well, particles at the interface in phase space travel at momenta ranging from $-k_F$ to $+k_F$, so that the inclination of the interface increases with time. When orbitals reflect from the right-hand side, the momentum component in the Wigner function reverses sign, giving rise to a counterclockwise flow up the right-hand side of Fig. 37 and back to the left across the top. The flow in phase space across the top also shows very clearly the behavior discussed in the preceding section, whereby that portion of the momentum distribution of the projectile which is displaced beyond the Fermi surface of the target simply propagates through the system and is eventually emitted from the other side. The behavior of two interpenetrating Fermi gases, which is discussed in detail by Bertsch (1978a) thus explains the qualitative dynamics within the single well of the compound system.

The detailed shape of the Wigner function is complicated and cannot be understood solely in terms of the Fermi gas model. The irregularities in shape reflect single-particle effects, or, equivalently, the nonlocal condition $\rho^2=\rho$. By virtue of the complicated structure of the Wigner function as a function of k at fixed z, it is evident that at the stages of the reaction shown in the figure, the system is far from thermal equilibrium. Even at later times, and in collisions of finite slabs in which significant reflections have occurred from the edges of the potential well, plots of the one-body density matrix, equivalent to the Fourier transform of the Wigner distribution, indicate that the system remains far from thermal equilibrium (Bonche, Koonin, and Negele, 1976).

The TDHF results for the Wigner function have been compared with analogous mean-field evolution via the Vlasov equation, Eq. (3.25), by Tang (1981). Whereas the qualitative behavior expected from Fermi-gas arguments is well reproduced, the TDHF and Vlasov results differ in quantitative detail. Ironically, for the sizes of systems relevant to nuclei, numerical integration of the Vlasov equation is technically more difficult and more expensive than solution of the TDHF equations, so it is presently not clear if the Vlasov equation will be of practical value.

In summary, because of the weak coupling between longitudinal and transverse degrees of freedom in mean-field dynamics, collisions of semi-infinite slabs display the essential phenomena of the theory in a particularly clear and unencumbered form. The strong dissipation, leading to either deeply inelastic scattering or fusion, the emission of particles in the forward direction, and the lack of longitudinal equilibrium exhibited in the slab collisions of this section are salient features of the more realistic calculations presented in the final section.

VII. APPLICATION TO PHYSICAL SYSTEMS

The cumulative evidence from previous sections suggests that the time-dependent mean-field approximation is a viable starting point for a systematic theory of nuclear dynamics. In addition to the formal arguments, the success of the mean-field approximation for stationary states and the degree to which slab collisions reproduce the salient features of heavy-ion reaction phenomenology strongly motivate the application of the general time-dependent mean-field theory to finite nuclei.

A. Approximations

Application of even the lowest-order mean-field approximation to all but the lightest nuclei presents a computational problem of formidable proportions, requiring the solution of coupled integrodifferential equations for complex single-particle functions of four continuous variables for each particle. Reduction of the mean-field theory to manageable proportions therefore requires the introduction of additional approximations. As discussed in Sec. II.B.2, one crucial simplification is utilization of an appropriate effective interaction.

In addition, it is essential to drastically reduce the number of degrees of freedom in the full TDHF problem such that the essential dynamics is contained in those degrees of freedom which have been retained. The primary means of reducing degrees of freedom is to utilize symmetries which are exactly maintained by the mean-field equations or to impose constraints on the form of the single-particle wave functions. With practical restrictions on the form of the effective interaction and wave functions, special cases may require the use of the filling approximation to deal with partially filled shells and time-dependent pairing to change the occupation numbers when single-particle level crossings occur.

Finally, even after the number of spatial and spin-isospin degrees of freedom has been reduced as much as possible, it is still necessary to replace the infinite number of degrees of freedom associated with continuous space-time variables by a finite number of discrete variables. It is argued below that this reduction is best accomplished by utilizing a discrete lattice in space-time, and the salient aspects of evolution of the resulting discrete finite-difference equations are briefly reviewed. A more detailed discussion of many of these approximations may be found in lectures by Koonin (1979) and Negele (1978b).

1. Effective interaction

As shown in Sec. II.B, the essential physics of a realistic G matrix with phenomenological adjustment to obtain proper saturation and binding energy is contained in a Hamiltonian density of the form Eq. (2.14b), specified either by the DME functional or a phenomenological Skyrme force. The form of interaction utilized most commonly in time-dependent mean-field calculations is a slightly modified version of the Skyrme Hamiltonian density (Hoodbhoy and Negele, 1977; Negele *et al.*, 1978). In addition to zero-range density-independent and

density-dependent terms, which may be interpreted as a linearized density expansion around the saturation density, the Skyrme force contains two types of momentum-dependent terms which may be interpreted as the leading terms in a gradient expansion of a finite-range interaction. The first term, involving the Galilean-invariant combination $(\rho_q\tau_q - J_q^2)$ arises from the nonlocality of the Hartree-Fock potential and is retained in its original form. Here τ_q denotes the kinetic energy density Eq. (2.12b) for neutrons or protons, J is the current density

$$J(R)=\sum_\nu \mathrm{Im}[\psi_\nu^*(R)\nabla\psi_\nu(R)] , \tag{7.1}$$

which vanishes in the ground state but contributes in a general time-dependent state, and the isospin label q distinguishes protons and neutrons. The second momentum-dependent term in the Skyrme force involves gradients of the density and essentially arises from truncating a Taylor-series expansion of the convolution of the density with a finite-range two-body force. From both physical and numerical considerations, it is preferable to replace it by convolution with a finite-range force, with a Yukawa potential being technically convenient. Thus the effective Hamiltonian density utilized in time-dependent mean-field calculations has the following form:

$$\begin{aligned} H=\int H(r)d^3r=\int d^3r\Bigg[&\frac{\hbar^2}{2m}(\tau_n+\tau_p)+\frac{t_0}{2}\left[(2+x_0)\rho_n\rho_p+\frac{(1-x_0)}{2}(\rho_n^2+\rho_p^2)\right] \\ &+\frac{t_1+t_2}{4}[(\rho_n+\rho_p)(\tau_n+\tau_p)-(J_n+J_p)^2] \\ &+\frac{t_2-t_1}{8}(\rho_n\tau_n-J_n^2+\rho_p\tau_p-J_p^2)+\frac{t_3}{4}(\rho_n\rho_p^2+\rho_p\rho_n^2)\Bigg] \\ &+\frac{v_L}{2}[E_y(\rho_n,\rho_n)+E_y(\rho_p,\rho_p)]+v_U E_y(\rho_n,\rho_p)+\frac{e^2}{2}\int\int d^3r\,d^3r'\frac{\rho_p(\mathbf{r})\rho_p(\mathbf{r}')}{|\mathbf{r}-\mathbf{r}'|} , \end{aligned} \tag{7.2}$$

where the Yukawa contribution is defined

$$E_y(\rho_q,\rho_{q'})=\int\int d^3r\,d^3r'\frac{e^{-\mu|r-r'|}}{\mu|r-r'|}\rho_q(r)\rho_{q'}(r') \tag{7.3}$$

and the labels p and n denote summation over only proton or neutron orbitals, respectively. Although second- and higher-order effects of the tensor force are implicitly included in the central effective interaction, no explicit tensor or spin-orbit interaction is included.

One linear combination of the five phenomenological Skyrme parameters (Vautherin and Brink, 1972) is undetermined by the volume energy, surface energy, symmetry energy, and saturation density (as reflected in charge radii). The undetermined combination, determining the relative importance of momentum dependence and density dependence in producing saturation, is conveniently specified by the effective mass m^*/m, which ranges from roughly 0.3 to 1 for the most commonly used Skyrme forces. Since microscopic nuclear matter calculations indicate that m^*/m is on the order of 0.6 to 0.7, the most physical Skyrme forces are interactions II and III, with $m^*/m=0.58$ and 0.76, respectively. In addition, as noted in Sec. II.B.2, they agree closely with the DME functional.

Several sets of parameters defining the Hamiltonian density, Eq. (7.2), are specified in Table II. The nonlocal interaction SK II is straightforwardly derived from the Skyrme II interaction with $m^*/m=0.58$ (Hoodbhoy and Negele, 1977). This has become the standard nonlocal interaction appropriate for spin-saturated systems with unequal numbers of neutrons and protons and has been used by Bonche *et al.* (1979), Davies (1979), Davies and Koonin (1981), Davies, Maruhn-Rezwani *et al.* (1978), Davies, Sandhya Devi, and Strayer (1979, 1980, 1981a, 1981b), Dhar (1979), Dhar and Nilsson (1978, and 1979), Dhar *et al.* (1981), Krieger and Davies (1978), Krieger and Weiss (1981), Negele *et al.* (1978), Sandhya Devi, Dhar, and Strayer (1981), Sandhya Devi, Strayer, Davies, Koonin, and Dhar (1981), and Sandhya Devi, Strayer, Irvine, and Davies (1981). To bracket the physical range of effective mass, the parameters of the interaction SK III, derived from the Skyrme III force with $m^*/m=0.76$, are also tabulated in Table II.

In addition to these two realistic interactions, the parameters of two simplified interactions utilized in the earliest TDHF calculations are also recorded in Table II. A purely local interaction, with $m^*/m=1$, yields significant simplifications by eliminating the current terms in Eq. (7.2) and decoupling the transverse wave functions for semi-infinite slabs. This case reduces to the interaction Eq. (6.56) used for the original slab calculations, and its parameters are tabulated in the column marked *local* in Table II. This force, which contains no isospin dependence, was derived only for $N=Z$ mirror nuclei and has been used in calculations of light nuclei by Bonche, Grammaticos, and Koonin (1978), Cusson *et al.* (1981), Cusson, Maruhn, Stöcker (1980), Cusson and Meldner (1979), Davies, Feldmeier *et al.* (1978), Flocard, Koonin, and Weiss (1978), Koonin, Davies *et al.* (1977), Koonin, Flanders *et al.* (1978), Krieger and Davies (1979), Maruhn-Rezwani, Davies, and Koonin (1977), and Weiss (1977). Finally, an additional technical sim-

plification utilized in early calculations was to replace the finite-range local interaction by a zero-range interaction, with the parameters tabulated under the heading zero-range in Table II. It was used in early work by Koonin (1976), Cusson, Smith, and Maruhn (1976), and Cusson, Maruhn, and Meldner (1978), and as pointed out by Bonche, Grammaticos, and Koonin (1978) has an unphysically small surface energy and correspondingly sharp surface, giving rise to unrealistically low fusion cross sections.

2. Symmetries

One general technique for significantly reducing the number of dynamical degrees of freedom is specification of an initial wave function possessing symmetries which also occur in the mean field. The time-dependent mean-field equations automatically preserve any such symmetries in time. Thus it is possible to select targets, projectiles, and initial conditions which preserve reflection, inversion, spin, and axial symmetry under evolution in the mean field. Such solutions are very special. Not only are they especially cheap to calculate, because they evolve in a limited space, but for the same reason they also have less freedom for randomization and thus dissipation and equilibration. The essential fact to bear in mind is that in considering a realistic ensemble of initial conditions, these special symmetric cases receive negligible weight and one must be alert to the possible unrealistic consequences of such symmetries.

A few computational results suggest that symmetric initial conditions are not misleading. For example, three-dimensional calculations of head-on collisions do not differ qualitatively from those at small but finite impact parameters. Similarly, the qualitative behavior of collisions with identical target and projectile is the same as for asymmetric collisions.

3. Reduction of degrees of freedom by constraints

In addition to utilizing symmetries to reduce the number of degrees of freedom, it is also possible to impose simplifying constraints on the wave function. In the case of symmetries, the evolution of the wave function is governed by the exact mean-field equations, and the physical approximation lies in interpreting the result as being representative of more general initial conditions. In contrast, imposition of a constraint yields new dynamical equations which are physically distinct from the original mean-field equations.

A simple example is to constrain the spatial wave functions for neutrons and protons to be identical for $N=Z$ nuclei. With this isospin constraint and the spin-independent interaction Eq. (7.2), a single spatial wave function represents four nucleons, protons, and neutrons with either spin projection; and the original mean-field for protons and neutrons has been replaced by that for particles with effective charge $\frac{1}{2}$. Given that the Coulomb interaction is much weaker than the strong interaction, this approximation is physically reasonable for a variety for applications. Where the total dissipation is of quantitative interest, however, such freezing of the isospin degrees of freedom can cause significant discrepancies. An example is the fusion cross sections discussed subsequently in Fig. 43, for which Krieger and Davies (1978) show that the dissipation, and thus the low-energy cross sections, is significantly reduced by imposition of an isospin constraint.

Whereas an isospin constraint reduces the number of degrees of freedom by a factor of $\frac{1}{2}$, much larger reductions may be achieved by restricting the spatial wave functions to depend upon two, rather than three, spatial coordinates. One useful two-dimensional approximation arises from requiring the mean field to be axially symmetric. This may be accomplished, for example, by constraining the single-particle wave functions to have the form

$$\Phi_\nu = e^{-i\eta L_y} e^{i\chi(r,z,\phi)} \psi_\nu(r,z) e^{im_\nu\phi} , \tag{7.4}$$

where r,z,ϕ are cylindrical coordinates in an intrinsic frame which is rotated an angle η about the y axis relative to the laboratory frame, χ is a coherent velocity field, and m_ν is the orbital angular momentum projection along the symmetry axis. Application of the time-dependent variational principle, Eq. (3.1), with a determinant of wave functions of the form (7.4) yields canonical equations with the Hamiltonian (Feldmeier, 1977; Negele, 1977)

$$H = \mathscr{H}[(\psi_\nu(r,z)e^{im_\nu\phi})^*, \psi_\nu(r,z)e^{im_\nu\phi}] + \frac{L^2}{2\mathscr{I}[\rho,\chi]} , \tag{7.5}$$

where $\mathscr{H}$ is the Hamiltonian, Eq. (3.5), for the axially symmetric wave functions in the intrinsic frame, and the moment of inertia $\mathscr{I}$ is a specified functional of the density and velocity field χ. Physically, the moment of inertia corresponds to irrotational flow, and Eq. (7.5) yields the unconstrained TDHF equations in the two limits of zero and infinite impact parameters. Alternatively, an axially symmetric approximation may be obtained by postulating the Hamiltonian Eq. (7.5) (Koonin, 1976) and adopting a physically motivated prescription for the moment of inertia. For separated ions, $\mathscr{I}$ is taken to be that of two separated point particles

$$\mathscr{I}_{\text{point}} = m\frac{A_1A_2}{A_1+A_2}R^2 , \tag{7.6a}$$

where R denotes the distance between the centers of mass, and when the target and projectile are significantly overlapping, the rigid body moment of inertia is used,

$$\mathscr{I}_{\text{rigid}} = m\,2\pi\int dr\,dz\,(z^2+r^2/2) , \tag{7.6b}$$

The validity of the axial approximation and optimal definition of the moment of inertia have been investigated by Davies *et al.* (1978) by comparison with three-dimensional calculations of $^{16}O+{}^{16}O$ and $^{40}Ca+{}^{40}Ca$

collisions at cm energies of 0.4 and 1.3 MeV per particle above the Coulomb barrier. For impact parameters such that the three-dimensional calculation does not produce fusion, the axially constrained theory with moments of inertia (7.6a) and (7.6b) for separated and overlapping configurations yields an excellent approximation. In contrast, the fusion occurring in the three-dimensional calculations is not reproduced in the axially symmetric approximation, reflecting the fact that restriction to axially symmetric shapes has eliminated shape deformations crucial to the randomization of single-particle motion required for fusion. The irrotational moment of inertia, Eq. (7.5), arising from the assumption of a common velocity field χ for each single-particle wave function, Eq. (7.4), is considerably less accurate than Eqs. (7.6a) and (7.6b) indicating that this ansatz is too restrictive. It remains an open question whether allowing a different χ_ν for each wave function significantly improves the approximation.

For detailed calculations of collisions of heavy nuclei, the axially symmetric approximation is the only computationally viable theory. Based on the comparison with three-dimensional calculations for light nuclei, it is assumed to yield reliable results for nonfusion inelastic scattering events for cm energies of the order of 1 MeV per particle above the Coulomb barrier. Results based on this approximation will be presented subsequently in Figs. 41, 43, 45, and 47–49.

A second constraint to reduce the dynamics to two spatial dimensions is to require that each wave function have the separable form of a component in the reaction plane multiplied by a normal component

$$\psi_\nu(r,t)=\phi_\nu(x,y,t)\chi_\nu(z,t) . \tag{7.7}$$

Head-on axially symmetric calculations and full three-dimensional calculations support the intuitive expectation that very little equilibration occurs out of the reaction plane, since single-particle orbitals with high initial momenta in the reaction plane acquire relatively insignificant transverse momentum components from reflections at the well edge. The ansatz, Eq. (7.7), capitalizes on this lack of equilibrium out of the reaction plane, while allowing maximal freedom for motion in the reaction plane. The randomization arising from multiple reflections in an arbitrarily shaped cavity should be more accurately reproduced by this wave function than by an axially constrained one, thus yielding a more accurate description of dissipation and fusion for large impact parameters.

As in the axially constrained case, one must derive or define equations of motion for wave functions of the form (7.7). The most theoretically appealing method would be to apply the time-dependent variational principle to obtain equations for ϕ_i and χ_i, but for technical reasons this approach has not been implemented. For light nuclei, a natural approximation is suggested by the fact that harmonic oscillator functions are separable and yield reasonable approximations to Hartree-Fock wave functions. Thus, a sensible trial solution is (Sandhya Devi and Strayer, 1978a, 1978b)

$$\psi_i(r,t)=\phi_i(x,y,t)\chi_i^{\mathrm{HO}}(z) , \tag{7.8}$$

where the oscillator size parameter may be determined by minimizing the ground-state energy with the trial function. The equations of motion for ϕ_j using an effective Hamiltonian density which produces a local Hartree-Fock potential are

$$i\dot{\phi}_\nu=\left[-\frac{\hbar^2}{2m}\left(\frac{\partial^2}{\partial x^2}+\frac{\partial^2}{\partial y^2}\right)+\langle T_z\rangle_\nu+W_\nu(x,y)\right]\phi_\nu , \tag{7.9a}$$

where W_ν is related to the full local Hartree-Fock potential by

$$W_\nu(x,y)=\int dz\,|\chi_\nu^{\mathrm{HO}}(z)|^2 W(x,y,z) \tag{7.9b}$$

and

$$\langle T_z\rangle_\nu=\frac{\hbar^2}{2m}\int dz\left|\frac{d\chi_\nu^{\mathrm{HO}}}{dz}\right|^2 . \tag{7.9c}$$

Static and time-dependent separable solutions using Eqs. (7.9) have been compared with three-dimensional results by Koonin *et al.* (1978). For the light, oscillator-like nuclei ^{16}O and ^{40}Ca, the static densities agree reasonably well, especially if one averages the shapes in the z direction and in the x-y plane, and the binding energies and rms radii agree to within 2%. For heavier nuclei, significant discrepancies arise from the fact that oscillator functions do not produce saturating density distributions. In the Thomas-Fermi limit, for example, the density distribution generated by harmonic oscillator functions is given by an inverted parabola raised to the $\frac{3}{2}$ power. It remains an open question whether a fully variational calculation with the general wave function (7.7) is significantly better in heavy nuclei. The agreement between separable wave functions of the form (7.8) and exact three-dimensional calculations for the scattering of $^{40}\mathrm{Ca}+{}^{40}\mathrm{Ca}$ at 278 MeV is striking. In addition to agreement in final scattering angles, final fragment angular momenta and energies agree within 2% at all impact parameters, and the same fusion window from $L=30\hbar$ through $L=80\hbar$ occurs in both calculations.

The separable approximation is thus in many respects complementary to the axially symmetric approximation. In contrast to the axial symmetry constraint, the separable approximation enforces a sharp dichotomy between shape deformations in the reaction plane, which are crucial to the randomization required for fusion, and transverse degrees of freedom, which are frozen out. It yields an accurate approximation for both fusion and inelastic scattering of light nuclei and is used extensively in the calculations summarized subsequently in Figs. 41, 42, 45, and 46. Unlike the axial-symmetry constraint, it is not applicable to nuclei much heavier than the Ca isotopes, and does not yield the exact solution for head-on collisions.

4. Occupation numbers

In the mean-field approximation, open-shell nuclei possess multiply degenerate ground states, so that there is no unique initial condition for TDHF evolution. As a result of omission of the spin-orbit force, even nuclei corresponding to physically closed subshells also suffer from this ambiguity with the effective Hamiltonian density Eq. (7.1). Hence an approximation specifying unique and physically motivated occupation numbers is required for most heavy-ion collisions.

The simplest approximation is the familiar filling approximation, in which valence nucleons are uniformly distributed throughout the partially filled valence shell. The one-body density matrix, Eq. (3.15), is thus replaced by the generalization

$$\rho(x,x')=\sum_i n_i\psi_i^*(x')\psi_i(x) , \tag{7.10}$$

where the time-independent occupation numbers are defined to be $n_i=1$ for filled shells, $n_i=m/2(2l+1)$ for a shell of orbital angular momentum l containing m particles, and $n_i=0$ for unoccupied shells. The resulting mean field is spherically symmetric, eliminating the necessity of integrating over initial configurations corresponding to all relative orientations of deformed target and projectile.

An alternative approach would be to solve time-dependent pairing or time-dependent Hartree-Fock-Bogoliubov equations. Formally, the Hartree-Fock-Bogoliubov theory is quite appealing, having the same form as Eq. (3.20a)

$$i\dot{K}=[M,K] , \tag{7.11}$$

where the augmented matrices are defined by

$$K\equiv\begin{bmatrix}\rho & \chi\\ -\chi^* & 1-\rho^*\end{bmatrix} , \tag{7.12a}$$

$$M\equiv\begin{bmatrix}h-\lambda & u\\ -u^* & -(h-\lambda)^*\end{bmatrix} , \tag{7.12b}$$

$$\chi(r,r')=\langle\psi(r')\psi(r)\rangle , \tag{7.12c}$$

$$u(r,r')=\tfrac{1}{2}\int\int v(r,r';r'',r''')\times\chi(r'',r''')dr''dr'' , \tag{7.12d}$$

ρ and h are defined in Eqs. (3.12) and (3.18), and the chemical potential λ constrains the mean particle number. Although $K^2=K$ as $\rho^2=\rho$, the trace of K is infinite, so, unlike the TDHF case, Eq. (7.11) cannot be solved by evolution of a finite number of eigenfunctions of K. Given the technical difficulties in solving the TDHF equations, it is not surprising that numerical solution of Eq. (7.11) is presently impractical.

A much simpler approximation which retains some of the same physics is obtained by application of the time-dependent variational principle to a BCS wave function with the constraint that the gap remain constant (Błocki and Flocard, 1976). To within a phase factor, the single-particle wave functions evolve according to the TDHF equations. The BCS u's and v's, defined with the convention that u_j is real, are determined by the equations of motion:

$$i\frac{d}{dt}|v_j|^2=\Delta(u_jv_j-u_jv_j^*) \tag{7.13a}$$

and

$$i\frac{d}{dt}(u_jv_j)=2u_jv_j(\varepsilon_j-\lambda)+\Delta(2|v_j|^2-1) , \tag{7.13b}$$

where

$$\varepsilon_j=\int\phi_j^*h\phi_j , \tag{7.13c}$$

the Lagrange multiplier λ is defined to conserve particle number

$$\lambda=\frac{\left[N\Delta+\sum_{j>0}[\varepsilon_j(u_jv_j+u_jv_j^*)-\Delta]\right]}{\sum_{j>0}(u_jv_j+u_jv_j^*)} , \tag{7.13d}$$

and the occupation probabilities in the density matrix, Eq. (7.10), defining the mean field, are given by $n_j=|v_j|^2$.

Since no matrix elements of an effective interaction are evaluated with the constant gap constraint, Eqs. (7.13) involve negligible computational effect. This approximation is commensurate with other approximations made in obtaining the phenomenological effective interaction, since the gross features are correctly reproduced by using the experimental value of Δ. The time-dependent occupation probabilities specified in this approximation are qualitatively important when a constraint or symmetry would otherwise prevent mixing between two single-particle levels which cross during the shape deformation of the mean field, and a specific example is discussed below in the case of induced fission. Time-dependent mean-field calculations with BCS occupation probabilities have been reported by Cusson *et al.* (1981), Cusson, Maruhn, and Stöcker (1980), Cusson and Meldner, (1979); and Negele *et al.* (1978). The other calculations involving open-shell nuclei have utilized the filling approximation.

5. Discretization and evolution approximations

The continuous space-time variables in the TDHF initial-value equations, Eq. (3.7), or in the periodic self-consistent equations for nuclear eigenstates, Eq. (5.75), and spontaneous fission, Eq. (5.134), must be approximated by a finite number of degrees of freedom. The two most obvious techniques are truncation of an expansion in a complete set of functions and utilization of a discrete mesh in space and time.

Experience in static Hartree-Fock calculations indicates that coordinate space calculations, which either

directly or implicitly through a numerical integration algorithm assume that wave functions are defined on a discrete mesh, are superior to expansion in a set of basic functions, such as harmonic oscillator functions. Since shape degrees of freedom are essential, it is crucial that truncation or discretization errors be shape independent. In the case of deformed nuclei, the accuracy of an expansion in oscillator functions is highly shape dependent, so that even gross qualitative features of the results may be contaminated by basis constraints. Even a 14-oscillator shell basis, for example, is barely adequate for heavy deformed nuclei (Negele and Rinker, 1977) and is quite unreliable for calculation of fission barriers. The fact that there are no realistic analytically solvable models necessarily implies that in general there is no optimal basis for truncated expansions. In contrast, the equivalence of all points on a uniform spatial mesh essentially eliminates shape dependence in coordinate-space calculations. Furthermore, the fact that the maximum rate of spatial variation in all low-energy processes is specified by the Fermi wavelength provides a scale such that discretization errors may be absolutely controlled. Hence, except for some early exploratory calculations (Cusson and Maruhn, 1976; Maruhn and Cusson, 1976), TDHF calculations presently utilize a discrete mesh.

In formulating a mean-field theory on a mesh in coordinate space, it is extremely useful to replace the spatial integrals in the action, Eq. (3.1), which is a functional of A single-particle wave functions, by discrete sums with suitable weights yielding an approximate discretized action which is a function of the values of each of the single-particle wave functions on each of the mesh points. In the limit of small mesh spacing, of course, the discretized action approaches the true action. However, for any finite mesh spacing, variation of the discretized action yields a well-defined set of differential equations in time and difference equations in spatial mesh labels which approximate the TDHF equations. Such a discretized functional yields exact conservation of discrete approximations to the energy, momentum, and angular momentum, eliminates various consistency difficulties which arise in discretizing the TDHF equations directly, guarantees Hermitian approximations to the single-particle Hamiltonian, and provides a convenient conceptual framework for thinking about the structure of the resulting equations.

The simplest example of discretization of the kinetic energy is the approximation for each Cartesian coordinate:

$$\int dx\, \psi^*(x)\left[-\frac{d^2}{dx^2}\right]\psi(x)\approx\frac{1}{\Delta x}\sum_i |\,\psi(x_{i+1})-\psi(x_i)\,|^2 . \tag{7.14}$$

Variation of this expression yields the standard three-point difference formula for the kinetic energy operator in the single-particle equation. Generalization of Eq. (7.14) to contain ψ's at three adjacent mesh points with appropriate coefficients (Flocard, Koonin, and Weiss, 1978) yields the corresponding five-point formula. The accuracy of the three- and five-point formulas is indicated by the fractional errors they yield for the kinetic energy of nuclear matter of $\frac{1}{28}(k_F\Delta x)^2$ and $\frac{1}{378}(k_F\Delta x)^4$, respectively, corresponding to underestimates of the kinetic energy on a 1-fm mesh of 6.2% and 0.8%, respectively. Because of the ease of dealing with sparse matrices, for a given accuracy it is most efficient in Cartesian coordinates to utilize the five-point formula with correspondingly fewer mesh points. Discretization in cylindrical coordinates is discussed by Davies and Koonin (1981), Koonin *et al.* (1977), and Hoodbhoy and Negele (1977), who present explicit evaluation of correction terms and comparison with exact Hartree-Fock results.

For the periodic boundary value problems, Eq. (5.75) and Eq. (5.134), in which space and time enter equivalently, it is obvious that time derivatives should be treated analogously to spatial derivatives. The approximation of the time derivative in the action analogous to Eq. (7.14) is

$$\int dt\, \psi^*(t) i\frac{\partial}{\partial t}\psi(t)\approx\sum_j\frac{i}{2}[\psi^*(t_{j+1})+\psi^*(t_j)] \times[\psi(t_{j+1})-\psi(t_j)] , \tag{7.15}$$

and its variation yields the three-point formula for the first derivative with respect to time in the single-particle equation. An analogous five-point formula may be straightforwardly derived and is utilized in the calculations reviewed in Sec. VII.F below.

In contrast to the periodic boundary value problem, space and time play dissimilar roles in the TDHF initial-value problem, Eq. (3.7), and are thus treated inequivalently. Instead of varying an expression for the action discretized in time to obtain finite difference equations, evolution from time t_n to t_{n+1} is accomplished by a unitary approximation to the evolution operator

$$\psi_i^{(n+1)}=U_{ij}\psi_j^{(n)} , \tag{7.16}$$

where (n) denotes the time and the indices i and j label discrete spatial coordinates. Denoting the discretized single-particle Hamiltonian at an appropriate intermediate time by h, the basic approximations for the evolution operator are of the form

$$u\approx e^{-ih\Delta t/\hbar} \tag{7.17a}$$

or

$$u\approx\frac{1-\frac{ih\Delta t}{2\hbar}}{1+\frac{ih\Delta t}{2\hbar}} . \tag{7.17b}$$

Three-dimensional Cartesian calculations utilize a series expansion of (7.17a) (Flocard, Koonin, and Weiss, 1978), whereas axially symmetric calculations use the Peaceman Rachford or local one-dimensional variations of Eq. (7.17b) (Davies and Koonin, 1981). The practical-

ity of both these procedures hinges crucially on the fact that only multiplication of sparse matrices or inversion of tridiagonal matrices is required. Energy conservation, which is automatic for variation of an action discretized in space and continuous in time, can also be maintained for evolution by the approximations, Eq. (7.17), if the terms in h arising from two-and three-body forces are expressed in terms of specific combinations of $\rho^{(n+1)}$ and $\rho^{(n)}$ (Flocard, Koonin, and Weiss, 1978).

Typical three-dimensional calculations involve the order of 15 000 spatial mesh points with a mesh spacing $\Delta x \sim 1$ fm, and axially symmetric calculations utilize an order of magnitude fewer mesh points with $\Delta x \sim 0.5$ fm. Wave functions are typically evolved several hundred time steps of magnitude $\sim 5 \times 10^{-24}$ S. Energy conservation and orthonormalization of single-particle wave functions are typically enforced to fractions of a percent. Studies of numerical accuracy with smaller spatial and time intervals and tests such as comparison of axial and three-dimensional calculations of head-on collisions confirm the reliability of the discretization and evolution approximations described in this subsection and ensure that the results reviewed in the remainder of this section reflect mean-field dynamics and not spurious numerical effects. An alternative technology utilizing fast Fourier transform and predictor corrector algorithms is described by Cusson, Maruhn, and Meldner (1978).

B. Qualitative features

Many qualitative features of the mean-field dynamics of heavy-ion collisions may be seen in contour plots of the density distribution in the reaction plane integrated with respect to the normal to the reaction plane. The essential features at sequential times are clearly displayed in the single case of the $^{16}O + {}^{40}Ca$ collisions shown in Figs. 38–40 for three initial angular momenta (Weiss, 1977). Similar plots for many other reactions in the low-energy regime may be found in the literature including $^{4}He + {}^{40}Ca$ (Weiss, 1977), $^{16}O + {}^{16}O$ (Cusson, Smith, and Maruhn, 1976; Cusson, Maruhn, and Meldner, 1978; Flocard, Koonin and Weiss, 1978), $^{40}Ca + {}^{40}Ca$ (Bonche, Grammaticos, and Koonin, 1978), $^{86}Kr + {}^{139}La$ and $^{84}Kr + {}^{209}Bi$ (Davies, 1979; Davies, Sandhya Devi, Strayer, 1981) and $^{136}Xe + {}^{209}Bi$ (Dhar *et al.*, 1981).

Figure 38 displays the unrestricted three-dimensional evolution of a nearly central collision. The laboratory energy of 316 MeV corresponds to a cm energy per particle above the Coulomb barrier of roughly 3.6 MeV, so that on the basis of slab dynamics the projectile is expected to pass through the target. As seen in the figure, in which the ^{16}O nucleus approaches from the upper right-hand corner, this expectation is borne out. Although the rate of separation of the fragments is much slower than the initial approach indicating significant longitudinal equilibration, there is little indication of excitation of transverse modes; supporting the assertion that the mean field does not induce significant excitations perpendicular to the reaction plane. The predominant excitation is observed to be an axially symmetric octupole oscillation. The approximate axial symmetry of the density suggests that head-on collisions are in fact reasonably representative of general collisions at small but finite impact parameters.

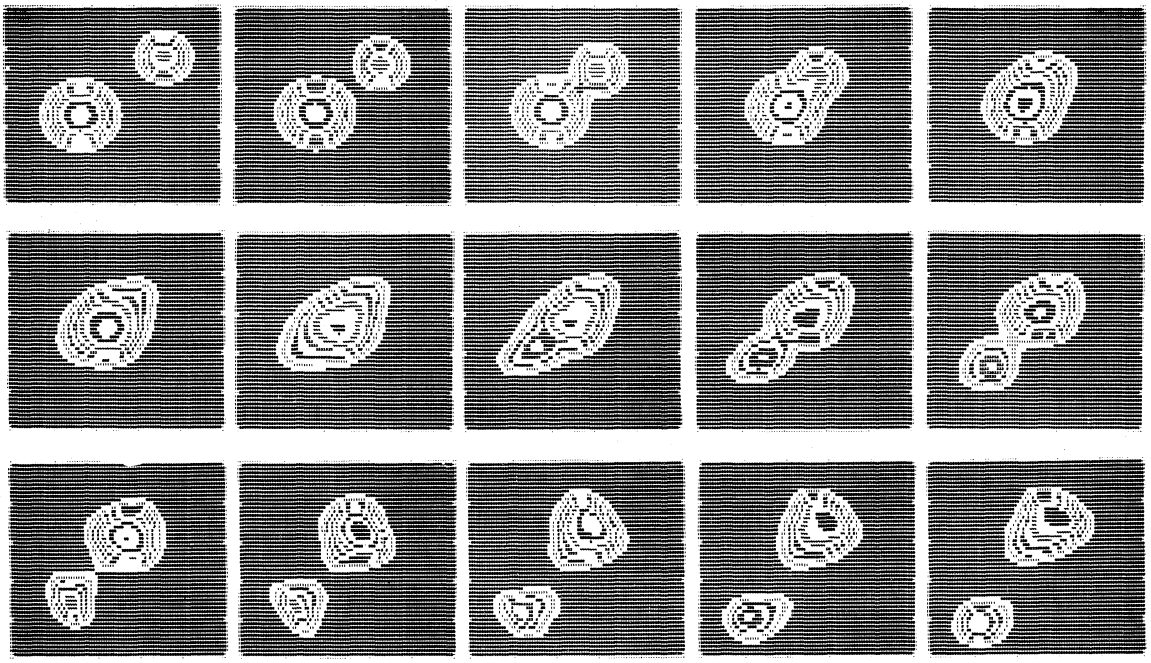

FIG. 38. Contour plots at sequential times of the density in the cm integrated over the normal to the reaction plane for $^{16}O + {}^{40}Ca$ collision at a laboratory energy of 315 MeV. The initial angular momentum $l = 20\hbar$ corresponds to a nearly head-on collision.

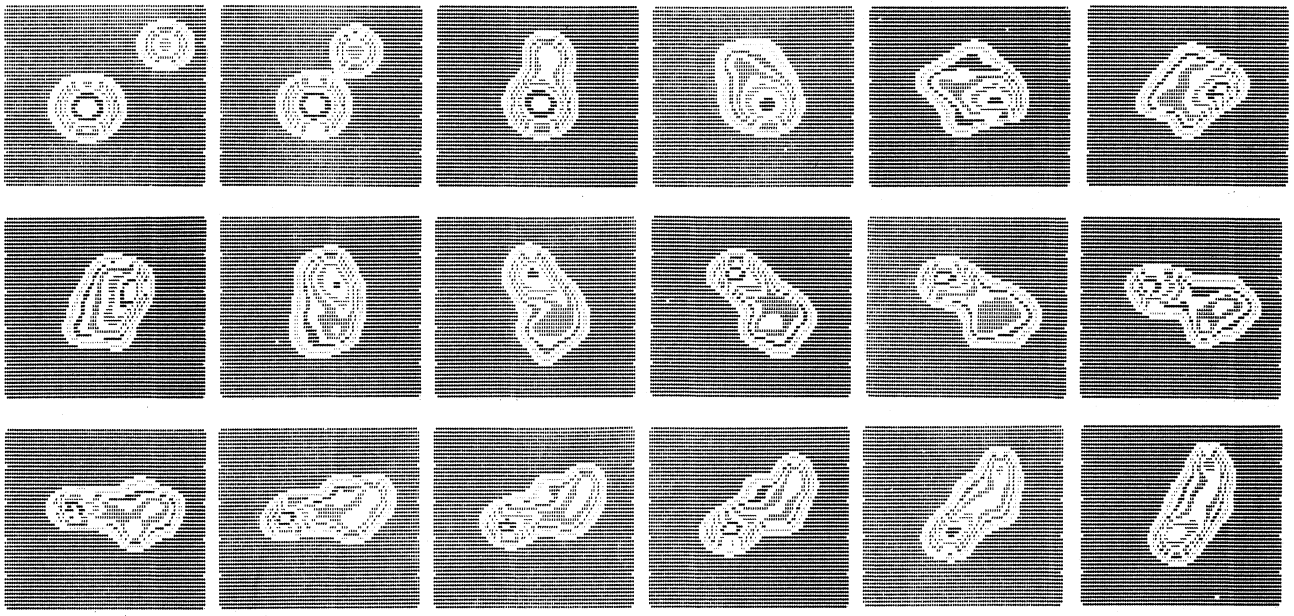

FIG. 39. Contour plots for the same reaction as in Fig. 38 with an initial angular momentum of $l=60\hbar$.

Evolution of a collision with higher angular momentum, $l=60\hbar$, leading to fusion is shown in Fig. 39. Here the projectile moves to the left with a much smaller downward velocity component and is captured by the target leading to a tumbling compound nucleus analogous to the compound slabs in slab fusion events. From the complicated sequence of shapes, it is evident that the randomization of single-particle wave functions reflected from the well edges plays a significant role in dissipating the original collective translational energy. Whereas it is clear that most of the intermediate shapes could be approximated qualitatively by axially symmetric configurations, the axial approximation would yield quantitative inaccuracy at energies of several MeV A^{-1}.

Finally, Fig. 40 shows a peripheral collision with $l=80\hbar$, in which the projectile moving to the left with a

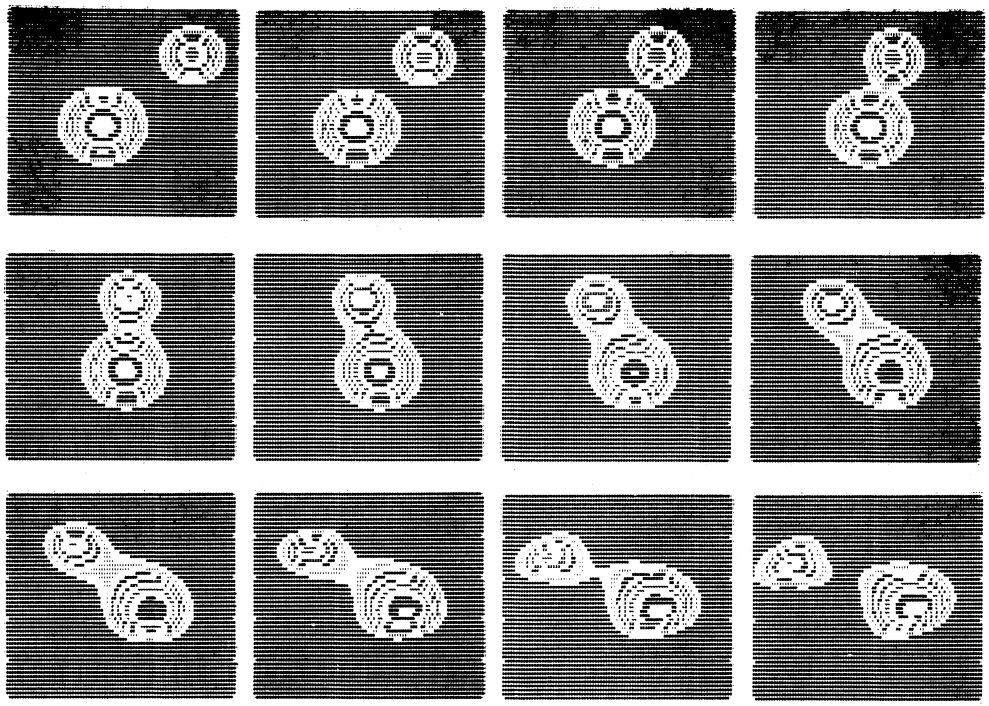

FIG. 40. Contour plots for the same reaction as in Fig. 38 with an initial angular momentum of $l=80\hbar$.

negligible downward velocity component grazes the surface of the target and separates, having undergone significant dissipation. The shapes in this case are much more axially symmetric, consistent with the fact that the axial constraint yields an adequate description of inelastic scattering even when it is inadequate for fusion.

After we have seen the salient features of forward transmission, fusion, and deep-inelastic scattering for three impact parameters in a single nucleus, it is useful to consider the systematic behavior for all impact parameters and a range of target and projectile masses. Several gross features of systematics are evident from the deflection functions, specifying the center of mass scattering angle, θ_{cm}, as a function of initial angular momentum l presented in Fig. 41. This figure summarizes results of three-dimensional calculations of $^{16}O+{}^{16}O$ (Flocard, Koonin and Weiss, 1978) and $^{40}Ca+{}^{40}Ca$ (Weiss, 1977); separable calculations of $^{16}O+{}^{93}Nb$ (Sandhya Devi *et al.*, 1981); and axially constrained calculations of $^{86}Kr+{}^{139}La$ (Davies, Sandhya Devi, and Strayer, 1979), $^{89}Kr+{}^{209}Bi$ (Davies *et al.*, 1978), and $^{136}Xe+{}^{209}Bi$ (Dhar *et al.*, 1981). Similar calculations, not included in the figure, have been performed for the sytems $^{28}Si+{}^{28}Si$ (Bonche *et al.*, 1979), $^{40}Ar+{}^{58}Ni$ (Koonin, 1979), and $^{84}Kr+{}^{208}Pb$ (Davies *et al.*, 1978). The cm energy per particle, calculated relative to Coulomb energies defined at quarter-point radii tabulated by Huizenga (1975) range from 0.35 to 1.28 for the system shown in Fig. 41 with the axially symmetric calculations being restricted to the lowest energies to maximize their accuracy.

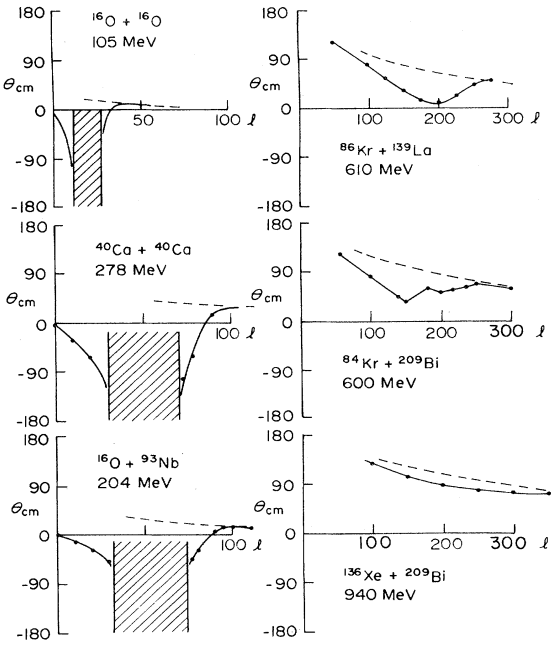

FIG. 41. Deflection functions (solid lines) specifying the TDHF scattering angle in the cm, θ_{cm}, as a function of initial angular momentum l specified in units of $\hbar$. The projectile lab energies are specified for each reaction, and correspond to cm energies per particle above the Coulomb barrier of 1.28, 1.07, 1.19. 0.70, 0.41, and 0.35 MeV for the lightest through heaviest systems, respectively. The dashed curves denote pure Coulomb deflection functions, the shaded areas denote fusion regions, and the solid points indicate results for individual TDHF calculations. Note that for the two symmetric collisions, the scattering angle is defined modulo 180°, and the unconventional choice of 0° at $l=0$ has been made to correspond to the projectile passing through the target as observed in asymmetric collisions.

The deflection functions in Fig. 41 display several semiclassical features common to classical phenomenological models of heavy-ion collisions. Collisions at large impact parameters are dominated by the Coulomb interaction, and the deflection function thus approaches that of pure Coulomb scattering at large l. In light nuclei, as the impact parameter decreases, the nuclear attraction overcomes the Coulomb repulsion, shifting the deflection from positive to negative angles. Still further reduction of the impact parameter yields fusion, indicated by the shaded region for which no scattering angle is defined. As the charges of the target and projectile increase, the relative importance of the Coulomb interaction increases. For the $^{86}Kr+{}^{139}La$ system, the Coulomb repulsion is sufficiently strong that the nuclear potential no longer results in negative scattering angles. The difference between the TDHF and Coulomb deflection functions continues to decrease smoothly with increasing charge until for the heaviest system, $^{136}Xe+{}^{209}Bi$, the mean-field result is qualitatively quite similar to that for pure Coulomb scattering. The absence of fusion for the three heaviest systems results from the low energies of $0.3-0.4$ MeV A^{-1}, and is discussed in Sec. VII.C below.

In addition to these semiclassical aspects, the deflection functions in Fig. 41 also display several features unique to mean-field theory. As already seen in Fig. 38, for sufficiently small impact parameters at high enough energies, the projectile does not dissipate all its translational energy and passes through the target. In addition to $^{16}O+{}^{40}Ca$, this transmission window is observed in $^{16}O+{}^{93}Nb$ for angular momenta below $30\hbar$. Similar behavior is also observed in $^{16}O+{}^{16}O$ and $^{40}Ca+{}^{40}Ca$, although because of the identity of target and projectile one cannot distinguish between forward and backward scattering, and the deflection function is only defined modulo 180°. A second feature is that single-particle effects can introduce fluctuations, as seen, for example, in the $^{84}Kr+{}^{209}Bi$ deflection function near $l\sim 175\hbar$ or in the sensitivity of the fusion region to small changes in incident energy.

A final qualitative feature of mean-field dynamics is particle emission. As discussed in Sec. VI.D5 and shown in Fig. 35, high-momentum components of single-particle wave functions propagating through the well emerge in the forward direction. Just as these low-amplitude components were not visible on linear plots of slab collisions, Figs. 31–33, they are also not apparent in Figs. 38–40. Recent separable calculations of $^{16}O+{}^{93}Nb$ with sufficient attention to numerical accuracy (Sandhya Devi *et al.*, 1981) display the same particle emission seen in slab collisions and expected from Fermi

gas estimates. In this work, contour plots are generated of the neutron density in the range between 1% and 10%. For a head-on collision, as the oxygenlike fragment emerges in the forward direction, a low-density component of high-momentum neutrons is seen to propagate beyond the front of the fragment well and escape in the forward direction as in Fig. 35. Since in such an asymmetric collision it is meaningless to consider ^{93}Nb propagating through an ^{16}O nucleus, the present considerations apply only in the forward direction of the smaller nucleus propagating through the larger or for nearly symmetric collisions. To the degree to which the axial approximation applies, at finite angular momentum one would expect high-momentum components to be emitted in the forward direction in the rotating frame and with a probability which decreases with increasing angular momentum reflecting the decreased component of relative velocity along the symmetry axis. This expectation is well borne out in the separable calculations, which do not enforce such symmetry in the reaction plane. Fermi gas estimates using the criterion Eq. (6.63) in the rest frame of the ^{93}Nb target agree semiquantitatively with the actual mean-field results for both the emission probability and angle as a function of angular momentum, although numerical uncertainties in evaluating the velocity of the emitted components preclude quantitative velocity comparison. In spite of the ambiguities of interpreting properties of final states in the TDHF initial-value problem and the fact that particle emission from collision processes is ignored, it is interesting that the mean-field prediction for the neutron multiplicity in coincidence with deep-inelastic final states of 0.19 is consistent with the experimental result of 0.15 ± 0.5 (Gavron *et al.*, 1982). Calculations of forward emission have also been performed for collisions of ^{4}He, ^{12}C and ^{197}Au projectiles on ^{12}C and ^{197}Au targets (Stöcker *et al.*, 1981). Although strong forward emission is observed, at the much higher energies in this work, ranging from laboratory energies per projectile particle of $30-85$ MeV A^{-1}, physical interpretation becomes much more difficult. The validity of the mean-field approximation is highly suspect at these energies, and even within the mean-field framework it is difficult to define the frame in which to apply the criterion, Eq. (6.63).

A second aspect of particle emission concerns the formation of alphalike clusters in the neck region of low-energy separating fragments. It has already been shown in connection with Fig. 34 that infinitesimal changes in initial conditions determine whether there is a relative abundance or deficiency of single-particle wave functions in the neck region of a scissioning system and that these single-particle effects may qualitatively affect the nature of the final state. In realistic geometry, it is therefore expected that initial conditions may be found giving rise to an aggregation of single-particle wave functions in the neck region of a scissioning nucleus which produce a sufficiently large density fluctuation that an alphalike cluster asymptotically separates from the two receding major fragments. Examples of such effects have been observed in 710 MeV ^{86}Kr + ^{139}La collisions at angular momenta near $100\hbar$ (Davies, Sandhya Devi, and Strayer, 1979), in 1130 MeV ^{136}Xe + ^{209}Bi collisions at angular momenta near $100\hbar$ (Dhar *et al.*, 1981), and in the induced fission of ^{236}U (Negele *et al.*, 1978). Experimentally, alpha emission from the neck of moderately heavy systems in deep-inelastic scattering is known to be large (Miller *et al.*, 1978), and in ^{236}U fission the probability of emitting an alpha particle from the neck region is 1 in 600. Thus, although there is presently no precisely formulated mean-field reaction theory for the probability of such emission, it is interesting and suggestive that such events occur in the TDHF initial-value problem.

C. Fusion

One of the least ambiguous observables which may be calculated in the mean-field theory is the fusion cross section. Extensive calculations and comparisons with experiments have been carried out for light nuclei, yielding satisfactory quantitative agreement. Since the crucial prerequisite for the fusion of two colliding ions is dissipation of the initial collective relative translational energy, this agreement constitutes strong support for the validity of the mean-field dissipation mechanism.

1. The fusion regions

In the TDHF initial value problem, the fusion cross section is calculated as (Koonin, 1979)

$$\sigma_{\rm fus}(E)=\pi\lambda\!\!\!^{-2}\sum_{l<}^{l>}(2l+1)\,, \tag{7.18}$$

where $\lambda\!\!\!^{-}$ is the reduced wavelength for motion in the incident channel and the sum extends over all impact parameters for which the projectile and target fuse into a single compound system. The regions in E and l for which TDHF calculations are observed to fuse are shown in Fig. 42 for four typical reactions: ^{16}O + ^{16}O, calculated in three dimensions (Bonche, Grammaticos, and Koonin, 1978), ^{16}O + ^{24}Mg calculated in the separable approximation (Krieger and Weiss, 1981), and the systems ^{28}Si + ^{28}Si and ^{16}O + ^{40}Ca calculated both in the separable approximation and in three dimensions (Bonche *et al.*, 1979).

All the results in Fig. 42 show the same qualitative behavior. In the present semiclassical approximation, there is no fusion below the Coulomb barrier. For energies slightly above the Coulomb barrier in these light systems, fusion occurs for head-on collisions and all impact parameters up to a critical peripheral value, corresponding to $l>$, beyond which all impact parameters yield inelastic scattering. As the energy increases further, a threshold is reached beyond which nearly head-on collisions below a lower cutoff $l<$ do not fuse, but rather as in Fig. 38, the projectile is transmitted through the target and emerges in the forward direction. As the energy is further increased, the $l>$ and $l<$ cutoffs come

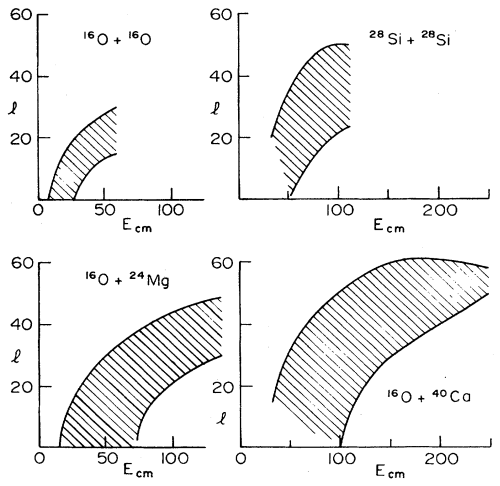

FIG. 42. Fusion regions, indicated by shaded areas, specifying the ranges of initial angular momentum l in units of $\hbar$ and cm energy, E_{cm}, in MeV for which the TDHF initial value problem leads to a final state interpreted as a fused compound system.

closer together, and eventually at a sufficiently high energy no impact parameters yield fusion. The three cases shown in Figs. 38–40 were selected to be representative of the regions below $l<$, between $l<$ and $l>$, and above $l>$, respectively.

Systematic calculations of the fusion regions for heavy systems comparable to those summarized in Fig. 42 are unavailable due to the prohibitive expense of three-dimensional calculations and the limitations of the axial approximation to low energy and the separable approximation to light systems. Head-on collisions of $^{86}Kr + ^{139}La$ and $^{89}Kr + ^{209}Bi$ have been calculated by Davies, Sandhya Devi, and Strayer (1979, 1981). As in the case of light systems, below a low-energy threshold of $E_{lab}=650$ and 850 for the La and Bi cases, respectively, the Kr projectile does not fuse, but rather bounces back; above a high-energy threshold of 850 and 1100 MeV, respectively, the Kr projectile passes through the target; and for intermediate energies, fusions occur. The behavior of these heavy systems using the SK II interaction differs from light systems in two respects. Whereas the low-energy cutoff for fusion in light systems occurs at the Coulomb barrier, for these heavy systems it occurs considerably above the barrier. This dynamic result reflects the macroscopic behavior pointed out by Nix and Sierk (1977) that, in order for the dynamical path to pass inside the fission saddle point and thus produce fusion, systems beyond mass 220 must exceed an energy threshold higher than the Coulomb barrier. A second difference is that, below the energy threshold for fusion, long-lived resonances are observed, analogous to the resonances in slab collisions seen at low energy in Fig. 34. Recent calculations by Davies, Sandhya Devi, and Strayer (1981) using the SK III interaction of Table II indicate significant interaction dependence in the low-energy cutoff. The SK III interaction yields a cutoff for $^{86}Kr + ^{139}La$ 150 MeV lower than SK II, so that the long-lived resonances observed with SK II evidently fuse with SK II.

In the context of purely classical models, the most dramatic feature of mean-field fusion dynamics is the presence of the transmission window below $l_<$. It is therefore important to understand its origin, assess whether corrections to the mean field will eliminate it, and obtain a definitive experimental test of this prediction.

The mechanism is clearly the same mean-field transmission seen in slab collisions, and the thresholds in finite nuclei may be partially understood by a Fermi gas argument by Wong (1979). In the case of particle emission in which only a few particles originating in the projectile escape from the far side of the target, it is clear that the escaping particles arise from the high-momentum components which traverse the potential well most rapidly, so the far edge of the nuclear potential from which they emerge is virtually unaffected by the collision. Thus the obvious frame in which to apply the escape criterion, Eq. (6.63), is the rest frame of the target. As more and more target particles interact with the surface, it is slowed down, brought to rest, and finally accelerated in the opposite direction. It is physically plausible that flow-through and thus transmission occur when the criterion, Eq. (6.63), is satisfied in a frame representing an average velocity of the surface during the time projectile particles are impinging on it. Wong assumes that the appropriate frame is the c.m. one, in which case the transmission criterion becomes

$$\frac{(k_F+k)^2}{2m} \geq \frac{k_F^2}{2m}+\mu \ , \tag{7.19}$$

where k is the momentum per particle of a nucleus in the cm frame. For a Fermi energy $\varepsilon_F=35$ MeV and a removal energy of 8 MeV appropriate to finite nuclei, Eq. (7.19) specifies transmission when the cm energy per particle above the Coulomb barrier exceeds 0.41 MeV. The corresponding threshold in $^{16}O + ^{16}O$ of $E_{cm}=28.4$ is in reasonable agreement with the TDHF results in Fig. 42 of 27 MeV. For slab collisions in which there is no Coulomb force, the separation energy equals the binding energy per particle of 16 MeV, so the criterion, Eq. (7.19), yields a threshold of 1.52 MeV per particle, in qualitative agreement with the calculated value of 2 MeV per particle in Fig. 34. Wong shows that the systematic behavior of the transmission window is reproduced by Eq. (7.19) for a variety of target and projectile combinations. If application of the escape criterion in the cm frame is quantitatively reliable, it has the interesting consequence that the transmission threshold decreases as the effective mass is decreased.

Unfortunately, there is no direct experimental test of the mean-field transmission prediction. The strongest indirect evidence for the window is the agreement with experiment of mean-field predictions for fusion cross sections discussed subsequently in connection with Figs. 43–45. Although, by Eq. (7.18), only the combination

$(l_>+1)^2-(l_<+1)^2$ is experimentally determined, the agreement seen in Fig. 43 for $^{16}O+^{16}O$ would be replaced by overestimates of up to 33% at the highest energies if all impact parameters below $l_<$ were assumed to fuse. Thus, if the mean-field theory is in error in predicting the transmission window, it mysteriously makes compensating errors in $l_>$ such as to reproduce observed fusion cross sections.

Experimental attempts to look for the transmission window in $^{16}O+^{16}O$ (Kox, Cole, and Ost, 1980) and $^{27}Al+^{32}S$ (Natowitz *et al.*, 1979) reach opposite conclusions and are subject to controversial model assumptions. A careful measurement of the fragment kinetic energies at forward angles in $^{16}O+^{16}O$ collisions at $E_{cm}=34$ MeV has been made by Lazzarini *et al.* (1981). As seen in Fig. 42, this energy is slightly above the predicted threshold, and trajectories up to $6\hbar$ are predicted to yield inelastic scattering in the forward direction instead of fusion. Whereas the predicted events of $4\hbar$ and $6\hbar$ are in definite disagreement with the data, the measurement is so close to the threshold, which in turn is subject to significant theoretical uncertainties, that the existence of the transmission phenomenon is not ruled out by this experiment. Thus as yet the phenomenon has been neither unambiguously confirmed nor disproven experimentally.

2. Fusion cross sections

Fusion cross sections, defined by Eq. (7.18), have been calculated as a function of bombarding energy for the following systems: $^{12}C+^{14}N$ (Maruhn-Rezwani, Davies and Koonin, 1977); $^{12}C+^{16}O$ and $^{12}C+^{18}O$ (Krieger and Davies, 1979); $^{16}O+^{16}O$ (Bonche, Grammaticos, and Koonin, 1978; Krieger and Davies, 1978); $^{16}O+^{24}Mg$ (Krieger and Weiss, 1981; Sandhya Devi, Dhar, and Strayer, 1981); $^{16}O+^{27}Al$ (Sandhya Devi, Dhar, and Strayer, 1981); $^{16}O+^{40}Ca$ and $^{28}Si+^{28}Si$ (Bonche *et al.*, 1979); and $^{40}Ca+^{40}Ca$ (Bonche, Grammaticos, and Koonin, 1978; Krieger and Davies, 1978). Theoretical results are compared with experimental data in Figs. 43–45 for three systems which are both representative of results throughout the region and subject to a minimum of technical and theoretical uncertainties.

Figure 43 compares two sets of TDHF calculations for $^{16}O+^{16}O$ with experimental data of Conjeaud *et al.* (1977). Theoretical results are presented as error bars reflecting the uncertainty in locating $l_>$ and $l_<$ with the discrete values of angular momenta utilized in the calculations. In addition to displaying excellent agreement with experiment, this figure shows the relative insensitivity of $^{16}O+^{16}O$ results to the interaction and computational constraints. The three-dimensional calculation of Bonche, Grammaticos, and Koonin (1978), denoted by open circles, used the local interaction of Table II and constrained the isospin by constraining proton and neutron wave functions to be identical. The axially constrained calculations by Krieger and Davies (1978), denoted by triangles, utilized the nonlocal interaction SK II of Table II and had unconstrained isospin. Additional evidence from other calculations indicates comparable insensitivity to independent changes in constraints and the interaction.

Mean-field calculations of Sandhya Devi, Dhar, and Strayer (1981) for $^{16}O+^{24}Mg$ are compared with experimental data of Tabor *et al.* (1978) in Fig. 44. Since no isospin constraint is imposed on the calculation, the full nonlocal SK II interaction is used, and the validity of the separable approximation for light systems has been well verified by detailed comparisons with three-dimensional calculations, these results are expected to be theoretically reliable. The excellent agreement with experiment is comparable to that obtained in $^{16}O+^{16}O$.

Several approximate theoretical calculations for $^{40}Ca+^{40}Ca$ fusion cross sections are shown in Fig. 45. The axially constrained calculations of Krieger and Davies (1978) with unconstrained isospin utilizing the local and nonlocal SK II interactions of Table II are denoted by open squares and triangles, respectively. Note that compared with $^{16}O+^{16}O$, this system is more sensitive to the interaction with the nonlocal interaction yielding somewhat lower cross sections. Three-dimensional calculations of Bonche, Grammaticos, and Koonin (1978) with constrained isospin and utilizing the local interaction of Table II are denoted by open circles. Again in contrast to the $^{16}O+^{16}O$ case, one observes a significant difference between calculations utilizing the same interaction but different constraints. Since the accuracy of the axial constraint has been verified at low energies, the important difference between the local calculations at low energies is the isospin constraint. The fact that cross sections with unconstrained isospin (open squares) are several hundred mb higher than with constrained isospin (open circles) indicates that the Coulomb force is strong enough in this system to induce quantitatively significant dissipation. Two sets of experimental data for $^{40}Ca+^{40}Ca$ are compared with the theoretical predictions in Fig. 45. The earliest data by Doubre *et al.* (1977) are denoted by crosses and are in serious disagreement with theory at low energy. Since both the mean-field theory and technical approximations utilized in the calculations should be most accurate near threshold, such disagreement, if substantiated, would have serious implications. Two recent experiments, however, yield different low-energy fusion cross sections which are consistent with each other and with theory. The data of Tomasi *et al.* (1982) are denoted by the solid circles in Fig. 45 and are observed to agree as well with mean-field theory as the data for lighter systems shown in Figs. 43 and 44. As seen in Fig. 4 of the paper of Tomasi *et al.*, the unpublished results of Barreto *et al.* (1980) are also in excellent agreement with these new data. Thus the $^{40}Ca+^{40}Ca$ system now appears to provide a rewarding example of genuine predictive power of the mean-field theory and vindication of the effort to avoid phenomenological tampering with the underlying theory.

Results for the other light systems for which fusion

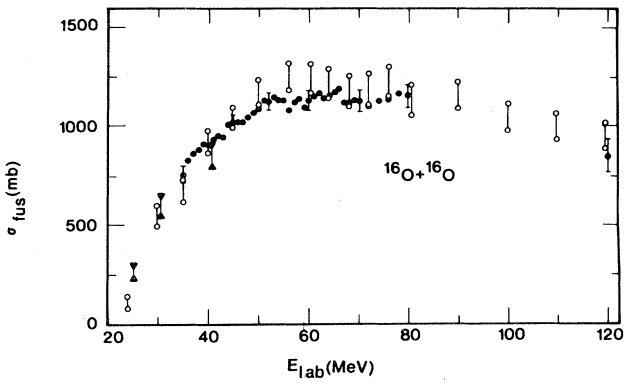

FIG. 43. Fusion cross sections as a function of energy for $^{16}O+^{16}O$. Open circles denote three-dimensional calculations with the local interaction and constrained isospin. Triangles indicate axially constrained calculations with the SK II interaction and no isospin constraint. Experimental data are denoted by solid circles.

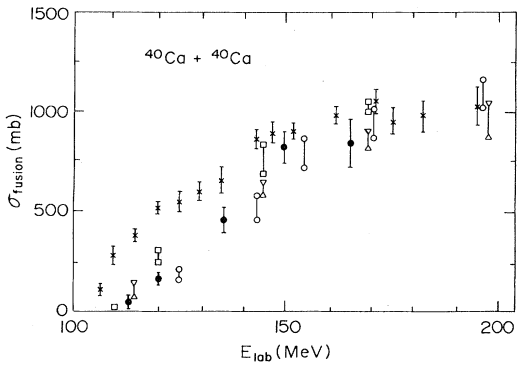

FIG. 45. Fusion cross sections for $^{40}Ca+^{40}Ca$ as in Fig. 43. Open squares and triangles denote axially constrained calculations with no isospin constraint utilizing the local interaction and the SK II interaction, respectively. Open circles indicate three-dimensional calculations with constrained isospin. Experimental data by Doubre *et al.* and by Tomasi *et al.* are denoted by crosses and solid points, respectively.

cross sections have been compared with experiment are roughly comparable to those shown in Figs. 43–45. Calculations for $^{16}O+^{40}Ca$ show the same sensitivity to constraints and the interaction as $^{40}Ca+^{40}Ca$ and yield comparable agreement. Results for $^{16}O+^{24}Mg$ using five different Skyrme forces display much less interaction sensitivity than the heavier systems. Open-shell systems, in which the filling approximation is made, do not differ appreciably from the closed-shell systems shown here. In general, the quantitative agreement with experiment is satisfactory, with discrepancies of at most 20–30%.

For technical reasons, no systematic calculations exist in heavy nuclei. Davies, Sandhya Devi, and Strayer (1979) estimate a lower limit to the fusion cross section for $^{86}Kr+^{139}La$ at 710 MeV to be 118 mb on the basis of axially constrained calculations. This result is consistent with the experimental upper limit of 500 mb by Vandenbosch *et al.* (1978). A similar lower bound of 100 mb is obtained by Davies, Sandhya Devi, and Strayer (1981) for $^{84}Kr+^{209}Bi$ which is again safely below present experimental bounds for low-energy reactions.

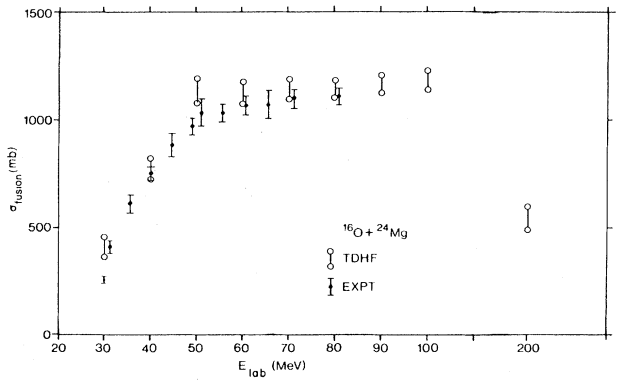

FIG. 44. Fusion cross sections for $^{16}O+^{24}Mg$ as in Fig. 43. Open circles denote calculations using the separable approximation, the SK II interaction, and no isospin constraint. Solid circles indicate experimental data.

In summary, the success of the mean-field theory in predicting fusion cross sections for light systems provides substantial evidence for the validity of the theory. Technical limitations presently preclude meaningful comparisons in heavier systems, and as yet there exists no definitive experimental test of the predicted transmission for nearly central collisions.

D. Deep inelastic scattering

A different and potentially sensitive test of many aspects of mean-field dynamics is provided by the striking features of heavy-ion inelastic scattering. The dissipation and relaxation observed in strongly damped collisions and the systematic behavior throughout the Periodic Table of fragment mass and energy distributions as functions of scattering angle place stringent demands on a microscopic theory having no free parameters.

A convenient way of summarizing experimental data for comparison with the semiclassical results of the TDHF initial-value problem is provided by a Wilczyński plot, displaying contours of the double-differential cross section for the projectilelike fragment as a function of energy and angle. Each impact parameter in a TDHF calculation yields a single point in the E-θ plane, and in the semiclassical limit these points should reproduce the major qualitative features of the contour plot, with a high density of points corresponding to high cross section and corrections to the semiclassical approximation presumably defining the falloff away from the semiclassical trajectory.

Such Wilczyński plots may be constructed for all the systems cited in Sec. VII.B for which deflection functions have been calculated. Four representative curves

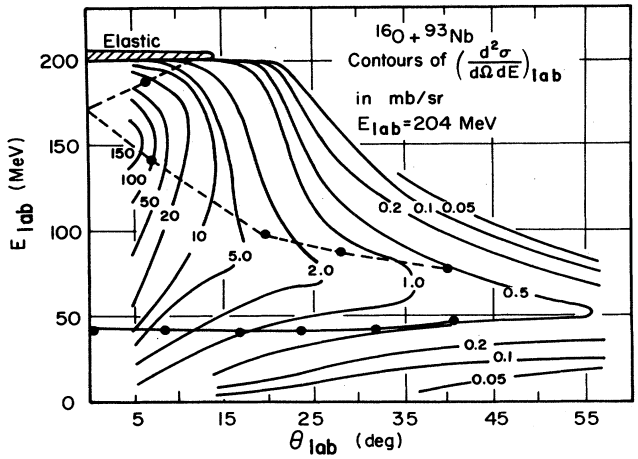

FIG. 46. Comparison of mean-field predictions with the experiemental Wilczyński plot for $^{16}O+^{93}Nb$ at $E_{lab}=204$ MeV. Calculated points, denoted by solid points, are connected by dashed lines above the fusion region and solid points below the fusion region to guide the eye.

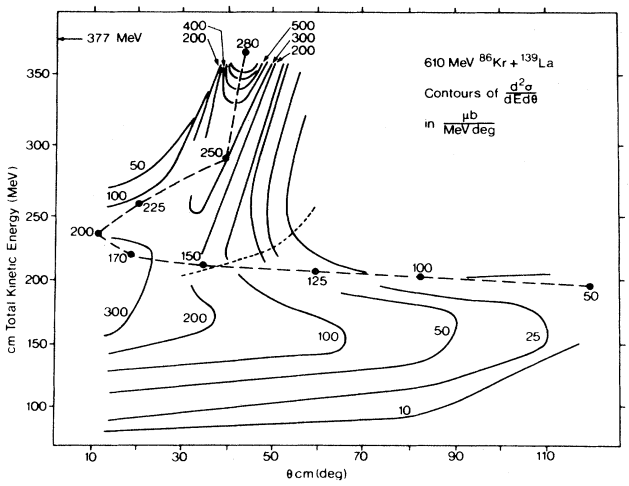

FIG. 47. Wilczyński plot as in Fig. 46 for $^{86}Kr+^{139}La$ at $E_{lab}=610$ MeV. The calculated points are labeled with the orbital angular momentum.

are shown in Figs. 46—49, corresponding to four systems which have been discussed and referenced in Sec. VII.B and for which deflection functions are presented in Fig. 41.

The experimental data of Obenshain *et al.* (1981) is compared with TDHF results in the Wilcyński plot shown in Fig. 46. For arbitrarily large impact parameters, there is negligible energy loss and these Coulomb trajectories lie on a horizontal line corresponding to the elastic peak in Fig. 46. Below $l\sim 100\hbar$, the deflection function in Fig. 41 decreases with decreasing l, and the trajectory in Fig. 46 passes through zero degrees. Although negative-angle scattering has been indirectly confirmed in light systems using photon polarization to infer the angular momentum direction, the cross sections depend only on the magnitude of the scattering angle, and the Wilczyński plot thus does not distinguish positive and negative scattering angles. The negative-angle branch above the fusion region is indicated by the dashed line and corresponds quite closely to the ridge passing downward and to the right in the figure. This agreement indicates that the mean field not only qualitatively reproduces the dissipation occurring in strongly damped collisions, but also quantitatively predicts the nontrivial angular dependence of the energy loss. The branch below the fusion region is indicated by the solid line, but is quantitatively less important due to the small weighting of low-impact parameters.

A similar comparison is shown for $^{86}Kr + ^{139}La$ in Fig. 47, based on the experimental data of Vandenbosch *et al.* (1978). For this heavier system, the deflection function is everywhere positive. The trajectory follows the pronounced ridge in the experimental data from the elastic peak at the grazing angle down to the Coulomb barrier of approximately 220 MeV at the minimum scattering angle. The experimental data display a horizontal ridge slightly below the Coulomb barrier extending to large scattering angles, and this qualitative behavior is reproduced by the mean-field trajectory but with a shift of roughly 50 MeV in energy loss.

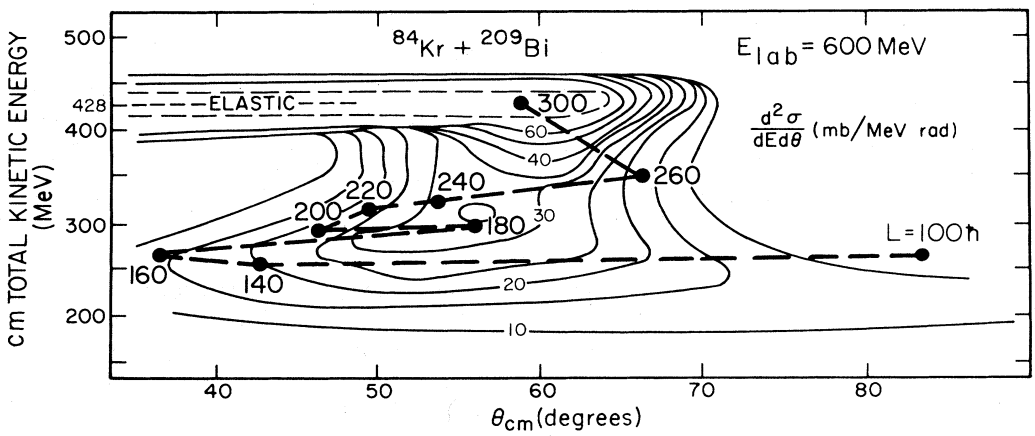

FIG. 48. Wilczyński plot as in Fig. 47 for $^{84}Kr+^{209}Bi$ at $E_{lab}=600$ MeV.

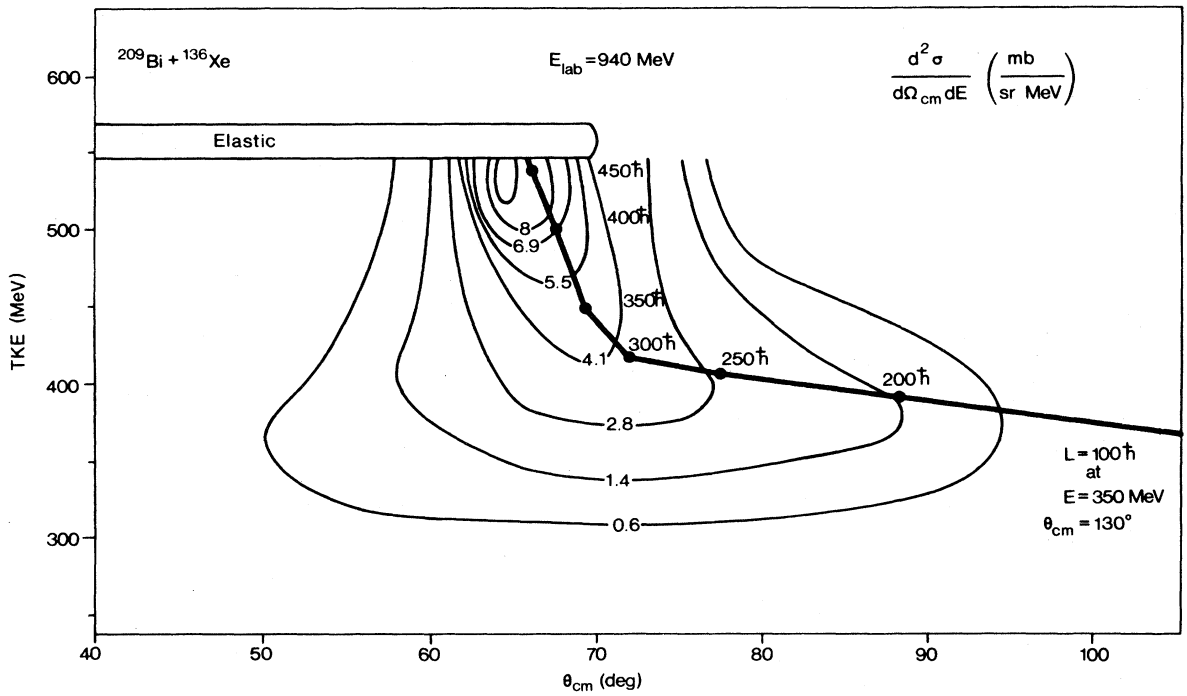

FIG. 49. Wilczyński plot as in Fig. 47 for ^{136}Xe+^{209}Bi at E_{lab}=940 MeV.

Figure 48 compares experimental data for ^{84}Kr + ^{200}Bi (Wolf *et al.*, 1974; Wolf and Roche, 1976) with mean-field predictions seen in Fig. 41. The deflection function is qualitatively similar to that for ^{86}Kr + ^{139}La, but the minimum scattering angle now is much larger, giving rise to concentration of scattering at the rainbow angle in the region of 50°. Instead of a monotonically decreasing ridge, this system displays a local maximum in the deep-inelastic region near the rainbow angle. Again, the mean field reproduces the average trend from the elastic peak down to the minimum angle near the Coulomb barrier energy of approximately 310 MeV, exhibiting some single-particle fluctuations, as already discussed in connection with Fig. 41. Strongly damped events at low-impact parameter qualitatively reproduce the horizontal ridge extending to large scattering angles but again underestimate the energy loss by up to 50 MeV.

A final Wilczyński plot is shown in Fig. 49 for ^{209}Bi + ^{136}Xe, using the data of Schroder and Huizenga (1977) and Schroder *et al.* (1978). The Coulomb energy is so high in this system that the deflection function is monotonic with no rainbow scattering. The experimental data comprise a single ridge passing downward and to the right, which is well reproduced by the mean-field theory.

The salient features of the distributions of projectile-like fragments in energy and angle are thus systematically reproduced throughout the Periodic Table. It should be emphasized that the results shown here are genuinely representative of the level of agreement with experiment obtained for all the systems and energies referenced in Sec. VII.B in connection with calculations of deflection functions. The primary quantitative deficiency is the apparent underestimation of the energy damping at low-impact parameters. This apparent discrepancy is clouded by several experimental and theoretical uncertainties. Although the lowest l point in the ^{84}Kr + ^{209}Bi calculation at 600 MeV appears to conflict with the data in Fig. 48, the data were analyzed ignoring the fact that the mass of the projectilelike fragment is significantly larger than 84 for large scattering angles, leading to a spurious decline in the back-angle ridge. Analogous calculations for the essentially similar reaction ^{84}Kr + ^{209}Pb at 494 MeV (Davies, Maruhn-Rezwani, *et al.*, 1978) yield quantitative agreement with the ridge at backward angles. In the case of ^{86}Kr + ^{139}La, the mass distribution for the most strongly damped events is comprised of two components, one centered around the projectile mass and one centered around symmetry, and the mean-field result should be compared to data with the latter fusion-fission component removed. Finally, aside from these experimental considerations, the possibility exists that the axial constraint is less accurate in representing the dissipation in heavy systems than is presently assumed. For all these reasons, then, the quantitative tests of mean-field dissipation at backward angles are presently indecisive.

Other observables beside the fragment kinetic energy in principle may be compared with experiment as a function of the scattering angle. The mean mass number of the projectilelike fragment may plausibly be approximated by the number of particles in the TDHF final state, and its qualitative behavior with scattering angle is reproduced. In contrast, the dispersion in particle number, as discussed in Secs. III.A.4, II.B.1, and VI.D, re-

quires dynamical treatment of two-body correlations which are neglected in the mean-field theory. Not surprisingly, this dispersion is underestimated by an order of magnitude in TDHF calculations. To the extent to which one is willing to use the scattering angle as a clock to determine the contact time, the equilibration of various degrees of freedom in the one-body density matrix may be studied and compared with diffusion and transport theories as discussed by Davies, Maruhn-Rezwani, *et al.* (1978) and Koonin (1979).

In summary, subject to the conceptual limitations of the TDHF initial-value problem and the approximations required to render numerical solution of the mean-field equations practical, the microscopic TDHF theory with no free parameters is remarkably successful in predicting the salient features of deep-inelastic scattering throughout the Periodic Table. These results, combined with the fusion cross sections reviewed in the preceding section, constitute the primary experimental evidence for the validity of mean-field dynamics.

E. Fission

In principle, spontaneous and induced fission provide a rich testing ground for the mean-field theory. The quantum mean-field theory of tunneling decay derived in Sec. V.E contains the combined physics of the collective dynamics of shape degrees of freedom and single-particle effects and should be capable of describing the systematic behavior, complete with shell fluctuations, of partial widths to decay by symmetric and asymmetric fission modes throughout the Periodic Table. Although implementation of the theory was straightforward in the one-dimensional model in Sec. VI.C.3, a realistic calculation in three spatial dimensions for a heavy nucleus is beset with formidable obstacles. Implementation of the corresponding generalization to induced fission (Kerman and Levit, 1981) is even more impractical, since at finite temperature the self-consistent equations require solution for the unoccupied as well as normally occupied orbitals. Only in the semiclassical approximation above the fission barrier does the computational problem reduce in scope to that of the TDHF initial-value problem, and this limit is treated in the following section.

1. Semiclassical approximation to induced fission

For induced fission near threshold, the initial condition for the separating fragments corresponds to a wave packet of collective shapes passing close to the fission saddle-point configuration with low collective velocity. Analogous to the TDHF initial-value problem for scattering, then, the natural initial condition for induced fission at threshold is to release the system from an initial configuration infinitesimally beyond the saddle point. Since, experimentally, the most probable fission fragment kinetic energies display smooth behavior as a function of fissility, systematic calculation of the final fragment kinetic energies should provide another test of dissipation in the mean-field theory. In addition, such calculations provide insight into the shapes and time scale involved in the passage from saddle to scission.

The induced fission of ^{236}U in this semiclassical approximation has been calculated by Negele *et al.* (1978). As is clear from previous discussion of collisions, computational considerations require constraint to axial symmetry in order to render the calculation feasible. In contrast to the case of collisions, however, evolution of an axially symmetric configuration beyond the saddle point is totally misrepresentative of nearby slightly asymmetric configurations. Since the axially symmetric Hamiltonian does not connect different angular momentum and parity substates, Nilsson levels cross with no mixing and the orbital occupation is locked in orbitals for which the total energy eventually increases with increasing deformation and fission is impossible. In contrast, for any finite axial asymmetry, levels do not cross and there is no impediment to the descent to scission.

To obtain nontrivial dynamics with an axially symmetric constraint, it is necessary to allow the residual interaction to mix the states which are not connected by the mean field, and the simplest treatment uses the constant-gap pairing approximation, Eq. (7.13). The conceptual limitation is that the gap must represent not only the true pairing matrix elements, but also the average effect of the mean-field matrix elements which have been artificially suppressed by symmetry. The gap, Δ, is therefore taken as a phenomenological parameter with the physical constraint that it should be somewhat greater than the pairing value. In the space employed in the calculation, values of $\Delta=2$ and 6 MeV correspond to the two-body matrix elements $G\simeq 0.17$ and 0.29 MeV, respectively. For comparison, $23/A$ yields $G\simeq 0.1$ and realistic reaction matrix elements range from 0 to 0.4 MeV in this region of the Periodic Table (Negele, 1970b), so these values are representative of the range of physical interest.

The sequence of densities occurring during fission of ^{236}U for $\Delta=2.0$ MeV is shown in Fig. 50. Salient qualitative features include the preservation of uniform surface thickness and formation of a highly elongated neck which ruptures rapidly.

Quantitative results depend significantly upon the value of the phenomenological gap Δ. As Δ is increased from 2.0 to 6.0 MeV, the transfer of probability to lower energy orbitals is facilitated, with the result that the transit time from 1 MeV below the saddle point to scission is decreased from 3.4 to 2.2×10^{-21} s and the dissipation is decreased, yielding an increase in the final translational kinetic energy from 142 to 166 MeV. Experimentally, the most probable fission-fragment kinetic energy is 168.0 ± 4.5 MeV (Burnett, 1963), reflecting roughly 18 MeV of dissipation relative to the theoretical macroscopic result in the absence of viscosity. Thus variation of Δ in the physically reasonable range yields uncertainty in dissipation of the order of the experimental effect, and the present practical restriction to axial symmetry thus precludes a quantitative test of the mean-field theory.

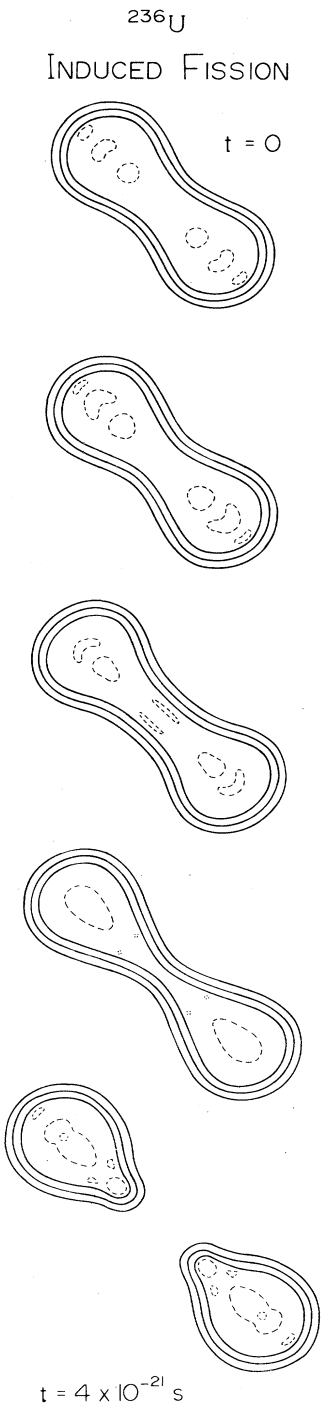

FIG. 50. Contour plots of the nuclear density in a plane containing the symmetry axis at time intervals of 4×10^{-21} s during induced fission of ^{236}U. The outer solid lines denote densities of 0.02, 0.08, and 0.14 fm^{-3}, and the dashed lines denote a density of 0.16 fm^{-3} and thus reveal shell fluctuations.

2. Spontaneous fission

The computational scale of the self-consistent periodic eigenvalue problem, Eq. (5.134), for the bounce solution governing spontaneous fission is much larger than that of the TDHF initial value problem, and the results are correspondingly meager.

An exploratory calculation has been performed for ^{8}Be in three spatial dimensions plus time, using the local interaction of Table II and the method of solution described in Sec. VI.C1 (Negele, 1980). Unfortunately, in the case of ^{8}Be the spurious cm motion error varying as $1/A$ introduces an error of the order of 16 MeV between the energy of the parent nucleus and the two daughters, when the physical Q value is of the order of only kilovolts. Since as yet no practical method for treating this effect in mean-field theory has been developed, the effective Hamiltonian must be modified to cancel the cm error in order to obtain fission, and there is no reason to believe such a major modification is quantitatively reliable. In the referenced calculation, the strength of the Coulomb interaction was enhanced by increasing the charge of the proton as a prelude to investigating fission systematics as a function of fissility.

Figure 51 shows perspective plots of the half-density surfaces for the bounce solution for symmetric fission of ^{8}Be at sequential times. One feature of the fission of this system which is not at all representative of heavy fissile nuclei is the fact that the turning point at the entry to the classically allowed region is far past the scission point, so that the bounce solution near $\tau=0$ corresponds to two well-separated alpha particles. Thus, although this schematic ^{8}Be calculation plays a useful role in demonstrating the feasibility of solving the self-consistent tunneling problem and in developing techniques for heavier systems, it has little direct physical relevance.

The feasibility of calculating fission in systems as large as ^{28}Si and ^{32}S, with suitably enhanced proton charge, offers several interesting possibilities. Since the crossing of Nilsson levels is already important in this region, it is possible to study directly the breaking of axial symmetry in the self-consistent bounce solution. Direct comparison with adiabatic reductions and formulations in terms of a single collective variable will be possible with the same effective interaction. Finally to the extent to which $A\approx30$ is large enough to embody liquid drop behavior, the dependence of the penetrability on fissility may be calculated by keeping A fixed and increasing e^2. Thus, although we are presently very far from a realistic microscopic fission calculation for uranium, there do exist viable avenues of investigation.

F. Pion condensation

A final, highly speculative application of mean-field dynamics to finite nuclei is the search for pion condensation in heavy-ion collisions (Krewald and Negele, 1980). This application is speculative not only because a definitive calculation lies well beyond present capabilities, but also because collision energies are involved which approach or exceed the limits of validity of the mean-field approximation. Nevertheless, the intrinsic interest of the

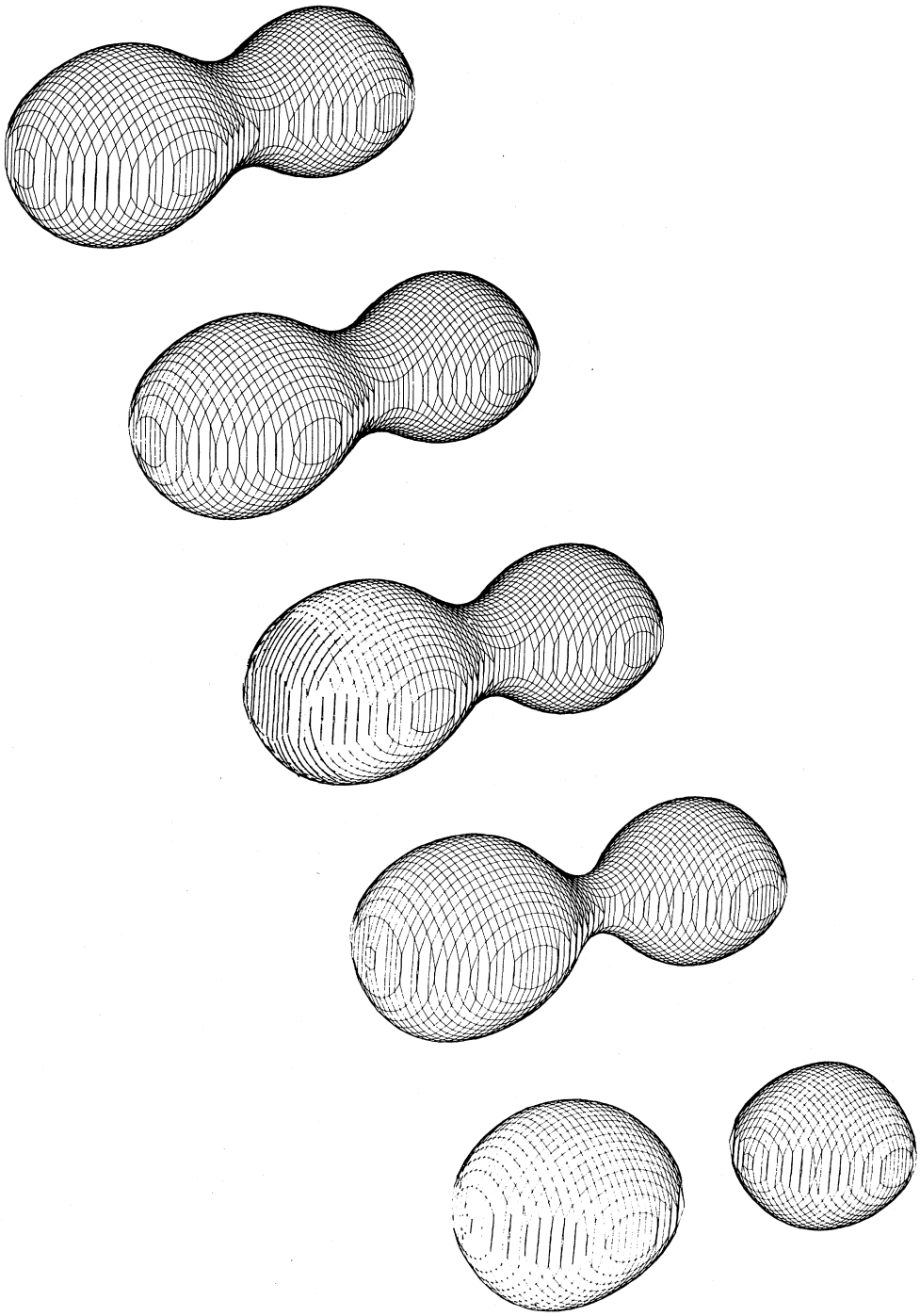

FIG. 51. Surfaces, shown in perspective, of constant density equal to one-half nuclear matter density at sequential times for spontaneous fission of ^{8}Be.

phenomenon merits a brief review.

Pion condensation (Migdal, 1972a, 1972b; Sawyer, 1972; Scalapino, 1972; and Migdal, 1978) arises from the instability of nuclear matter at sufficiently high density with respect to excitations with the quantum numbers of the pion. In the static limit, it is described in terms of spin-isospin excitations with an effective interaction containing the one-pion exchange potential, and as the density increases, spin-isospin modes become progressively softer until they become self-sustaining at the critical density. In the mean-field approximation, a π^0 condensate corresponds to coherent spin-isospin density fluctuations such that layers of excess spin-up protons and spin-down neutrons alternate with layers of excess spin-up neutrons and spin-down protons. (Takatsuka and Tamagaki, 1978; Takatsuka *et al.*, 1978). The nonzero

expectation value of the source term $\nabla\cdot\langle\sigma\tau\rangle$ plays the role of the expectation value of the pion field or order parameter in the condensed phase. Since the time-dependent mean field describes the evolution of the matter densities of the colliding nuclei, includes the RPA fluctuations with respect to the instantaneous one-body density matrix, and governs the nonlinear growth of a condensate in the self-consistent field, it provides a unified microscopic description of pion condensation in heavy-ion collisions.

The critical density for pion condensation during a nuclear collision is much lower in the mean-field theory than in a treatment assuming local equilibration. The essential mechanism may be seen by comparing a system of two interpenetrating Fermi gases with a single Fermi gas of the same total density. For a single Fermi gas of nuclear matter at density ρ, the driving term for the instability in the RPA propagator is the zero-frequency Lindhard function (Lindhard, 1954), $\Pi_0(q,k_F)$, where $k_F=(3\pi^2\rho/2)^{1/3}$. In contrast, for two separated Fermi spheres representing interpenetrating gases each of density $\rho/2$, and for the most favorable case of condensate momentum $\mathbf{q}_c$ perpendicular to the beam direction, the driving term becomes $2\Pi_0(q_c,2^{-1/3}k_F)$ (Gyulassy and Greiner, 1977). The multiplicative factor of 2 increases the driving term much more than shifting the argument to $2^{-1/3}k_F$ decreases it, reflecting the physical fact that the phase space for particle-hole excitations of momentum q_c around the surface of two separated Fermi spheres is much larger than that around a single larger Fermi sphere corresponding to the same total density. The net effect is that the condensation threshold occurs in the two-gas problem at a total density of roughly one-half that for a single equilibrated gas. Since realistic estimates for the threshold in an equilibrated gas are in the range of 1.5—3 times nuclear matter density and the corresponding thresholds for colliding nuclei are thereby reduced to 0.75—1.5 times nuclear matter density, this effect could be absolutely crucial in producing pion condensation in a feasible experiment. This significant feature of the mean-field theory is completely lost, however, if pion condensation is included only in an equation of state depending on the density, as in the calculations by Pirner *et al.* (1979) and Stöcker *et al.* (1980).

In the exploratory calculations of Krewald and Negele (1980), head-on axially symmetric collisions of $^{15}N+{}^{15}N$ were calculated in the time-dependent mean-field approximation using the Hamiltonian density

$$\mathscr{H}=H+\frac{t_4}{2}(\mathbf{S}_p+\mathbf{S}_n)^2+\frac{t_5}{2}(\mathbf{S}_p-\mathbf{S}_n)^2 -\frac{1}{2}\left[\frac{f^2}{\mu^2}\right]E_Y[\nabla\cdot(\mathbf{S}_p-\mathbf{S}_n),\nabla\cdot(\mathbf{S}_p-\mathbf{S}_n)]\ , \tag{7.20}$$

where the spin density is defined

$$\mathbf{S}_q(r)=\sum_\nu \Psi_\nu^{*s,q}(r)\sigma_{ss'}\Psi_\nu^{s',q}(r)\ , \tag{7.21}$$

H denotes the Hamiltonian density Eq. (7.2), the Yukawa convolution is defined in Eq. (7.3), f and μ are the effective pion coupling constant and mass, the charge subscript q denotes either protons or neutrons, s indicates the spin projections, and σ denotes Pauli matrices. The effective interaction thus includes the one-pion exchange potential plus zero-range $\sigma\cdot\sigma$ and $\sigma\cdot\sigma\tau\cdot\tau$ components, and the parameters were adjusted to reproduce realistic calculations of pion condensation thresholds and appropriate Landau parameters. Since π^+, π^0, and π^- modes are nearly degenerate in collisions involving nuclei with nearly equal neutron and proton densities, the calculation was simplified by omitting all charge-changing components and thus considering only π^0 condensation.

Calculations were performed at a cm energy per particle of 20 MeV so as to obtain most of the enhancement of the Lindhard function for two separated Fermi spheres without totally invalidating the mean-field approximation, and detailed plots of $\nabla\cdot\langle\sigma\tau\rangle$ are presented in the original reference. Whereas nonlinear growth of the spin-isospin mode during the time of nuclear overlap is clearly observed, it is not dramatic and results in no significant signature in the final collision fragments. It is an open question as to how large the growth would be for a full three-dimensional calculation of Pb + Pb, where the larger overlap time, the greater spatial extent, and possibility of planar rather than cylindrical fluctuations are all much more conducive to the growth of an instability.

Even in the event that a short-lived pion condensed state with pronounced spin-isospin instabilities should arise in actual collisions and be adequately approximated in mean-field calculations, the fact that it is not accessible to external probes, such as electrons, photons, or pions, renders it a nontrivial problem to verify its existence unambiguously. Possible signatures, such as pion emission or spin-isospin correlations, are beset with uncertainties. Hence, it is possible that pion condensation may in fact occur in these intermediate-energy heavy-ion reactions as a result of the favorable phase space, and nevertheless be relegated to the realm of speculation for lack of an adequate signature.

VIII. SUMMARY AND FUTURE OUTLOOK

The mean-field theory reviewed in this work provides the foundation for a systematic theory of a wide variety of problems in nuclear structure and dynamics. Reduction of the full Schrödinger equation to a theory involving the one-body density matrix is an immense simplification of the many-body problem, which, nevertheless, contains an infinite number of degrees of freedom from which the collective and single-particle variables relevant to a particular process emerge naturally. With an appropriate effective interaction based on the phenomenological knowledge of nuclear interactions and the saturation of nuclear matter, quantitative success is obtained in a variety of applications, ranging from the energies and density distributions of nuclear ground states to the calculation of fusion cross sections and the dissipation and

gross features arising in inelastic heavy-ion scattering.

A number of interesting formal and conceptual problems remain unresolved. Even at the level of the mean-field theory, new and more powerful techniques are needed to deal with large numbers of degrees of freedom. Instead of evolving $(A_1+A_2)\times N_x \times N_y \times N_z$ complex numbers, representing single-particle wave functions on a mesh, it would be desirable to reformulate the mean-field approximation in terms of a small number of the most relevant variables. Viable, controlled approximations to the TDHF theory are needed which clearly separate collective, single particle, and statistical effects and which deal efficiently with the truly statistical aspects. In situations in which single-particle behavior does not dominate the physics, it should be possible to formulate a much simpler theory involving only the nearly diagonal properties of the one-body density matrix (or, equivalently, low-momentum moments of the Wigner transform), utilizing the density $\rho(R)$, kinetic energy density $\tau(R)$, current density $\mathbf{J}(R)$, and spin density $\mathbf{S}(R)$. Similarly, it is equally desirable to formulate simplifications of the two-body time-dependent coupled-cluster equations, both to extract the essential physics from the complicated general formalism and to render quantitative calculations tractable.

The functional integral formulation also raises a number of significant unresolved problems. The most salient conceptual problem is that, in the absence of an expansion parameter, there is no criterion for choosing between equivalent exact expressions which yield differing lowest-order SPA results. Whereas the freedom in defining the mean field has been utilized thus far to embed desirable, previously known approximations in the functional integral formalism, it is necessary to learn to exploit this freedom to optimize corrections. Two particularly crucial areas for future efforts emphasized in Sec. V are the derivation of a scattering theory formulated in terms of few-body observables and the development of techniques to deal with the short-range repulsion in the nuclear interaction. Present methods of evaluating quadratic and higher-order corrections to the SPA are tractable only in simple cases for which the SPA equations can be solved analytically, and in which only one nontrivial space-time coordinate is involved. Clearly in the nuclear physics applications considered in this work, more powerful general techniques are needed, with the Monte Carlo method being a particularly promising possibility.

The region of validity of the mean-field approximation has yet to be understood quantitatively. Although systematic expansions in principle provide a framework for calculating or estimating errors, present considerations are limited to intuitive agruments. It has been argued above that the role of the Pauli principle in generating a large mean-free path justifies the mean-field description of low-energy collective modes, collisions slightly above the Coulomb barrier, and fission. Other interesting regions of validity, however, also seem possible. Whenever the process may be specified by the action of an external potential, the mean-field theory should provide an excellent description of the response of the system. Thus, peripheral and grazing collisions at arbitrarily high energies appear to fall within the purview of the theory, with the fragmentation of peripheral relativistic heavy-ion collisions being a particularly interesting possibility. Other applications might arise when one can isolate some region of a system in which particles have low relative momentum, such as the coalescence of final fragments from an excited intermediate system. In addition, applications in other fields, such as atomic physics, surely abound.

The initial exploratory phase of numerical calculations, reviewed in detail in Sec. VII, appears to be nearly completed, and significant technical advances and developments in computer capabilities are required for substantial new progress. Given that one of the virtues of the mean-field theory is its treatment of single-particle effects, it is clearly desirable to include eventually the spin-orbit interaction to obtain the proper single-particle level ordering. Similarly, systematic calculations of spontaneous fission lifetimes in the actinide region, investigation of spin-isospin instabilities in the collisions of heavy nuclei, and the inclusion of two-body collisions in the time-dependent coupled-cluster theory will be extremely interesting when technically feasible. For the present, however, possibilities for practical calculations offering significant new insights into mean-field dynamics are rather limited.

Experimentally, the primary challenge is to measure observables which definitively distinguish the mean-field theory from other approximations. During intermediate stages of evolution, the density distributions arising in the TDHF theory and fluid dynamics differ significantly. In a head-on collision, for example, the limited transverse equilibration in the mean-field theory yields compound systems which are always prolate, whereas fluid dynamics may yield intermediate systems which become highly oblate. As yet, however, no experimental signature of this qualitative difference has been found in the final-state observables. Even more dramatic are the mean-field predictions of the forward transmission window for small-impact parameters in fusion reactions and the possibility of large-amplitude spin-isospin fluctuations in higher-energy collisions of heavy nuclei. Given recent experimental advances in precision and specificity in coincidence experiments, serious effort should be addressed to formulating definitive tests of the mean-field theory.

In conclusion, it is clear from these and other open questions that nuclear dynamics continues to challenge our understanding of the physics of many-body systems. It is hoped that the modest successes of the mean-field theory reviewed in this work provide the impetus to meet this challenge.

ACKNOWLEDGMENTS

It is a pleasure to acknowledge the contributions of collaborators and colleagues both to my understanding of

mean-field theory and to this review. Steve Koonin has played a crucial role in virtually every phase of the development of the mean-field theory, and Shimon Levit was responsible for stimulating my interest in functional integral methods, as well as many of the developments in their application to nuclei. Other collaborators having significant impact on this work include P. Bonche, K. T. R. Davies, P. Hoodbhoy, S. Krewald, J. R. Nix, and B. Yoon. Stimulating discussions concerning various aspects of this work with M. Baranger, M. Beckerman, G. Bertsch, F. Coester, B. Day, H. Flocard, M. Gyulassy, A. K. Kerman, E. Moniz, D. Vautherin, F. Villars, M. Weiss, and J. Zabolitzky are also gratefully acknowledged. It is a pleasure to thank K. T. R. Davies, B. Day, J. Dubach, H. Flocard, S. Köhler, I. Sick, M. Strayer, and M. Weiss for providing results and original figures and to thank K. T. R. Davies and F. Coester for their comments on a draft of the manuscript. This work was supported in part through funds provided by the U. S. Department of Energy under Contract No. DE-AC02-76ER03069.

REFERENCES

Abers, E., and B. Lee, 1973, Phys. Rep. **9**, 1.
Abrikosov, A. A., and I. M. Khalatnikov, 1959, Rep. Prog. Phys. **22**, 329.
Agassi, D., H. J. Lipkin, and N. Meshkov, 1966, Nucl. Phys. **86**, 321.
Alhassid, Y., and S. E. Koonin, 1981, Phys. Rev. C **23**, 1590.
Alhassid, Y., B. Müller, and S. E. Koonin, 1981, Phys. Rev. C **23**, 487.
Bäckman, S. O., A. D. Jackson, and J. Speth, 1975, Phys. Lett. B **56**, 209.
Baranger, M., and M. Véneroni, 1978, Ann. Phys. (N.Y.) **114**, 123.
Bargmann, V., 1961, Commun. Pure Appl. Math. **14**, 187.
Barreto, J., G. Auger, H. Doubre, M. Langevin, and E. Plagnol, 1980, Annual Report IPN Orsay (unpublished).
Baym, G., 1962, Phys. Rev. **127**, 1381.
Baym, G., and L. Kadanoff, 1961, Phys. Rev. **124**, 287.
Bender, C., F. Cooper, and G. Guralnick, 1977, Ann. Phys. (N.Y.) **109**, 165.
Bender, I., D. Gromes, H. Rothe, and K. Rothe, 1978, Nucl. Phys. B **36**, 259.
Berezin, F. A., 1966, *The Method of Second Quantization,* (Academic, New York).
Bertsch, G. F., 1977a, Phys. Rev. C **15**, 713.
Bertsch, G., 1977b, private communication. See also Negele 1977, p. 79.
Bertsch, G. F., 1978a, "Dynamics of heavy ion collisions," in *Nuclear Physics with Heavy Ion and Mesons,* edited by R. Balian, M. Rho, and G. Ripka, Les Houches Summer School XXX (North-Holland, Amsterdam), Vol. 1, p. 175.
Bertsch, G., 1978b, Z. Phys. A **289**, 103.
Bertsch, G., and D. Mundinger, 1978, Phys. Rev. C **17**, 1646.
Bethe, H. A., 1931, Z. Phys. **71**, 205.
Bethe, H. A., 1971, Annu. Rev. Nucl. Sci. **21**, 93.
Blaizot, J. -P., 1980, Phys. Rep. **64**, 172.
Blaizot, J. -P., and H. Orland, 1980, J. Phys. (Paris), Lett. **41**, L53.
Blaizot, J. -P., and H. Orland, 1981, Phys. Rev. C **24**, 1740.
Błocki, J., and H. Flocard, 1976, Nucl. Phys. A **273**, 45.
Bonche, P., K. T. R. Davies, B. Flanders, H. Flocard, B. Grammaticos, S. E. Koonin, S. J. Krieger, and M. S. Weiss, 1979, Phys. Rev. C **20**, 641.
Bonche, P., B. Grammaticos, and S. E. Koonin, 1978, Phys. Rev. C **17**, 1700.
Bonche, P., S. Koonin, and J. W. Negele, 1976, Phys. Rev. C **13**, 1226.
Bondorf, J. P., J. N. De, G. Fai, A. O. T. Karvinen, and B. Jakobsson, 1979, Phys. Lett. B **84**, 163.
Bondorf, J. P., J. N. De, G. Fai, A. O. T. Karvinen, B. Jakobsson, and J. Randrup, 1980, Nucl. Phys. A **333**, 285.
Burnett, D. S., 1963, Lawrence Berkeley Laboratory Report No. UCRL-11006.
Calogero, F., and A. Degasperis, 1975, Phys. Rev. A **11**, 265.
Campbell, D., 1978, "Nuclear physics in one dimension," in *Nuclear Physics with Heavy Ions and Mesons,* edited by R. Balian, M. Rho, and G. Ripka, Les Houches Summer School XXX (North-Holland, Amsterdam), Vol. 2, p. 673.
Campbell, D., 1979, *Proceedings of a Conference on Time Dependent Hartree-Fock Method,* edited by P. Bonche, B. Girard, and Ph. Quentin (Editions de Physique, Saclay).
Campbell, D., and Y. T. Liao, 1976, Phys. Rev. D **14**, 2093.
Campbell, D., and J. W. Negele, 1981 (to be published).
Campi, X., and D. W. L. Sprung, 1972, Nucl. Phys. A **194**, 401.
Ceperley, D., G. V. Chester, and M. H. Kalos, 1977, Phys. Rev. B **16**, 3081.
Chaumeaux, A., V. Layly, and R. Schaeffer, 1977, Phys. Lett. B **72**, 33.
Coester, F., 1958, Nucl. Phys. **7**, 421.
Coester, F., and H. Kümmel, 1960, Nucl. Phys. **17**, 477.
Coleman, S., 1977, "The uses of instantons," in *The Whys of Subnuclear Physics,* edited by A. Zichichi (Plenum, New York), p. 805.
Conjeaud, M., S. Harar, F. Saint-Laurent, J. M. Loiseaux, J. Menet, and J. B. Viano, 1977, Proceedings of the International Conference on Nuclear Structure, Tokyo, 663.
Coon, S. A., and H. S. Köhler, 1974, Nucl. Phys. A **231**, 95.
Creswell, C., A. Hirsch, W. Bertozzi, J. Heisenberg, M. V. Hynes, K. DeJager, S. Kowalski, H. Miska, B. Norum, F. N. Rad, C. P. Sargent, T. Sasanuma, and W. Turchinetz, 1981, MIT preprint.
Cusson, R. Y., and J. Maruhn, 1976, Phys. Lett. B **62**, 134.
Cusson, R. Y., J. A. Maruhn, W. Greiner, and H. Stöcker, 1981, preprint.
Cusson, R. Y., J. A. Maruhn, and H. W. Meldner, 1978, Phys. Rev. C **18**, 2589.
Cusson, R. Y., J. A. Maruhn, and H. Stöcker, 1980, Z. Phys. A **294**, 257.
Cusson, R. Y., and H. W. Meldner, 1979, Phys. Rev. Lett. **42**, 694.
Cusson, R. Y., R. K. Smith, and J. A. Maruhn, 1976, Phys. Rev. Lett. **36**, 1166.
Dashen, R. F., B. Hasslacher, and A. Neveu, 1974a, Phys. Rev. D **10**, 4114, 4130.
Dashen, R. F., B. Hasslacher, and A. Neveu, 1974b, Phys. Rev. D **12**, 2443.
Dasso, C. H., T. Døssing, and H. C. Pauli, 1979, Z. Phys. A **289**, 395.
Davies, K. T. R., 1979, Oak Ridge National Laboratory Report No. ORNL/TM-700.
Davies, K. T. R., H. T. Feldmeier, H. Flocard, and M. S. Weiss, 1978, Phys. Rev. C **18**, 2631.

Davies, K. T. R., H. Flocard, S. Krieger, and M. S. Wiess, 1980, Nucl. Phys. A **342**, 111.
Davies, K. T. R., and S. E. Koonin, 1981, Phys. Rev. C **23**, 2042.
Davies, K. T. R., V. Maruhn-Rezwani, S. E. Koonin, and J. W. Negele, 1978, Phys. Rev. Lett. **41**, 632.
Davies, K. T. R., R. J. McCarthy, J. W. Negele, and P. U. Sauer, 1974, Phys. Rev. C **10**, 2607.
Davies, K. T. R., R. J. McCarthy, and P. U. Sauer, 1972, Phys. Rev. C **6**, 1461.
Davies, K. T. R., K. R. Sandhya Devi, and M. R. Strayer, 1979, Phys. Rev. C **20**, 1372.
Davies, K. T. R., K. R. Sandhya Devi, and M. R. Strayer, 1980, Phys. Rev. Lett. **44**, 23.
Davies, K. T. R., K. R. Sandhya Devi, and M. R. Strayer, 1981, preprint.
Day, B. D., 1967, Rev. Mod. Phys. **39**, 719.
Day, B. D., 1978, Rev. Mod. Phys. **50**, 495.
Day, B. D., 1981a, Phys. Rev. Lett. **47**, 226.
Day, B. D., 1981b, Phys. Rev. C **24**, 1203.
Dechargé, J., and D. Gogny, 1980, Phys. Rev. C **21**, 1568.
DeJager, C. S., H. DeVries, and C. DeVries, 1974, At. Data Nucl. Data Tables **14**, 479.
Desplanques, B., and J. F. Mathiot, 1982, Phys. Lett. (in press).
De Tourreil, R., and D. W. L. Sprung, 1973, Nucl. Phys. A **201**, 193.
deWitt Huberts, P. K. A., *et al.*, 1971, Phys. Lett. B **60**, 157.
Dhar, A. K., 1979, Phys. Rev. Lett. **42**, 1124.
Dhar, A. K., and B. S. Nilsson, 1978, Phys. Lett. B **77**, 50.
Dhar, A. K., and B. D. Nilsson, 1979, Nucl. Phys. A **315**, 445.
Dhar, A. K., B. S. Nilsson, K. T. R. Davies, and S. E. Koonin, 1981, Daresbury preprint No. G53AAG.
Dirac, P. A. M., 1930, Proc. Cambridge Philos. Soc. **26**, 376.
Dirac, P. A. M., 1933, Phys. Z. Sowjetunion, Band3 Heft1.
Dolan, L., 1976, Phys. Rev. D **13**, 528.
Doubre, H., A. Gamp, J. C. Jacmart, N. Poffé, J. C. Roynette, and J. Wilczyński, 1977, Orsay Report No. IPNO-PhN-77-26.
Dubach, J., 1980, Nucl. Phys. A **340**, 271.
Faddeev, L. D., 1976, "Introduction to functional methods," in *Methods in Field Theory,* edited by R. Balian and J. Zinn-Justin, Les Houches Summer School XXVIII (North-Holland, Amsterdam), p. 1.
Fai, G., and J. Nemeth, 1973, Nucl. Phys. A **208**, 463.
Fantoni, S., B. L. Friman, and V. Pandharipande, 1981, Phys. Lett. B **104**, 89.
Feldmeier, H. T., 1977, Oak Ridge National Laboratory report No. ORNL/TM-6053.
Fetter, A., and J. D. Walecka, 1971, *Quantum Theory of Many-Particle Systems* (McGraw-Hill, New York).
Feynman, R., and A. Hibbs, 1965, *Quantum Mechanics and Path Integrals* (McGraw-Hill, New York).
Flocard, H., S. E. Koonin, and M. S. Weiss, 1978, Phys. Rev. C **17**, 1682.
Friar, J. L., and J. W. Negele, 1975, Adv. Nucl. Phys. **8**, 219.
Friar, J. L., and J. W. Negele, 1977, in *Proceedings of the 1977 Bates Linac Summer Study,* edited by A. Bernstein, Laboratory for Nuclear Science, MIT.
Frois, B., J. B. Bellicard, J. M. Cavedon, M. Huet, P. Leconte, P. Ludeau, A. Nakada, Phan Xyan Ho, and I. Sick, 1977, Phys. Rev. Lett. **38**, 152.
Galitskii, V. M., 1958, Sov. Phys.—JETP **7**, 104.
Gavron, A., R. L. Ferguson, F. E. Obenshain, F. Plasil, G. R. Young, G. A. Petitt, K. A. Geoffroy, D. G. Sarantites, and C. F. Maguire, 1982 (to be published).
Glick, A. J., H. J. Lipkin, and N. Meshkov, 1965, Nucl. Phys. **62**, 211.
Gogny, D., 1975, "Self-consistent pairing calculations," in Nuclear Self-Consistent Fields, edited by G. Ripka, and M. Porneuf, (North-Holland, Amseterdam), p. 333.
Gogny, D., 1979, "Theories of the nuclear ground state beyond Hartree-Fock," in *Nuclear Physics with Electromagnetic Probes,* edited by H. Arenhövel and D. Drechsel, Lecture Notes in Physics (Springer, Berlin), Vol. 108, p. 88.
Goldstone, J., 1957, Proc. R. Soc. London, Ser. A **239**, 267.
Goldstone, J., and K. Gottfried, 1959, Nuovo Cimento Ser. X **13**, 849.
Griffin, J. J., M. Dworzecka, K. K. Kan, and P. C. Lichtner, 1979, *Proceedings of a Conference on Time Dependent Hartree-Fock Method,* edited by P. Bonche, B. Girard, and Ph. Quentin (Editions de Physique, Saclay).
Gutzwiller, M. C., 1967, J. Math. Phys. **8**, 1979.
Gutzwiller, M. C., 1969, J. Math. Phys. **10**, 1004.
Gutzwiller, M. C., 1970, J. Math. Phys. **11**, 1791.
Gutzwiller, M. C., 1971, J. Math. Phys. **12**, 343.
Gyulassy, M., and W. Greiner, 1977, Ann. Phys. (N.Y.) **109**, 485.
Hadjduk, Ch., and P. U. Sauer, 1979, Nucl. Phys. A **322**, 329.
Hamada, T., and I. D. Johnston, 1962, Nucl. Phys. **34**, 382.
Hoodbhoy, P., and J. W. Negele, 1977, Nucl. Phys. A **288**, 23.
Hoodbhoy, P., and J. W. Negele, 1978, Phys. Rev. C **18**, 2380.
Hoodbhoy, P., and J. W. Negele, 1979, Phys. Rev. C **19**, 1971.
Hubbard, J., 1959, Phys. Rev. Lett. **3**, 77.
Huizenga, J. R., 1975, Nukleonika **20**, 292.
Jeukenne, J. P., A. Leujeune, and C. Mahaux, 1976, Phys. Rep. **25**, 83.
Kalos, M. H., D. Levesque, and L. Verlet, 1974, Phys. Rev. A **9**, 2178.
Kan, K. K., 1980, Phys. Rev. C **22**, 2228.
Kan, K. K., J. J. Griffin, P. C. Lichtner, and M. Dworzecka, 1979, Nucl. Phys. A **332**, 109.
Kerman, A. K., and S. E. Koonin, 1976, Ann, Phys. (N.Y.) **100**, 332.
Kerman, A. K., and S. Levit, 1981, Phys. Rev. C **24**, 1029.
Kerman, A. K., S. Levit, and T. Troudet, 1982, MIT preprint.
Kleinert, H., 1977, Phys. Lett. B **69**, 9.
Kleinert, H., 1978, Fortschr. Phys. **26**, 565.
Kleinert, H., and H. Reinhardt, 1979, Nucl. Phys. A **332**, 331.
Köhler, H. S., and H. Flocard, 1979, Nucl. Phys. A **373**, 189.
Koonin, S. W., 1975, Ph.D. thesis, Massachusetts Institute of Technology (unpublished).
Koonin, S. E., 1976, Phys. Lett. B **61**, 227.
Koonin, S. E., 1979, "The time-dependent Hartree-Fock description of heavy-ion collisions," in *Heavy Ion Interactions at High Energies,* edited by D. Wilkinson, Progress in Particle and Nuclear Physics (Pergamon, Oxford), Vol. 4, p. 283.
Koonin, S. E., K. T. R. Davies, V. Maruhn-Rezwani, H. Feldmeier, S. J. Krieger, and J. W. Negele, 1977, Phys. Rev. C **15**, 1359.
Koonin, S. E., B. Flanders, H. Flocard, and M. S. Weiss, 1978, Phys. Lett. B **77**, 13.
Kox, S., A. J. Cole, and R. Ost, Phys. Rev. Lett. **44**, 1204.
Kramers, H. A., 1926, Z. Phys. **39**, 828.
Krewald, S., and J. W. Negele, 1980, Phys. Rev. C **21**, 2385.
Krieger, S. J., and K. T. R. Davies, 1978, Phys. Rev. C **18**, 2567.
Krieger, S. J., and K. T. R. Davies, 1979, Phys. Rev. C **20**, 167.

Krieger, S. J., and M. S. Weiss, 1981, Phys. Rev. C. **24**, 928.
Kümmel, H., 1974, Nucl. Phys. A **228**, 272.
Kümmel, H., K. Lührmann, and J. Zabolitzky, 1978, Phys. Rep. C **36**, 1.
Kuratsuji, H., and T. Suzuki, 1980, Phys. Lett. B **92**, 19.
Landau, L. D., 1957, J. Expt. Theor. Phys. (U.S.S.R.) **32**, 59.
Lapedes, A., and E. Mottola, 1982, Princeton preprint.
Lazzarini, A., H. Doubre, K. T. Lesko, V. Metag, A. Seamster, R. Vandenbosch, and W. Merryfield, 1981, Phys. Rev. C **24**, 309.
Levit, S., 1980, Phys. Rev. C **21**, 1594.
Levit, S., J. W. Negele, and H. Orland, 1981 (to be published).
Levit, S., J. W. Negele, and Z. Paltiel, 1980a, Phys. Rev. C **21**, 1603.
Levit, S., J. W. Negele, and Z. Paltiel, 1980b, Phys. Rev. C **22**, 1979.
Lichtner, P., and J. J. Griffin, 1976, Phys. Rev. Lett. **37**, 1521.
Lindhard, J., 1954, Kgl. Dansk. Videnskab. Selsk. Mat.-Fys. Medd. **28**, No. 8.
Lipkin, H. J., N. Meshkov, and A. J. Glick, 1965, Nucl. Phys. **62**, 188.
Lührmann, K. H., 1977, Ann. Phys. (N.Y.) **103**, 253.
Martin, P. C., and J. Schwinger, 1959, Phys. Rev. **115**, 1342.
Maruhn, J. A., and R. Y. Cusson, 1976, Nucl. Phys. A **270**, 471.
Maruhn-Rezwani, V., K. T. R. Davies, and S. E. Koonin, 1977, Phys. Lett. B **67**, 134.
McGuire, J., 1965, J. Math. Phys. **6**, 432.
Meshkov, N., A. J. Glick, and H. J. Lipkin, 1965, Nucl. Phys. **62**, 199.
Migdal, A. B., 1972a, Zh. Eksp. Teor. Fiz. **61**, 2209 [Sov. Phys.—JETP **34**, 1184].
Midgal, A. B., 1972b, Zh. Eksp. Teor. Fiz. **62**, 1621 (Sov. Phys.—JETP **35**, 845).
Midgal, 1978, Rev. Mod. Phys. **50**, 107.
Miller, J. M., G. L. Catchen, D. Logan, M. Rajagopalan, J. M. Alexander, M. Kaplan, and M. S. Zisman, 1978, Phys. Rev. Lett. **40**, 100.
Monkhorst, H. J., 1977, J. Quantum Chem. **511**, 421.
Natowitz, J. B., G. Doukellis, B. Kolb, G. Rosnev, and Th. Walcher, 1979, Nukleonika **24**, 443.
Negele, J. W., 1970a, Phys. Rev. C **1**, 1260.
Negele, J. W., 1970b, Nucl. Phys. A **142**, 225.
Negele, J. W., 1971, Phys. Rev. Lett. **27**, 1281.
Negele, J. W., 1977, "Overview of the time dependent mean-field theory," in *Proceedings of the Topical Conference on Heavy-Ion Collisions,* NTIS, U.S. Department of Commerce, CONF-770602, p. 73.
Negele, J. W., 1978a, "Nuclear matter theory," in *Nucleon-Nucleon Interactions—1977,* edited by D. F. Measday, H. W. Fearing, and A. Strathdee, AIP Conference Proceedings **41**, p. 104.
Negele, J. W., 1978b, "Nuclear dynamics: the time-dependent mean-field approximation and beyond," in *Theoretical Methods in Medium-Energy and Heavy-Ion Physics,* edited by K. W. McVoy and W. A. Friedman (Plenum, New York), p. 235.
Negele, J. W., 1979, *Nuclear Structure and Heavy-Ion Collisions,* Varenna Summer School LXXVII (Soc. Italiana di Fisica, Bologna, Italy).
Negele, J. W., 1980, Proceedings of an International Conference on Extreme States in Nuclear Systems, Dresden, edited by H. Prade and S. Tesch, Zfk Rossendorf Report, Dresden.
Negele, J. W., S. E. Koonin, P. Möller, J. R. Nix, and A. J. Sierk, 1978, Phys. Rev, C **17**, 1098.
Negele, J. W., S. Levit, and Z. Paltiel, 1979, *Proceedings of a Conference on Time Dependent Hartree-Fock Method,* edited by P. Bonche, B. Girard, and Ph. Quentin (Editions de Physique, Saclay).
Negele, J. W., and G. Rinker, 1977, Phys. Rev. C **15**, 1499.
Negele, J. W., F. Serr, and G. Vichniac, 1982 (to be published).
Negele, J. W., and D. Vautherin, 1972, Phys. Rev. C **5**, 1472.
Negele, J. W., and D. Vautherin, 1975, Phys. Rev. C **11**, 1031.
Negele, J. W., and K. Yazaki, 1981, Phys. Rev. Lett. **47**, 71.
Nix, J. R., and A. J. Sierk, 1977, Phys. Rev. C **15**, 2072.
Nohl, C. R., 1976, Ann. Phys. (N.Y.) **96**, 234.
Obenshain, F., R. L. Ferguson, F. Plasil, A. H. Snell, and G. R. Young, 1981 (unpublished).
Ohnuki, Y., and T. Kashiwa, 1978, Prog. Theor. Phys. **60**, 548.
Orland, H., 1980, *Conférence sur les Méthodes Mathématiques de la Physique Nucléaire,* College de France.
Orland, H., 1981, private communication.
Orland, H., and R. Schaeffer, 1978, Z. Phys. A **290**, 191.
Pandharipande, V. R., and R. B. Wiringa, 1979, Rev. Mod. Phys. **51**, 821.
Patrascioiu, A., 1981, Phys. Rev. D **24**, 496.
Payne, G. L., J. L. Friar, B. F. Gibson, and I. R. Afnan, 1980, Phys. Rev. C **22**, 823.
Pirner, H. J., K. Yazaki, P. Bonche, and M. Rho, 1979, Nucl. Phys. A **329**,
Polyakov, A. M., 1977, Nucl. Phys. B **121**, 429.
Rajaraman, R., 1975, Phys. Rep. C **21**, 227.
Ray, L., 1979, Phys. Rev. C **19**, 1855.
Reed, M., and B. Simon, 1972, *Methods of Modern Mathematical Physics* (Academic, New York), Secs. VIII.8 and X.11.
Reid, R. V., 1968, Ann. Phys. (N.Y.) **50**, 411.
Reinhardt, H., 1978, Nucl. Phys. A **298**, 77; **306**, 38.
Reinhardt, H., 1979a, J. Phys. G **5**, L91.
Reinhardt, H., 1979b, Nucl. Phys. A **331**, 353.
Reinhardt, H., 1980, Nucl. Phys. A **346**, 1.
Reinhardt, H., 1981, Nucl. Phys. A. **367**, 269.
Reinhardt, H., 1982, Nucl. Phys. (in press).
Richert, J., D. M. Brink, and H. A. Weidenmüller, 1979, Phys. Lett. B **87**, 6.
Sandhya Devi, K. R., A. K. Dhar, and M. R. Strayer, 1981, Phys. Rev. C **23**, 2062.
Sandhya Devi, K. R., and M. R. Strayer, 1978a, Phys. Lett. B **77**, 135.
Sandhya Devi, K. R., and M. R. Strayer, 1978b, J. Phys. G **4**, L97.
Sandhya Devi, K. R., M. R. Strayer, K. T. R. Davies, S. E. Koonin, and A. K. Dhar, 1981, preprint.
Sandhya Devi, K. R., M. R. Strayer, J. M. Irvine, and K. T. R. Davies, 1981, Phys. Rev. C **23**, 1064.
Sawyer, R. F., 1972, Phys. Rev. Lett. **29**, 382.
Scalapino, D. J., 1972, Phys. Rev. Lett. **29**, 386.
Schonhammer, K., and O. Gunnarsen, 1978, Phys. Rev. B **18**, 6606.
Schroder, W. U., J. R. Birkelund, J. R. Huizenga, K. L. Wolf, and V. E. Viola, Jr., 1978, Phys. Rep. **45**, 301.
Schroder, W. U., and J. R. Huizenga, 1977, Annu. Rev. Nucl. Sci. **27**, 465.
Sick, I., 1974, Phys. Lett. B **53**, 15.
Sick, I., J. B. Bellicard, J. M. Cavedon, B. Frois, M. Huet, P. Leconte, A. Nakada, Phan Xuan Ho, S. Platchkov, P. K. A. deWitt Huberts, and L. Lapikas, 1977, Phys. Rev. Lett. **38**, 1259.

Sick, I. *et al.*, 1979, Phys. Lett. B **88**, 245.
Sick, I. *et al.*, 1975, Phys. Rev. Lett. **35**, 910.
Sperr, P., T. H. Braid, Y. Eisen, D. G. Kovar, F. W. Prosser, J. P. Schiffer, S. L. Tabor, and S. Vidgor, 1976, Phys. Rev. Lett. **37**, 321.
Sperr, P., S. Vidgor, Y. Eisen, W. Henning, D. G. Kovar, T. R. Ophel, and B. Zeidmann, 1976, Phys. Rev. Lett. **36**, 405.
Sprung, D. W. L., and P. K. Banerjee, 1971, Nucl. Phys. A **168**, 273.
Stöcker, H., R. Y. Cusson, J. A. Maruhn, and W. Greiner, 1980, Z. Phys. A **294**, 125.
Stöcker, H., R. Y. Cusson, J. A. Maruhn, and W. Greiner, 1981, preprint.
Stratonovich, R. L., 1957, Dokl. Akad. Nauk. SSSR **115**, 1907; [Sov. Phys.—Dokl. **2**, 416 (1958)].
Strayer, M., W. Bassichis, and A. Kerman, 1973, Phys. Rev. C **8**, 1269.
Suzuki, T., H. Hyuga, and A. Arima, 1979, Z. Phys. A **293**, 5.
Tabor, S., D. Geesaman, W. Henning, D. Kovar, K. Rehn, and F. Prosser, 1978, Phys. Rev. C **17**, 2136.
Takatsuka, T., and R. Tamagaki, 1978, J. Phys. Soc. Jpn. Suppl. **44**, 495.
Takatsuka, T., K. Tamiya, T. Tasumi, and R. Tamagaki, 1978, Prog. Theor. Phys. 59, 1933.
Tang, H., 1981, Phys. Lett. B **101**, 10.
't Hooft, G., 1976, Phys. Rev. Lett. **37**, 8.
Thouless, D. J., 1972, *The Quantum Mechanics of Many-Body Systems* (Academic, New York).
Tomasi, E., D. Ardovin, J. Barreto, V. Bernard, B. Cauvin, C. Magnago, C. Mazur, C. Ngô, E. Piasecki, and M. Ribrag, 1982, Nucl. Phys. A **373**, 348.
Tomoda, T., and A. Sevgen, 1982, Z. Phys. A **304**, 221.
Troudet, T., 1982, Ph.D. thesis, Massachusetts Institute of Technology (unpublished).
Vandenbosch, R., M. P. Webb, P. Dyer, R. J. Pugh, R. Weisfield, T. D. Thomas, and M. S. Zisman, 1978, Phys. Rev. C **17**, 1672.
Varma, G. K., and L. Zamick, 1977, Phys. Rev. C **16**, 308.
Varma, G. K., and L. Zamick, 1978, Nucl. Phys. A **306**, 343.
Vautherin, D., and D. M. Brink, 1972, Phys. Rev. C **5**, 626.
Weiss, M. S., 1977, Fizika **9**, Suppl. 3, 315.
Wigner, E. P., 1930, Phys. Rev. **40**, 749.
Wolf, K. L., and C. T. Roche, 1976, "The interaction of very heavy ions with heavy targets," in *Proceedings of the Symposium on Macroscopic Features of Heavy Ion Collisions,* Argonne, Illinois, ANL Report No. ANL/PHY-76-2 (unpublished), Vol. I, p. 295.
Wolf, K. L., J. P. Unik, J. R. Huizenga, J. Birkelund, H. Freiseleben, and V. E. Viola, 1974, Phys. Rev. Lett. **33**, 1105.
Wong, C. Y., 1979, *Proceedings of a Conference on the Time Dependent Hartree-Fock Method,* edited by P. Bonche, B. Girard, and Ph. Quentin (Editions de Physique, Saclay).
Wong, C. Y., and K. T. R. Davies, 1980, Phys. Lett. B **96**, 258.
Wong, C. Y., and H. H. K. Tang, 1978, Phys. Rev. Lett. **40**, 1070.
Wong, C. Y., and H. H. K. Tang, 1979, Phys. Rev. C **20**, 1419.
Yang, C. N., 1967, Phys. Rev. Lett. **19**, 1313.
Yoon, B., and J. W. Negele, 1977, Phys. Rev. A **16**, 1451.
Zabolitzky, J. G., 1980, *Advances in Nuclear Physics* (Plenum, New York), Vol. 12.
Zabolitzky, J. G., 1981, Bochum preprint.
Zakharov, V. F., and A. B. Shabot, 1972, Sov. Phys.—JETP **34**, 62.